Feasibility of the motorized momentum exchange tether system:

An investigation of system risk compared against conventional launch vehicle alternatives, accounting for vehicle and tether span failures

by

Christopher Hayward Draper

15 September 2006

A dissertation submitted to the Faculty of Engineering, University of Glasgow, in fulfilment of the requirements for the degree of Doctor of Philosophy.

UNIVERSITY
of
GLASGOW

ProQuest LLC.
789 East Eisenhower Parkway
P.O. Box 1346
Ann Arbor, MI 48106 – 1346

Abstract

This thesis examines the feasibility of a motorized momentum exchange tether (MMET) system being used to perform commercial space launches. The MMET system is an on-orbit launch concept that could be used to reduce the cost of access to space, thereby catalysing a broader range of space-enabled business concepts. The research presented in this thesis assumes this cost of access to space for a reasonable launch system can be presented as the adverse financial risk of its operation. Under this assumption, the research concludes that an MMET-based system would be a feasible alternative to an equivalently capable conventional system if the risk associated with the system is less than that associated with the alternative. To illustrate the concepts and approaches presented within, this thesis presents an assessment of the proposed Lunar Staged MMET (LSM) mission, an assessment that indicates the MMET is a feasible alternative for completing such a mission under specific analytical and market conditions.

The expected financial risk is presented in this thesis as the product of the mission cost and the probability of mission failure. The cost of each mission is calculated from the perspective of the end customer, and the long-term price of such services is computed using publicly available data and the assumption that the commercial space industry can be modelled as an oligopoly. Support for such a model is contained in the literature and through this research, which compares the quarterly financial data published by the Boeing Company against the international commercial launch rate.

The probability of system failure associated with an MMET-based unconventional launch system must account for a number of factors. For the first, conventional stage of the system, assessing the probability of stage failure is found through an examination of observed failure rates relative to conventional engineering reliability estimates for conventional launch vehicles. Through this examination, a novel approach to calculating the rate at which the probability of failure for vehicles produced within a variant class changes as a function of time is presented, an approach that offers a valid technique for applying reliability growth across a series of vehicles that are best considered to be independent vehicles. The thesis goes on to

present the results of research into various component aspects that are vital to the design and analysis of a tether-based system. First, the research explores the strength of tethers modelled as braided aramid ropes, which supports claims of strain dependence regarding aramid fibre strength that can have significant strength benefits and indicates that this phenomenon should be accounted for in any operational architecture. Second, the thesis presents an empirical hypervelocity impact effects equation calibrated for use with tethers, which indicates that the currently accepted approach to oblique hypervelocity impacts may not be appropriate for tether analyses. Thirdly, research into fractured impactor dispersion after a hypervelocity impact on tether targets is presented, which indicates that the commonly accepted one-impact-one-failure assumption employed for multi-line tether analyses may not be sufficient. TetherLife, an analytical program developed to calculate the expected lifetime of an MMET system given various sub-span parameters, employs the products of these research areas to calculate the mean time to failure for a range of tether sizes and orientations.

After combining the probability of failure associated with the conventional launch vehicle component of the MMET-based unconventional launch system, the probability of failure associated with the MMET system, the probability or failure associated with handing a payload between systems, and the likely cost of deploying a suitable set of MMET systems, a comparison can be made between the financial risk associated with completing a specific mission using an MMET-based unconventional launch system verses completion of the same mission using conventional means. For the LSM mission examined within the research, an MMET-based system would be a reasonable option if an average of 85 missions per year are required, contingent on specific analytical assumptions. While such a number of lunar supply missions are not currently required, the conclusion that the MMET system can be an alternative to a conventional system under various circumstances offers support for continuing current research on system design and analysis.

Table of Contents

Acknowledgements

This work is dedicated to R.C. Oarrie, without whose inspiration I may have taken the easy way out.

Throughout the course of my work here at the University of Glasgow, I have received invaluable technical guidance and support from a diverse range of sources, including: Prof. Matthew Cartmell, Mr. David McKenzie, Mr. Kenneth Stevenson, Prof. Mark Burchell (University of Kent), Dr. Nial Friel (University of Glasgow, Statistics), Mr. Robin Milne (University of Glasgow, Economics), Dr. Phil Harrison, Dean John Hancock, Prof. John Weaver (University of Glasgow, Department of Electronics and Electrical Engineering), Mr. Kaz Piechowiak, Mr. Brian Robb, Mr. Alex Torry, Mr. Ewan Russell, Dr. Graham Green, Dr. Donald Balance, and Dr. Margaret Lucas.

While we may get wrapped up in the research from time-to-time, it must be remembered that the efficient completion of this thesis relied heavily on the operational support provided by Ms. Pat Duncan, Mrs. Evelyn McDonald, Ms. Fiona Downie, Miss Jane Livingston, Miss Marilyn Dunlop, Miss Jennifer Young, Mrs. Christine Cooke, and, up until her departure, Ms. Marion Richardson. While all those Professors, Doctors, and technicians kept the technical portions of my thesis on track, you got me over the real world hurdles, for which I cannot thank you enough.

Outside Glasgow, I must thank Mr. Phil Brinkman (FAA), Dr. Paul Wilde (ACTA – Houston), and Dr. Jon Collins (ACTA – Torrance) for the technical support you have provided. Since my arrival in Washington, DC, you have always been there to support and inspire my work. Without you, I probably would have left aerospace years ago.

More than anyone, though, I must thank Prof. Matthew Cartmell. Coming to Glasgow was one of the best decisions I have ever made. I cannot thank you enough for offering me this opportunity.

Thank you.

Preface

This thesis strives to analyse the design and cost conditions that would indicate the motorized momentum exchange tether (MMET) concept being developed at the University of Glasgow is a feasible alternative to a conventional launch vehicle concept. In response to concerns that the cost of access to space is too high, many novel launch concepts have been developed. The types of concepts vary widely from structures stretching all the way to a geosynchronous orbit, to rockets launched from balloons. All of these concepts offer hope for bringing down the cost of access to space. However, when resource allocation is required, some concepts may warrant immediate study, while others may require advancements in core technologies.

It is argued that, if a system reduces the cost of access to space, such a system will enable space-based commercial opportunities. For example, if the cost of transport to the moon were reduced, maybe a business concept would emerge that relies on this low-cost transport. If the rationalization is that a better system enables commercial achievement, it seems logical that a new technology like the MMET should be judged using proven metrics derived from the commercial launch environment.

The commercial launch market is both small and fluid. With companies such as Arianespace, Boeing, Chelomei, General Dynamics, Hughes, Korolev, Lockheed Martin, McDonnell Douglas, Mitsubishi, and Orbital Sciences not only entering and exiting the market in various forms and performing various roles within the industry that range from simple manufacturing to launch operations; agencies and organizations such as the European Space Agency (ESA), the Japan Aerospace Exploration Agency (JAXA), the National Aeronautics and Space Administration (NASA), the United States Air Force (USAF), and the United States Navy (USN), varying and redefining their roles and oversight within space launch operations; and new organizations such as International Launch Services (ILS), Sea Launch, and SpaceX emerging to navigate niches within an industry that is rife with overcapacity, the task of defining a feasible launch system alternative is not a trivial proposition. Even with an ever evolving pool of suppliers and technologies, and a reportedly large potential market of customers, the number of commercial launches performed

throughout the entire world has rarely reached or exceeded fifty launches in any given year. With the current level of overcapacity reported in the market, the cost of access to space has already dropped significantly, and is likely to be well below the publicly stated prices.

Because the market is so small, any release of information is thought to remove the competitive advantage of an organisation. For this reason, it is very hard to find publicly available information about the commercial market that is based on current data. Furthermore, it is similarly difficult to find hard information on the contracting principles employed for the "average" contract, as each is developed on a case-by-case basis. With a history of less than 20 years, the commercial launch market is difficult to quantitatively analyse.

With an acceptance of the significant uncertainty associated with the industry data, combined with a task to assess a launch concept that has yet to be fully designed and tested, this thesis offers a guide for where future work should be focussed on the MMET system. The novelty in this research has been to integrate various, apparently disparate themes, in order to create an entirely new feasibility study and assessment. Very few assessments of this kind have been rigorously completed for unconventional launch system concepts, and, as far as the author knows, no other analysis has currently reached the level of fidelity achieved within for a tether-based space system.

This thesis lays out its fundamental approach, a process for implementing those fundamentals for the purposes of an on-orbit launch system concept like the MMET, and presents an application of those fundamentals for a specific mission. While this work focuses on assessing unconventional systems that employ tether-based on-orbit launch systems, the principles presented and the methods by which they are applied could potentially be applied to other systems.

The thrust of this work is in establishing a methodology that selects the better of two reasonable launch system choices. The analyses presented herein take a holistic approach to assessing a launch system option. In the same way risk accounts for more than reliability, launch system feasibility accounts for more than functionality. If a

system is cheaper, this decrease in cost may be offset by a decrease in reliability, a situation that must be identified and considered.

As defined within, the major aspects that must be accounted for when selecting a conventional launch system are identified in Fig 1. As evident from Fig 1, a conventional launch system is one that takes a payload from the surface of the earth to its final destination, without assistance from propulsive components or systems that are not present at the time of launch.

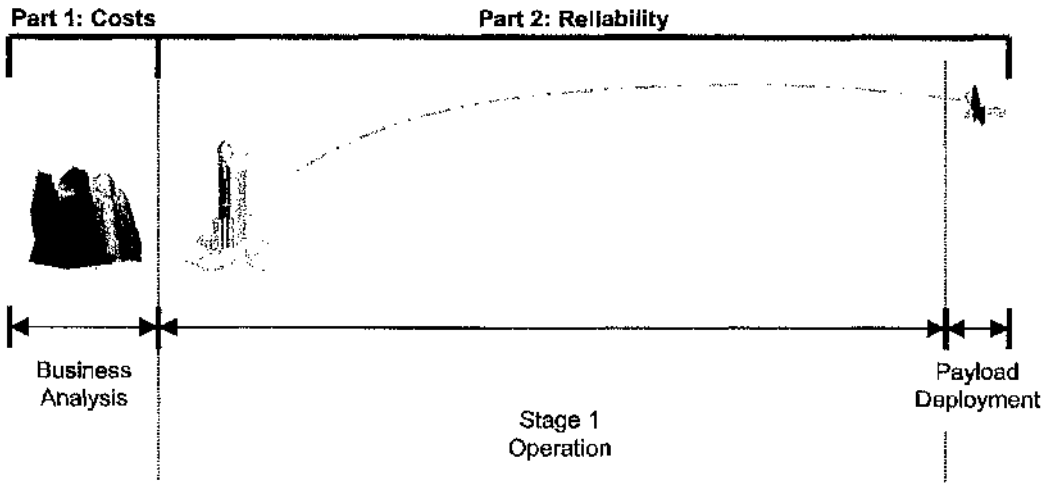

Figure 1: Model of a conventional launch system operation.

On-orbit launch system concepts employ smaller conventional launch vehicles as a component of the overall launch system, as identified in Fig 2. To be considered a feasible launch system option, this work asserts that an unconventional launch system must undergo a holistic examination equivalent to that for a conventional system. As in the case of a two-stage MMET-based on-orbit launch system like that presented in Fig 2, such an analysis at the system stage level is significantly more complex.

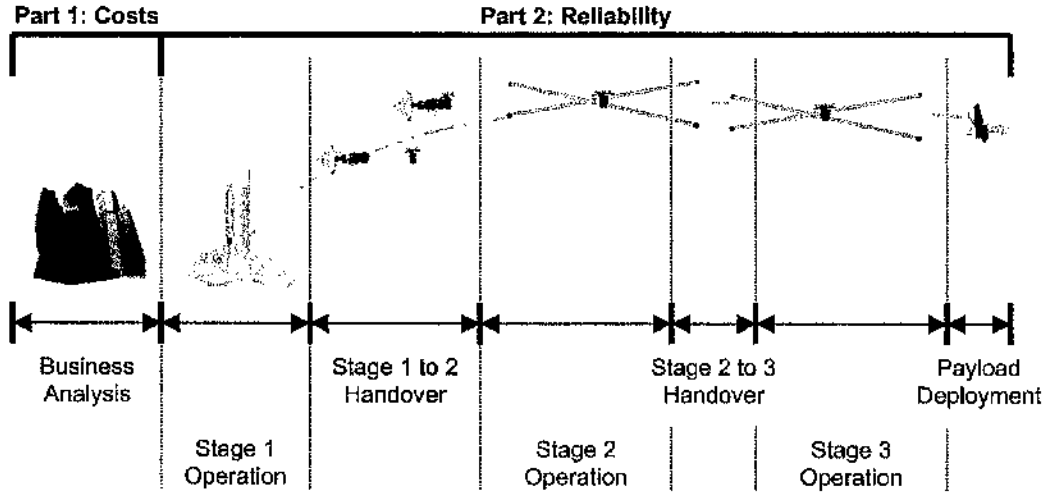

Figure 2: Model of an unconventional launch system employing two staged MMET systems.

Caution is urged when navigating through this thesis as the terminology employed by conventional mission analysts and unconventional system designers does not always agree. Terms used in this document must be interpreted in the context of this document. For example, this work considers the entire operation of the conventional launch vehicle identified in Fig 2 to be a single stage. From the perspective of the unconventional system, this is valid. However, for an individual who is familiar with the term *stage* as it applied to a conventional space launch vehicle, this perspective may conflict with his or her inherent understanding.

This thesis employs a commercial perspective to the analysis of the MMET, focusing on when it would become financially feasible. While every transaction in the commercial environment is complex, the research has worked to identify the core mechanisms in each transaction, so that a reasonable choice methodology is applied.

Chapter 1

Past Work

There exists a wide range of unconventional launch systems and launch system concepts. Many of these systems and concepts involve unique staging options designed to reduce the cost of access to space. One of these concepts is the MMET, which is currently undergoing development at the University of Glasgow.

1.0 Unconventional launch systems

An unconventional launch system is considered to be any that employs a mixture of dissimilar propulsive systems, any of which may require conventional chemical rocket propulsion, to take a payload from the surface of the earth to its final destination. According to this definition, there is currently only one unconventional launch system that is regularly employed for orbital launch missions, and this is the Pegasus launch system. The Pegasus launch system is composed of two stages, as previously defined. The first stage of this unconventional launch system is the Lockheed L-1011 aircraft, and the second stage is the Pegasus vehicle. For Pegasus-style architectures, earlier stages carry subsequent stages until they are required. Although only currently capable of completing suborbital missions, the Scaled Composites Spaceship One and its derivatives also employ this Pegasus-style architecture. In addition to unconventional systems like Spaceship One, many other concepts including various single-stage-to-orbit systems were proposed during the Ansari X-Prize competition. Many of the various concepts for such launch systems are discussed in documents such as DOT (2006) and Ashford (2002), or through examination of the relevant European Space Agency (ESA) or National Aeronautics and Space Administration (NASA) websites.

In contrast to the Pegasus-style architecture, an on-orbit launch system does not require the initial stages to carry all later stages. An on-orbit launch system is a propulsive system that remains on orbit between missions, and propels any payload it receives either onto its final destination or onto another on-orbit launch system stage. Within this class of concepts are those that are tether-based. An overview of the general tether concepts and tether-based launch applications currently under

investigation can be attained through examination of Cosmo and Lorenzini (1997), Johnson *et al.* (1999), Carroll (1986), Bekey (1983), or Forward and Hoyt (1999).

Tether-based systems are any space structure for which long, fibrous lines are an intrinsic component. Such concepts are primarily divided into the electro-dynamic tether, which is a system that uses conductive material within the tether span to allow the passage of current as it moves through the magnetosphere; and the momentum exchange tether, which is a long structure that transfers large tangential velocities to a payload at its tip by hanging, oscillating, or rotating about its centre of mass. The most widely considered studies of momentum exchange tethers, herein referred to as *passive* momentum exchange tethers, are those in which angular rotation is initiated through gravitational and inertial imbalances induced by a highly elliptical orbit. Examples of such systems are presented and discussed in Forward and Hoyt (1999) and also include hybrid systems like the MXER tether discussed in Sorensen (2003).

The main problem with passive momentum exchange tether systems is that, as the system releases its payload, it experiences a substantial de-orbit. Some current concepts, such as the MXER presented in Sorensen (2003), reorient themselves electrodynamically after de-orbit using energy gathered with their conductive tethers while the systems are passing through the magnetosphere. At present, systems like the MXER are still in the development phases, and require a great amount of further research, according to Sorensen (2004). Regardless of the current development state, many limitations inherent in passive momentum exchange tether systems are hard to overcome. Such limitations include their dependence on an elliptical orbit to force localised motion, which means that such systems lose their altitude advantage at the time they are undergoing their most rapid rotations. At the same time, the initial condition precision required for such systems, as identified in Eiden and Cartmell (2003), is significant.

As a counter to the problems of a passive system, the motorized momentum exchange tether (MMET) system under development at the University of Glasgow allows mission planners to both take advantage of the altitude benefits associated with a highly elliptical orbit by retaining some reasonable independence between the local

angular velocity of the system and the orbital position, thereby increasing the mechanical advantage available to the system; and operate in an out of plane manner that allows for less costly plane changes, thereby opening up unconventional launch sites for use in conventional mission.

1.1 Motorized momentum exchange tether

The MMET concept has undergone significant development since its introduction by Cartmell in Cartmell (1996). System introduction was quickly followed-up by two feasibility studies presented in Cartmell (1997a) and Cartmell (1997b), which determined that the system concept could be dynamically sound. In short, the MMET concept attempts to conserve angular momentum by counter-rotating two sets of payload and counterweight assemblies. By conserving a high proportion of angular momentum, the MMET will not experience as much of a rapid, post-mission de-orbit, as is inherent in other concepts. Further, this dependence on a counterweight to produce angular velocities in the system makes its operation independent of orbital position. As mentioned, such independence allows the system to release its payloads with the maximum possible imparted tangential velocity while at apogee, as opposed to perigee where passive systems must release to achieve the same conditions; or place payloads onto out-of-plane trajectories, which is currently not proven to be operationally feasible for passive systems. Work since the initial feasibility assessment has focused on validating the initial models and increasing the MMET model complexity, such as implementing deployment constraints, orbit eccentricity, and oblate Earth models.

Such tether work has been presented within a range of Journals and conference proceedings. The first public introduction of the MMET system came in Cartmell (1998), which introduced the system in terms of the general findings presented in Cartmell (1996-1997b). From there, an application of the concept was discussed in Cartmell and Ziegler (1999), which presented a further analytical study of the concept feasibility, with further studies of work supporting and developing these concepts presented in papers such as Ziegler and Cartmell (2000a), Ziegler and Cartmell (2000b), and Ziegler and Cartmell (2001).

The conclusions of these studies were supported by a testing regime discussed in Cartmell and Ziegler (2000), Cartmell and Ziegler (2001), Cartmell and Ziegler (2002), and Cartmell *et al.* (2003). It is during these experimental tests that an ESA funded scale model of the MMET was constructed and demonstrated in Glasgow, the results supportive of the concept.

Building on from this experimental success is the dynamic modelling work of Ziegler (2003), McKenzie *et al.* (2004), Cartmell and D'Arrigo (2005), and McKenzie and Cartmell (2005). Such analytical works have assisted in the development of more complex and sophisticated mission proposals such as Draper *et al.* (2004) and Cartmell *et al.* (2004).

While such research offers strong support for the feasibility of the system dynamics, there is currently no complete and publicly available research concerning how an MMET system would interact with the orbital environment.

1.2 Analytical components required for this research

The conclusions to how an MMET system would react with the orbital environment presented herein arise from research that has developed a risk assessment methodology and analytical package that calculates the lifetime of an MMET system, within the constraints of the model and available data. In conjunction with this engineering risk assessment, the system is assessed in the context of the commercial market, with conclusions being presented as to its financial viability. A research remit of this complexity requires an investigation of many topics. The main topics required, and a discussion of the literature relevant to this research, is presented in this section.

1.2.1 Commercial launch market

To understand the viability of an unconventional launch system within the commercial market, the commercial market must be defined and understood. This work accepts the working definition of the commercial space launch industry employed by Gabler (1991). Such a definition, which is based on the amount of government controlled operational oversight and financial support, would include all

space launches conducted for non-government customers by current operators such as Boeing Company, Lockheed Martin, Orbital Sciences, Sea Launch, and Arianespace. This is not an exhaustive list of commercial operators, and these operators are not exclusively involved in the commercial space launch industry, with many also conducting launches for government organisations.

When examining the launch market, the commercial launch rate is of primary concern. In the United States, any launch that is not conducted on behalf of the government or one of its agents is considered a commercial launch that must be licensed by the Department of Transportation (DOT). In other parts of the world, the regulator framework is not in place to allow for such a clear distinction, a distinction that identifies the relationship of the end user to its respective government. When assessing the commercial designation of non-US launches, the DOT generally considers a launch to be commercial if it is internationally competed. For the comparison of international launch rates and market shares, it is the DOT designation of what is a commercial launch that is accepted for use within the research presented here. The recent history of all commercial launches and activities is obtained by examination of DOT (1998b-2006), with any launch dates and details further cross-referenced against sources such as Isakowitz *et al.* (1999), Wade (2003), Chang (1996), Chang (2000), Smith (2005a), and Smith (2005b).

While it is clear and verifiable when a vehicle launches and, in the case of a commercial payload, what the payload is and who owns it, the cost of that launch is very hard to determine, based on publicly available data. Gabler identifies this issue, citing the oligopolistic nature of the industry as the cause. Despite its likely inaccuracy, this research examines the only publicly available compilation of commercial launch vehicle cost estimates, which are presented in DOT (1998b-2004). These estimates are compared against corporate financial filings submitted to the US Security and Exchange Commission (SEC) by US commercial space launch vehicle manufacturers. While it is reasonable to assume that the data provided to the SEC can be considered valid, as the legal reach of the SEC is significant and proven, the level of clarity offered by government mandated financial filings varies drastically between the different operators in the US. For example, almost no information can be inferred

about the launch activities of Lockheed Martin based on annual reports like Lockheed Martin Corporation (2003), with the figures presented those of Orbital Sciences in Orbital Science Corporation (2003) being marginally better. As a counter, the Boeing Company offers a significant level of insight into its commercial launch affairs, even if its investor-focused documents highlighting activities specific to each business line are neither externally audited nor offer a designation between internal and external revenues. In the context of the information that is commonly available in the public domain regarding the financial activities of commercial launch operators, a wealth of information is gained by examination of Boeing (1998a-2004d).

A further source of financial information, although the publicly available information is edited or censored by DOT in an attempt to remove the possibility that any competitive advantage could be lost, is obtained through an examination of Boeing (2002e), Boeing *et al.* (2000), Boeing *et al.* (2002), and Sea Launch (2002). These documents offer industry reaction to the regulations proposed by DOT around the turn of the century, and offer insight into projected costs associated with regulatory compliance and the operational mechanisms that drive such cost predictions. While these documents must be examined in the context of a persuasive argument, in which facts are presented in a light that is intended to lead the reader towards a desired response, the methodologies employed within these documents are informative.

These cost predictions and forecasts are only valid, though, in the terms of the projections from which the calculations are derived. Here again, two sides looking for funding within a competitive and political arena often dictate the arguments presented in the public literature. While it is evident that the commercial space industry is not a highly recognized contributor to the world economy by the average person, nor is its history dating back to the 1960s widely known or understood, the DOT is responsible for regulating the affairs of the commercial space transportation industry, as they are conducted by US citizens. Within the political arena that the DOT must operate, the importance of an organization dictates the funding it receives. Without funding, organizations like the Office of the Associate Administrator for Commercial Space Transportation (AST), within the Federal Aviation Administration (FAA) of the DOT, cease to exist. With the desire for self-preservation evident, DOT

publishes market projections on a regular basis. These projections are contained in documents such as DOT (1998-2004), COMSTAC (1997-2004), and Office of Commercial Space Transportation (1995), which is the previous title for AST within DOT. The ensuing launch rates and commercial studies have repeatedly proven the projections of DOT, and its industry partnership organizations such as COMSTAC, to be wildly inaccurate when examined in retrospect against documents such as Decker (2004), Smith (2005a), Smith (2005b), and Holtz-Eakin (2003). As with all predictions that are performed in the context of speculative markets, such as that of Johnson (1998), care must be taken in examining the source, its motivations, and the possible contribution of the work to the overall understanding of the market, actions that are taken during the course of the research discussed and presented herein.

When examining the motivations and subtleties associated with the launch industry, this research calls primarily on historical works like those of Gabler (1991), Decker (2004), Smith (2005a), Smith (2005b), and Holtz-Eakin (2003), and Krige (1999), with anecdotal insight from news sources at the time like Tully (1985), when examining the dawning of US regulatory policy towards commercial space launch activities; Wilhelm (2000), when examining the emergence of vehicles like the Delta III that were constructed in response to the anticipated needs of the commercial market; and Figler (2001) or Young (2001), when exploring the kinds of arguments that grab public attention, as did the inquiry by the city of Los Angeles as to whether satellites could be considered taxable under the rules governing terrestrial assets.

As discussed later, international activities have had a significant influence on the emergence and development of the commercial launch industry. The driving force provided by Arianespace in forcing the development of a transparent commercial market within the US is evident in documents such as Gabler (1991), Hermida (1997), Krige (1999), and Smith (2005a). Without the European influences discussed in these documents, it is clear that the international launch market would not be sufficiently developed for creating the currently emerging opportunities in space.

Because market forces acting on the commercial space transportation industry result in a competitive need for financial obscurity, proving how the industry really works

with only publicly available information is difficult. The research presented herein draws from a wide range of publicly available sources in an attempt to develop support for general trends on how the market would react to an unconventional system. Given the case-by-case nature dictating all financial decisions within an inherently risky industry, the predictions presented by this research must be viewed in the context of the uncertainty inherent in the available and employed data.

1.2.2 Risk-based decisions in the commercial market

As discussed later, this work makes the assumption that the commercial launch industry is risk averse. This assumption is made in the context of standard economic and financial assumptions highlighted in texts such as Stockman (1999), which offers a microeconomic perspective on the subject; Brealey and Myers (2003), which indicates that the concept is also accepted in finance texts; and Kotz and Johnson (1986), which address the concept as it applies generally within the study of economics. Nowhere in the literature, even though the industry is founded on inherently ultra-hazardous technologies as identified by DOT (2002), are the business practices of the commercial launch industry reported to be more accepting of greater corporate risk than organizations in other industries.

With such an assumption, this work then calls on the works of Guikema and Pate-Cornell (2002), Parkinson (1999), Smith *et al.* (1997), Weigel and Hastings (2004), and Livesey (1987), which identify methods that account for the measure and selection of systems based on the criteria of risk-minimization. As this concept of risk mitigation is supported within the literature, this work adopts a selection method consistent with the literature.

1.2.3 Launch vehicle costs

As discussed with regards to the commercial market, identifying the true cost of a commercial launch is difficult, given competitiveness within the commercial launch industry. While the aforementioned discussion of the commercial market to be presented in Chapter 2 of this work discusses the general trends and movements within the commercial launch industry, and how such movements are supported by the financial data available within the public domain, Chapter 3 compares actual costs

as stated in DOT (1997-2004) with those presented in Wade (2004) to gain an understanding of the general cost associated with various vehicles of differing capability. The validity of each of these sources is assessed and suitably verified through a comparative examination of Gabler (1991), Decker (2004), Smith (2005a), Smith (2005b), Isakowitz *et al.* (1999), and Holtz-Eakin (2003). The examination presented in Chapter 3 presents cost approximations under the assumption that the estimates presented in the literature are suitably valid.

1.2.4 Conventional launch vehicle failure rates

As financial risk is identified in the literature and discussed in Section 1.2.2 to include both cost and probability of failure, the probability of failure associated with conventional launch vehicles must be assessed. Assessing the probability of failure, however, is more complex than dividing the number of success a vehicle completes by the number of attempts it makes, as is done in Isakowitz *et al.* (1999), Chang (1996), Chang (2000), and other less sophisticated techniques discussed in DOT (2002b). Understanding how to appropriately calculate the probability of occurrence for an event with a small number of attempts is highly debatable, with significant financial implications discussed by Air Force Space Command (2004) and DOT (2002a) regarding launch approval.

There are a wide range of techniques that are commonly accepted to calculate the true probability that a launch vehicle will fail, the main techniques presented and discussed in Guikema and Pate-Cornell (2004), Guikema and Pate-Cornell (2005), and DOT (2002b). While it is obvious that these calculations are in conflict with both the reliability engineering analyses and risk assessments conducted with conventional techniques like those presented in Lewis (1996) and Stamatelatos (2002), as identified by Fragola and Collins (2004), these top-down analyses based on observed flight data offer greater assurance that the public is protected to an appropriate level.

The problem with the analyses presented by Guikema and Pate-Cornell is that they are both invalid, and proved to be invalid by their own conclusions. In these works, analysts employ an assumption that similar launch vehicles can be modelled as Bernoulli trials of a random event. McCartney *et al.* (1993), in conjunction with the

conclusions of Chang, clearly identify that this assumption is invalid, as do the conclusions presented in Guikema and Pate-Cornell (2005) that indicate that the probability of success associated with each launch increases with time and experience.

This research presents the first statistically valid method that accounts for this increase in vehicle reliability, while also drawing a connection between the probability that the vehicle will launch successfully (i.e., the observed success rate) and the reliability calculation for the vehicle (i.e., the designed success rate). This methodology is developed based on the assertions of Neyman, presented in Collani and Draeger (1999).

From this understanding of the current vehicle reliability levels, and how these levels will change throughout time, an approximation of the likely vehicle reliability for a conventional vehicle can be assessed as a function of time.

1.2.5 Tether rendezvous and handover

Assuming a successful launch, an unconventional launch system that incorporates an MMET must perform, at least, one successful orbital rendezvous. This could occur either when the MMET is fully extended, which is the basis for previous work by Cartmell and Ziegler; or when the system is fully retracted, which is the basis of Draper *et al.* (2004) and this research. However, rendezvous is not assured, as evident in the report of Berger (2005) on the 15 April 2005 failure of the Demonstration of Autonomous Rendezvous Technology (DART) mission.

The orbital dynamics of a rendezvous are clearly defined for systems that can be suitably modelled as a point mass, an understanding of such calculations achievable through examination of texts such as Thomson (1986). For missions like the one proposed in Cartmell *et al.* (2004), the payload must not only rendezvous with the initial MMET system, but must then be released and rendezvous with a second MMET. With an examination of the system orbital dynamics of both MMET systems, initial conditions can be determined that would produce a perfect handover, without outside interference.

Within the literature, Williams *et al.* (2005) presents a discussion of how to improve the probability of a successful handover by shifting the mass within the tether system so as to modify the system rotation. Similar to Cartmell *et al.* (2004), where optimum handovers are discussed alongside possible corrective actions that may be necessary in the presence of mission error, this work does not examine the probability of occurrence associated with likely errors, nor discuss the likelihood that the system will be able to correct such errors. Unlike investigations like Cartmell *et al.* (2004) and Williams *et al.* (2005) that focus on correcting errors in the tether-based systems, this research focuses on the equations needed to correct an improperly released payload, and offers a methodology from which the probability of failure for a known systemic error can be calculated. This methodology has not been previously presented for the MMET or other tether-based systems.

1.2.6 Orbital debris environment

While operational risks are inherent in any multi-component system, the orbital environment offers failure sources that may not be intuitively obvious. While first-order system concept investigations consider altitudes of greater than 100km to be part of a frictionless environment, Justus (1995) is just one of many sources that prove this characterisation is not sufficient for mission design and risk assessment.

There are currently tonnes of orbital debris fragments and disused rocket stages orbiting the earth. This man-made debris, combined with naturally occurring micrometeorites, present a dangerous environment where the significant relative velocities between orbiting objects result in frequent hypervelocity impacts. Understanding where these pieces of debris are most dense and most lethal to spacecraft as a result of hypervelocity impact has been a task originating in the 1960s with works like Cour-Palais (1969) and culminating in the recent publication of computer-based finite element models like ORDEM2000 and MASTER99, described in Liou *et al.* (2000) and Bendisch *et al.* (2000), respectively. For the purposes of this research, these models are considered the most sophisticated and accurate currently available to the public, with components built on the earlier modelling work such as that of Kessler *et al.* (1988) and Kessler *et al.* (1991).

The creation and validation of these models has been an extensive activity that is not addressed in this work. The research presented here assumes the models employed by the US National Aeronautics and Space Administration (NASA) and the European Space Agency (ESA) are sufficiently vetted and in agreement with published data. Of the multitude of work called on by these models is that presented in documents such as Goldstein (1998), Hörz *et al.* (1999), Kessler *et al.* (1970), Kessler *et al.* (1988), Krisko *et al.* (2000), Levine (1991), Levine (1992), Levine (1993), Schumus et al. (2000), Settecerri and Stansbery (1997), Settecerri *et al.* (1997), Settecerri *et al.* (1999), Stansbery *et al.* (1996), Stansbery *et al.* (1995), Stansbery *et al.* (1994), and Zhang and Kessler (1993). These documents discuss a range of data collection and processing topics ranging from initial collection techniques to the Long Duration Exposure Facility (LDEF) analysis and results, and the Haystack observations to the debris growth models for predicting how the environment changes over time.

When comparing the output of ORDEM96 and ORDEM2000, Liou *et al.* (2000) do not identify any significant differences in the calculated debris densities produced by both models over various inclinations and orbits. Although there will be a loss in fidelity as a result of the decreasing model complexity, the acceptability of the models presented in Tribble (2003) is assumed sufficient as there were no significant alterations made since the models presented in Tribble (1995), even with the introduction of new information, and the use of references by Tribble (1995) that were also employed during the creation of the methodology associated with ORDEM96. It is assumed within this research that comparisons between the output produced by the models presented in Tribble (2003) and the ORDEM2000 model outputs were conducted, and the differences were negligible within the context of the fidelity achievable via Tribble (2003). Considering the level of fidelity employed within Tribble (2003), it is assumed in this research that any model employing the equations presented in Tribble (2003) will produce a suitable engineering estimate of the orbital environment.

1.2.7 Spacecraft risk

The orbital environment poses significant risks to spacecraft, which have led to various examinations of operational systems, research into proposed systems, and design guidelines for mission planners. While the design guidelines may not be able to precisely model the effects identified in the historical studies, they are suitable engineering estimates that are accepted as sufficient analyses by practitioners.

Regarding historical studies, the Shuttle, the LDEF, MIR, and the Hubble space telescope have all made significant contributions to the collection and cataloguing of orbital environmental effects on spacecraft. Historical studies examining the observable effect of the orbital environment on an range of systems and missions are presented in the works of Christiansen *et al.* (1997), Bedingfield et al. (1996), Burt and Christiansen (2001), Christiansen (1998), Cour-Palais (1985), Graham *et al.* (2000), Hyde *et al.* (2000a), Hyde *et al.* (2000b), Kessler (1993), *Kuriki et al.* (1997), Levine (1991), Levine (1992), Levine (1993), Paul *et al.* (1997), and See *et al.* (1990).

With the benefit of a significant historical background, sophisticated research analyses have been performed on theoretical systems in an attempt to gain a high fidelity understanding of how certain systems react to specific environmental elements. Such research studies add to the understanding of the environmental effects on spacecraft in their ability to improve the understanding of acceptable analysis techniques. Examples of these research studies can be found in works such as Christiansen *et al.* (1992), Drolshagen (2002), Hyde *et al.* (2001), James *et al.* (1994), Tribble (1995), Tribble (2003), Kessler (1981), Kessler *et al.* (1996) McBride and McDonnell (1999), Schonberg and Yang (1993), Rex (1997), and Robinson (1999).

By examining the level of fidelity attainable in the context of the analytical cost required, an understanding of what is a reasonable level of analytical complexity can be determined. As has been proven by various analytical applications, the appropriate level of fidelity is often present in a range of design guides published by NASA. These guides include Cour-Palais (1969), Frost (1970), Kessler *et al.* (1972), Silverman (1995a), Silverman (1995b), NASA (1995), and Dooling and Finckenor (1999). As they have already been widely accepted and are currently promoted in

NASA guidance, this analysis of the MMET will assume the fidelity associated with NASA proposed design guidelines are sufficient for the analyses performed within this research.

As a result of the currently available design guidance, this work focuses on failures resulting from orbital debris and micrometeorite impacts onto tethers. The cross sectional area of the tether is modelled to decrease as a function of time based on atomic oxygen (AO) degradation, calling on the equations presented in Tribble (2003) to produce the analytical results of this orbital effect, equations that are consistent in scope and fidelity to those recommended by NASA. By maintaining this focus, the core issue under investigation is how a tether system will react to a hypervelocity impact, and how often such impacts are expected to occur.

1.2.8 Hypervelocity impact modelling

Hypervelocity impacts are typically considered those in which the speed of impact is greater than the speed of sound in both the target and impactor materials. Even thought the speed of sound in Aluminium is roughly 5.1km/sec, Tribble (2003) identifies a hypervelocity impact to be one where the impact speed is greater than 1km/sec, with impactor fracture and phase change occurring at impact velocities in excess of 2km/sec. As discussed in Davison *et al.* (1996), the highly localized damage around a hypervelocity impact location is caused by the greater rate of energy delivery relative to the rate at which each material is able to dissipate energy. This imbalance renders the material strength insignificant at the time of impact and causes an initial hydrodynamic flow of material near the impact location. This hydrodynamic phase causes hypervelocity impact craters to generally resemble a water splash in thick, ductile materials.

There are two main approaches to modelling hypervelocity impacts, one employing hydrocode techniques, and the other empirical in nature. Hydrocode modelling is a finite element approach that applies fluid dynamic concepts to solids. Because the energy imbalance resulting from a hypervelocity impact causes a hydrodynamic phase near the impact, hydrocode techniques must account for energy and momentum transfers and balancing within the impactor and target when both are transitioning

between solid and liquid states. An understanding of hydrocode modelling and other finite element techniques as they pertain to hypervelocity impacts can be gained through examination of documents such as Anderson (1987), Campbell and Vignjevic (1997), Collins (2002), Eftis *et al.* (2001), Fahrenthold and Horban (1999), Fahrenthold and Horban (2001), Fahrenthold and Koo (1997), Gerassimenko (2001), Hayhurst *et al.* (1995), Hiermaier *et al.* (1997), Pierazzo and Collins (2003).

Empirical modelling of hypervelocity impact effects is widely used by spacecraft mission analysts for assessing the probability of failure associated with a spacecraft. To construct empirical models, researchers rely on hypervelocity impact tests and examinations like those presented in Bernhard *et al.* (1995), Burchell and Grey (2001), Burchell and Whitehorn (2003), Burchell *et al.* (1999), Burt and Christiansen (2001), Christiansen *et al.* (1993), Cour-Palais (2001), Cour-Palais (1985), Dahl and Schultz (2001), Grey and Burchell (2004), Lamontage *et al.* (1999), Neish and Kibe (1997), Orphal (1999), Orphal and Anderson (1999), Orphal and Anderson (2001), Paul *et al.* (1997), Schonberg (1989), and Zukas and Gaskill (1996) to develop relationship concepts that can be reduced down to the kind of proposals presented in Baker (1995), Walker (2001), or Schonberg and Ebrahim (1999). Many of the relationships, such as penetration depth in a semi-infinite target being directly related to the impact velocity to the 2/3-power, are incorporated in the equations most widely employed by spacecraft analysts and presented in Cour-Palais (1969), Frost (1970), and Elfer (1996) and investigated by Hayashida and Robinson (1991).

Both modelling approaches rely on test data for calibration, so neither can be considered fundamentally more accurate, even though hydrocode modelling is significantly more complex and computationally costly.

1.2.9 Tensile strength of aramid fibres

The strength of aramid fibres, called by their trade names of Kevlar and Twaron, is dependent on strain rate. This dependence is identified in Teijin (2005a) for strain rates associated with Twaron rope applications. However, considerably more interest has been in testing aramid fibres for use in ballistic shields. As a result, the bulk of literature on aramid tensile testing, such as that conducted by Allen *et al.* (1992),

Benhoulo *et al.* (1997), and Wang and Xia (1999) focuses on significantly higher strain rates than those examined here.

While material strength is identified as a significant contributor to the empirical equations like the Rockwell equation presented in Hayashida and Robinson (1991) or the 1992C equation presented in Penson (2003), it is not clear that the tensile strength of a tether has a significant effect on the outcome of a hypervelocity impact, nor is such an idea supported by the discrepancy in results identified in this work and those of McBride and Taylor (1997).

1.2.10 Hypervelocity impact testing on tether fibres and ropes

The amount of hypervelocity impact test data for tether targets is quite small. Prior to this research, the literature contains tests as identified in Hayashida and Robinson (1993), Penson and Burchell (2003), Sabath and Paul (1997), McBride and Taylor (1997), and Van Noord and Robinson (2002). While all offer discussions of the tests performed and the damage observed, the works offer few conclusive results. Further, concepts or theories that may emerge from the literature cannot be proven without a more significant impact-testing regime than is conducted either in support of the cited literature or in support of this research.

When examining the results presented in Sabath and Paul (1997), it is identified that the lethal impactor diameter for a Kevlar target is greater than that of Spectra. When examining the results presented herein for Twaron against the results of McBride and Taylor (1997) for Spectra targets, this relationship that Kevlar is able to sustain damage from larger impacts is again supported. When examining the impact site presented in both McBride and Taylor (1997) and presented herein, there are indications that the molten stage evident in metallic impacts and identified herein is also present in tether impacts. This difference in susceptibility could be the product of the lower melting temperature associated with Spectra. Such a conclusion is intuitively reasonable and in agreement with commonly accepted concepts of hypervelocity impact failure mechanisms. However, there does not exist enough data within the literature, nor was enough data produced during the course of this research, to fully investigate such a theory.

1.2.11 Post-hypervelocity impact dispersion of impactors and ejecta

The secondary effects of a hypervelocity impact, whether it is the dispersion of lethal impactors borne of the shattered initial impactor or spallation from the backside of a semi-infinite plate, are well studies for perpendicular impacts down to highly oblique impacts. Such investigations are the basis for bumper plate design, as the concept of secondary lethality following impact with a flat plate is far from controversial. Within the literature, a significant discussion of this issue can be understood through examination of texts such as Stilp (1997), Gardner and Burchell (1997), Christiansen *et al.* (1992), Christiansen *et al.* (1993), Cour-Palais (1985), Frost (1970), Orphal (1999), Orphal and Anderson (2001), Schonberg (1989), and Schonberg and Ebrahim (1999).

Prior to this research, no work has been publicly released that characterises the secondary effects of a debris impact with a tether target. Conventional risk assessment approaches like Hoyt and Forward (1998) do not consider secondary effects, resulting in a one-impact-one-failure assumption that may be inappropriate if significant debris dispersion is likely. Within the literature cited above regarding secondary impactor dispersion, the angle of dispersion is stated to vary depending on the materials and conditions present at impact. While this dispersion angle is characterised by Gardner and Burchell (1997) to be around 10-degrees for oblique impacts between 50-degrees and 75-degrees, an investigation of Stilp (1997) clearly identifies that these angles are not always so restricted.

1.2.12 Tether impact risk

The current literature on tether failure does not maintain a careful distinction between the probability of impacting a tether, and the probability of failure. This is because most failure assessments are focused on hanging tethers, which remain oriented along the gravity gradient for the duration of their mission. This historical tendency to produce analytical solutions focussed on hanging tether systems is evident in NASA (1995), which purports to offer a suitable solution for assessing the probability that a space tether will fail during a mission.

Most tether analyses identify a threshold debris size, which is then considered the lethal impactor. After identifying what is a lethal impactor, the analysis seeks to characterize the debris flux associated with that debris size, and calculate the probability of failure from that, generally employing some form of the Poisson distribution. This is the fundamental theory employed in Gettins *et al.* (2004), Anselmo and Pardini (1999), and McBride and Taylor (1997). This approach is not suitable for the MMET because the system is not stationary relative to the gravity gradient. Because it is not stationary relative to the gravity gradient, the impact velocity relative to the local impact plane is not uniform. If the velocity is not uniform, then the system is not equally susceptible at all instants, thereby invalidating the assumption that a single debris size can be considered lethal at all times.

Patera (2002) offers an analytical approach for calculating the probability that a tether will collide with another satellite. While this analysis is consistence with Collision on Launch Analysis (COLA) approaches described in DOT (2002a-2002b) and the literature it references, such a technique is only of value when the trajectory of both objects is known. For this research, it is assumed that a suitable COLA has been completed throughout the expected lifetime associated with the tether.[i] Consequently, the significant contribution Patera (2002) makes to this analysis is the realization that the casualty area of the tether, which has a direct relationship with the probability of impact, includes the width of the impactor. While important, this is not unique to Patera (2002), as an equivalent assertion is also implied in the computational results presented in texts such as McBride and Taylor (1997).

As a side note, while it reports to be relevant to the discussion of tether failure analyses, the corporate restrictions that have obviously limited the kind of data that can be presented in Strumfels (2001) render the work of little benefit. Possibly interesting from the perspective of an independent data point, so little is revealed about the underlying methodology that the work does not offer any indication of how to repeat the results presented within.

This research independently investigates both the probability that the system will be impacted, followed by the probability that the impact would result in a failure. Once

the average rate of lethal impact is known for a particular mission, the level of redundancy built into the tether system will dictate the system lifetime.

1.2.13 Tether mission failure analyses

There have been numerous works published on the topic of tether system failure, but none have addressed the specific issues relevant to a MMET system, the fact that one impact may result in more than one failure, and the presentation of analysis techniques that can be repeatedly applied, within an analytical environment that employs commonly accepted orbital debris models. For example, even though Anselmo and Pardini (2005) employ accepted debris models and a redundancy approach that is mathematically logical, the use of non-dimensional constants that "cannot be easily estimated" and a reliance on general approximations for determining acceptable failure conditions would make the results difficult to replicate from their fundamental origin.

Similar arguments regarding repeatability can be supported after examination of work like that of Forward and Hoyt (1995) and Hoyt and Forward (1998). In Hoyt and Forward (1998), the analysis uses metrics that do not directly relate to conventional metrics, even though the system could be described in such terms, as it is in this research. In addition to these unique metrics, the issue of multiple failures per impact is ignored, as with Anselmo and Pardini (2005). As demonstrated later, this condition of multiple failures per impact could have a significant effect on the failure calculations presented in Hoyt and Forward (1998) and Forward and Hoyt (2005).

Disregarding issues of analytical repeatability, both the aforementioned analyses and those of Van Der Heide and Kruijff (2001) and Van Noord and Sturmfels (2001) all rely on the assumption that a tether system can be assessed by assuming a specific debris impactor is lethal at all times, and that each impact will only result in one failure. So long as these assumptions are present, the resulting analyses will not be applicable to all MMET systems or missions.

A final failure investigation examined by this work is that of Chobotov (1999) which addresses the issue of tether on tether collisions. It is assumed within this research

that mission planning will prevent such a failure mode through the mission design process.

1.3 Lunar Staged MMET (LSM) mission: definition and overview

The *LSM mission*, as it is refereed to herein, is a two-stage Earth-to-moon mission proposed in Cartmell *et al.* (2004) at the Russian Academy of Sciences 2004 Summer School in St. Petersburg. The LSM mission employs two MMET systems, the centre of one located on a low earth orbit (LEO) and the other on an elliptical earth orbit. As presented, the orbital, operational, and system parameters for the LEO and EEO systems are as follows:

Table 1 Orbital, operational, and system parameters for the LSM mission.

	LEO system	EEO system
Orbital parameters		
Perigee Altitude (Ht_P)	350 km	632 km
Eccentricity (e)	0.152	0.732
Operational parameters		
Angular velocity at centre (ω_{op})	-4. 37E-3 rad/sec	1.07E-2 rad/sec
System parameters		
Propulsive sub-span length (L)	200 km	75 km

For the LEO system, the negative angular velocity at the central facility indicates that it is rotating in a retrograde manner. This retrograde rotation is required so that the linear velocity vector of the LEO system tip, relative to the Earth, is identical to that of the receiving EEO system tip. As presented in Cartmell *et al.* (2004), the LEO system is not changing the payload altitude by imparting a significant in crease in tangential velocity; it is, effectively, lifting the system from a lower orbit and handing it to the EEO system. After the payload is received by the EEO system, the system rotation imparts a significant tangential velocity to the payload at release that places

the payload onto an appropriate trajectory for rendezvous with the moon. The stages associated with the LSM mission are graphically presented in Fig 1.

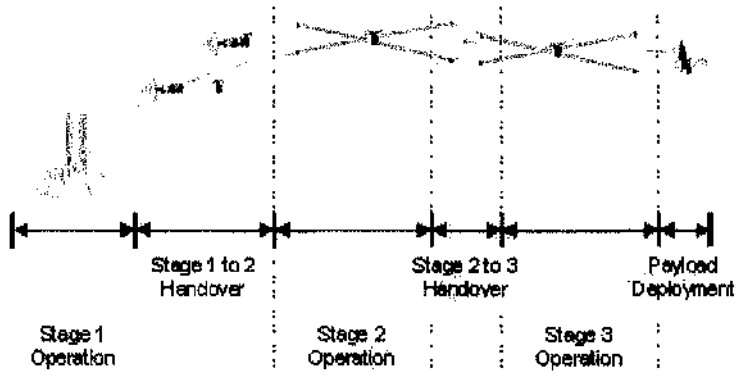

Figure 1 Operational overview of the LSM mission.

This work examines the LSM mission only from the perspective of primary failures.[ii] A failed handover is discussed in Cartmell *et al.* (2004) with a discussion as to how the payload would be recovered.[iii] The research presented in this thesis assumes that, if the LEO and EEO systems are out of synchronisation such that a handover failure is possible, retrieval as discussed is not sufficiently feasible.

The principles and techniques presented in this work will be illustrated using the LSM mission. This work will finish by determining if it is feasible for the LSM mission to be completed using a two-stage tether-based on-orbit launch system, or whether employing a single conventional launch system is more appropriate.

Chapter 2

Selection Criteria

When presented with a wide range of launch system options for use in the commercial market, mission planners must employ a consistent, economically sound selection criterion. This Chapter discusses the factors and events that led to the growth of the commercial space launch industry, the economic theories this work assumes are valid when modelling the commercial market, and a selection criterion that is valid within such economic models.

2.0 The commercial space transportation market

The commercialisation of space activities in the United States began in 1962 with passage of the Communications Satellite Act, codified as Public Law (P.L.) 87-624. Passage of this law enabled private sector organizations to engage in the commercial communications satellite business. Since passage, according to Smith (2005b), "commercial communications satellites have been chiefly a private sector activity." While the business of satellite communications was becoming commercial, US companies could only secure launch services from the US government.

The recent emergence of a commercial launch market began around the time that the European Space Agency-developed (ESA) Ariane vehicle made its first flight in 1979, and began operational launches in 1982 according Smith (2005a). While its first eight launches delivered government payloads, the 1980s saw the emergence of an international commercial launch market. With regards to the US, deregulation of the commercial space launch industry began on 16 May 1983 with the issuance of the National Security Decision Directive No. 94. To further promote commercialisation of the space launch industry, the Reagan administration placed authority for the regulation of commercial space activities with the US Department of Transportation (DOT) on 24 February 1984 with Executive Order 12465 (49 FR 7211); provided the space sector with various tax incentives and benefits on 20 July 1984 through the National Policy on the Commercial Use of Space (White House 1984); and simplified launch licensing procedures with the Commercial Space Launch Act of 1984 (P.L. 98-

575, 49 USC 2601-2603). Amid this flurry of activity, new companies began to enter the US commercial space transportation industry, as did Arianespace.

According to a number of sources, including Krige (1999), Hermida (1997), Gabler (1992), Smith (2005a), and Smith (2005b), while the Reagan administration was promoting commercialisation of the expendable launch vehicle (ELV) market during the early 1980s, it was also supporting a protectionist policy with regards to the Shuttle by pricing its commercial launch services at levels well below their commercial value. To grow its market share around the world and the US, Krige (1999) and Tully (1985) report that Arianespace began to systematically price its launch services below those of the Shuttle. While the pricing of the Shuttle for commercial payloads was preventing US commercial space launch suppliers from entering the market, Arianespace launched its first commercial satellite for a US customer on 23 May 1984. Two days later, Transpace Carriers Inc (TCI) of Greenbelt, Maryland, USA, filed a petition of unfair practices against Arianespace and its consortium of 11 backing governments with the Office of the US Trade Representative. According to Smith (2005a) and Krige (1999), it was claimed that the European governments were unfairly subsidising Arianespace.

After an investigation of the complaint by TCI, Smith (2005a) noted that all governmental parties agreed the financial assistance provided to Arianespace by ESA and its member countries was not any greater than that provided to the Shuttle. At the same time the Office of the US Trade Representative was engaged in an investigation launched by the TCI petition highlighting the impact of government subsidies on free trade in the commercial space transportation industry, Krige (1999) notes that the Reagan administration was in the process of approving the Phase III pricing policies that would set the fiscal year 1988-1991 prices for commercial launches on the Shuttle. After receiving urging from NASA Administrator James Beggs, claiming that the Shuttle was a "national asset" that would "not be able to compete effectively with the European Ariane launch vehicle," Krige (1999) reports that Reagan approved a pricing of the Shuttle that would continue to undercut US ELV suppliers. With the US and the involved European governments agreeing to future discussions on commercial launch vehicle pricing practices, the TCI action produced neither an

immediate nor a long-term resolution. As reported by Smith (2005a) and Krige (1999), talks on the entry of non-market economies into the commercial space industry were agreed to in 1990, but only a single talk on the subject was held in 1991.

For TCI, which held the right to purchase Delta II vehicles for commercial applications, its petition does not appear to have produced the intended outcome. While its petition did cause both the US and the involved European states to admit that both offered financial assistance for the Shuttle and Ariane vehicles, respectively, the talks did not end these subsidies. Consequently, the competitive disadvantage impeding commercial suppliers like TCI from entering the launch services industry had not diminished. However, the failure of Challenger on 28 January 1986 shifted policy in favour of a more competitive commercial launch market.

In its infancy, Hermida (1997) identifies the full allocation of risk to the commercial launch service suppliers, combined with early Ariane and Shuttle-launched kick-motor failures reported by Tully (1985), as a driving factor for producing insurance costs that made ELV suppliers uncompetitive when compared to the Shuttle. While the exact cause is unknown, it is likely that both the Challenger accident and the AIAA lobbying effort reported in Hermida (1997) had significant roles in the policy and legal shifts that helped increase commercial launch activity through the 1990s.

In the wake of the Challenger failure, Hermida (1997) highlights that the Reagan administration "prescribed that the Space Shuttle would only be used for those payloads which require the unique characteristics of the NASA Space Transportation System." In effect, this removed the Shuttle from the commercial market. In so doing, a significant entry barrier was removed for commercial launch service suppliers.

While the exit of the Shuttle from the commercial market removed subsidised competition from the US government, commercial launch service providers remained fully liable for the risk associated with their operations until 1988. In 1988, by amending the Commercial Space Launch Act, the DOT was authorized to administer

a risk allocation scheme similar both to that proposed by the AIAA proposal cited in Hermida (1997) and to the system employed by NASA for its Shuttle program. As codified in the DOT regulations contained in Part 14 of the US Code of Federal Regulations, Chapter III, so long as the licensed commercial launch operator is in possession of a reasonably priced level of insurance greater than or equal to that required by the DOT for a specific launch, the US government will indemnify up to $1.5 billion worth of third-party damage in excess of that covered by the required insurance. The US Congress extended this indemnification in 2004 for a further 5 years by passing P.L. 108-428. By extending this indemnification mechanism, as argued in DOT (2002c), the DOT believes such measures ensure US commercial launch service suppliers remain capable of competing in the world market.

The changes implemented through the 1980s have produced an environment where non-government launch service providers are sourcing vehicles designed for the commercial market. This increase and change in the types of customers purchasing hardware and services from launch vehicle manufacturers has produced modified variants designed for the commercial market such as the Titan II; vehicles that are made of surplus government components such as the Taurus; and new variants and families specifically designed for the commercial market such as Pegasus, Delta 3, and Falcon. In this politically described "free market" environment of decreasing regulation, manufacturers are competing to design better, lower cost vehicles in an attempt to cater to commercial customers.

In the midst of the current and projected success in the late 1990s, the US Air Force attempted to make its EELV program a flagships for the possibilities of the commercial space launch market. Smith (2005a) identifies the beginning of the EELV program as a $30 million appropriation in 1995, with a goal to reduce launch costs by 25%. Lockheed and McDonnell Douglas were awarded development contracts worth $60 million each in 1996. As a side note, McDonnell Douglas merged with Boeing in 1997, with Boeing now listed as the operator for the Delta IV EELV program, while current Delta II launch licenses with the FAA are still held by McDonnell Douglas. In an attempt to take advantage of the cost saving projected via the commercial market, the US Air Force stated its intentions to interact with the

EELV program as a commercial customer. To this end, instead of having the two EELV projects compete with the loser being down-selected, the US Air Force would offer minimal research and development funding to each, with all further development costs being recouped via future commercial sales. In 1998, both Boeing and Lockheed were each issued $500 million in research and development funding and received US Air Force orders of 19 launches for $1.38 billion and nine launches for $650 million, respectively, according to Smith (2005a). It is further reported in Smith (2005a) that this research accounted for approximately 20% of the Delta IV development costs.

With the collapse of the commercial launch market around the turn of the century, the original, commercial sales-based agreements reached between the US Air Force and the manufacturers became untenable. To this end, Wade (2006) reports that the launch price for each EELV vehicle was raised to $138 million in November 2004, Lockheed was allowed out of its contract agreements at Vandenberg, and the program violation of "Nunn-McCurdy" spending restrictions saw the US Air Force certify that further funding of the EELV program is essential for US national security. Smith (2005a) notes that this certification was given in agreement with the DOD "assured access" to space policy, a policy codified in P.L. 108-136. Even with the anti-trust issues concerning Boeing that publicly emerged in 2003, and House Report (H.Rept.) 108-553 that questioned the need for two EELV programs, the Bush administration space transportation policy issued in December 2004 is reported by Smith (2005a) to support both programs. In support of the assured access policy, the 24 satellite launches that were to be competed for between Boeing and Lockheed were awarded evenly to the two companies.

It is currently unclear how the EELV program will be considered in terms of the commercial space industry. Currently, the outcome of a Space Exploration Technologies Corporation protest filed on 15 August 2005 and reported in BNA (2005b) regarding this non-competed award is unknown. Additionally, Lockheed and Boeing are currently planning to merge their respective EELV operations into a joint venture called United Launch Alliance (ULA), reported in sources such as Smith (2005a) and BNA (2005a), to save the programs considerable costs. While it is clear

that the US Air Force, Boeing, and Lockheed Martin are not acting in an economically independent manner with regards to the EELV program, such an example does not discount the choice mechanisms governing private sector launch service suppliers and customers. With Boeing publicly retreating from the commercial sector, even though Smith (2005a) further states that it may reconsider this decision, it is clear that the commercial launch market is capable of forcing out historically dominant organizations if they are not commercially viable, offering support for the theory that commercial operations are economically independent.

For the purposes of this work, the commercial space launch market includes all activities carried out under a license issued by the US Department of Transportation. Within this market, it is assumed that all launch vehicle suppliers and customers are acting in accordance with traditional Theory of the Firm and the Theory of Markets as discussed in Pass and Lowes (1992).

2.1 Modelling the commercial launch market

Within the Theory of Markets, it is important to understand which construct best models an examined industry so as to better understand how decisions taken by one participant are likely to affect the market. While the traditional Theory of the Firm states that all participants seek profit maximisation and price is adjusted to find equilibrium between supply and demand, knowing which model is appropriate for a certain market will allow analysts to predict how the market share of each participant will change as price changes, based on the supply and demand characteristics within the market.

2.1.1 Previous work

After examining the commercial space transportation industry during its emergence, Gabler (1992) assumes that the market could be modelled as a non-collusive oligopoly. This conclusion is reached by examining the number of participants in the market, product variability, cost of entry for new participants, stability of publicly available prices, and the prevalence of price wars.

With regards to the number of participants, Gabler (1992) mentions three launch service suppliers within the US, with four further organizations attributed to Europe, China, the former Soviet Union, and Japan, which are not examined here because of concern for data accuracy and the interpretation of a commercial launch within these countries. Within the US, the three launch service suppliers mentioned are General Dynamics Commercial Launch Services, McDonnell Douglas Commercial Delta, and Martin Marietta Commercial Titan. Orbital Sciences is briefly mentioned with regards to its first Pegasus launch, but is not considered a launch service supplier for the purposes of Gabler (1992). With regards to commercial customers for medium to large launch services, Gabler (1992) states that there were no more than 50 in existence at that time.

While Gabler (1992) discusses commercial suppliers and commercial customers, national governments are also discussed as participants in the commercial launch market. While national governments may have been the most significant customer for most suppliers at the time of Gabler (1992), it is questionable whether including national governments as true commercial customers is valid. For example, the level of oversight provided by a government for a mission launched on a commercial vehicle is far more stringent than that provided by a commercial customer. As discussed in Krige (1999), national governments traditionally rely heavily on oversight to ensure mission success. In contrast, commercial customers ensure mission success through economic means such as those discussed in Gabler (1992), where the market price is discounted for a less reliable vehicle. Gabler (1992) also mentions that governments are often restricted from choosing international launch service suppliers as a result of national policies. For these reasons, it does not seem reasonable to consider launches conducted on behalf of national governments as commercial launches. However, as the amount of data analysis is minimal in Gabler (1992), his inclusion of national governments has no practical effect. With or without national governments, the number of suppliers is still quite small in terms of the number of customers, which is the first requirement for an oligopoly stated in Pass and Lowes (1993).

Even with only seven suppliers worldwide, Gabler (1992) identifies 20 vehicles that are available through the commercial market. This high number of vehicles relative to the number of suppliers supports the concept of differentiated products discussed by Pass and Lowes (1993). In context, it must be understood that the first commercial launch conducted by a US supplier occurred in August of 1989. In three years, the commercial launch market expanded to include the 20 vehicles identified by Gabler (1992) with only 22 total launches occurring under DOT license by the end of 1992. While there are significant environmental concerns that must be accounted for when selecting a launch vehicle, it could be argued that the commercial launch industry did not need so many options. If it is true that the number of different variants is higher than that required by the industry, the commercial space transportation industry is likely to share a trait of many oligopolies where product differentiation is driven by advertising and marketing.

Such a situation is highlighted by the differences between McDonnell Douglas and General Dynamics. By the end of 1992, McDonnell Douglas had launched 13 Delta II vehicles under DOT license and General Dynamics had launched six Atlas vehicles. While the fairing size and solid rocket motor quantity and orientation vary, Delta II variants are often considered sufficiently similar to be grouped into a single failure analysis as is done in Gabler (1992). While the validity of such a grouping is often questioned from a reliability standpoint, the fact that it is grouped together in Gabler (1992) offers an indication that the advertising and marketing of the Delta II vehicle focuses on the long-term success and flexibility of the vehicle. At the same time, Gabler (1992) identifies four different Atlas variants available to the commercial market. As a counter to the likely Delta II marketing approach, the number of variants indicates the 'imaginary' differences discussed in Pass and Lowes (1993).

The cost of entry for new suppliers is discussed in conceptual terms within Gabler (1992). In 1992, all of the vehicles discussed in Gabler (1992) were derived from previously developed core technology. The only organization that was not relying on current core technology for its research and development was Orbital Sciences. While it is likely it was only able to secure its funding as a result of a contractual agreement with NASA, which appears to have culminated in a $35 million contract in

1986 for the transfer orbit stage (TOS) vehicle, $50 million in research and development funding for the project was secured from private investors between 1984 and 1985, according to Orbital (2005). In 2005, this amount would be equivalent to $84 million using the Price Producer Index for aerospace products and parts manufacturing. In addition to organizational start-up costs, such a financial burden could be considered a significant barrier to entry. However, what is not mentioned in Gabler (1992) is the lower cost of entry approach taken by Transpace Carriers, Inc., (TCI) in 1984. By being a distributor of launch services through its agreement with McDonnell Douglas, TCI entered the commercial launch market without the significant research and development costs experienced by Orbital Sciences. However, as evident by the current existence of Orbital Sciences, it is debatable as to whether the method in which TCI entered the market could be considered equivalent to the methods used by the other organizations listed as suppliers in Gabler (1992).

With regards to price stability, or *price stickiness*, Gabler (1992) makes reference to the fact that the publicly stated prices are stable, yet does not offer a significant history to prove their stability over time. As previously stated, this is likely to be due to the fact that the commercial market was still in its infancy in 1992. However, Gabler (1992) does offer reference as to the origin of the commonly accepted prices. Gabler (1992) identifies that the price per launch for the Atlas and Delta families of vehicles in 1992 is very similar to the price per launch estimated for government flights of the same vehicle. This similarity offers an indication that the prices charged for government launches may be a likely source for the publicly stated prices presented to commercial customers.

While Pass and Lowes (1993) identify that participants are likely to avoid price wars because of the market share relationships explained using the kinked-demand curve, Geroski *et al.* (1985), Porter (1985), Friedman (1983), Fellner (1949), and Eichner (1976), indicate that a desire to avoid price wars does not actually prevent price wars. In the commercial market, Gabler (1992) employs the example of ArabSat 1C as a publicly disclosed price war occurring in the late 1980s. In this competition, a service that was anticipated to sell for $45 million was devalued by bids of $35 million and $25 mission from European and Chinese officials, respectively. The eventual contract

was awarded to the Europeans, although the reasons for such selection are unclear, as is the cause of the price war. It is theorised by Gabler (1992) that the Chinese "cheated" the market equilibrium, as it is termed in Geroski *et al.* (1985) and others, for which the Europeans demonstrated that competing with prices below equilibrium would not be accepted by the industry.

While the level of data analysis presented in Gabler (1992) offers indications that the non-collusive oligopoly was a suitable model for the commercial space transportation industry at the time of its emergence, such conclusions are not based on how the financial state of each company reacts to changes in the market. In an effort to determine whether the financial implications expected for an organisation operating within an oligopoly exist in the current commercial launch market, this research examined the financial data presented by the Boeing Company in the context of the launch rate reported by the FAA within the commercial market.

2.1.2 Examining Boeing market share

Boeing Corporation presents the most complete financial data set of all the current commercial launch participants. In its quarterly and annual reports, Boeing breaks its revenues and earnings into various segments, within which launch services are identified. This work compiled all reports for which the revenue and earnings could be partially attributed to a commercial launch. From an investigation of quarterly reports, the quarterly earnings as a percentage of revenue are presented in Fig 2.1.

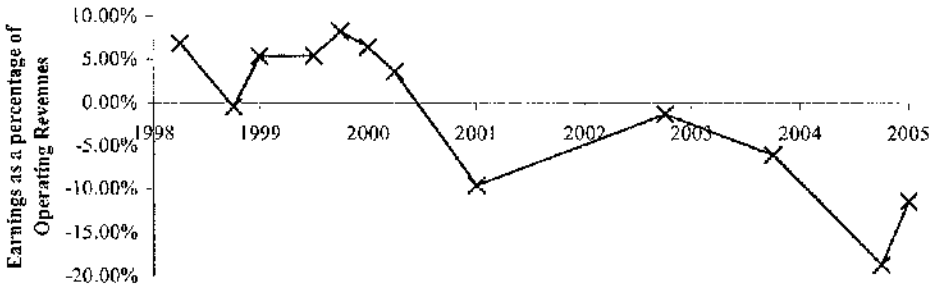

Figure 2.1 Boeing Commercial Launch Service earnings as a percentage of operating revenue for all quarters during which the revenue for a launch operation was presented.

It is useful to examine Fig 2.1 both in the context of important events at Boeing, and in the context of the launch market, described in terms of launches per quarter in Fig 2.2. With regards to events at Boeing, the first Delta III failure occurred on 27 August 1998, the second on 5 May 1999. Because the revenues associated with a particular launch cannot be directly related to a particular event, Fig 2.1 only indicates that these failures may have attributed to the drop in earnings observed in the later quarters of 1998. While the drop in earnings around 2000 likely results from the combined events of EELV development at a time of market cooling, the drop in earnings around 2003 is likely to have been driven by the legal action and launch reassignments taken by the USAF identified in sources such as Decker (2004), Smith (2005a), Smith (2005b), and Holtz-Eakin (2003). Such activities led to Boeing announcing it would pull its Delta IV out of the commercial market.

Not only are events at Boeing important to consider when examining the company earnings, Boeing market share must also be understood in the context of the world launch market. With regards to the international commercial market as a whole, there was a significant spike in activity between 1997 and 2000, which is mirrored in Fig 2.1. After the second quarter of 2001, there is a large jump in the launch rate that is driven by non-US commercial launches. This trend of non-US commercial launches driving the launch rate generally continues to the present time. Following the turn of the century and into the present day, launch capacity has actually increased with the introduction of new vehicles and families. This increase in supply and identified

decrease in number of launches indicates that the industry is again at significant levels of overcapacity, and indication that is supported by works such as DOT (2001a – 2006) or Smith (2005b)

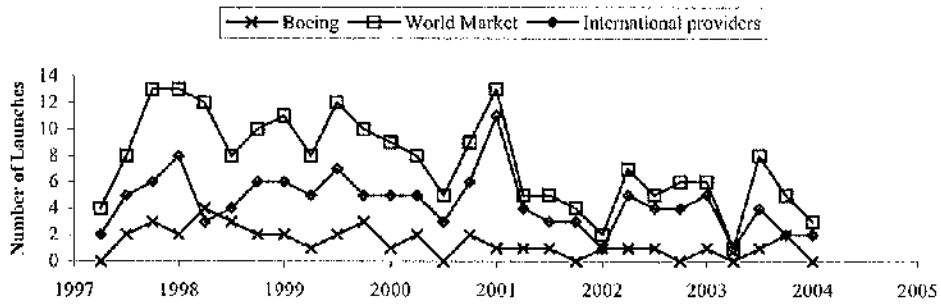

Figure 2.2 Number of launches conducted by Boeing each quarter and the corresponding number of launches occurring within the entire world commercial launch market.

Figure 2.3 presents the market share and change in market share for vehicles attributed to Boeing, symmetrically smoothed over five months. While there does appear to be a decreasing trend over time, the average change in world market share between 1997 and 2004 is zero with a standard deviation of 20%. The average market share over this time period is 18% with a standard deviation of 13%. Further, the correlation between world market share and earnings is –0.05.

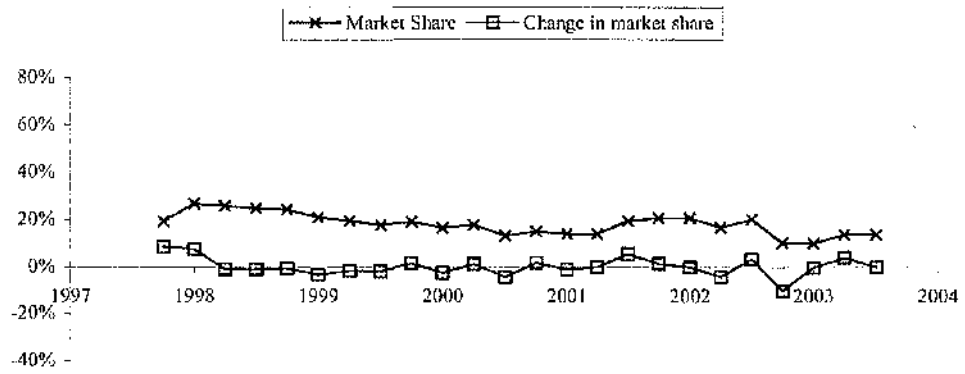

Figure 2.3 Boeing world market share and change in World market share, symmetrically smoothed over five financial quarters.

Similar results are obtained when examining the Boeing market share relative to the US market. Because the US market is only 40% of the international market, on average over the time period, the Boeing market share relative to the US commercial launch industry is significantly more volatile. Even with this volatility, the average percentage change in US market share over the examined time period is again zero, but with a standard deviation of 55%. The average US market share is 48% with a standard deviation of 32%. The correlation between the US market share and Boeing earnings is –0.03.

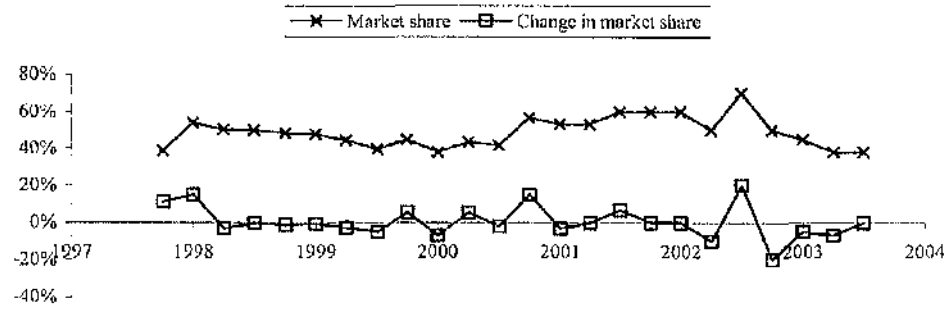

Figure 2.4 Boeing US market share and change in US market share, symmetrically smoothed over five financial quarters.

Between 1997 and 2004, the commercial launch industry experienced a significant rise up until around mid-2000 before experiencing a steady decline. Because there are two distinct market models within the time period, the average market share relative to the world and the US market during this decline may be of note. Over this period, Boeing market share exhibited an average annual change of –2% with a standard deviation of 26% relative to the world market and –4% with a standard deviation of 70% relative to the US market. The correlations between market share and earnings for these two reference markets are –0.15 and –0.22, respectively.

When examining these relationships it is important to note that the launches attributed to Boeing include both Delta vehicles and the Zenit 3SL by Sea Launch. Sea Launch is an international joint venture owned by Boeing and Energia. Sea Launch is included in the Boeing history because it is contributing to Boeing profits and it is assumed neither would directly compete with the other.

2.1.3 Boeing as support for the oligopoly model

As previously discussed, if the commercial launch industry can be appropriately modelled as a non-collusive oligopoly, the number of launch service suppliers would be small so that the pricing of one participant would affect the market price, the barriers to entry are high, the change in price would tend to be minimal over time, and organisations would accept a decrease in profits in order to maintain market share. Indicators of these characteristics are observed through an examination of the Boeing financial data and market share history.

With regards to the number of participants, the average market share between 1998 and 2004 captured by Boeing is 15% relative to the world market and 47% relative to the US market. With such influence, it is likely that the price adjustments Boeing makes would have significant implications for the other participants in the market. Therefore, the first condition of whether the market can be modelled as an oligopoly appears to be met.

The cost of research and development has not decreased in significance since Orbital Sciences entered the industry. As stated in Smith (2005b) and Krige (2003), Boeing

is reported to have written-off $2 billion in development costs for the Delta IV. In addition to hefty research and development costs, P.L. 108-136 and its codifying of the assured access to space policy focused on the two EELV variants has hampered the ability of independent companies to win long-term government contracts. Such an issue is currently being debated in response to SpaceX filing a legal action against the USAF that is discussed in BNA (2005b) for awarding twenty launches evenly between the two EELV variants without a public competition. All of these factors indicate significant barriers to market entry.

By examining Boeing earnings in the context of market share, the data indicates that suppliers will decrease their price in an effort to maintain market share. While there was a small average decrease in market share during the current market downturn, the correlation between market share and earnings demonstrates an effective independence between the two. What is interesting to note is that this desire to maintain market share is not coming as a result of a traditional price war, in which Friedman (1983) asserts that the origins either lie in a desire to (i) attack a participant who has attempted to cheat the other participants in the market or (ii) to drive a participant out of the market. In this case, prices are being cut in response to overcapacity.

However, while a conventional price war ends when each losing participant leaves the market, market forces do not wholly govern the commercial launch industry. Because access to space is a policy adopted by the US, and because the other countries whose citizens are participants in the market as identified by the subsidies to Arianespace cited in the complaint by TCI, it is unlikely that traditional launch manufacturers, who are also currently operating as launch service suppliers, will ever be forced out of the market. While Smith (2005b) mentions the Boeing claim and supposed reassessment of its desire to remove the Delta IV from commercial competition, it is expected that a launch service supplier will continue to compete, even in the face of significant financial losses, because the probability of government support is high.

If such theories regarding strategic dependence on government support are valid, the oligopoly construct may not be a suitable model. Further, if the price stickiness

observed in Gabler (1992) and identified in the next chapter accurately represents the actual pricing employed by commercial launch suppliers, it is unlikely that the current price decreases that would result in the severe decrease in earning during the market downturn would be expected. In an attempt to remain in an environment where demand is rapidly shrinking and supply is increasing, the market price for launch services is likely to drop much more quickly than that identified in DOT figures or projections.

The largest inhibitor to clearly assessing the validity of the oligopoly model is the lack of clarity with regards to industry data. Uncertainty, as it pertains to the oligopoly, is discussed in Geroski *et al.* (1985). While the nature of the launch industry and the operational constraints associated with a series of launches cannot be overlooked, the volatility associated with the Boeing market share between 2000 and the present day could be examined relative to an oligopoly model with imperfect information.

2.2 Cash flow overview for the launch industry

While the monies and accounting practices associated with the commercial launch industry are large and complex, the basic cash flow associated with it is no different to that of any other transaction. It must be noted that, while the commercial space transportation industry includes space tourism, this work only considers orbital missions designed to deliver payloads onto either an Earth orbit or an escape trajectory. Payload delivery remains the bulk of commercial space launch business according to documents produced by the DOT. As the MMET system is intended for payload delivery, and may not yet be shown to be capable of achieving many of the stringent environmental requirements associated with human passengers, its feasibility will be assessed relative to the economic forces governing those commercial participants when purchasing and supplying payload delivery services.

Most commercial space launch operations begin because an organisation requires a commercial capability attainable through the use of a unique space-based asset. For an agreed price, the end customer pays a launch services provider to deliver this

capability. For its services, the launch service supplier retains a portion of the price as profit. The cash flow associated with these transactions is presented in Fig 2.5.

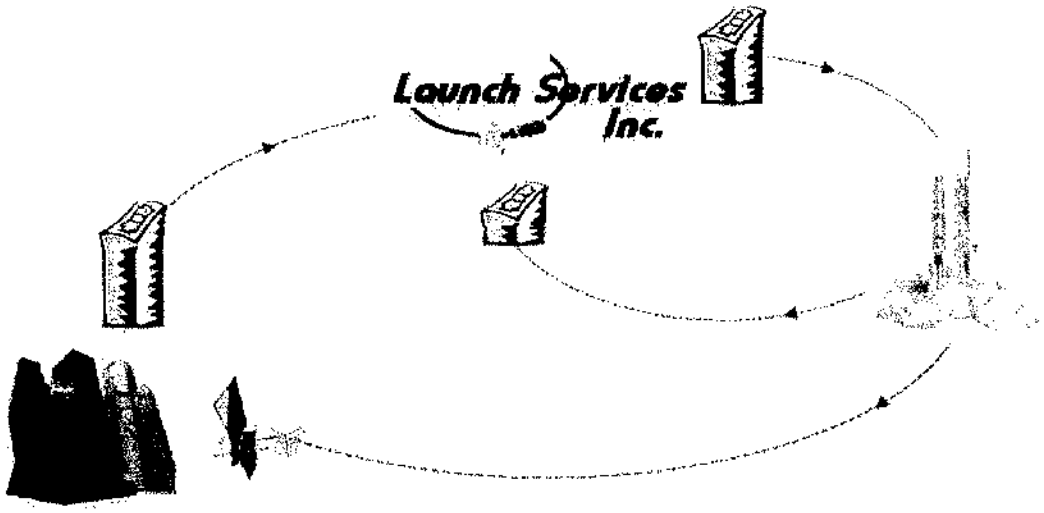

Figure 2.5 Illustration of the commercial space launch industry cash flow. The end customer (bottom left) pays a launch services supplier (top) to place a payload into orbit. Of the monies paid by the end customer, a portion pay for the launch (right) and a portion are retained as profit. The launch delivers the payload to its intended orbit for the end customer.

As a result of the Commercial Space Launch Act Amendments of 1988, Federal regulations (14 CFR, Chapter 3) require all parties to a US launch must agree to cross-waivers that absolve all participants from liability in the event of a failure. Further, as discussed by Holtz-Eakin (2003), there are indications that launch providers are moving away from re-flight provisions. In the early years of the commercial launch industry, Gabler (1992) comments that customers often purchased assurances from the vehicle supplier so that, in the event of a failure, the costs associated with a follow-on flight would be less significant. Such cost reductions could be as straightforward as a reduced price for the manufacture and launch of a second vehicle, or an indirect reduction in cost such as launch priority. In the case of launch priority, whereby the re-flight would have priority over other orders that the supplier is committed to completing, the adverse cost of the failure is reduced because the length of time that the end customer is without its asset is less than it would have been

without the re-flight provisions. While contract terms for commercial launches are not publicly available, the discussion in Holtz-Eakin (2003), combined with the customer history associated with the Delta 3 vehicle on its second and third launch attempts, does offer indications that the increases in reliability seen throughout the launch vehicle market is decreasing the likelihood that customers are requiring or purchasing re-flight provisions.

Another change in commercial space industry practice is with regards to ownership. While the more traditional concept of space-based assets sees them purchased and owned by the end user, as is the case with XM Radio, organizations are beginning to move towards a service-oriented purchasing approach. In the same way the US Navy and Air Force are entering into agreements like those discussed in Holtz-Eakin (2003) where the government does not own the asset that is being launched, commercial customers are often purchasing exclusive use of the service provided by the satellite while another company retains ownership of the satellite. Such agreements were identified in the controversy reported by journalists such as Young (2001), Patsuris (2001) and Figler (2001) when Los Angeles County attempted to tax Hughes satellites as movable property owned by Hughes Electronics, even though the satellites were producing revenue for the legally separate, but wholly owned, entity called DirectTV. Hughes Electronics was formed in 1985 as a wholly owned subsidiary of General Motors (GM) when it purchased the Hughes Aircraft Company from the Howard Hughes Medical Institute. Since then, the satellite manufacturing operations were sold to Boeing in 2000, and the company was split from GM in 2003, allowing News Corporation to purchase over one-third of the company. The kinds of acquisitions, sales, mergers, and property ownership agreements prevalent in the commercial launch and space services industry require case-by-case analysis for most commercial launch transactions.

While the case-by-case complexity associated with a commercial launch agreement may be significant, there is no indication that the fundamental relationships identified in Fig 2.1 are invalid. This work assumes the validity of such a cash flow relationship between the generalised participants, regardless of the specific interactions and legal boundaries relating each.

2.3 Perspective: on a mission for the generalised end customer

It is assumed that the generalised commercial space launch industry is made up of end customers and launch service suppliers. Furthermore, as will be discussed later, it is assumed that the end customer has a right to choose any supplier. Therefore, for a system employed by a supplier to be deemed economically feasible, it must present a competitive advantage that would cause the customer to choose it.

As previously discussed, an individual or organization becomes an end customer within the commercial space launch industry when a capability it is seeking would only become available after the launch of a space-based asset. The end customer could take a number of organization shapes, and the product could be sold using a wide range of accounting devices, but the functionality of the agreement must remain; a payload must be functionally delivered. Therefore, no concern is given to the type of asset, the ownership of the asset, or the relationship between end customer, launch supplier, and system manufacturer.

2.4 Choice: presenting the options and the selection criteria

As it is assumed previously that all customers and suppliers are acting in accordance with traditional Theory of the Firm and the Theory of Markets as discussed in Pass and Lowes (1992), it will be further assumed that such theories also govern the choices of the generalised end user and supplier. While the Theory of Markets assumes the actions of participants are constrained by the market construct, the traditional Theory of the Firm enables an assumption that the participants are motivated by profit maximisation.

It is a fundamental principle in economics to assume that a rational person, when presented with a choice between multiple options, will choose the option with the greatest worth. While worth could be expressed in terms of any quality, economics has a tendency to make choices based on monetary approximations of worth. By projecting the worth of each option into the same time, a rational person will choose the option with the greatest monetary value.

When projecting each option into the present, there may be significant levels of uncertainty associated with the worth of an option. In such cases, it is standard to examine the distribution of probable outcomes for each option multiplied by the corresponding probability distribution. The mean value of the resulting distribution is considered to be the *expected worth*. While a comparison of the expected worth for each option may be best examined in the context of the variance associated with each, it is commonly accepted that the expected worth is suitable for decision making purposes.

Since it is assumed that all participants in the commercial space industry are attempting to maximize profit, it is assumed that a rational participant, when faced with a choice involving many options, will choose the option with the greatest expected profit. As discussed later, the price of a product fluctuates within the constraints of its market so that the demand for the product, based on its price, equals the supply. Therefore, suppliers are incapable of independently pursuing profit maximization through price adjustments. Since the market defines the price of a launch service commodity, and that price is equal at any point in time for all options that provide an equivalent service based on our definition of the industry cash flow model, participants can only maximize profits independently by reducing the expected cost of an option.

The cost of a system is directly related to its adverse economic risk. The risk of an option is fundamentally equivalent to its expected worth. In engineering applications, though, risk carries the connotation of being associated with adverse outcomes. For the purposes of this work, the adverse economic risk of a system is equal to the relative price of the system multiplied by its probability of failure. Given the assumptions stated above, it is assumed that a reasonable participant in the commercial space industry will choose a launch system that presents the least adverse economic risk when compared against all other options.

When comparing two reasonable options, A and B, this work assumes option A will be chosen over option B if the following inequality holds true:

$$p_{f,A}C_A < p_{f,B}C_B \tag{2.1}$$

Where:

$p_{f,A}$ = Probability that option A will fail

C_A = Cost of option A

$p_{f,B}$ = Probability that option B will fail

C_B = Cost of option B

When comparing two reasonable options for which the risk of A is equal to the risk of B, it is reasonable to assume that one would choose the option with a lower probability of failure. This likely choice is assumed to be based on the risk-adverse nature of organisations. While the risk allocation scheme imposed by the DOT in the United States does remove legal exposure, a system failure is possibly more detrimental to the commercial fortunes of the company, if the assessment offered by Krige (2003) is valid.

It must also be clear as to what is a reasonable option. An option is reasonable if, assuming failure, the company is able to continue trading. If a launch option is so expensive or risky that system failure would bankrupt the organization, it is assumed to be an unreasonable option. Past history, however, has not always proven that companies only choose reasonable options. Especially in the commercial space industry, where novelty can trump traditional business sense as demonstrated by Beale Aerospace or the Conestoga program, companies often appear to accept higher risks than traditional firms. However, such a conclusion that there is a corporate culture within commercial space organizations that make them less risk averse does not seem to have support within the literature.

2.5 LSM: examination of the options

Completing the LSM mission with a conventional launch vehicle could be costly, depending on payload mass, because of the required vehicle size. As proposed, the

LSM mission would reduce this cost by using a small conventional launch system followed by two staged tether systems. However, the multiple handoffs and systems employed significantly increase the mission risk.

For a mission to succeed, all stages must succeed. For the LSM mission, the probability of failure associated with the mission is calculated as follows:[iv]

$$p_{f,RAS} = 1 - \left[(1 - p_{f,LV})(1 - p_{f,H1})(1 - p_{f,T1})(1 - p_{f,H2})(1 - p_{f,T2})\right] \qquad (2.2)$$

Where:

$p_{f,RAS}$ = Probability that the LSM mission will fail

$p_{f,LV}$ = Probability that the conventional launch vehicle will fail

$p_{f,Hi}$ – Probability that the i^{th} handover will fail

$p_{f,Ti}$ = Probability the i^{th} tether system will fail

If the mission risk associated employing the two-stage MMET system is less than that for the same mission completed with a conventional launch vehicle, the conclusions of this thesis are predicated on the assumption that the MMET-based system would then be economically feasible for such a use.[v]

Chapter 3

Launch Vehicle Costs

There is a wide range of conventional launch system options open to the customer. These all vary in cost and capability. This section presents the various vehicles available within the commercial launch market, and some of the various sources for pricing information on these vehicles.

3.0 Current commercial vehicles

This work is examining the economic feasibility of employing an MMET-based unconventional launch system for use in the US commercial launch market. As a conventional system is required for the first stage, it is assumed that the vehicle that would be chosen would come from those currently available within the commercial market, or from future vehicles that will emerge.

Data on the capability of, and publicly stated end user price for, all vehicles employed under a DOT launch license is published quarterly. This work cross-references the information provided by the DOT against that provided by Astronautix. Astronautix gathers its information from a number of sources, often from Jonathan's Launch List or sources of similar reputation. Jonathan's Launch List provides a mirror for the list of all United Nations registered orbital objects and mission insights published by the site author that are routinely respected and relied upon by the respective USAF and DOT launch safety organisations.

3.1 Vehicle capabilities

This work considers a vehicle to be available to the commercial launch market if that vehicle has previously been employed for a DOT licensed launch. Table 3.1 presents the maximum payload, as reported by Wade (2006), each vehicle that meets such a requirement could transport either to LEO or to a geosynchronous transfer orbit (GTO).

Table 3.1 All commercial vehicles launched between 1 Jan 1997 and 1 Jan 2005.

	Payload to LEO (kg)	Payload to GTO (kg)
Athena 1	820	--
Athena 2	2,065	--
Atlas 5 401	12,500	5,000
Atlas 5 521	13,950	6,000
Atlas II	6,580	2,810
Atlas IIA	7,280	3,039
Atlas IIAS	8,610	3,630
Atlas IIIA	8,640	4,055
Atlas IIIB	10,718	4,500
Delta 2 7XXX	5,089	1,818
Delta 4 Medium (4,2)	11,700	5,300
Delta III	8,292	3,810
Pegasus 1	375	--
Pegasus XL	443	--
Taurus	1,363	431
Zenit 3SL	--	5,250

No information is given by Wade (2006) with regards to the lifting capability of the Zenit 3SL for LEO destinations. For this reason, the cell for this value is marked '--'. Based on its stated capability with regards to GTO, it is assumed that the vehicle is capable of lifting around 13 tonnes to LEO. For the Pegasus 1, Pegasus XL, Athena 1, and Athena 2, it is understood that Wade (2006) does not state that these vehicles are sold on the commercial market for purposes of a mission requiring GTO injection.

Current research conducted at the University of Glasgow does not anticipate employing an MMET for missions with payloads less than one-tonne nor greater than three-tonnes. An investigation of Table 3.1 demonstrates that most vehicles are capable of performing such a task.

3.2 Price over time

Because of the time value of money, it is a fundamental concept in both economics and finance that a commodity, such as a commercial launch, will not cost the same in two different time periods. Further, it is a basic tenant of such a theory that the value of monies that will be received in the future is less than monies received today because equivalence is based on the opportunity cost of capital. Hence, if a launch

that occurred ten years ago is of equivalent value to a launch that occurs today, the earlier launch would have been priced much less than the launch price stated today.

The DOT publishes the stated launch price for each commercial vehicle that is launched each year. Because of the competitive advantage that companies would lose if the actual contract price were known, the DOT either publishes a cost spread or a point estimator. Based on Boeing (2002a), as will be discussed in a later section, the amount of monies written off for a demonstration flight of the Delta III vehicle, plus 15% of that value, equals the upper limit of the price spread stated by the DOT. When creating point estimators out of each price spread stated by the DOT, this 15% relationship is used to calculate a point estimate from the spread.

For all vehicles with more than two flights between 1997 and 2005, Fig 3.1 presents either the point estimate, or the calculated point estimate based on the data, presented in DOT (1997 – 2004).

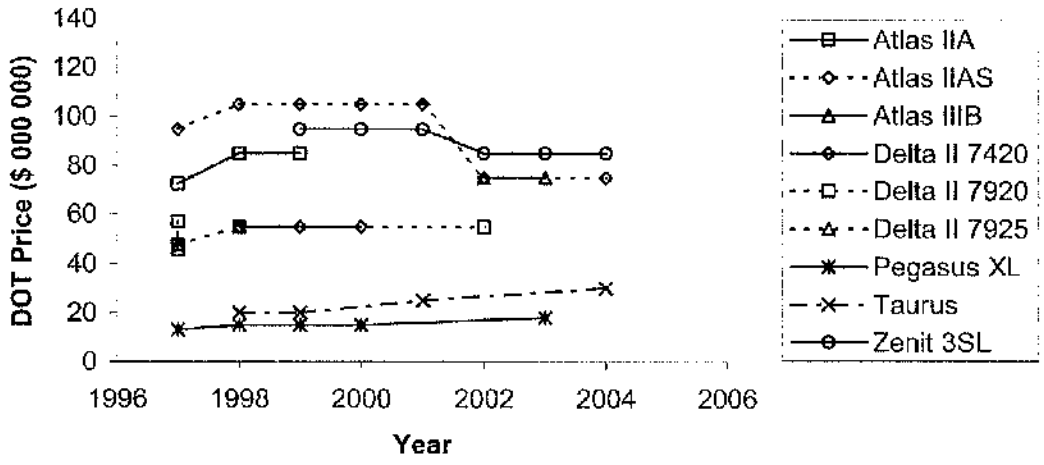

Figure 3.1 Price per launch listed by the DOT at the time of launch for each vehicle with more than two commercial flights between 1997 and 2005.

Examination of the graph shows the price for most vehicles rising until the turn of the century, after which the prices for most vehicles fall again. This rise in price corresponds to the increase in market demand and subsequent slowdown seen in the

United States. While discussed in more detail in the next chapter, this rise and fall in the launch rate was due to speculation in the communications and technology market, speculation that led to a market crash just after the turn of the century.

Assuming the prices listed by the DOT are valid, Fig 3.2 presents these values in terms of dollars in 2005. The conversions made in this work employ the Price Producers Index values for aerospace products and parts manufacturing (PCU3364, based June 1985), published by the US Bureau of Labour and Statistics.

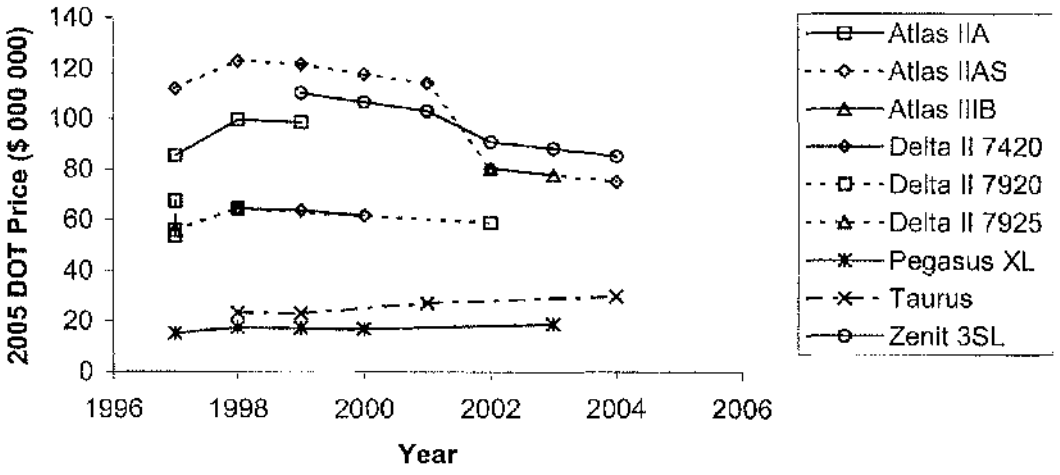

Figure 3.2 Price per launch for the flights listed by the DOT for each vehicle with more than two commercial flights between 1997 and 2005, adjusted to reflect dollars in 2005.

Examination of Fig 3.2 relative to Fig 3.1 shows a more pronounced drop in price for the majority of vehicles after the technology market crash in the early 2000s. However, unofficial data obtained from sources in the DOT indicates that the actual price of vehicles between 2001 and 2003 fell well below that stated publicly in DOT data. While publicly unverifiable, it was reported from such sources that an exclusive launch on the Sea Launch Zenit 3SL in the summer of 2002 could be secured for as little as $45 million.

When examining data for the Athena 1 and Atlas IIIA in Tables 3.1 and 3.2, the pre-2000 increase and the post-2000 decrease are clearly observed. While it is clear that

there would have been a rise in price when demand was at an all-time high during the late 1990s, and a similar drop in price as the level of overcapacity in the launch market skyrocketed after 2000, it is unclear whether any of the price data offered by the DOT is valid, or whether that obtained through Astronautix is robust enough from which one could develop trends.

Table 3.2 Price data for the Athena 1 vehicle.

Vehicle:	Athena 1			Destination Orbit:	LEO
Launch Year	Astronautix Price Year	DOT Price ($ 000 000)	Astronautix Price ($ 000 000)	2005 DOT Price ($ 000 000)	2005 Astronautix Price ($ 000 000)
1997	2000	15	17	18	19
1999	2000	17	17	20	19

Table 3.3 Price data for the Atlas IIIA vehicle.

Vehicle:	Atlas IIIA			Destination Orbit:	GEO
Launch Year	Astronautix Price Year	DOT Price ($ 000 000)	Astronautix Price ($ 000 000)	2005 DOT Price ($ 000 000)	2005 Astronautix Price ($ 000 000)
2000	1999	105	105	118	122
2004	1999	75	105	75	122

An examination of Fig 3.1 and Fig 3.2 demonstrates that there are two vehicles that do not rise and fall in accordance with the commercial launch. These vehicles are the Taurus and Pegasus XL vehicles that were developed and introduced in the mid-1990s. Unlike the Zenit 3SL, though, both of these vehicles were either significantly altered users of surplus technology or new systems with no flight history. Because of this, it is anticipated that this consistent rise in price corresponds to an increase in consumer confidence with regards to these vehicles. Because Orbital Sciences is a company that was founded with an intention to service the commercial launch market, it is assumed by this work that its slow-growth pricing practices are driven by conventional approaches to new technology. The Sea Launch Zenit 3SL, being a joint venture of international organisations with long standing histories with government contracts employing proven launch technology, is likely to have established a pricing structure in line with other government employed launch vehicles. This difference in

management and technological origin is likely to be the reason for the significant difference in price history with regards to these vehicles over the examined time period.

3.3 EELV inconsistency

One of the more interesting inconsistencies in the DOT data and the Astronautix data is that seen when examining the Atlas V and Delta IV prices. While the originally intended price of both the Atlas V and Delta IV is consistent with that stated by the DOT, these prices do not take into account the well-publicised increase in price estimates corresponding to the commercial launch market crash.

One of the contract terms discussed in Holtz-Eakin (2003) is the "best-customer clause." This clause states that neither Boeing nor Lockheed may sell their vehicles to commercial customers for less than the price each is charging the government. As a result of the contract negotiations discussed in Smith (2005a) and Smith (2005b) that led to the price increase of $7.807 billion discussed in Decker (2004) for the first round of government EELV contracts, in addition to other cost overruns and recalculations, the price per vehicle increased significantly from the initial estimates of around $72 million per flight, likely to be equivalent to that stated by Wade (2006).

Table 3.4 Price data for the Atlas V, 401 vehicle

Vehicle:	Atlas 5 401			Destination Orbit:	GEO
Launch Year	Astronautix Price Year	DOT Price ($ 000 000)	Astronautix Price ($ 000 000)	2005 DOT Price ($ 000 000)	2005 Astronautix Price ($ 000 000)
2002	2004	75	138	80	138
2003	2004	75	138	78	138

Table 3.5 Price data for the Atlas V, 521 vehicle

Vehicle:	Atlas 5 521			Destination Orbit:	GEO
Launch Year	Astronautix Price Year	DOT Price ($ 000 000)	Astronautix Price ($ 000 000)	2005 DOT Price ($ 000 000)	2005 Astronautix Price ($ 000 000)
2003	2004	85	138	88	138
2004	2004	85	138	85	138

Table 3.6 Price data for the Delta IV, Medium (4,2) vehicle

Vehicle:	Delta 4 Medium (4,2)			Destination Orbit:	GEO
Launch Year	Astronautix Price Year	DOT Price ($ 000 000)	Astronautix Price ($ 000 000)	2005 DOT Price ($ 000 000)	2005 Astronautix Price ($ 000 000)
2002	2004	85	138	91	138

It does not seem logical that the price stated by the DOT is accurate if it does not reflect the changes in launch price discussed in the literature. Nor does it seem logical that the organization would openly violate a contract requirement for the purposes of making a financial loss if the cost estimates provided to the USAF are valid. For these reasons, it seems logical to view the prices stated by the DOT with some scepticism; a scepticism that could be carried forward towards other vehicle prices.

3.4 Price to cost comparison

The first two Delta III missions, launching with commercial payloads, failed catastrophically. Having failed twice on the first two missions, Boeing could not find a customer for the third launch. To try and gain future customers by demonstrating the vehicle problems could be corrected, a demonstration launch was conducted in August 2000. In Boeing (2002a) the amount written off for this launch was stated as $78 million. This write-off is termed to be equal to the "costs" associated with the launch.

Table 3.7 Publicly stated prices for the Delta III on its first two launches

Vehicle:	Delta III			Destination Orbit:	GEO
Launch Year	Astronautix Price Year	DOT Price ($ 000 000)	Astronautix Price ($ 000 000)	2005 DOT Price ($ 000 000)	2005 Astronautix Price ($ 000 000)
1998	1999	90	90	105	104
1999	1999	90	90	104	104

As previously stated, the upper limit stated by the DOT is equal to this amount plus 15%. At the same time, the lower limit is 95% of this value. There is no information available to verify whether these costs included intra-corporation sales, which are counted into the quarterly revenue and earnings statements that Boeing publishes. If the write-off in 2000 accounts for internal sales, it is likely that such sales include profits earned by each department. If this is true, then the $78 million is likely to be similar to the actual minimum price Boeing would charge a commercial customer so as to ensure the company makes a suitable profit on the sale. If intra-company transactions are not accounted for, or these transactions do not produce profit margins equal to those the company would expect for sales to outside customers, then the point estimation methodology based on the 15% relationship is likely to be invalid.

3.5 Valid price estimates

An investigation of the numbers presented by the DOT, in conjunction with information available through other sources, raises serious concerns about their validity. While the numbers do appear to superficially correspond to the market movements between 1997 and 2005, there is little other support for their accuracy.

Additionally, the motives associated with the DOT values could be questionable. As with its many reports that exhibit unrealistic launch projections such as those presented in DOT (1996 – 2004), the launch prices published may be compromise values borne of industry pressure. In addition to its safety role, the DOT is also charged with promoting the industry. In the case of published launch values, it is logical to believe that cost estimates that do not offer full clarity would allow the DOT to achieve its promotion objectives without compromising its safety responsibilities. Therefore, it would not be operating in opposition to its remit while still supporting, and gaining the support of, the commercial launch industry.

It is also interesting to note that the rise and fall of the prices as stated by the DOT, even when adjusting such values to 2005 dollars, still does not mirror the volatility of the market over a corresponding period. While the prices reported by the DOT demonstrate maximum changes from peak to trough of around 50%, the launch rate fluctuated by nearly 400% during that same time period. When accounting for the generalised industrial attitude associated with the likely market model governing the commercial space launch industry, such dampened price movements are expected. However, if the movements are theoretically expected, and there is the possibility that ulterior motives may exist with regards to reporting accuracy, serious questions must be asked about the validity of the price data provided by the DOT.

The DOT does have a political element incorporated into its role and remit; an element that independent repositories such as Astronautix do not have. For this reason, it is likely that the price estimates provided by Wade (2006) are the most accurate available in the public domain.

3.6 Future prices

As previously mentioned, the price of a commodity fluctuates in accordance with the constraints of the specific market model so as to equalize the supply and demand. To this end, there are many factors that affect the future price of each launch vehicle. However, so long as there exists a commercial market where the needs are not uniform across all customers, there will likely continue to be a range of prices and capabilities.

At the same time, the argument does exist that the cost reductions attainable with conventional, chemical-based propulsion systems are limited. Even as efficiency increases through optimised chemical types or mixtures; or chamber, tubing, or nozzle geometries; Sutton and Biblarz (2001) note that there are limits to the amount of energy that can be released using chemically propulsive means. With these limitations, there will always be a base price for conventional chemically propelled launch vehicles within the commercial space launch market.

3.7 LSM: completing the mission using a conventional launch system

All previous work at the University of Glasgow has focused on MMET missions with payloads of either 2.5 tonnes or less. Considering a suitable safety factor of 20% may be assumed to be a reasonable design requirement, it seems prudent to select a conventional launch vehicle for incorporation into the two-stage tether system that has a rated capacity of around, but no less than, three tonnes.

3.7.1 LEO options for the first stage of the LSM mission

From Table 3.8, it can be observed that the two vehicles that satisfy such a requirement are the Delta II and the Atlas II.

Table 3.8 Commercial launch vehicles with a stated capability of launching to LEO payloads greater than two-tonnes but less than 10 tonnes

	Payload to LEO (kg)	Payload to GEO Transfer (kg)
Athena 2	2,065	--
Delta 2 7XXX	5,089	1,818
Atlas II	6,580	2,810
Atlas IIA	7,280	3,039
Delta III	8,292	3,810
Atlas IIAS	8,610	3,630
Atlas IIIA	8,640	4,055

While the on-orbit dynamics of an unbalanced handover are still under investigation, it could be possible that a single MMET may be designed such that it is capable of delivering two payloads during one mission. If this is the case, the total payload mass for two 2.5 tonne payloads to LEO is five tonnes, which could be accomplished with a Delta II. However, for three-tonne payloads, an Atlas II would be required. Considering the Delta II is approximated by Wade (2006) to cost $70 million in 2005 dollars while the Atlas II costs $107 million, first investigations seem to indicate a small change in individual payload mass could have significant cost implications.

However, while not discussed in full at this point of the work, the reliability of each vehicle must be taken into account. If the calculated reliability of the Atlas II is significantly higher than that of the Delta II, it could present the conventional launch

option with least risk. In such a case, even though it is more expensive, it could be considered a better choice from a holistic mission standpoint.

3.7.2 Options for performing the LSM mission with a conventional vehicle

While it is clear that the Delta II and Atlas II are capable of carrying the payloads destined for operation to the first-stage MMET, the cost of putting each MMET system onto its working orbit must be examined. At this point in the work, the size of each MMET system is unknown. The size of each system is determined by the desired system reliability, a factor that will be discussed later. Until the required MMET system size is calculated, an appropriate vehicle for lifting the system into orbit cannot be determined. The cost of deploying each MMET will be discussed in a later section after the size of each system is known.

As a conventional alternative to the two-stage MMET system, the only vehicle currently built that is capable of completing the LSM mission is the Delta IV-Heavy. Therefore, for comparative purposes, the cost of the vehicle required to complete the LSM mission is reported by Wade (2006) to cost $254 million per launch.

Chapter 4

Reliability of Conventional Launch Vehicles

Calculating the probability that a future space launch vehicle will fail is of great interest, and the techniques employed for such endeavours are the source of great debate. By understanding the current probability that a specific launch vehicle can be launched successfully, and how that probability will change as a function of time using the methodology presented herein, probability of success estimates can be developed for conventional launch system components for the purposes of assessing the LSM mission.

4.0 Introduction

Space launch operations are inherently ultra-hazardous. Consequently, because all risk cannot be removed from such operations, the responsible safety organizations in the United States employ a regime of risk mitigation and residual assessment. After imposing operational requirements that reasonably minimize all known risks, every US space launch is then subjected to a quantitative analysis of all residual risk.

The United States Air Force (USAF), National Aeronautics and Space Administration (NASA), and the Department of Transportation (DOT) all have the ability to impose a wide range of launch restrictions depending on this quantitative analysis, as identified in Air Force Space Command (2004) and DOT (2006). The quantitative metric used by these organizations to assess residual risk for operational purposes is termed *expected casualty*. An expected casualty computation for debris impact must be completed for every military, scientific, and commercial launch. The expected casualty of an entire launch is the aggregation, over the entire mission, of the risk at any instant. The contribution to expected casualty resulting from the risk associated with impacting debris at any instant is expressed, mathematically, as follows:

$$E_c(i,j) = P_{I,j,i}\rho_{P,j,i}A_{C,j,i} \tag{4.1}$$

Where:

$E_c(i,j)$ = expected casualty contribution of the j^{th} location at the i^{th} instant.

$P_{I,j,i}$ = probability of impacting the j^{th} location at the i^{th} instant.

$\rho_{P,j,i}$ = population density of the j^{th} location at the i^{th} instant.

$A_{C,j,i}$ = casualty area relative to the j^{th} location at the i^{th} instant.

A discussion of the concepts and current applications of expected casualty are provided by Philipson (1995), which also discusses the expected casualty requirements for toxic release and blast overpressure analyses. While the routines and algorithms required for implementation of these two risk sources are not presented within, it is understood that they, too, share a similar relationship with probability of failure. The use of geometric probability employed by Kiureghian (2001) also applies to the Maximum Probable Loss (MPL) insurance metric, which has significant DOT licensing implications, as discussed in DOT (2002a).

By examination, it is clear that expected casualty for debris impacts is directly dependent on the probability of impact estimate, which is directly dependent on the probability that the vehicle will fail a certain time prior to impact. While an acceptable value for $\rho_{P,j,i}$ is directly dependent on the fidelity and timeliness of the employed data, the launch vehicle casualty area multiplied by the probability that debris will impact an examined area is a function of (i) the vehicle break-up analysis, (ii) the fidelity and timeliness of the employed weather data, and (iii) the probability that the launch vehicle will fail at the i^{th} event time. There are acceptable metrics for a sufficient vehicle break-up analysis and accepted standards for weather data. However, determining a launch vehicle's probability of failure is generally a topic that is fiercely debated by many competing interests. In this environment where program costs are measured in billions of dollars, government safety organizations

must adopt metrics for assessing expected casualty that are not only fundamentally and computationally valid, but must also be fair, understandable, and repeatable.

Engineering reliability analyses employ a wide range of stochastic techniques for assessing the probability that a system will fail over a particular span of time. The literature on such techniques is vast and well researched, an overview available through examination of textbooks or practitioner guides, such as Lewis (1996) or Stamatelatos (2002). While mathematically valid, results of launch vehicle reliability analyses that rely solely on component or sub-system test data are identified by safety organizations and academics, as in DOT (2002) and Fragola and Collins (2004), to be in conflict with observed flight histories, as presented in Chang (1996), Chang (2000), or Isakowitz *et al.* (1991); or analyses of such flight history, like those presented in Guikema and Paté-Cornell (2004) and Guikema and Paté-Cornell (2005).

Given the conclusions of Chang (1996), which do not fault vehicle design on a general level while identifying infancy failures in the propulsive system as the primary cause of vehicle failure since 1958, this discrepancy is likely to be due to unforeseen interactions between the launch vehicle, its components, its operational processes, and the launch environment. An example of an unforeseen operational failure mode is evident when examining the Atlas/Centaur (AC) failures on missions AC-70 and AC-71. McCartney *et al.* (1993) present the findings of the AC-71 failure investigation, identifying a change in operational practice borne of efficiency driven modifications initiated as early as AC-62, six years prior to the investigated failure, as the root cause for the performance anomalies which resulted in the loss of both AC-70 and AC-71. Such an example demonstrates that a sound vehicle design can be operated in a manner that produces an unforeseen failure mode. As an example of uncertainty regarding how a component behaves under launch conditions, Chang presents a discussion of the Titan 34D mission that failed on 18 April 1986. As identified by Chang, the cause of this failure is attributed to a crack in the solid rocket motor propellant. While analyses indicated that the crack would not cause a failure, Chang (1996) identifies that burn-through occurred and resulted in vehicle loss. In combating such failures, an organization must be capable of collating and disseminating past experiences for application on future missions. Indicating the

importance of knowledge collation and dissemination, of the nineteen recommendations for launch vehicle reliability enhancement identified in Chang (2000), only four were design specific.

The persistence of these unforeseen failure modes is likely due to the relatively small amount of operational data available for launch vehicles. While systems that are traditionally analyzed with the conventional reliability engineering techniques presented in Lewis (1996) are capable of being developed in identical batches and repeatedly tested in sufficiently identical environments under operational conditions, the financial risk associated with launch vehicle programs, identified in Parkinson (1999), is a factor that severely limits the number of operational tests that can be conducted for each program, often limiting operational datasets to less than tens of flights per variant. However, as evident through examination of the cause associated with the AC-70 and AC-71 failures, significant design modifications occur after every launch, regardless of outcome. Consequently, it is likely that a significant number of potentially catastrophic failure modes remain undetected for long periods of time, as did the failure mode associated with both AC-70 and AC-71; and various operational characteristics of a component or system may not be fully understood, as identified on the Titan 34D mission discussed by Chang, resulting in significant performance uncertainty. To combat the component and sub-system uncertainty that produces significant errors when predicting launch vehicle reliability using bottom-up techniques, DOT (2002b) states that safety organizations employ top-down probability of failure assessments that incorporate observed flight histories.

There are a number of documents in the current literature that offer representations of the kind of top-down analytical approaches that are identified in DOT (2002) as traditionally acceptable to safety organizations. Because of the operational or design modifications made after each launch, the number of flights made by truly identical vehicles is rarely more than one. Despite this fact, most analytical techniques group vehicles to increase dataset size. The first of these techniques requires the analyst to group similar vehicles, often based on family or variant designation, and assess the probability of failure for each group over that composite data set. Guikema and Paté-Cornell (2004) presents an example of this commonly accepted approach using both

frequentist-based and Bayesian-based calculations. Regardless of statistical technique, the analyst must assume that each launch vehicle is sufficiently identical such that the observed flight history can be considered a realization produced by a set of Bernoulli trials. The problem with this assumption is that, not only does the discussion presented in McCartney *et al.* (1993) indicate that this assumption is invalid, later investigations completed by Guikema and Paté-Cornell, and presented in Guikema and Paté-Cornell (2005), offer indications that reliability growth is an observable phenomenon within launch vehicles. If true, such a phenomenon invalidates the fundamental assumption of identical vehicles that is required for the earlier analyses presented in Guikema and Paté-Cornell (2004) and cited by safety organizations in DOT (2002).

The analysis of vehicle flight history intended to investigate the prevalence of infancy failures performed in Guikema and Paté-Cornell (2005) indicates that improvements in the average failure rate of vehicles that DOT considers similar, as per DOT (2002), can be observed through the mean estimate of a frequentist analysis, although the Smith-Satterwaite *t*-test indicates such movements are not statistically significant; or through Bayesian-based Markov Chain Monte Carlo (MCMC) analyses, which offer more conclusive results. In addition to a variant-specific analysis over all tested flights, the inter-generational analysis performed by Guikema and Paté-Cornell indicates the existence of intra-family changes in variant success rate. Both of these conclusions are consistent with the results presented in Chang (1996), Chang (2000), and McCartney *et al.* (1993), and offer conceptual support for DOT guidance presented in DOT (2002) that "operator learning" (i.e., reliability growth) should be accounted for in a top-down analysis performed for launch safety purposes. However, such agreements offer further indications that the simplifying assumption of Bernoulli trials intrinsic to most conventional launch vehicle analyses is invalid. While indications of reliability growth are identified and discussed in Guikema and Paté-Cornell (2004) and Guikema and Paté-Cornell (2005), which, if verifiable, would invalidate the assumption of Bernoulli trials employed in their work, neither proposes a method for applying such observations to a specific vehicle, variant, family, or operator.

Reliability growth modeling is widely employed when assessing developing systems. A recent overview of generally accepted reliability growth models for repairable systems is discussed in Walls *et al.* (2005), and an investigation of the general framework, traditional reliance on logarithmic relationships, and benefit of Bayesian implementation techniques discussed by Jewell (1984). While the benefits to reliability growth estimation in software analysis and general engineering analyses are discussed relative to the assumptions of logarithmic and monotonic growth relationships, as in Quigley and Walls (1999), Quigley and Walls (2003), and Walls and Quigley (2001), a body of work on removing such assumptions also exists, including Ansell *et al.* (1997) and Ansell *et al.* (1999). Consistent with the conclusions of McCartney *et al.* (1993), which indicate that not every design modification leads to a reliability improvement, Ansell *et al.* (1997) and Ansell *et al.* (1999) discusses how innovations (i.e., system modifications) affect the local system reliability profile. However, the definition of a repairable system stated by Lugtigheid *et al.* (2004) clearly excludes expendable launch vehicles, invalidating a direct application of these techniques.

It may be logical to try and draw parallels between expendable launch vehicle reliability growth and either Shuttle or nuclear delivery systems. However, Shuttle is a repairable system, as identified in Kaplan (1990), and reliability conclusions gained through an examination of repairable systems cannot be directly applied in a valid manner to expendable systems, as per the conclusions of Lugtigheid *et al.* (2004). At the same time, while not repairable, the analysis of weapon systems identified in Fries and Easterling (1999) require expert guidance for producing the prior modification function used to model system degradation. While computationally accurate, and even with research into techniques for selecting objective priors like that presented in Vaurio (1992), many analysts raise concerns about the selection of prior and update functions in Bayesian analyses.

For Bayesian risk-assessment techniques, the selection of a prior is an issue that is specifically raised with regards to launch vehicles by Philipson (1995), and is an issue which applies not only to his previous work contained in Philipson (1989) that is specifically identified in the critique, but is a contentious point with various

mitigating approaches and explanations, with only a small segment of this voluminous discussion identified in works such as Koop (2003), Poirier (1995), and Spiegelhalter *et al.* (2003). This contention is not unique to the launch industry, and is widely discussed in general texts on Bayesian analysis, and specifically highlighted in the practitioner guide developed by Spiegelhalter *et al.* (2003) for the WinBUGS software, the package that was used to develop the results presented in the works of Guikema and Paté-Cornell.

The reason Bayesian analysis techniques are contentious is because the prior distribution, which is set by the analyst, is highly influential for small datasets. Since the number of flights that make up a standard dataset for a launch vehicle analysis is quite small, the prior set by the analyst has the ability to dominate the results. To correct for such influence, many turn to a range of non-informative analytical techniques, like those identified in Guikema and Paté-Cornell (2004), Guikema and Paté-Cornell (2005), Koop (2003), or Poirier (1995); or other, less sophisticated launch vehicle probability of failure computations within the literature, like those discussed in DOT (2002), which rely primarily on the ratio of observed successes to attempts, thereby diminishing analytical subtleties. While this decrease in analytical subtlety may be undesirable, Philipson (1995) highlights that such subtlety is only as valid as the methodology with which the prior is selected.

Even though Philipson identifies elements that make it debatable to claim any failure analysis is objective, based on the accepted limitations of commonly accepted frequentist forecasting techniques like those presented in Guikema and Paté-Cornell and the intrinsic subjectivity of selecting appropriate priors, government safety organizations regulating commercial launch operations require such analyses for launch approval, as discussed in Air Force Space Command (2004) and DOT (2006). While a fully objective launch vehicle failure probability analysis with low uncertainty based solely on the outcome of observed attempts is not achievable, supplemental analytical metrics can be developed that are stochastically valid.

In these top-down analyses, factors such as "learning" are specifically highlighted in DOT (2002). To account for this phenomenon of increasing reliability that is

indicated by the results presented in Guikema and Paté-Cornell (2005), it is the responsibility of the safety organizations to minimize subjectivity as much as possible. In an effort to reduce subjectivity, DOT (2002) identifies the government proposal to account for learning by examining the 65% confidence interval for the true probability of failure calculated with the binomial distribution given the total number of successes observed out of the total number of attempted flights. While this use of the Clopper-Pearson confidence intervals does produce a moving midpoint as a result of the narrowing confidence boundaries, these movements are a function of decreasing uncertainty. To state that the change in midpoint estimator is an indication of reliability growth is invalid and arbitrary. However, while the Department of Transportation approach is clearly invalid, it is just as invalid to apply the results of Guikema and Paté-Cornell because they are obtained under the simplifying model that each vehicle is a Bernoulli trial relative to its data set. Because the frequentist and Bayesian techniques that are described in DOT (2002) violate the analytical requirement for Bernoulli trials, a stochastically valid method must be proposed that allows safety organizations to increase the predicted probability of success associated with each launch, in accordance with commonly accepted reliability growth theory, while maintaining the validity and objectivity of the probability growth technique.

This work proposes a methodology that assesses the organizational capability of a launch vehicle operator to learn from past experience based on the observed flight history of its launch vehicle variants. This work begins by presenting the core methodology, followed by an approximation for this methodology using a logarithmic, monotonic simplification that retains its fundamental validity. After presenting the approach and discussing its applications, the results of an investigation into the learning rate exhibited by current commercial vehicles is presented that uses this simplified model, leading to a concluding discussion that identifies the benefits of employing the presented methodology.

4.1 Learning Methodology

Considering the vast differences in scale between the data sets used by launch vehicle analysis practitioners and those typically used by reliability growth practitioners, the two analytical paradigms seem to share few similarities. While traditional reliability

growth models focus on repairable and mass-produced systems, launch vehicle operators manufacture statistically unique vehicles that share little more than general design parameters. In the context of the conclusions presented in Chang (1996) and Chang (2000), no group of orbital launch vehicles could be selected out of all flights conducted since 1958 that are sufficiently identical so as each could be considered a Bernoulli trial. Because stochastically characterizing the reliability growth of a space launch vehicle in a valid manner is not possible under current manufacturing limitations, this work proposes a shift in focus with regards to launch vehicle failure probability estimation.

Instead of examining the probability that a launch vehicle will succeed, this work shifts the emphasis to calculating the probability that the next vehicle an operator launches will successfully complete its mission. This is a subtle, yet vital, distinction to ensure analytical validity. By shifting the analytical landscape in this manner, greater justification can be developed for prior distributions employed within Bayesian analyses, thereby diminishing the current concerns of subjectivity raised in work such as Philipson (1995). At the same time, under such an analytical paradigm, the contributions of Guikema and Paté-Cornell (2004) and Guikema and Paté-Cornell (2005) become far less significant than the work presented in papers such as Garber and Paté-Cornell (2004), Souder *et al.* (2005), McManus *et al.* (1993), and Walls and Quigley (2001), which focus on characterizing the knowledge collation and dissemination capabilities of an organization by objectively quantifying the effectiveness of its managerial and communication processes. Where such an approach offers significant benefit is in its application to range safety requirements. DOT (2002) identifies that range safety organizations currently consider both (i) the reliability analyses performed by operators and (ii) the top-down analyses performed by range safety organizations to be valid and accurate approaches to calculating the probability that a vehicle will fail, even though the two methodologies produce significantly different results. The shift in analytical emphasis presented here would remove that logical inconsistency.

In accordance with the observations and concepts of non-monotonic reliability growth presented in the literature, identified in works such as Chang (1996), Chang (2000),

McCartney *et al.* (1993), Ansell *et al.* (1997), and Ansell *et al.* (1999); this work proposes a *learning parameter* that is applied to the operator. This learning parameter, under investigation at the University of Glasgow, applies to each vehicle based on the number of flights for that variant, the date of the next attempt, the date of the original attempt for that variant, the number of variants developed prior to the current variant, and the total number of prior flights over all variants. Multiplying the operator developed engineering reliability calculation by this learning parameter would produce the probability that the operator will complete its next launch in a successful manner. By accounting for these factors, the learning parameter could model the demonstrated ability of an operator to learn during the development of a variant, an ability that may be greater after the development of prior variants. Such capabilities would be consistent with the indicated requirements identified in Guikema and Paté-Cornell (2005).

4.1.1 Relating the probability that each mission will succeed to the calculated vehicle reliability

The fact that many analyses assume the flight history for a variant can be considered a set of Bernoulli trials, as is done in conventional launch vehicle analysis literature such as DOT (2002), Guikema and Paté-Cornell (2004), Guikema and Paté-Cornell (2005); allows the flight sequence to be ignored. However, ignoring the sequence of successes and failures is proved to be invalid and is to be identified in Guikema and Paté-Cornell (2005), Collani and Draeger (2001), and Kotz and Johnson (1986), as the reason the confidence bounds for a frequentist analysis are so wide. By accounting for the realization corresponding to the observed flight history, relative to all the possible realizations for that number of trials, a Neyman acceptance region approach can develop relatively narrow boundaries that contain the true probability of success for that realization. By removing the assumption of Bernoulli trials and solving for the acceptance region in a manner that is identical to that employed when solving for the Clopper-Pearson confidence intervals, an acceptable interval bounding the true probability of occurrence for each attempt can be found for each proposed learning parameter.

When removing the assumption of Bernoulli trials, the analysis relates the probability that the operator will complete the next mission successfully to the vehicle reliability calculated for that mission via the learning parameter. For each launch attempt, the true probability that the i^{th} attempt of the j^{th} variant employed by that operator will be successful, $p_{s,i,j}$, is related to the vehicle reliability for that launch as in Eq. 4.2.

$$p_{s,i,j} = L\left(i_j, j, t_i, t_{0,j}, \left[\left(\sum_{k=1}^{j-1} N_k\right) + i\right]\right) R_{i,j} \tag{4.2}$$

Where:

L – learning parameter

t_i = date of the i^{th} launch attempt

$t_{0,j}$ – date of the first launch of the j^{th} variant

N_k = number of launches preformed by the k^{th} variant

$R_{i,j}$ = design reliability calculation for the i^{th} attempt of the j^{th} variant

Based on this relationship, which is capable of modelling the true probability that the next launch conducted by an operator will be successful, the observed histories of all variants relevant to a specific operator can be used to calibrate the learning parameter for that operator.

4.1.2 Calibrating the learning parameter for an operator using only observed flight history

As discussed, the Clopper-Pearson confidence intervals that are widely cited by frequentists depend on the aggregate outcome of all relevant realizations representing the observed launch vehicle success sequence, not the specific order of failures and successes. This aggregation results in very wide confidence intervals that are incapable of distinguishing between a series of events that represent failures on the

first three attempts and successes thereafter, a series of observations that would offer a strong indication of meaningful operator learning; and a series that exhibits three random failures, a scenario that would not indicate learning.

To account for order, calibration of the operator learning parameter proposed herein relies on the Neyman concept of acceptance regions as they were further investigated, and termed prediction regions, in Collani and Draeger (2001). Like the Clopper-Pearson technique, the Neyman concept of acceptance regions proposes a method that calculates an interval containing the true probability of success for an examined event, where the probability that the interval contains the true probability of success for the vehicle, β, is set by the analyst. Collani and Draeger (2001) presents the concept driving the technique as follows:

"1. There is a quantity of interest $\breve{p}$ with unknown actual value $p \in \left[\underline{p}, \overline{p}\right]$.

2. There is a random variable of interest $\breve{X}$ with uncertain outcome $\breve{x} \in \{0,1\}^n$."

This approach dictates that the aim of the first requirement above is to find the actual value of p by defining a set $C \subset \left[\underline{p}, \overline{p}\right]$, and the second aims to make inference about the uncertainty of the observed outcome, $\breve{x}$, by using a set $A \subset \{0,1\}^n$. As these two requirements are fundamentally interlinked, one finds a measurement interval C (i.e., a bounded set most similar to a confidence interval) by first computing acceptable prediction regions, $A_{\breve{X}}^{(\beta,n)}(p)$, and then sequentially solving from the null set of $\{0,1\}^n$ to the final realization.

A prediction region is acceptable when the error associated with the interval is at its minimum and the probability that the interval will contain p is greater than or equal to the selected β level, a value that is similar to the Clopper-Pearson confidence level. These requirements are defined mathematically as follows:

$$Q_{\{0,1\}^n}\left(A_{\breve{X}}^{(\beta,n)}(p)\right) = \min \tag{4.3}$$

$$P_{\vec{X}}^{(p)}\left(A_{\vec{X}}^{(\beta,n)}(p)\right) \geq \beta \tag{4.4}$$

Where:

$Q_{\{0,1\}^n}$ = marginal measure

$A_{\vec{X}}^{(\beta,n)}$ = β-prediction region for the random sample

p = true probability of occurrence

$P_{\vec{X}}^{(p)}$ = conditional distribution of the random sample

β = confidence level

In practice, finding the Neyman measurement procedures requires the practitioner examine the observed realization, $\vec{x}$, relative to the other 2^n permutations possible for those n trials. Each permutation, $\vec{x}_i$, has a probability of occurrence, $\mathrm{P}_{\vec{X}}^{(p)}(\vec{x}_i)$, equal to the product of occurrence for its constituent events. To find the lower limit, $l_{\hat{p}}^{(\beta,n)}$, and the upper limit, $u_{\hat{p}}^{(\beta,n)}$, respectively, of the measurement procedure (i.e., the numerical range within which the true probability will be contained with a probability equal to or greater than β), the following inequalities must be solved for p:

$$\sum_{i=1}^{j-1} \mathrm{P}_{\vec{X}}^{(p)}(\vec{x}_i) \geq \beta \tag{4.5}$$

$$\sum_{i=j+1}^{2^n} \mathrm{P}_{\vec{X}}^{(p)}(\vec{x}_i) \geq \beta \tag{4.6}$$

This approach of summing over all relevant realizations is functionally identical to the approach used to compute Clopper-Pearson confidence intervals. While the assumption of Bernoulli trials allows the Clopper-Pearson approach to use aggregate realizations, Collani and Draeger (2001) identifies that there is no statistical

requirement that either this assumption or the ensuing simplifications be implemented. While the Neyman approach is employed herein to account for the order within a set of trials where the probability of occurrence associated with each event changes between each trial, enacting the simplifications present in the Clopper-Pearson method would cause the Neyman approach to produce the same results. For each proposed learning parameter, whether proposed as a step in a MCMC analysis or within an iterative process, the acceptance region approach outlined above verifies whether a proposed learning parameter produces valid results that agree with the observed flight histories, and rejects any that do not.

4.2 Approximating learning using logarithmic and monotonic simplifications

In accordance with commonly accepted reliability growth theories, like those presented in Jewell (1984), Ansell *et al.* (1997), and Ansell *et al.* (1999), this work assumes that the probability of success for each launch can be related using a logarithmic relationship that is unique for each variant. As the unique logarithmic relationship for each variant can be defined using a pair of shape and size parameters, this approximation assumes the ability of an operator to learn can be represented using a joint-distribution constructed with the shape and size parameters calculated for each of its vehicle variants. Therefore, this model assumes that the operator is most capable of displaying an ability to learn that is consistent with the rate most frequently observed when examining the flight history of all its variants.

For each variant, the probability that the launch operator will successfully complete the i^{th} mission is presented in Eq. 4.7, below. The probability of success for each mission is presented in terms of the maximum probability of success, p_{∞}, attainable for that variant. When solving for acceptable shape and size parameters, the model is calculating interval boundaries around this maximum probability of success value. As per the learning model presented above, this maximum value would generally be restricted by an upper boundary equal to the engineering reliability estimate for the variant. Since this examination does not consider the reliability estimate for any variants, the model solves for this maximum probability of success with no prior knowledge, thereby using unity as an upper boundary.

$$p_i = p_\infty - ke^{-\alpha\frac{T}{T_0}} \tag{4.7}$$

The α and k constants are the shape and size parameters, respectively, defining the rate of learning exhibited by the observed flight history of each variant.[vi] These parameters are related to, and only valid for, a reference time, T_0, that is set by the analyst, which may or may not correspond to a specific launch date.

4.2.1 Important considerations for the presented simplifications

While an improvement over traditional techniques that are fundamentally invalid, such as those identified and presented in DOT (2002), Guikema and Paté-Cornell (2004), Guikema and Paté-Cornell (2005); this approximation does not offer the flexibility required to model reliability changes like those observed by Chang (1996), Chang (2000), or McCartney *et al.* (1993); or the concepts discussed by Ansell *et al.* (1997), because it does not model the mechanics of operator learning. This approximation is only capable of modeling movements that are consistent with the average change in system reliability resulting from design or operational modifications, using approximations that are presented as acceptable within the literature, as presented in Lewis (1996) and Jewell (1984). Additionally, the approach presented within does not account for the intra-generational invalidity inherent in the research presented in Guikema and Paté-Cornell (2005), where neither changes in learning rate nor changes in technological maturity are considered. However, by limiting the dataset to those vehicles that were initially designed and constructed primarily for commercial purposes, or those that underwent significant modifications after 1980 in response to the needs of the commercial market, it is assumed that this issue is suitably mitigated. This assumption is supported by an examination of the learning parameters for all variants produced by Orbital Sciences, which indicates that the shape parameter dependence on the introduction date for each variant is 2%, while the dependence is 7% for the size parameter. Such levels of dependency support the assumption that significant analytical effects caused by intra-family learning are mitigated herein as a result of restricting the investigation to commercially developed vehicles introduced within the examined time period.

After accounting for model limitations, various functional aspects of the model or its results must be considered. First, an analyst must ensure that the reference date is consistent for all variants under investigation throughout a multi-variant examination, or when applying the results to an analytical forecast. The shape and size parameters are tied to this reference date, making any conclusions erroneous if they are applied to an analysis based on any other reference date. The reference date for analyses presented herein is chosen to make the ratio of launch date to reference date less than one, so as to maximize the number of valid combinations produced for each analysis. An appropriate reference date and its effect are specific to each analysis, however, and must be considered on a case-by-case basis.[vii]

Secondly, like conventional approaches such as the Clopper-Pearson confidence intervals, the intervals containing the probability that an operator will successfully complete a mission will narrow as the flight history for a variant increases and, if the size parameter is positive, the midpoint of this interval will increase as the number of flights increases. This increasing midpoint is incorrectly interpreted in government texts, such as those presented in DOT (2002), to be an indication of learning. Such a conclusion is invalid in most cases because the assumption of Bernoulli trials identified within the Clopper-Pearson approach means that the boundaries are narrowing around a probability of success estimate that has been identical for all flights. Unlike this erroneous conclusion that one can model learning by examining a set of Bernoulli trials, the probability of success for each flight within the model presented herein will be changing. However, the probability of success on any attempt cannot be found by direct investigation of the changing confidence boundaries associated with an increasing dataset.

Such an application of the model is inappropriate and invalid. The primary problem with such an application is that the performed computations require the full dataset. Comparing a partial dataset to a whole dataset offers no benefit. The second major problem is that the model is solving for the maximum attainable probability of success for that operator calculated with the current flight history. Conceptually identical to the Clopper-Pearson approach that produces boundaries about a single value, the narrowing interval observed within the methodology presented herein

represents a decrease in uncertainty regarding the maximum probability of success term. While the magnitude of this value may fluctuate with new data as a result of decreasing skewness, comparing the maximum estimate from a less informed dataset offers no gain in understanding regarding the vehicle. To calculate the probability of success for any flight, shape and size parameters that most appropriately represent that variant must be used in conjunction with the maximum value estimate.

The third note of caution regards the use of the joint-distribution for each variant and the interval bounding the maximum probability of success estimate for the operator. Each probability of success interval is directly dependent on a specific pair of shape and size parameters. It is not valid to directly equate the 95% level of the shape and size joint distribution to the 95% level of a probability of success distribution aggregated over all variants. Relationships between shape and size parameters, and the ensuing probability of success boundaries relevant to each parameter pair, are found herein by performing a regression analysis. When using a third order regression in both shape and size parameters for vehicles within the examined dataset presented herein, as demonstrated later, such a regression accounts for up to 97% of all variations in the interval boundaries.

Finally, as with any other analytical method, very little information regarding changes within a vehicle can be attained if the vehicle has exhibited no failures. Unless a variant exhibits a launch failure, the shape and size parameters for the logarithmic and monotonic approximation will have mean and standard deviation values that account for all possible learning combinations. This general result would remain until a significant flight history is developed, after which the size parameter would begin to be narrow. This narrowing would not be the result of increasing information, though, but would be borne of the fact that the number of learning parameter combinations that can validly express the observed flight history would be shrinking based on the length of time between the first launch and the most recent launch. Considering the fact that the current flight history for most commercial variants examined herein is too small for this narrowing phenomenon to be reasonably observed, variants with no failures offer little benefit to this examination.

4.2.2 Example for a fictitious operator with multiple variants

To demonstrate this simplified model, this sub-section will examine an operator with three hypothetical variants to determine the shape and size parameters for this logarithmic and monotonic simplification of the learning parameter. The first vehicle of interest will have conducted two launches, the first on 11 August 2004, which is 38210 Julian, and the second occurring on 20 November 2004, which is 38311 Julian.[viii] For the analysis, the selected reference date is 40000 Julian. On these hypothetical launch dates, the first launch is observed to fail, while the second succeeds. As with the other two fictitious variants used in this example, the shape and size parameters will be examined over the intervals $0 \le \alpha \le 1$ and $-1 \le k \le 1$ with a certainty of 95% that the probability of occurrence is contained within the calculated interval.

By incorporating the fore stated data and parameters relevant to this example, Eq. 4.5 and Eq. 4.6 can be presented as in Eq. 4.8 and Eq. 4.9, below. Iteratively solving Eq. 4.8 for a defined pair of shape and size parameters will produce the lower boundary of an interval containing the maximum attainable probability that the operator can produce a successful launch, conditional on the those parameters being valid. Solving Eq. 4.9 in the same manner will produce the equivalent upper boundary.

$$\left[1-\left(p_{\infty,lb}-ke^{-\alpha\frac{38210}{40000}}\right)\right]\left[1-\left(p_{\infty,lb}-ke^{-\alpha\frac{38311}{40000}}\right)\right]\ge 0.95 \tag{4.8}$$

$$\begin{aligned}&\left[\left(p_{\infty,ub}-ke^{-\alpha\frac{38210}{40000}}\right)\right]\left[1-\left(p_{\infty,ub}-ke^{-\alpha\frac{38311}{40000}}\right)\right]+\ldots\\&\left[\left(p_{\infty,ub}-ke^{-\alpha\frac{38210}{40000}}\right)\right]\left[\left(p_{\infty,ub}-ke^{-\alpha\frac{38311}{40000}}\right)\right]\ge 0.95\end{aligned} \tag{4.9}$$

Using 10,000 uniformly distributed combinations of the shape and size parameters, and checking the solution obtained with each sample pair to ensure it does not violate the laws of probability, a quantitative and qualitative assessment of all valid learning parameter combinations for this variant are found to be joint-normally distributed

with a mean value for α of 0.583 with a standard deviation of 0.284, a mean value for k of 0.134 with a standard deviation of 0.081, and a correlation of 0.405.

As a note of caution, it must be remembered that the learning parameters developed are dependent on the reference date. In the example presented above, the reference date is 40000 Julian. However, if this date were changed to 20000, the mean value of α would become 0.657 with a standard deviation of 0.265; the mean k would become 0.285 with a standard deviation of 0.21; and the correlation between the two would become 0.554. This represents a change of over 10% in both learning parameters, which could have a significant impact on any predictive calculations for which this technique could be applied.

In addition to this variant with two flights, the other two variants flown by this hypothetical operator have shape, size, and correlation values of 0.468 (0.187), 0.352 (0.189), and 0.376, respectively, for the first vehicle; and 0.564 (0.094), 0.287 (0.250), and 0.631, for the second vehicle, with the standard deviation for each applicable parameter contained within the parentheses. With an even weighting between these three variants, the shape, size, and correlation for the operator, with the relevant standard deviations in parenthesis, are 0.576 (0.204), 0.258 (0.208), and 0.260, respectively. For predictive calculations, these values would be assumed indicative of operator learning, offering an understanding of how rapidly the operator is capable of improving the probability that each of its launches will be successful. As previously mentioned, regressions of the probability intervals against the shape and size parameters must be performed to draw predictive conclusions regarding the probability that a manufacturer will succeed on a specific launch. Such calculations are performed for some of the variants examined in the following section.

4.3 Results for current commercial variants and operators

This section examines launch vehicles introduced after 1980, calculates the joint-distribution of shape and size parameters associated with each, and presents failure and operator data for selected vehicles. This analysis varies the shape and size parameters between zero and one, with a reference date of 40000 Julian (i.e., 6 July 2009). The number of parameter combinations used for each vehicle varies based on

the number of flights, and was selected to minimize the number of computations while retaining a suitable level of accuracy. Accuracy was ensured through a qualitative examination of the cumulative distributions for each of the parameters. The number of divisions per parameter is listed, the number of combinations being this value squared.

4.3.1 Identification and discussion of examined vehicles

The analysis discussed herein examined all commercial launch variants that first launched in an operational manner after 1 January 1980, and that underwent 20 or fewer launches before 7 December 2003. All vehicles from that dataset that exhibited one or more failures are listed in Table 4.1. The number of shape and size parameter divisions used for the analysis of each vehicle is presented in the third column from the right. The second to last column is the number of flights, N, and the final column is the number of failures for that variant.

As previously mentioned, for every vehicle that experiences no failures, the joint distribution defining its learning has standard deviations associated with each mean value that make the distribution uninformative. For these trivial data sets, the mean of each parameter is 0.5 with a standard deviation of 0.28. For this reason, such vehicles are not presented in Table 4.1.

Table 4.1: Shape and size parameter mean and standard deviation for each variant, correlation between the shape and size parameters, the number of divisions for each parameter used to develop the joint-distribution, the number of launch attempts per variant (N), and the corresponding number of failures (r).[ix]

Vehicle	a mean	a std	k mean	k std	correl	a/k div	N	r
Ariane 5G	0.5863	0.2988	0.3477	0.2083	0.4042	17	16	3
Pegasus XL	0.5982	0.3172	0.3839	0.2035	0.4067	7	20	3
Ariane 1	0.5635	0.2878	0.1950	0.1185	0.3331	89	10	2
Atlas E Extra	0.5744	0.2888	0.0837	0.0465	0.3718	47	8	2
Atlas I	0.5713	0.2860	0.0986	0.0599	0.3642	111	11	2
Titan 34D	0.5693	0.2863	0.0373	0.0207	0.3571	111	7	2
Ariane 2	0.5678	0.2865	0.1164	0.0707	0.3509	111	6	1
Ariane 3	0.5749	0.2858	0.0221	0.0104	0.3818	93	11	1
Ariane 42P	0.8205	0.1147	0.0256	0.0000	0.0000	39	15	1
Athena 2	0.5783	0.2848	0.0634	0.0381	0.3893	113	3	1
Atlas G Centaur	0.5731	0.2903	0.0177	0.0082	0.3903	111	7	1
Pegasus HAPS	0.5716	0.2861	0.1202	0.0738	0.3660	111	2	1
Taurus	0.5808	0.2850	0.0419	0.0243	0.3996	111	5	1
Titan 401A Centaur	0.5844	0.2957	0.0113	0.0039	0.4920	111	9	1
Titan 401B Centaur	0.5792	0.2852	0.0414	0.0239	0.3941	111	7	1
Titan 402B/IUS	0.5781	0.2848	0.0631	0.0379	0.3886	111	5	1
Titan 403A	0.5745	0.2861	0.0399	0.0226	0.3779	111	5	1
Titan II/SLV	0.5770	0.2873	0.0302	0.0143	0.3889	68	13	1
Zenit 3SL	0.6235	0.3123	0.0502	0.0227	0.5015	31	14	1

From Table 4.1, the likely learning exhibited by the operators on various programs can be compared. For example, the higher *k*-value for the Pegasus HAPS variant indicates that its operators learned qualities that allowed it to more significantly improve the probability that each successive launch would be successful than did the team operating the Atlas G Centaur. This seems intuitively reasonable since the Atlas was, theoretically, calling on more mature technologies than the Pegasus system at the respective time of each program.

It must also be noted that the *k*-value is not directly related to the number of failures. While vehicles with a high number of failures are likely to produce a situation where the program faces more opportunities to learn about its vehicle than programs with fewer failures, this increased learning is not always observed. For example, although the Titan 34D has had more opportunities to learn from its failures than the Ariane 2 vehicle, the larger size parameter presented in the table indicates that the organisation operating the Ariane 2 vehicle more completely incorporated the lessons learned from its past experiences.

Additionally, it must be noted that the sequence of vehicle failures has a large role in the development of these shape and size parameters, a quality that can be observed by examining variants with only one failure. For example, the Ariane 2 experienced its only failure on the first of six launches, while the Ariane 42P experienced its only failure on the seventh of 15 launches. These sequences, both quantitatively and qualitatively, indicate that the failure on the Ariane 42P was likely a random failure, while the Ariane 2 failure could have been the result of inexperience. This is further supported by the fact that the Ariane 42P came after the Ariane 2, which indicates that lessons learned from the Ariane 2 could have been employed on the later variant. While an examination of all variants across all vehicles does not offer strong quantitative support for such intra-family changes in learning rate, an examination of the Ariane learning parameter calculations for all vehicles with one or more failures indicates that 12% of the shape parameter calculation can be attributed to the introduction date of the variant, with the size parameter having a 19% dependence on the introduction date. These values do offer support for an application of the intra-family results presented in Guikema and Paté-Cornell (2005) and discussed in DOT (2002) to the Ariane variants. While a limited mechanism for applying such results could be accomplished using simple regression, this is not examined here.

4.3.2 Probability of success interval regressions for specific variants

The shape and size parameters, by themselves, do not offer insight into the probability that an operator will conduct a successful launch. For every combination of shape and size parameters, there will be a unique maximum attainable probability of success interval, calculated using Eq. 4.5 and Eq. 4.6. Consequently, it is not only important

to understand the learning rate of a specific operator, but also the relationship between the learning parameters and the maximum probability of success interval.

This work uses a multi-variable, third order linear regression to relate the shape and size parameters associated with a specific variant to its corresponding maximum probability of success interval. Table 4.2 presents these regression coefficients for the Ariane 2, the Ariane 42P, Atlas G Centaur, and Pegasus XL. These vehicles were chosen for further analysis based on the distinguishing qualities discussed above regarding their rate of learning and overall success rate. For all regressions presented, the regression constants are valid for the 95% confidence level and there is no significant F-statistic for the regression as a whole. A third-order regression, with respect to both shape and size parameters, was chosen to minimize the non-linearity and heteroskedacity observed in lower order regressions.

Table 4.2: Regression coefficients defining the upper and lower boundaries of the probability interval within which the probability that an operator will successfully complete a mission with the identified variant for any launch, based on the currently observed flight history of each variant

Vehicle	int	a	a^2	a^3	k	k^2	k^3	R^2
Ariane 2								
ub	0.953	-0.012	0.013	-0.009	0.897	-5.295	9.847	0.923
lb	0.074	-0.049	0.000	0.000	0.724	0.000	-2.218	0.966
Ariane 42P								
ub	1.000	0.000	0.000	0.000	0.000	0.000	0.000	1.000
lb	0.793	-0.019	-0.006	-0.005	1.001	-1.476	0.697	0.946
Atlas G Centaur								
ub	0.996	0.000	0.000	0.000	0.000	0.000	0.000	1.000
lb	0.577	-0.051	0.181	-0.215	0.000	80.459	-1993	0.895
Pegasus XL								
ub	0.783	-0.106	0.000	0.000	0.810	0.000	0.000	0.960
lb	0.087	-0.163	0.000	0.000	0.853	-0.370	0.000	0.964

Examination of Table 4.2 offers some very interesting insights. When examining the intercepts, the Ariane 2 and Pegasus XL both exhibit a very low lower boundary intercept, while, for the upper boundary intercept, the Ariane 2 is very high relative to the Pegasus XL. While further supported by examination of Table 4.3, this is likely

the result of (i) the greater size parameter for Pegasus XL and (ii) the wider interval for Ariane 2 resulting from a less significant flight history.

Also interesting are the results of the Ariane 42P and the Atlas G Centaur. Both have similar shape and size parameters, both have one failure each, and both have an upper boundary that is defined by a single value. What is interesting is the fact that the maximum attainable probability of success for the Ariane 42P operator is bounded by unity, while that of the Atlas G Centaur is slightly less. While the quantitative difference is minimal, it is still interesting to note that the number and order of failures has a noticeable impact on these calculations, as is expected. Compared against the Ariane 42P flight history, discussed above, the Atlas G Centaur experienced its single failure on the second to last flight in its history. As previously discussed, the sequence of observed failures is what causes the decreased upper boundary observed in Table 4.2, and offers an indication that the random failures associated with the Atlas G Centaur may have farther reaching consequences than those associated with the Ariane 42P.

From these regression coefficients, the expected upper and lower boundaries of the interval containing the maximum probability that an operator will conduct a successful launch can be found for each variant by solving the regression for the mean values of the shape and size parameters. The results of this calculation are presented in Table 4.3.

Table 4.3: Average shape and size parameters for each variant identified and the upper and lower boundaries containing the maximum probability associated with an operator successfully launching its variant, based on the currently observed flight history of each variant

Vehicle	a mean	k mean	correl	ub - inf	lb - inf
Ariane 2	0.5678	0.1164	0.3509	0.9975	0.1269
Ariane 42P	0.8205	0.0256	0.3509	1.0000	0.7956
Atlas G Centaur	0.5731	0.0177	0.3903	0.9961	0.5813
Pegasus XL	0.5982	0.3839	0.4067	1.0303	0.2629

When examining Table 4.3, the calculated upper boundary for the Pegasus XL operator violates the laws of probability theory, a mathematical issue that is common with confidence interval computations. Identical to current practice in binomial and Bayesian problems where this exact situation occurs, the Pegasus XL would have an upper boundary of unity, as opposed to the presented value of 1.0303.

From Table 4.3, a few very important conclusions could be drawn. First, although the Atlas G Centaur was most likely designed and assessed to have a probability of success on each mission no less than 99.7%, this computation implies that its current flight history indicates there is less than a 2.5% chance that its operator could achieve such a level of success. At the same time, while the examined flight history for the Pegasus XL indicates that its operator could still achieve a probability of successfully launching a mission that exceeds 99.7%, it is possible that this probability could be as little as 26%.

When comparing worst-case scenarios, there is only a 2.5% chance that the maximum probability of success attainable for the Pegasus XL operator is less than 26%. At the same time, it is equivalently unlikely that the Atlas G Centaur operator will exhibit an ability to launch its vehicles with a probability of success less than 58%. While this worst-case scenario is less than 2.5% probable, the worst-case scenario for the Atlas G Centaur is much better than that of the Pegasus XL. This difference in worst-case scenario is likely a function of the number of failures relative to the number of flights

for each variant and the order of the failures within the flight history. This same relationship between the number of flights and uncertainty is seen using classical binomial and Bayesian analytical approaches, while the order of the failures has already been identified as a cause for prolonging the convergence of the interval containing the probability that an operator can successfully launch its vehicles.

In addition to future predictions, the learning parameter approximation can be used to look backwards at intervals bounding the probability associated with an operator successfully launching the first vehicle within an examined variant. For the Pegasus XL, the figures above predict that the true probability associated with its operator successfully completing the first mission to be less than 70% but greater than -6%. As with the previous situation where the maximum attainable probability is calculated to be greater than unity, this negative number would be raised to zero. Therefore, the revised estimate associated with the probability that the first Pegasus XL launch would have been successful was less than or equal to 70%.

4.3.2.1 Accounting for operators with multiple variants

Calculating the shape and size parameters that approximate operator learning for a specific variant using the logarithmic and monotonic assumptions presented within is a straightforward and objective exercise. For an operator of a single variant, such an analysis is both valid and significantly more objective than analyses that currently claim to achieve the same goals. However, when an operator is responsible for multiple variants, the analytical complexity and subjectivity increase significantly.

4.3.2.2 Orbital Sciences

Orbital Sciences operate a number of variants, six of which were examined for this study. These six vehicles are the Pegasus, Pegasus H, Pegasus HAPS, Pegasus XL, Pegasus XL/HAPS, and Taurus. Of these six, the examined histories of three variants did not exhibit an unsuccessful mission. These three are the Pegasus, Pegasus H, and Pegasus XL/HAPS variants. For each of these variants that had not exhibited a failed mission, both the shape and size parameters have a mean of 0.5 and a standard deviation of 0.28. How these vehicles are treated in an analysis of the rate at which Orbital Sciences learns will have a significant effect on the results.

Table 4.4 presents three different groupings of the variants operated by Orbital Sciences. The first line presents the calculation for operator learning if all variants are considered and equally weighted in the calculation. Because half of the variants operated by the company have not failed, the parameters estimating organizational learning produce results similar to the trivial case discussed earlier. When examining just the Pegasus vehicles, where three out of five variants have exhibited no failures, the results are just as trivial. It is not until the analysis excludes all variants without one or more failures that the organizational learning approximation begins to vary significantly from the trivial case.

Table 4.4: Average values for the shape and size parameters calculated using various groupings of Orbital Sciences launch vehicle variants

Group	mean a	std a	mean k	std k	correl
Orbital (all vehicles)	0.55	0.30	0.34	0.29	-0.02
Pegasus (all variants)	0.54	0.30	0.40	0.29	0.00
Orbital (all variants that exhibited at least one failure)	0.59	0.30	0.18	0.19	0.22

Examples such as this for Orbital Sciences highlight the importance of examining the knowledge collation and dissemination mechanisms employed within an organization. Such an examination is required to assess whether all variants are equally representative of a single operator, or whether operations within a single organization are so different for specific variants that the inclusion of a specific variant would invalidate the results of the analysis. For example, both Lockheed Martin and Boeing each own the intellectual property rights associated with a range of vehicle variants. However, it may be reasonable to argue that designating either Lockheed Martin or Boeing as an operator may offer little analytical benefit when assessing specific variants produced by each organization. How variants are attributed to an operator is open to debate and, based on the conclusions of Chang, should depend on the level and rate at which information is shared between variant programs.

4.4 Knowledge collation and dissemination systems

The concept of using organizational knowledge collation and dissemination processes as a characteristic for delineating launch vehicle operators was raised earlier in this work, with use of such a metric supported by the accepted recommendation for improving on launch vehicle failure rates, given the observation and analysis of launch failures occurring after 1958. As discussed earlier, learning is an activity that requires not only the acquisition of past experiences, but also an ability to apply the lessons learned from these experiences to future situations. Within an organization, to ensure lessons are recognized, retained, and applied, a system must exist that collates and disseminates data about past projects. If two programs have equal access to a shared information repository, it can be argued that the variants produced by those programs could be considered to have the same operator.

There is a large body of literature on the topic of qualitatively and quantitatively assessing the functionality of an organization, a small segment of it available through examination of Garber and Paté-Cornell (2004), Souder *et al.* (2005), McManus *et al.* (1993). As identified in these works, there are statistical methods that are currently being applied to characterize the effects organizational structures have on the retention and dissemination of knowledge within an organization. If the conclusions of Chang (1996) and Chang (2000) are valid, the complexity of a launch system may not be as important a consideration when assessing the probability that an operator will conduct a successful launch as the rate at which an organization is able to learn from its mistakes. As only four of the 19 recommendations for launch vehicle reliability enhancement identified within Chang (2000) were design specific, this issue of knowledge collation and dissemination appears vital for future space launch assessments.

4.5 Recent developments and analytical implications

Of greatest note with regards to recent launch vehicle history is the initial Delta 4-Heavy demonstration launch on 21 December 2004. While Boeing considered the flight a success from the point of view a mission demonstration, this research would consider the flight a failure. Due to underperformance early in the flight, the vehicle

failed to reach its intended orbital parameters. While the intended final destination was a circular, 36,350 km orbit, the vehicle reached an elliptical orbit of 19,035 km at perigee and 36,413 km at apogee. From a commercial mission perspective, this would be considered a failure.

The number of flights for both the Delta IV and the Delta IV-Heavy is not significant enough to be able to draw long-term conclusions. Many vehicles, such as those developed by Orbital Sciences, have experienced early failures from which the vehicles have gone on to exhibit exemplary reliability. There is no conclusive proof that such a situation cannot again occur with the Delta IV-Heavy. Therefore, as it cannot be proven otherwise, it is assumed that the probability of success associated with the Delta IV and its variants is at the US Air Force mandated level of 0.997.

4.6 LSM mission: conventional risk

Given the limited number of vehicles that are capable of carrying out the LSM mission for both a 2500 kg and 3000 kg payload, and the cost per vehicle for the required orbits as discussed in Chapter 3, the most cost effective vehicles are found to be the Delta IV-Heavy if the LSM mission is to be completed using just conventional means; and the Delta II, for the conventional component of the tether-based unconventional system. As the Delta II is not examined herein because it has not experienced any failures, this work assumes that it, as well, has a probability of success per mission of 0.997, as per the design.

With this information, the values for the risk assessment of each option are presented in Table 4.5. If a value cannot be calculated at this point based on the information currently presented in this work, the cell is left blank.

Table 4.5 Values currently calculated for the LSM mission risk assessment.

	Conventional	MMET-based
C_{LV}	$254M	$70M
$C_{MMET,1}$	--	
$C_{MMET,2}$	--	
$p_{f,LV}$	0.003	0.003
$p_{f,H1}$	--	
$p_{f,T1}$	--	
$p_{f,H2}$	--	
$p_{f,T2}$	--	

Chapter 5

Successful Handovers

With staged MMET systems like that proposed for the LSM mission, understanding the probability that a handover will be accomplished successfully is vital when performing a reliability analysis of the whole system. This work offers an indication of the inherent insertion accuracy for conventional vehicles and provides a methodology for calculating the probability of a successful rendezvous between two MMET systems that are staged as they are in the LSM mission.

5.0 Handovers in staged systems

All multi-stage unconventional launch systems that do not incorporate a Pegasus-style architecture must handover a payload from one system to another. Despite precise orbital dynamic models, space launch missions are not free of error. While the orbital dynamics governing most conventional space systems are known, Berger (2005) identifies that even conventional systems executing a traditional rendezvous are prone to failure.

When examining rendezvous operations that involve tether systems, only Draper *et al.* (2004) addresses the probability of failure associated with random operational errors. While other papers such as Williams *et al.* (2005) and Cartmell *et al.* (2004) identify the issue of errors at the time of handover, both assume that the location and orientation of the tether at release or rendezvous is nominal. Williams *et al.* (2005) assumes the orientation of the tether can be corrected by changing the location of a mass located on the tether, thus correcting initial errors in tether orientation so that the system becomes properly oriented at the time of rendezvous to produce system success. Unlike the tether errors examined in Williams *et al.* (2005), Cartmell *et al.* (2004) only accounts for operational handover failures, but does not account for failures caused by misalignment of the tether systems, nor does it address the issue of tethers that are unsynchronised.

While it does seem intuitively likely that a payload handover between the tips of two rotating structures with radii on the order of hundreds of metres may not occur as planned, as identified in Cartmell *et al.* (2004), it does not seem reasonable that the cause of failure would not be attributed to errors in system orientation. While a precise estimate of accuracy is not possible without a greater understanding of the control systems that would be incorporated, it is reasonable to believe that the ideal orbit associated with a missed handover like that presented in Cartmell *et al.* (2004) may rarely be achieved. More likely is the situation where both the releasing and receiving systems are not ideally aligned at the time of handover. As an example of the causes associated with such random failures, the deorbit and reboost of the systems following each mission may put the MMET systems on unsynchronised orbits. Or, as a mission begins, the MMET systems may take longer than expected to spin-up, or the systems may start spinning up at the wrong time. Such random errors could be defined to within known tolerances, based on the currently unknown control systems that will be employed, these tolerances possibly being expressed in terms of the error in orbital position or system orientation. Regardless, it is likely that a small motor would be needed to ensure a significant probability of success when handing over payloads within a staged MMET system. Such a motor could place the payload onto a transfer orbit, given the velocity vector of the payload at the time of release, and would ensure a successful rendezvous with the receiving system.

5.1 Conventional rendezvous

It is rare that a conventional launch system will directly insert a payload into its final orbit. Whether a kick motor is employed for significant orbital changes, or spacecraft motors are used for small corrections, the insertion accuracy of conventional vehicles is not currently sufficient for ensuring rendezvous. This fact is obvious through examination of the insertion accuracies achievable with conventional launch vehicles. Launch vehicle manufacturers often provide performance data for their vehicles, which includes estimates of insertion accuracy. For the Delta II vehicle, Boeing (2000a) provides the following information with regards to its insertion accuracy.

Table 5.1 Insertion accuracy for a conventional Delta II mission

Number of Stages	Insertion Orbit	3-sigma limits at Perigee	3-sigma limits at Apogee	3-sigma limits on inclination
2	LEO	-25/+9.3 km	-9.3/+9.3 km	-0.05/-0.05 deg
3	GTO	-9.3/+9.3 km	--	-2/-6 deg

With the normal parameters presented in Table 5.1, rendezvous with an MMET would be highly unlikely without the assistance of a small motor. Assuming a payload could be successfully caught by a MMET if the payload is within 0.5 km and 0.5 degrees of its intended destination, there is only a 4.38% chance that the Delta II would produce a successful rendezvous. These tolerances are far greater than those accounted for in Cartmell *et al.* (2004), further illustrating the problems associated with the currently envisioned handover failure mode. While Cartmell et al. (2004) was not intended to be an exhaustive study of handover failure modes, the principles associated with the mission design do offer an indication of the tolerances required to complete the mission.

Considering the capabilities of a standard vehicle like the Delta II, to successfully rendezvous with the MMET system, a small motor would be needed. After separating from the conventional launch vehicle that brought the payload from the surface of the Earth, the payload would be on its insertion orbit. To travel from this insertion orbit so that it may rendezvous with the MMET system, the motors attached to the payload must place the payload onto a suitable transfer orbit. The insertion orbit may be so close to the MMET that this transfer orbit could appear functionally equivalent to small orbital corrections. At the same time, as identified through examination of Table 5.1, the insertion orbit could be so significantly different from the MMET orbit, on which the payload is intended to be, that a more obvious transfer orbit would be required. To both enter and exit from this transfer orbit, the payload motor must have sufficient propellant to produce the required impulses.

Calculating the impulse burns required to rendezvous given the spread of orbital conditions in Table 5.1 would require a use of the general orbital dynamic equations for intercept and rendezvous. As the information provided in Table 5.1 is quite broad,

a full analysis of all possible errors is computationally cumbersome and expensive, and will not be accomplished within this research or presented herein. The following section identifies a likely failure mode associated with the mission discussed in Cartmell *et al.* (2004), and presents a methodology for calculating the probability of success associated with such an operation, if the error distribution associated with orbital position and system orientation at the time of the intended handover is known. As previously stated, these errors are a direct product of the employed control systems, which are not currently known, making approximations of their accuracy speculative in nature.

5.2 MMET handovers

A payload is handed from one system to another by means of a successful rendezvous. When an MMET-based unconventional launch system only requires a single MMET, the only handover is between the conventional vehicle and the MMET system. If the location of the MMET tip with which the payload must rendezvous is known as a function of time, as well as the insertion orbit onto which the payload was delivered by the conventional launch vehicle component of the system, a transfer orbit and the required impulse burns for completing a successful rendezvous can be calculated in a straight-forward manner using texts such as Thomson (1986).

For the MMET deployment concept where rendezvous occurs when the tethers are fully retracted and the tethers are deployed during operation, calculating an appropriate transfer orbit only requires an understanding of the Keplerian orbits representing both the insertion orbit and the orbit of the MMET system. However, examining a staged handover where the tethers are fully extended and rotating at the time of handover produces non-trivial payload velocity vectors relative to the Keplerian orbit of each MMET central facility.

5.2.1 Staged handovers

For staged systems like those discussed in Cartmell *et al.* (2004), handover between two MMET systems occurs instantaneously, such that the payload being released by the first system is instantaneously received by the second system. To successfully complete such a mission, the tip of the releasing MMET is functionally rendezvousing

with the receiving tip. Considering the MMET systems typically examined by Cartmell are on the order of hundreds of kilometres in length, it must be understood that small angular errors relative to the central facility will produce significant distances between the tether tips. For an instantaneous handover, as required by the mission presented in Cartmell *et al.* (2004), handover is planned to occur when the two systems are aligned as presented in Fig. 5.1.

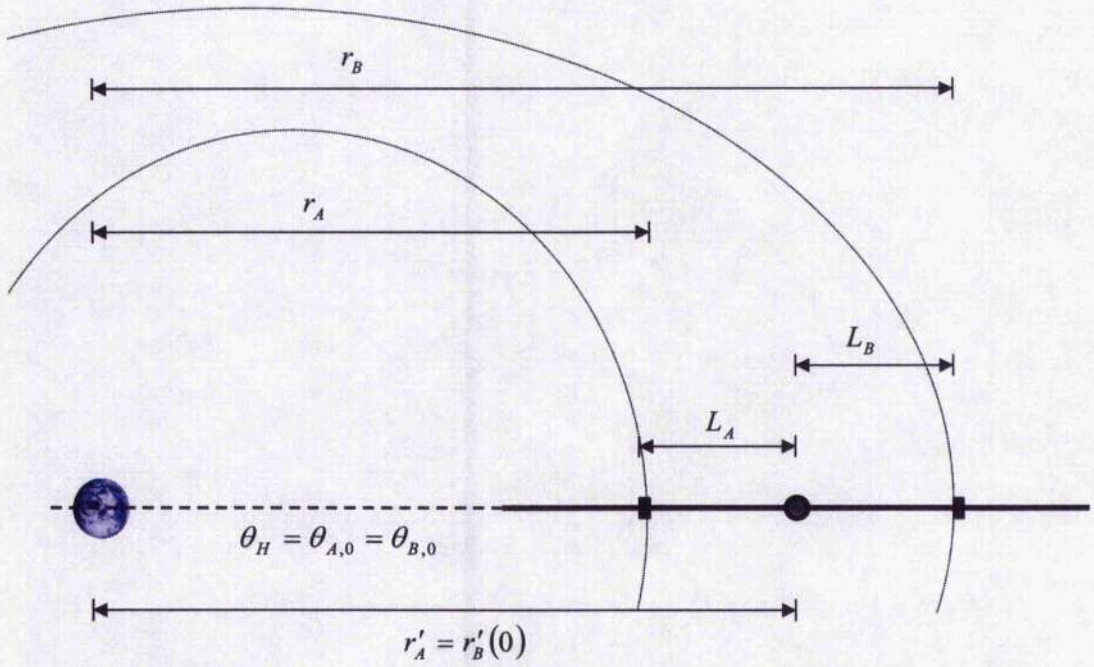

Figure 5.1: Illustration of an ideal handover between two momentum exchange tether systems, the releasing system identified as system A (left) and the receiving identified as system B.

As identified in Fig. 5.1, handover occurs at a specific orbital position relative to the orbit of each system, identified in the figure for both systems as θ_H. This location is represented for each MMET system as the angle between the location of handover and the perigee associated with the orbit for MMET system A and system B as $\theta_{A,0}$ and $\theta_{B,0}$, respectively. To gain the greatest altitude advantage achievable with each MMET system, θ_H is likely to correspond to apogee for system A, the lower altitude system; and perigee for system B, the higher altitude system.

Given the radius from the centre of the Earth to the central facility of system A and B, expressed as r_A and r_B, respectively; the length from the central facility of system A and system B to the tip of its respective system, expressed as L_A and L_B; the radius from the centre of the Earth to the releasing tether tip at the time of handover, r'_A; and the radius from the centre of the Earth to the receiving tether tip, zero seconds after the payload is released from the releasing tether tip, $r'_B(0)$; a number of important equalities can be derived, expressed in Eq. 5.1.

$$r_A + L_A = r_B - L_B = r'_A = r'_B(0) \tag{5.1}$$

The radius from the centre of the Earth to the receiving tether tip is expressed as a function of time after release in this situation to highlight the fact that, when calculating a suitable transfer orbit in the presence of location errors at release, the position of the receiving tether at release is not as important as its location after the transfer orbit is capable of being completed. As presented later, the radius from the centre of the Earth to the receiving tether tip at any instant is expressed as r'_B, the same radius at the time of release is expressed as $r'_B(0)$, and the radius from the centre of the Earth to the receiving tip a time t after release is expressed as $r'_B(t)$.

Ensuring each payload is released at the proper time and location is a daunting task, especially when the system size prevents rapid corrections in position or velocity. When considering the lower altitude MMET discussed in Cartmell *et al.* (2004), a one-degree error in tether orientation relative to the central facility will produce a tip displacement of nearly 3.5 km relative to the intended handover location. Considering the altitude of each mission, it is assumed that missions such as those discussed in Cartmell *et al.* (2004) will employ a combination of ground-based resources to synchronise the beginning of each mission, and on-board sensors that would ensure proper release. While there are many errors that could arise when synchronising the systems with ground-based systems, this work on handovers is only concerned with errors associated in positioning at release. As evident through examination of an error such as the one-degree orientation error discussed above,

whose magnitude may be considered minute in conventional engineering systems, the unique qualities intrinsic to the MMET concept mean that traditionally minute errors can have significant implications for mission success.

5.2.2 Non-optimal release

Considering the types of control systems that are likely to be employed for an MMET-based mission, this research anticipates that the two most likely errors with regards to handover would be observed in (i) orbital position and (ii) system angle. As identified in Fig 5.1, an ideal handover occurs when both systems are aligned with the gravity gradient at a designated handover location, θ_H. Errors in orbital position and system angle are identified in Fig. 5.2 for systems A and B, with the orbital position error, relative to θ_H, for each system identified as $\Delta\theta_A$ and $\Delta\theta_B$, respectively; and the tether orientation error for each system identified as $\Delta\phi_A$ and $\Delta\phi_B$, respectively.

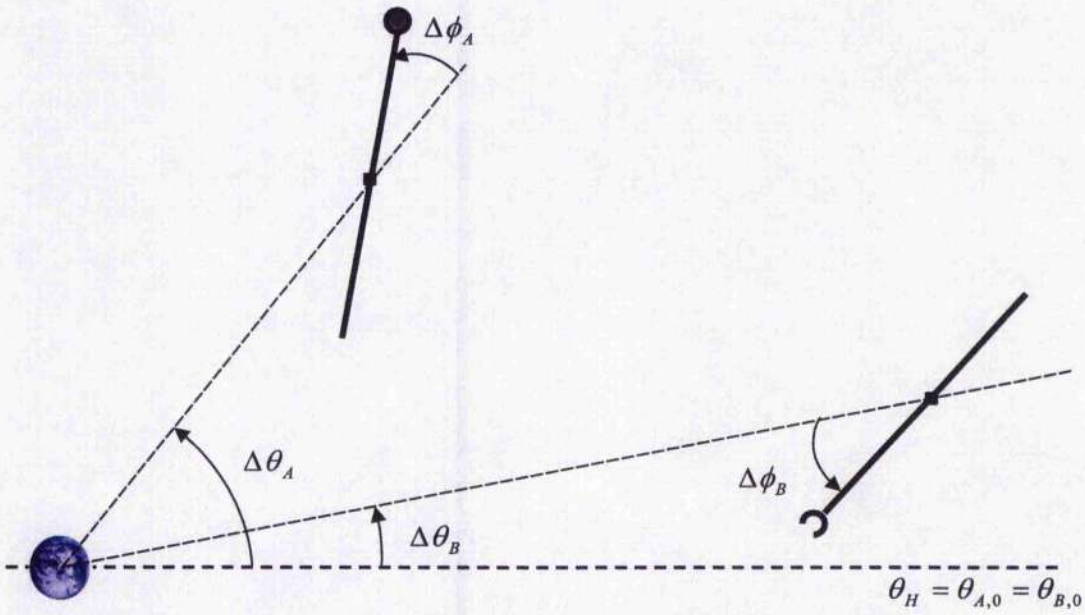

Figure 5.2 Errors in orbital position and system angle

It seems intuitively reasonable to assume that there is a high probability that such errors will exist. If such errors exist, a payload that is released in the presence of such

errors must be able to put itself onto a transfer orbit that will allow it to rendezvous with the receiving tip of the second tether, identified above as system *B*, to enable mission success. Based on the orbit of each MMET system, assuming the central facility of each will travel around the Earth in a Keplerian manner, the orientation of each system at release, and the time between release and recovery, *t*; a transfer orbit can be calculated that would allow the payload to successfully rendezvous with the receiving system.

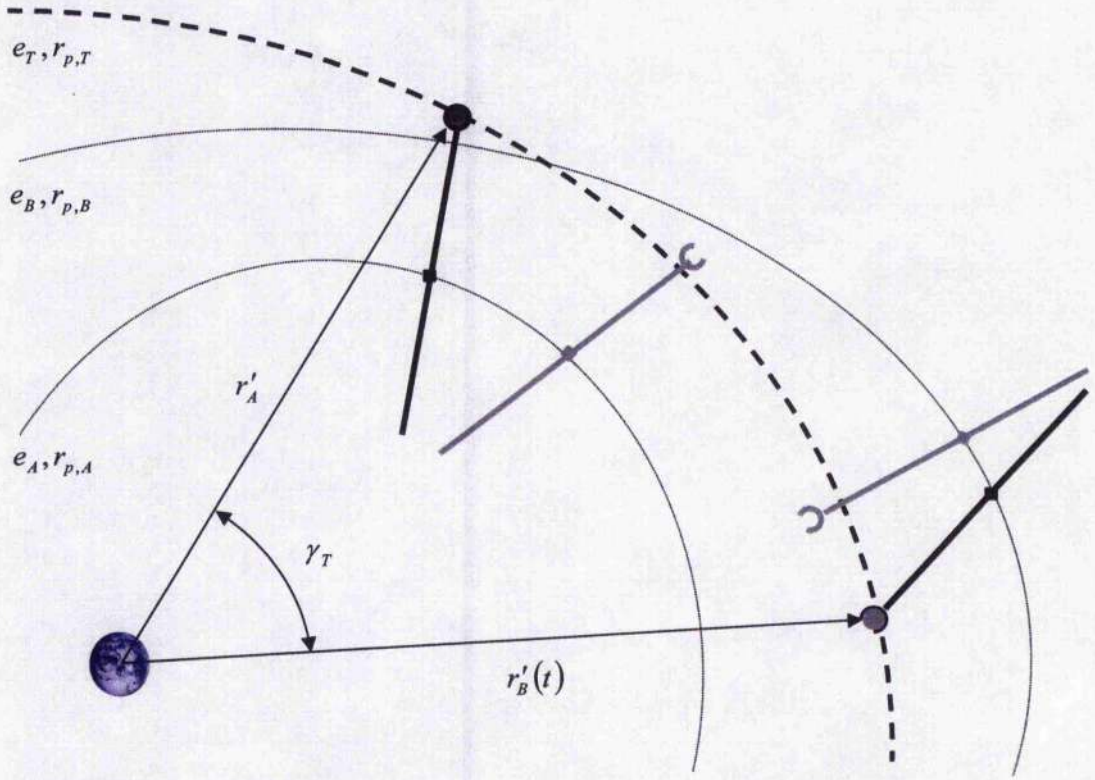

Figure 5.3 The three orbits required for a non-optimal handover: the releasing MMET (orbit *A*), the receiving MMET (orbit *B*), and the transfer orbit (orbit *T*)

In Fig. 5.3, the eccentricity and radius at perigee for the Keplerian orbit associated with the central facility of system *A*, the central facility of system *B*, and the transfer orbit are identified as e_A and $r_{p,A}$, e_B and $r_{p,B}$, and e_T and $r_{p,T}$, respectively. As discussed earlier, the time between release and recovery of the payload, *t*, is vital. Also important is the angle between the orbital location on the transfer orbit at

payload release and recovery, γ_T. This angle will be important later in this derivation when solving for suitable transfer orbit parameters.

Since it may not be immediately clear why the time between release and recovery is vital to these calculations, Fig. 5.4 and Fig. 5.5 highlight the position of systems *A* and *B* both at release and recovery. By examination of Fig. 5.4, both systems are shown at the time of payload release, in the presence of positional and orientation errors. As discussed earlier, the time dependent notation for the radius between the centre of the earth and the receiving payload tip is employed.

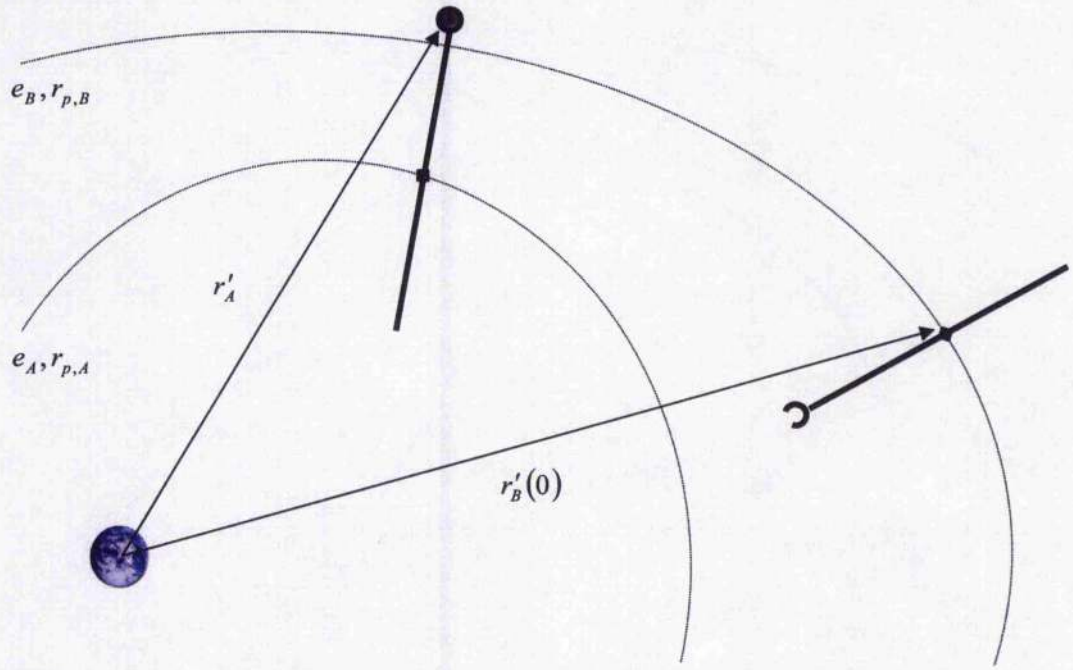

Figure 5.4 System *A* and *B* at the time of payload release.

After release, with the assistance of the motor discussed earlier, the payload will enter a transfer orbit, identified in Fig. 5.5 as in Fig. 5.3 with a thick dashed line. As the payload is travelling along this transfer orbit, it is assumed for the purpose of this research that both MMET system will continue to both travel along their respective orbits and rotate about their central facility. While the releasing payload will actually deorbit after release, the orbit of system *A* for the purposes of this methodology is only relevant immediately prior to release. The position of systems *A* and *B* after a

time t is identified in Fig. 5.5, as are both the release and recovery positions of the payload. As identified in Fig. 5.3, γ_T is measured from the radius of the payload at release to the radius of the payload at recovery, both radii being measured from the centre of the Earth.

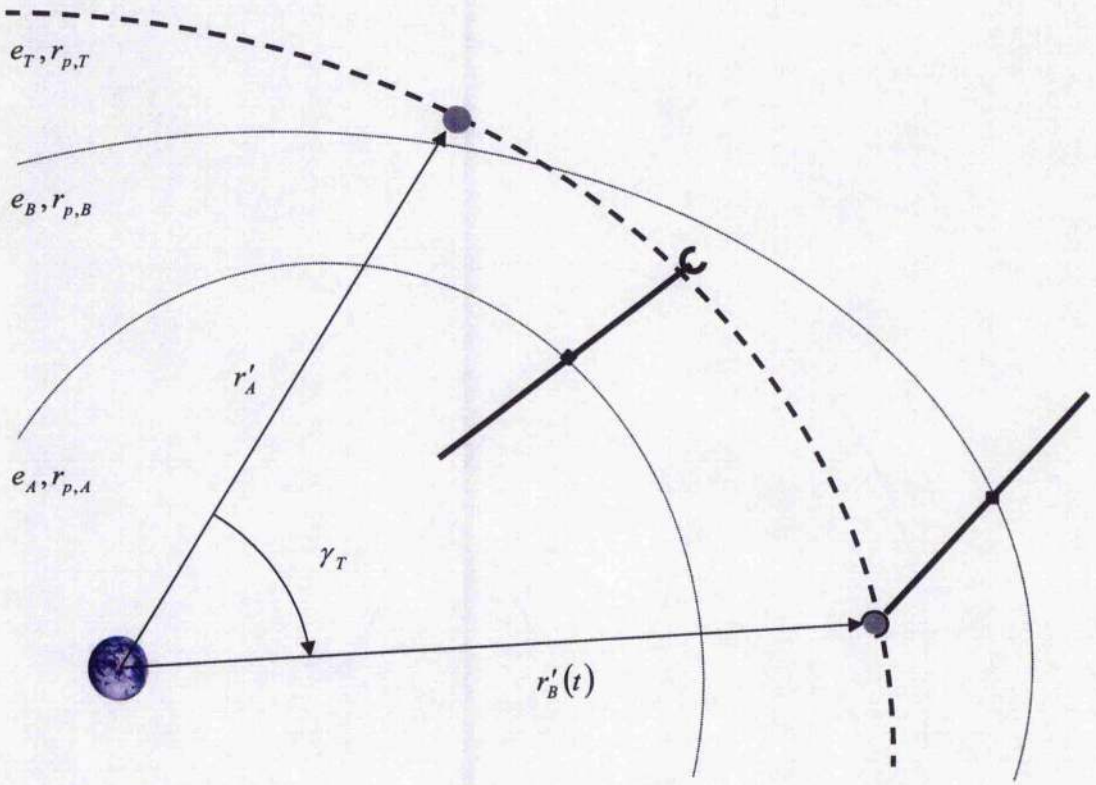

Figure 5.5 System A and B at the time of payload rendezvous, after it has traversed the transfer orbit.

Unlike conventional spacecraft, because of the size and rotation of the MMET systems, the velocity vector of the payload at release and of the vector that must be attained to ensure successful rendezvous at recovery are not defined solely by the Keplerian orbital parameters associated with the central facility of each system. Given the location, orientation, and operation of both MMET systems, the orbital parameters for the payload at release, and those required for the payload to ensure a successful rendezvous can be calculated.

5.2.3 Payload parameters at release and recovery

The orbital parameters of the payload at release and recovery can be presented in terms of the inertial reference frame. The velocity vector relative to the inertial frame for the tip of each MMET system is the sum of (i) the inertial velocity vector at the central facility and (ii) the local velocity of the tip relative to the central facility. The inertial velocity vector of the releasing tip of system A and its heading angle, v'_A and β'_A, respectively; and the velocity vector and heading angle for the receiving tip of system B, v'_B and β'_B, respectively; are presented in Fig. 5.6.

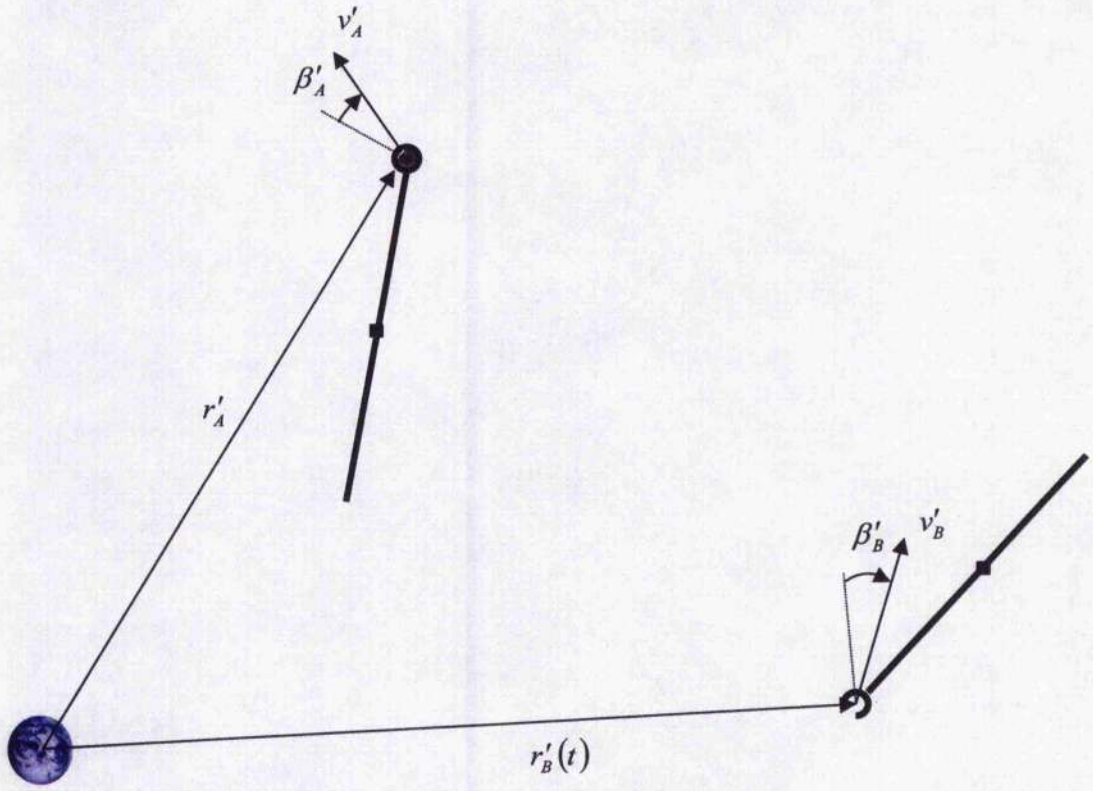

Figure 5.6 Initial orbital conditions for release from system *A*, and orbital conditions the payload must achieve at system *B* to ensure a successful rendezvous.

These velocity vectors for system A and B represent (i) the velocity vector that the payload will have at the time of release and (ii) the velocity vector that must be attained by the payload as it arrives at the receiving tip to ensure successful

rendezvous. As previously mentioned, these velocity vectors and heading angles are the sum of the velocity vector at the central facility of each system and the local velocity vector at the system tips. The velocity vector relative to the central facility for system A and B is identified in Fig. 5.7.

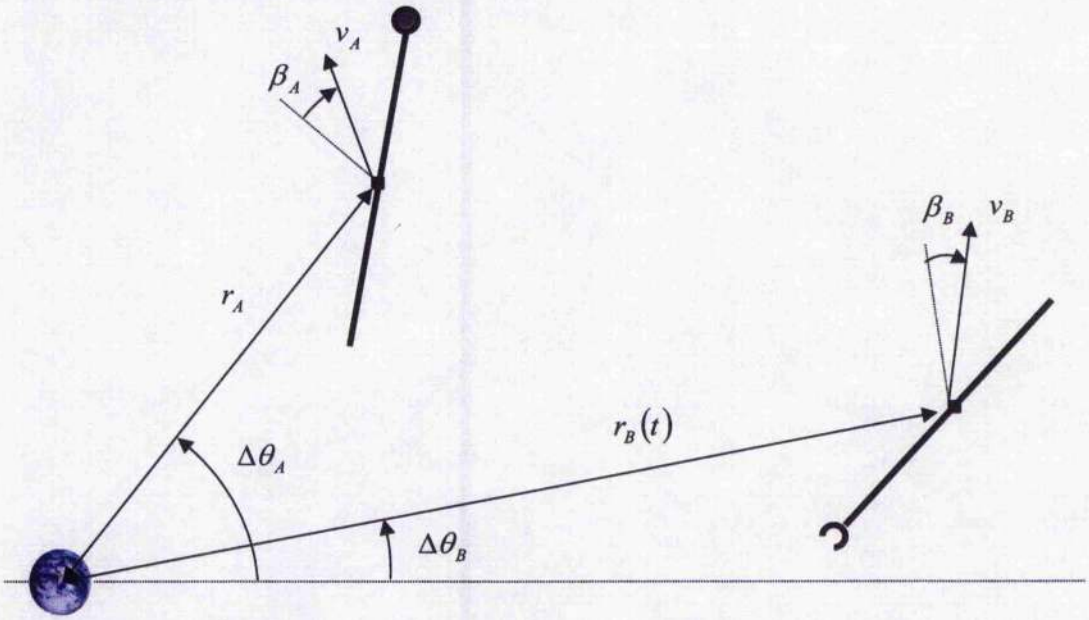

Figure 5.7 Conditions associated with the central facility of each MMET, assuming each travels along a Keplerian orbit, at the times of release and recovery.

The magnitude of the velocity vectors identified in Fig. 5.7 and their respective heading angles can be calculated based on the orbital position of the central facilities and the parameters of the orbits. Using the notation employed within Thomson (1986), the velocity and heading angle of the central facility of system A can be found as in Eq. 5.2 and Eq. 5.3, respectively. The velocity and heading angle for system B is calculated in an identical manner. While r_A represents the radius from the centre of the Earth to the central facility of system A at the time of release, there is no problem with substituting either r_B or $r_B(t)$ into Eq. 5.2 and Eq. 5.3, so long as r_B is the radius at a time, t, after release. In Fig. 5.7, a desire to emphasise the fact that payload recovery occurs a significant amount of time after release is the reason $r_B(t)$ is used.

$$v_A = \sqrt{K\left(\frac{2}{r_A} - \frac{(1-e_A)}{r_{p,A}}\right)} \tag{5.2}$$

$$\beta_A = \arccos\left[\frac{\sqrt{Kr_{p,A}(1+e_A)}}{r_A v_A}\right] \tag{5.3}$$

In these equations, K is the universal gravitational constant multiplied by the mass of the Earth, which is approximately equal to $3.985_{10}{}^{14}$. While Eq. 5.2 and Eq. 5.3 are currently expressed in terms of the radius to the central facility, relating these radii to orbital position is a straight-forward exercise, employing Eq. 5.4, which is presented in terms of system A. As with Eq. 5.2 and Eq. 5.3, system B would be treated in an identical manner to system A, when the orbital parameters are presented relative to the time of payload recovery.

$$r_A = \frac{1}{1+e_A\cos(\theta_{A,0}+\Delta\theta_A)} \tag{5.4}$$

While calculating the magnitude of the velocity vector and the heading angle for the central facility of system B at the time of recover is straight forward once the orbital location of the central facility is known, identifying this location for elliptical orbit requires an iterative treatment of the Kepler equation. The Kepler equation defines the motion of an object around a Keplerian orbit in terms of the variable ψ. As discussed in Thomson (1986), the variable ψ is related to the radius from the centre of the Earth to the orbiting body, r, in terms of one half the major axis, a, and the eccentricity of the orbit, e, as in Eq. 5.5.

$$\cos\psi = \frac{a-r}{ae} \tag{5.5}$$

For system B, this relationship can be expressed at the time of release and at the time of recovery, which occurs at a time, t, after release, as in Eq. 5.6 and Eq. 5.7, respectively.

$$\cos\psi_{B,0} = \frac{a_B - r_B(0)}{a_B e_B} \tag{5.6}$$

$$\cos\psi_{B,t} = \frac{a_B - r_B(t)}{a_B e_B} \tag{5.7}$$

With these relationships, for an object travelling along a Keplerian orbit for a known time, t, the relationship presented in Eq. 5.8 will hold.

$$\psi_B - e_B \sin\psi_B = t\sqrt{\frac{K(1-e_B)^3}{(r_{p,B})^3}} + \psi_{B,0} - e_B \sin\psi_{B,0} \tag{5.8}$$

By iteratively solving Eq. 5.8, the position of the central facility at the time of recovery, t, can be calculated. Once known, the position at any t will allow for the direct solution of the magnitude of the velocity vector and the heading angle associated with the central facility of system B.

While the velocity vectors associated with the central facilities of system A and B is assumed here to be defined by the Keplerian orbit of each, the local velocity vector of each tip is a function of the angular velocity of the system about its central facility and the sub-span length of each system. It is further assumed for this analysis that the angular velocity of the sub-spans about the central facility in an MMET system is functionally independent of orbital location. Current research into the MMET system does continue to support the initial indications of Cartmell (1996) that the orbital dynamic equations contain significant non-linear, inter-coordinate coupling. However, once these orbital dynamic equations are more fully derrived, independence could still be achieved through facility power variation. Further, the research presented herein assumes that the angular velocity of the tether spans about their respective central facilities is constant throughout the handover operation. Even if

further research into orbital dynamics indicates that ensuring such operational conditions are inefficient to meet, the core methodology presented here would remain valid. While the core methodology of finding a suitable transfer orbit for the payload given an accurate release and recover position would remain as presented, the equations for locating the facility and determining the orientation of system *B* would need to be modified so as to incorporate future results.

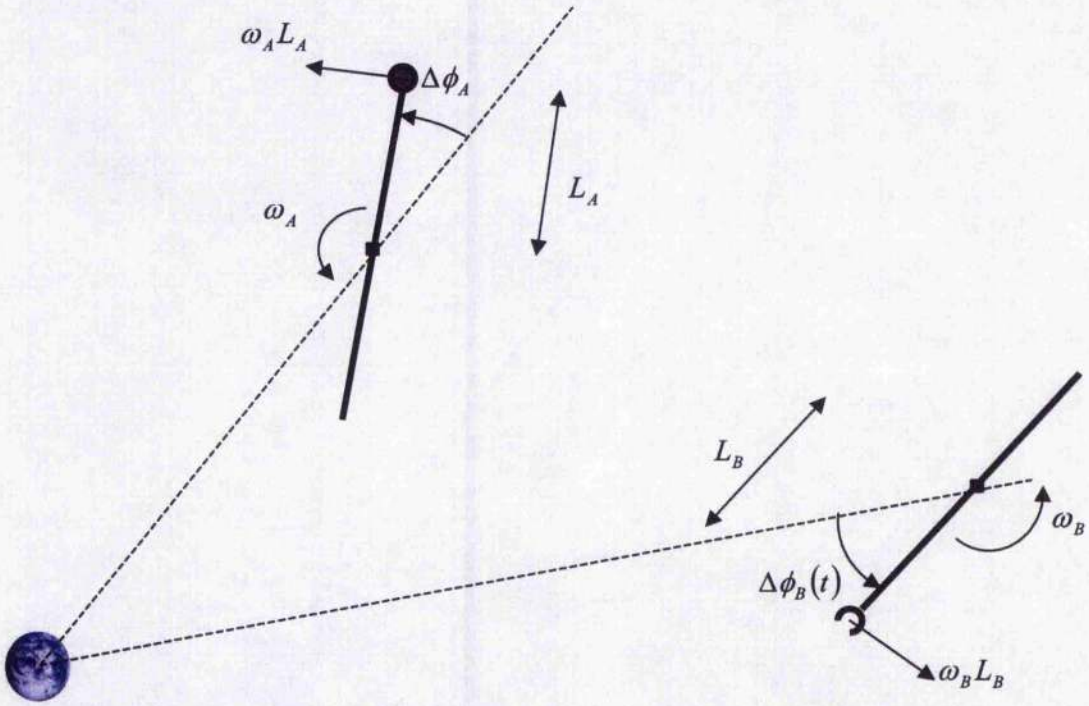

Figure 5.8 Local velocity vector at both the payload and the receiving system tip as a product of angular velocity and sub-span length

Given a constant angular velocity for the sub-spans of both system *A* and system *B*, the magnitude of the local velocity vector normal to the sub-span length for system *A* is equal to the product of the angular velocity at which the sub-spans are rotating about the central facility, ω_A, and the sub-span length, L_A. This product is identified in Fig. 5.8 for both systems *A* and *B*. Given the system orientation relative to the radius from the centre of the Earth to the central facility, the sum of the local velocity at the tip and the velocity vector of the central facility can be characterised in terms of

the sum of all radial components, $\sum v_{r,A}$, and all tangential components, $\sum v_{\theta,A}$, for system A as in Eq. 5.9 and Eq. 5.10, respectively.

$$\sum v_{r,A} = v_A \sin\beta_A - \omega_A L_A \sin\Delta\phi_A \tag{5.9}$$

$$\sum v_{\theta,A} = v_A \cos\beta_A + \omega_A L_A \cos\Delta\phi_A \tag{5.10}$$

With these velocity components, the magnitude of the resulting vector and its heading angle, relative to the central facility, can be found using Eq. 11 and Eq. 12, respectively. It is important to note that the magnitude of this velocity vector is equal to the inertial velocity vector of the payload at release, but the heading angle is presented in terms of the radius from the centre of the Earth to the central facility. To ensure this is highlighted, this heading angle is represented as $\beta_{A|r_A}$. As previously employed, variables that are presented in terms of the payload or the span tip are noted with an apostrophe.

$$v'_A = \sqrt{\left(\sum v_{\theta,A}\right)^2 + \left(\sum v_{r,A}\right)^2} \tag{5.11}$$

$$\beta_{A|r_A} = \arctan\left[\frac{\sum v_{r,A}}{\sum v_{\theta,A}}\right] \tag{5.12}$$

To convert this heading angle into one that is applicable to the payload at release, the angle, φ_A, between (i) the radius to the central facility of system A, r_A, and (ii) the radius from the centre of the Earth to the payload at release, r'_A, must be calculated. This angle is found for system A as in Eq. 5.13:

$$\varphi_A = \arcsin\left[\frac{L_A}{r'_A}\sin\Delta\phi_A\right] \tag{5.13}$$

Using this angle, the heading angle for the payload at release from system A, β'_A, is found as in Eq 5.14.

$$\beta'_A = \beta_{A|r_A} + \varphi_A \tag{5.14}$$

While fundamentally equivalent, care must be taken when solving Eq. 5.9 through Eq. 5.14 for system B as the reference defining $\Delta\phi_B(t)$ is not the same as that defining the same angle for system A. This change in reference modifies the negativity in Eq. 5.9 and Eq. 5.10. If ignored, the end results would be incorrect.

As with the earlier equations, it must be noted that finding the equivalent angle for system B requires the sign to be reversed.

With these initial conditions, the eccentricity and radius of perigee for the orbit associated with the payload at release can be calculated with Eq. 5.15 and Eq. 5.16, respectively.

$$e'_A = \sqrt{\left[\frac{r'_A(v'_A)^2}{K} - 1\right]\cos^2\beta'_A + \sin^2\beta'_A} \tag{5.15}$$

$$r'_{p,A} = \frac{(r'_A v'_A \cos\beta'_A)^2}{K(1+e'_A)} \tag{5.16}$$

Through an understanding of the payload orbit at release, and the location at which the payload must be after a time t to ensure rendezvous with the second MMET system, a transfer orbit can be calculated. Depending on the payload motor size, the payload will either be capable of making the burns required to both enter and exit form this transfer orbit, or the lack of adequate propellant will cause the errors present at the time of release to result in a handover failure.

5.2.4 Defining a suitable transfer orbit

As discussed, a non-optimal payload release can be successfully received by the second MMET system if the payload is placed on a suitable transfer orbit. Knowing the radius from the centre of the Earth to the payload at release, r'_A, and the radius from the centre of the Earth to the payload at the time of rendezvous with the second MMET, r'_B, and the angle between them, γ_T, the eccentricity, e_T, and the orbital location at release relative to perigee, $\theta_{T,A}$, for an appropriate transfer orbit can be found by iteratively solving Eq. 5.17 and Eq. 5.18, simultaneously.

$$\frac{r'_B}{r'_A} = \frac{1 + e_T \cos\theta_{T,A}}{1 + e_T \cos\left(\theta_{T,A} + \gamma_T\right)} \tag{5.17}$$

$$\psi_{B'} - e_T \sin\psi_{B'} = t\sqrt{\frac{K\left(1 - e_T\right)^3}{\left(r_{p,T}\right)^3}} + \psi_{A'} - e_T \sin\psi_{A'} \tag{5.18}$$

When solving Eq. 5.18, $\psi_{A'}$ and $\psi_{B'}$ are defined as in Eq. 5.19 and 5.20.

$$\cos\psi_{A'} = \frac{a_T - r'_A}{a_T e_T} \tag{5.19}$$

$$\cos\psi_{B'} = \frac{a_T - r'_B}{a_T e_T} \tag{5.20}$$

Once a suitable transfer orbit is found, as with the central facility of each MMET system, the parameters of the transfer orbit will dictate the magnitude of the velocity vector and the heading angle at any location on the transfer orbit. Upon release from the first MMET system, the motor must provide an impulse such that the velocity vector plus the imparted velocity provided by the motor produces the magnitude of the velocity vector and heading angle as identified in Eq. 5.21 and Eq. 5.22. At rendezvous with system *B*, Eq. 5.21 and Eq. 5.22 will calculate the velocity and heading angle for the payload on the transfer orbit at the location of rendezvous.

$$v'_{T,A} = \sqrt{K\left(\frac{2}{r'_A} - \frac{(1-e_T)}{r_{p,T}}\right)} \tag{5.21}$$

$$\beta'_{T,A} = \arccos\left[\frac{\sqrt{Kr_{p,T}(1+e_T)}}{r'_A v'_{A|T}}\right] \tag{5.22}$$

At the time of release, the velocity vector and heading angle produced by system A, and calculated using Eq. 5.11 and Eq. 5.12, must be modified using an impulse to achieve the vector magnitude and heading calculated using Eq. 5.21 and Eq. 5.22. At rendezvous with system B, the velocity magnitude and heading calculated using Eq. 5.21 and Eq. 5.22, using parameters that appropriately correspond to system B, must be modified with an impulse to produce the velocity magnitude and heading associated with the receiving end of system B, as calculated using Eq. 5.11 and Eq. 5.12.

These required impulses for entry onto and exit from this transfer orbit are identified in Fig. 5.9, as well as the velocity vector produced by system A at release and required by system B at rendezvous. Upon entry and exit, an impulsive thrust with a magnitude of Δv_A at release, and Δv_B at rendezvous with system B, must be applied to the payload at a heading angle of $\beta_{\Delta A}$ and $\beta_{\Delta B}$, respectively.

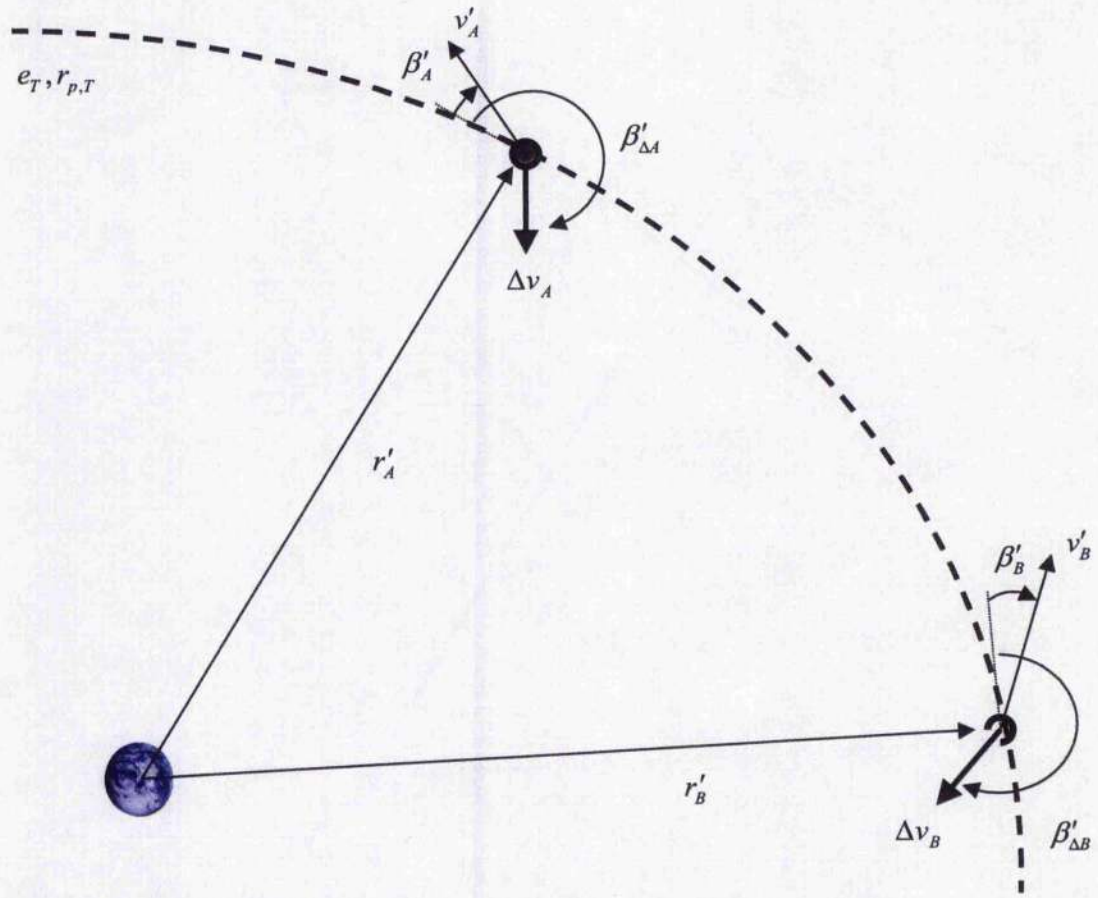

Figure 5.9 Diagram of the impulses and their directions required to enter, and then exit, the transfer orbit

The magnitude of the velocity vector and the heading angle of the impulse burn must be sufficient upon release such that the Eq. 5.23 and Eq. 5.24 agrees with Eq. 5.21 and Eq. 5.22.

$$v'_{T,A} = \sqrt{\left(v'_A \cos\beta'_A + \Delta v_A \cos\beta_{\Delta A}\right)^2 + \left(v'_A \sin\beta'_A + \Delta v_A \sin\beta_{\Delta A}\right)^2} \tag{5.23}$$

$$\beta'_{T,A} = \arctan\left[\frac{v'_A \sin\beta'_A + \Delta v_A \sin\beta_{\Delta A}}{v'_A \cos\beta'_A + \Delta v_A \cos\beta_{\Delta A}}\right] \tag{5.24}$$

When exiting the transfer orbit, the impulse and direction must be such that Eq. 5.25 and Eq. 5.26 are consistent with Eq. 5.11 and Eq. 5.12, when solved for system *B*.

$$v'_B(t) = \sqrt{\left(v'_{T,B}\cos\beta'_{T,B} + \Delta v_B \cos\beta_{\Delta B}\right)^2 + \left(v'_{T,B}\sin\beta'_{T,B} + \Delta v_B \sin\beta_{\Delta B}\right)^2} \tag{5.25}$$

$$\beta'_B(t) = \arctan\left[\frac{v'_{T,B}\sin\beta'_{T,B} + \Delta v_B \sin\beta_{\Delta B}}{v'_{T,B}\cos\beta'_{T,B} + \Delta v_B \cos\beta_{\Delta B}}\right] \tag{5.26}$$

To properly size the motor required for a sufficient level of mission assurance, the payload, M_p, and the initial motor mass, $M_{M,0}$, must be capable of producing all impulses required for the mission. This total impulse is equal to the sum of the impulses at both entry and exit. Using the rocket equation, the relationship between total impulse required for completing the rendezvous and the payload and initial motor mass are related as in Eq. 5.27, assuming all propellant is burnt after both operations, and assuming the motor characteristic is represented by the variable ν.

$$\Delta v_A + \Delta v_B = \nu \log\left(\frac{M_{M,0} + M_p}{M_p}\right) \tag{5.27}$$

With the rocket equation, which offers a relationship between change in propellant mass and impulse, the number of attainable orbits for a given motor size out of the number of possible orbits within reasonable parameters could be determined. From here, a probability of success could be developed per motor size.

It is unlikely that this probability of success estimate could be appropriately modelled with a standard normal distribution. For example, if the error in orbital angle is negative for the releasing system while it is positive for the receiving system, the probability of success is likely higher for a set motor size than it would be if the angle were reversed. Examining a sufficient number of combinations such that a probability of success for each motor size can be computed would require

development of an algorithm specifically designed with the equations presented above. Such an analysis has not been performed in support of this research.

5.3 LSM mission: handover risk

For the LSM mission, it is assumed that the analyst has appropriately sized a kick motor based on the errors specific to the employed MMET systems. If such a sizing has been conducted appropriately, it is assumed that the probability of successful rendezvous is in line with all other systems, being a probability of 0.997 that rendezvous will succeed at each stage.

Table 5.2 Values currently calculated for the LSM mission risk assessment.

	Conventional	**MMET-based**
C_{LV}	\$254M	\$70M
$C_{MMET,1}$	--	
$C_{MMET,2}$	--	
$p_{f,LV}$	0.003	0.003
$p_{f,H1}$	--	0.003
$p_{f,T1}$	--	
$p_{f,H2}$	--	0.003
$p_{f,T2}$	--	

Chapter 6

MMET Reliability

Chapter 6 through Chapter 10 address the probability of failure associated with an MMET system. Chapter 6 through Chapter 9 describe the experimental and analytical work that was done to develop a sufficient reliability estimate for the system. Chapter 6 presents an examination of the strength of aramid fibres like those that would be employed in space tether structures; Chapter 7 presents an empirical equation for predicting the outcome of hypervelocity impacts with tether structures; Chapter 8 presents work performed in the hypervelocity impact facility at the University of Kent, work that was performed to examine both (i) whether secondary debris clouds form as a result of an initial debris impact with a tether target and (ii) how such clouds propagate; and Chapter 9 discusses a Monte Carlo-based analysis approach for employing these previous elements to calculate reliability estimates for a momentum exchange tether system. Chapter 10 uses this analytical framework to assess the reliability of various tether configurations that could be employed for the LSM mission.

6.0 Background on aramid fibre strength testing

Of the researched tether concepts, Kevlar fibres are often a main structural component. While aramid fibres are reported to be extremely strong relative to their weight, this strength is identified in works such as Allen *et al.* (1992), Benhoulo *et al.* (1997), and Wang and Xia (1999), to vary as a result of factors such as loading rate or environmental conditions. Representative samples must be tested in order to understand how much, and under what conditions, this strength varies. Aramid fibres, such as Kevlar and Twaron, are increasingly popular for a wide range of uses. From bulletproof vests to space vehicle structures, these fibres exhibit properties that are uniquely beneficial to each intended use. Apart from its various benefits, one of the rare qualities aramid fibre possesses is its variation in strength as a function of load-rate.

The strength of a rope is often characterized by its *break strength*, which is the tensile force required to break the rope. For aramid fibres, it has been observed that the strain-rate has a significant impact on the break strength. In many cases, this difference could be on the order of 20% or more. If an aramid fibre strand, or rope composed of aramid fibre strands, is loaded at its optimal strain-rate, the observed break strength will be at a maximum. However, there are a number of factors affecting this optimum strain-rate, not all of which have been fully investigated or have become understood.

For the design of systems relying on aramid fibres to provide structure, understanding this optimal strain-rate could be significantly beneficial. By optimising a system so as to ensure aramid fibre members are loaded most effectively, significant increases in performance could be seen. This investigation provides a number of important data points for assessing how break-strength varies with strain-rate in aramid fibres, and how multi-strand braided rope performs as the number of constituent strands increases.

6.1 Material specifics: Twaron

The aramid fibre examined during this work was Twaron, produce by the Teijin Twaron Company.[x] The Teijin Twaron Company has classified each strand that made up the tested rope samples as Twaron 1680 dtex. Each strand of Twaron is a bundle of individual fibres, those fibres being oriented mostly parallel to each other.

Yarns and fabric strands are measured using two main types of linear density: a tex and a denier. A *tex* is the mass, in grams, of a piece of yarn or fabric strand that is1000 metres long and a *denier* is the mass per 9000 metres. The abbreviation *dtex* is short for decitex, and one *decitex* is the mass, in grams, of a yarn or fabric strand that is 10 000 metres long (i.e., one dtex is equal to 10 tex). For the Twaron tested during these experiments, while they are labelled as being 1680 dtex, Teijin Twaron measures its actual linear density to be 1730 dtex, as presented in Table 1. Table 1 also presents a number of other material characteristics reported by the manufacturer.

Table 6.1: Properties for the Twaron used in this work, as provided by Teijin Twaron on the data sheet designated as 04-007.

Mechanical Characteristics		
Linear density (Named)	1680	dtex
Linear density (Measured)	1730	dtex
Break strength (N)	350	N
Tenacity (mN/tex)	2023	mN/tex
Elongation at Break	0.0355	
Cord-Modulus (ASTM, GPa)	71	GPa

Properties		
Density of the polymer	1440 - 1450	kg/m3
Limiting Oxygen Index (LOI) depending on application	29, 36	% (powder, rope)
UV stability	Not good, needs protection	
Hydrolysis (water or steam)	Depending on temperature, severe strength loss occurs	
Decomposition temperature	> 450	°C
Heat resistance at 200°C , 48 hrs (residual strength)	90%	%
Linear coefficient of thermal expansion (axial, lateral)	-3.5, +2	ppm/K
Moisture content (dependent on stock circumstances)	4, 7	% (high, low)
Specific heat	1.42	J/gK

A quality of Twaron that is not noted in Table 6.1 is the strain-rate dependence of break strength. Such dependence is observed using charted results provided by Teijin Twaron and presented in Fig 6.1. This chart shows, for fibre strands that are twisted a stated amount, the break strength of those strands as a function of strain-rate. From Fig 6.1, it appears that the material break strength reaches a local maximum when the strain is increased at a rate between 9% and 20% per minute. While this rate seems to shift with the differing amount of twist experienced by the strand, it is assumed that each will have a local maximum that is not significantly greater than 100% strain per minute.

It is also important to note that the equipment used for this experimentation at the University of Glasgow was unable to replicate the results presented in Fig 6.1 because of equipment load-rate limitations. As the tensile testing machine used during these experiments was not capable of achieving an extension per minute of greater than 200 mm, and the minimum sample length required by the clamps is around 300 mm, the available equipment was not able to exceed the theoretical limit of 66% strain per

minute. As seen later in the presented results, the maximum strain rate used for this investigation was just less than 26%.

Another item of note when examining Fig 6.1 is that the break strength increases as the amount of twist increases before falling back significantly after the maximum presented at 80 rotations per metre. While it is not known what causes the increase in break strength for samples that are twisted less than or equal to 80 rotations per metre, it is assumed that the significant decrease after a certain threshold, a threshold that is believed to be at or around the 80 rotations per metre based on the information provided by Teijin Twaron and presented in Fig. 6.1, is due to inter-fibre (i.e. intra-strand) friction.

The final item that may be of interest when comparing the results presented in Fig 6.1 to the data presented in Table 6.1 is the correspondence of the maximum break strength cited for Twaron as being equivalent to an approximation of the local maximum for a Twaron strand subjected to a twist rate of 80 rotations per metre. Noting this is important in any future work that may be attempted with regards to modelling the Twaron rope. While it is assumed that there is no significant twist in the strands as they are braided into rope, as discussed below, a more accurate model of the manufacturing process would need be incorporated into any model of the rope strength and internal interactions.

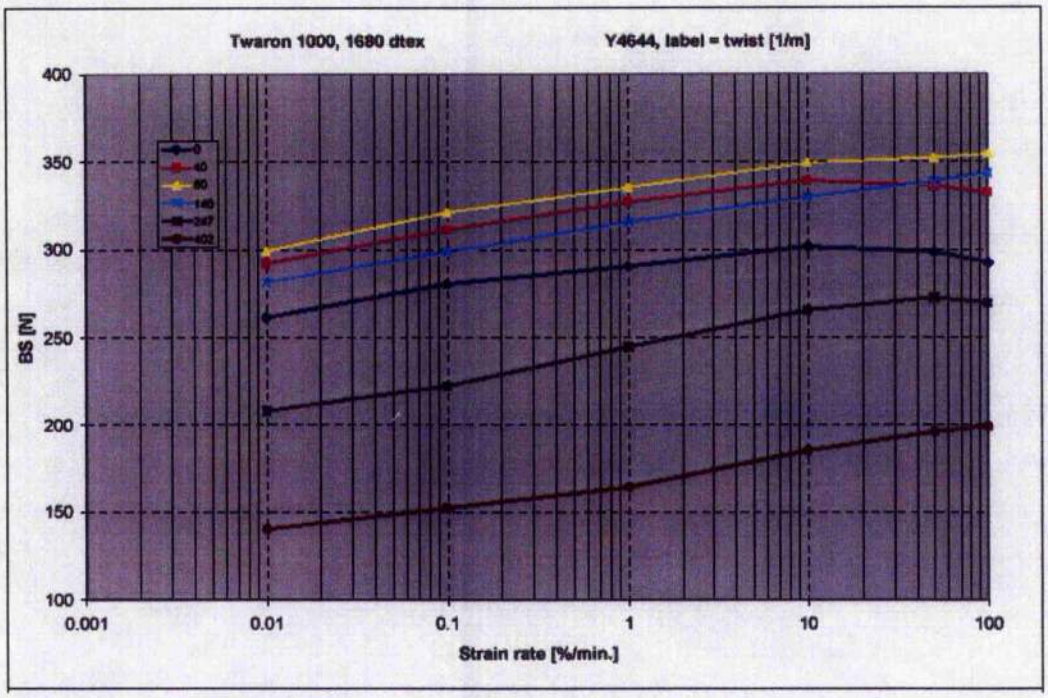

Figure 6.1: Twaron 1000, 1680 dtex, graph of break strength (N) verses strain rate for various amounts of material twist. This figure is supplied courtesy of Teijin Twaron, document number "Y4644+6649+6650+6962-Rate.xls / FigRate".

6.2 Manufacturing Twaron rope

The Twaron ropes examined in this work were manufacture by Culzean Fabrics of Kilmarnock, Scotland, using Teijin Twaron 1680 dtex Twaron strands. Two variations were examined for this work, one composed of four braided strands and one composed of eight braided strands. The strands were not pre-twisted before they were braided, nor were they intentionally twisted during the braiding process. The braiding process employed a standard over-over technique. A picture of a four-strand braided specimen is presented in Fig 6.2, separated so the braiding pattern can be observed. Also of note from the picture is the fact that the strands do not appear twisted relative to the braiding.

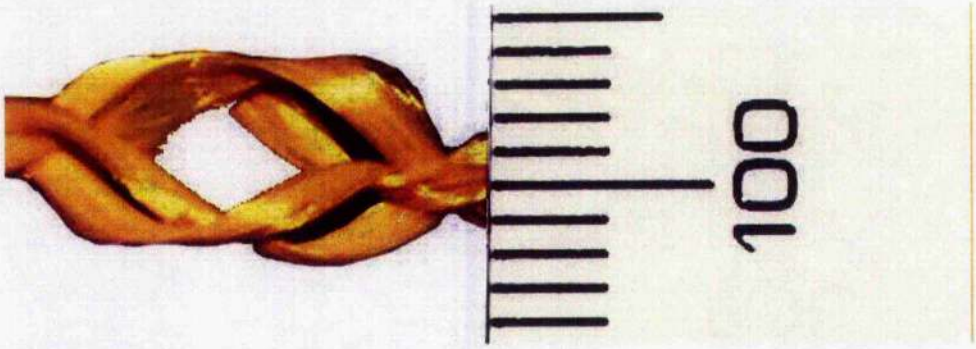

Figure 6.2: View of Twaron strands, spread to illustrate the braid pattern used in both the four-strand and eight-strand rope samples.

The eight-strand braid, which is not pictured, is identical in pattern to the four-strand rope.

6.3 Test apparatus

The four-strand and eight-strand Twaron ropes were tested using a Lloyds 10000, 50kN tensile testing machine. While the machine capability included loads up to 50kN, a 5kN load cell was used for these experiments, as its capability was more similar to the anticipated maximum loads. The test apparatus did not include feedback sensors, so each tensile test was conducted under a uniform extension rate set at a specific millimetre per minute rate for each test.

The Twaron rope samples were held during the tests using a split-cylinder clamp system, manufactured at the University of Glasgow. Each clamp is composed of a cylinder post, which is fastened to the base; and a split cylinder, which is not attached to either the base or the cylinder post. These components are identified in Fig 6.3. This split-cylinder design is not unique, as it is readily available within the yarn testing and manufacturing industry. The split-cylinder clamp manufactured by the University of Glasgow incorporated a free split cylinder (i.e., one that was not attached to the cylinder post when not in a test configuration) because of cost and manufacturing complexity considerations. This design did not produce any adverse effect on the results because all specimens were loaded into the clamps such that sample slack was removed prior to the specimen being pre-loaded. Once loaded, the

tension in the test specimen holds the split-cylinder clamp together, effectively self-securing the test specimen within the clamp. When placed together, the cylinder post and the split-cylinder are termed the *cylinder* within this work.

For these tests, each test specimen was wrapped around the cylinder for three full turns. As the free end of the specimen is clamped between the cylinder post and the split-cylinder, these three turns are counted from where the specimen exits this flat clamp face. Three turns were used because (i) it was observed that the free end did not noticeably slip in this configuration and (ii) every test that was conducted with fewer than three turns resulted in the specimen failure occurring outside the guage length, often somewhere on the cylinder and generally at the edge of the flat clamp face.

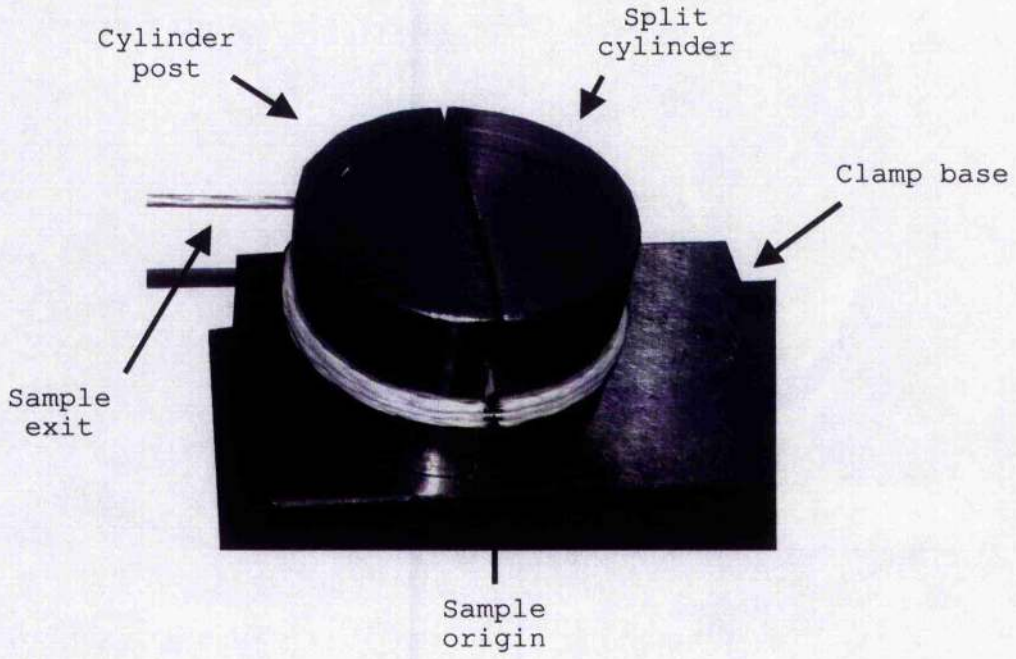

Figure 6.3: Illustration of the split-cylinder clamp securing a specimen in the test configuration.

To aid in the observation of sample slip around the cylinder and between the flat clamp faces, after loading the specimen into each clamp, the samples were marked at

the flat clamp face. These marks can be seen in Fig 6.3 just below the free end, called the *sample origin* in the picture. By marking all three loops on both sides of the flat clamp face, it was also observed that elongation occurred in the specimen for all locations along the cylinder and that the free end did not significantly slip from its original position.

After securing and marking the specimen using both split-cylinder clamps, the clamps were loaded into the tensile testing machine. A picture of the loaded machine is seen in Fig 6.4. Also in Fig 6.4 is a full view of the specimen loaded between the two split-cylinder clamps, with the gauge length identified. The gauge length is the distance between where each specimen begins to leave the split-cylinder clamps. For each test reported in this thesis, the specimen broke within this gauge length.

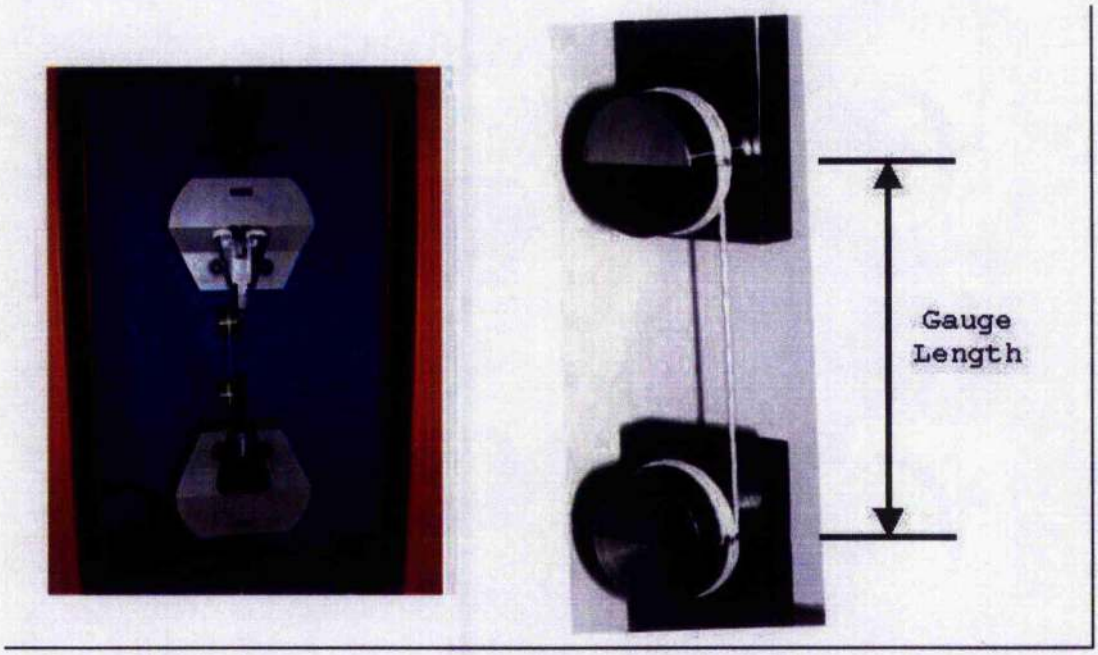

Figure 6.4: View of a sample in test configuration (left) and a close-up view of the specimen within the split-cylinder clamps, identifying the gauge length.

Once each specimen was loaded into the Lloyds machine, it was preloaded to 20kN, with a standard deviation of around 3kN, and the test conducted until failure. The test

finished when a significant portion of the specimen had failed due to tension in the strands.

6.4 Test results and discussion

Each test was named as per the designation system presented in Table 6.2. This naming system was used to aid in the data analysis by identifying the test conditions within the name.

Table 6.2 Naming system used to identify each test.

Test Designation: **XYWZZZZ**

X = Material type (T = Twaron, D = Dyneema)
Y = Number of strands composing specimen (Numeric)
W = Structure (S = Independent Strands, B = Braided)
Z = % elongation per minute, multiplied by 100 (4-digit numeric)

Using the naming system identified in Table 6.2, 13 successful tests were carried out on the rope specimens. A successful test was one where the specimen failure occurred within the gauge length. More tests were conducted with the four-strand braided rope because the distribution of results was not as expected. Since the eight-strand braided rope testing occurred after the data analysis of the four-strand results was completed, fewer tests were conducted on the eight-strand because the results, as they were obtained, were in closer agreement with the properties observed from the four-strand testing.

Table 6.3: Test Results

Test	Guage Length (mm)	Total Length (mm)	Pre-Load (N)	Extension mm/min	Strain /min	Break Force (N)	Stress at Break (MPa)
T4B0860	94	814	22	70	0.086	858	17861
T4B0915	45	765	27	70	0.092	1035	21528
T4B1261	81	801	20	101	0.126	1072	22306
T4B1414	93	813	20	115	0.141	961	19996
T4B1514	86	806	18	122	0.151	1080	22465
T4B1776	91	811	19	144	0.178	941	19583
T4B2026	75	795	22	161	0.203	1040	21647
T4B2555	63	783	20	200	0.256	886	18432
T8B0994	65	795	20	79	0.099	1451	15102
T8B1246	73	803	24	100	0.125	1849	19234
T8B1499	91	821	24	123	0.150	1723	17932
T8B1746	112	842	23	147	0.175	1443	15011
T8B1983	57	787	21	156	0.198	1046	10879

Using the results presented in Table 6.3, a second order polynomial was fitted to each data set using normal linear regression techniques. These regression lines are identified in Fig 6.5 and Fig 6.6, along with each data point.

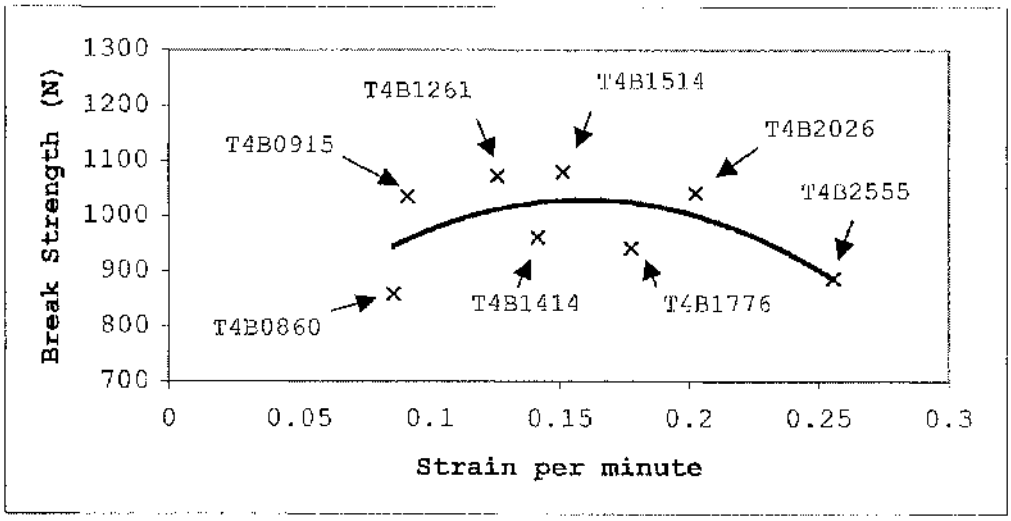

Figure 6.5 Break strength, in Newtons, as a function of percentage elongation per minute for ropes composed of four, simply braided Twaron strands.

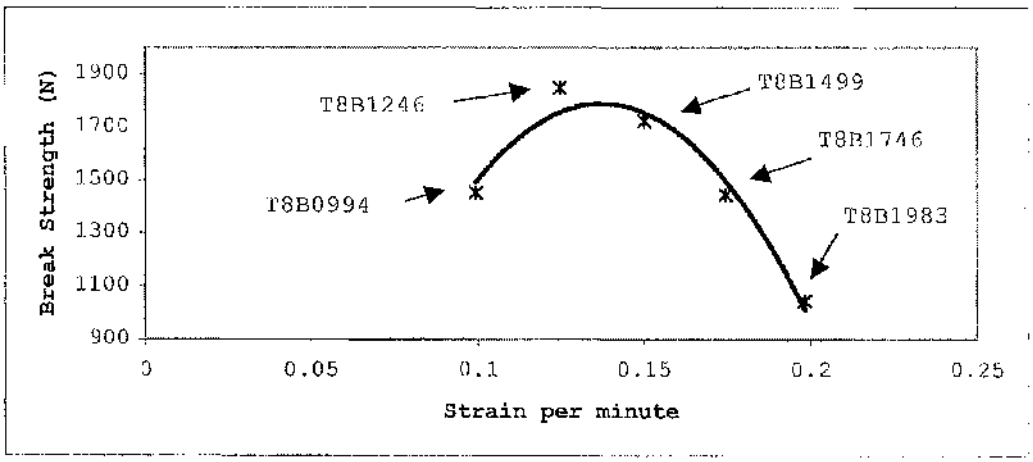

Figure 6.6 Break strength, in Newtons, as a function of percentage elongation per minute for ropes composed of eight, simply braided Twaron strands.

With this regression line, the standard deviation of the dataset was calculated based on error relative to this regression line. This use of the regression line in the calculation of standard deviation is assumed to be valid because the regression technique assumes the data points are normally distributed around the true values. After calculating the variance and standard deviation, a qualitative check for heteroskedacity did not raise concerns about the data fit.

The maximum break force observed during the testing of each rope, the maximum break force calculated using the regression curve, and the standard deviation associated with the regression curve are presented in Table 6.4. Of note, the maximum break force observed for the four-strand braided rope is well within one standard deviation of the calculated maximum break force, while the tested maximum for the eight-strand rope is barely within the one-sigma level. This is likely to be dependent on the number of tests, and is not an indication of greater variability in the eight-strand braided rope caused by an unknown mechanical explanation.

Table 6.4 Tested and calculated maximum performance for each rope.

	Max Break Force Tested (N)	Max Break Force Calculated (N)	Standard Deviation (N)
T4B*	1080	1028.79	67.87
T8B*	1849	1788.45	61.92

Also based on the calculated regression curves, Table 6.5 presents the strain per minute at the maximum calculated break force for each of the four-strand and eight-strand rope. While inconclusive based only on the limited number of data points presented in Fig 6.1, the results of Table 6.5 could be used in a model of the rope specimens to determine how much effective twist is present in each of the specimens. Understanding the amount of twist that is produced by the braiding process could allow for an optimisation of the braiding machine (i.e., the strands could be loaded with a certain pre-twist that produces an optimised amount of twist after that inherent in the braiding process is applied).

Table 6.5: Strain rate at calculated maximum break strength.

	Strain per minute at Max Break Strength
T4B*	15.96%
T8B*	13.72%

From previous observations, it was noted that the fibres within each braided strand do not appear to be twisted relative to the longitudinal axis of the strand. This would imply that the effective twist within each strand relative to the longitudinal axis of the rope is directly dependent on the number of strands present in the braid (i.e., for fewer strands, the twist is greater). This conclusion of *effective twist*, relative to the rope, seems to be supported by the decrease in the optimum strain per minute as the number of strands increase. From Fig 6.1, it is clear that the optimum strain rate increases with an increasing amount of twist for relatively low twist levels. While a qualitative

assessment of the eight-strand rope calculates the twist to be on the order of 50 revolutions per metre, thus placing both the four-strand and eight-strand rope into the low twist levels where a direct correlation is seen between optimum strain rate and twist, more research must be done in this area before these results of a twist/braid relationship can be accepted as anything more than anecdotal evidence.

6.5 Conclusions

The results presented in this chapter support the assertion that the maximum break strength of aramid fibres is directly related to strain rate. For many applications, understanding the quantity of this effect and the factors that would allow designers to maximise the potential of this effect is vital. As an independent assessment of the assertions made by Teijin Twaron about their product, the results of this work are very important to the materials community.

While important, this work is only a first step of the many required in the development of suitable models of aramid fibre interaction and performance when aramid strands are oriented into braided ropes and applied in space tether design. As an example of further work that must be completed for space tether applications, an important consideration examined by Wang and Xia (1999) is the effect of temperature on aramid strength. Consistent with the majority of available literature, while Wang and Xia (1999) focuses on research intended to offer insight into the ballistic properties associated aramid fabrics, the extreme temperature variations experienced by spacecraft offers cause for concern that the temperature relationships identified in Wang and Xia (1999) may significantly influence structural tether elements. While the dataset presented herein is too small to offer any more than circumstantial conclusions, this work does also offer evidence that (i) the strain rate produced during an MMET operation and (ii) the amount of twist in a braid has a direct effect on the break strength of an aramid rope. After further testing, this insight can be used to optimise manufacturing processes and MMET operations.

Chapter 7

Empirical Impact Equations

In the previous chapter, it was verified that the strength of a tether depends on the rate at which it is loaded. Further, with such a significant variability based on load, it must be assumed that the strength of the tether is not suitable for use as an input within empirical models. Such an assumption has significant consequences with regards to the empirical hypervelocity impact equations that would then be available to a tether-based system analyst, so a new equation must be developed for such a purpose.

7.0 Introduction

As mission planners look for systems to further reduce the cost of access to space, tether-based propulsive systems have gained considerable interest. However, the unique size and nature of space tether systems raises new analysis issues. While the failure equations, and their application, for assessing conventional on-orbit systems are known and widely accepted as suitable for traditional spacecraft, many of the assumptions and calibrations these equations employ are not suitable for tether-based systems.

All publicly available failure analyses of space tether systems have focused on environmental failures caused by particle impact, the most hazardous of such potential impactors being orbital debris. While it is always recommended that unconventional systems be tested in flight configuration to ensure analytical predictions are suitable, past tether failure analyses have employed empirical equations that approximate the results of a hypervelocity impact. While experimental tether impact analyses, such as those done in Hayashida and Robinson (1993), McBride and Taylor (1993), and Penson and Burchell (2003), perform predictions using equations such as the Fish-Summers and 1992C equations, respectively, and hypervelocity impact tests to experimentally assess the damage to tether strands, none have directly compared the result of experimental work with the predicted results in a manner that is more scientifically rigorous than qualitative observation.

This work takes a fresh look at the issue of empirically modelling hypervelocity impacts in the hopes of finding an equation that is better suited to analysing a tether-based space system.

7.1 Past work

The focus of this research is to aid risk analysis practitioners in their assessment of space tether systems. To this end, this research focuses on all known, empirically derived hypervelocity impact equations that have been applied either during a spacecraft development program or a space tether system lifetime assessment. Therefore, this work investigates the semi-infinite forms of the Fish-Summers, Schmidt-Holsapple, Rockwell, Cour-Palais, Modified Cour-Palais, and 1992C equations.

Starting in 1964, NASA began issuing space vehicle design criteria to offer designers uniform guidance with regards to the unique issues and challenges posed by the space environment. Such guidance was contained in documents such as Cour-Palais (1969) and Frost (1970), which offer guidance on protecting spacecraft from hypervelocity debris impacts through the use of empirical, environmental, and shielding models that were stated in these documents as being acceptable to NASA at the time. Later examination of these impact models by Hayashida and Robinson (1991) and the subsequent use of the Fish-Summers equation within the researched presented in Hayashida and Robinson (1993) indicate that these models are still acceptable to NASA.

During the Apollo program, NASA independently developed two impact equations, both of which accounted for material hardness. The first presented here was the Rockwell equation. The second is the Cour-Palais equation, as it is commonly referred to today, which was modified in the in the late 1980s and subsequently termed the Modified Cour-Palais equation.

It may be reasonable to note that none of the following equations are dimensionally balanced, although some do use dimensionless terms. This is not unusual for

empirical equations since they model effects and rarely employ a representation of the governing mechanism.

7.1.1 Fish-Summers

The Fish-Summers equation for semi-infinite targets was first introduced in May 1970 by V.C. Frost and is based on the hypervelocity impact studies conducted by R.H. Fish and J.L. Summers of NASA Ames Research Center. For application of the equation, Frost (1970) describes a semi-infinite body as one where "the depth of penetration [is] a small fraction of the plate thickness." Frost (1970) states that, if the penetration depth, relative to the target thickness, is limited to "25 percent or less, the plate may be considered semiinfinite [sic]." The semi-infinite form of the Fish-Summers equation is defined as in Eq. 7.1.

$$p = K_{\infty} m^{0.352} \rho_p^{\frac{1}{6}} v_n^{\frac{2}{3}} \tag{7.1}$$

Where

p = crater depth (cm)

K_{∞} = material constant for target

m = projectile mass (g)

ρ_p = projectile density (g/cm^3)

v_n = normal component of impact velocity (km/sec)

For the semi-infinite form of the Fish-Summers equation, the material constant is again defined by material properties and temperature. In Frost (1970), it is recommended that any unknown material constants must be found using hypervelocity testing, and the only two known constant values at the time of publication are reported to be 0.42 for Aluminium alloys and 0.25 for stainless steel. The results using the semi-infinite form of the Fish-Summers equation are considered by Frost (1970) to be "satisfactory" if not "somewhat conservative at the higher meteoroid velocities" since the experimental data was obtained at velocities at or

below 8 km/sec and extrapolated out. While deemed suitable for ductile metals, Eq 7.1 is identified in Frost (1970) to be of little use for low-ductility metals and "generally unsuitable for nonmetals [sic]."

According to Hayashida and Robinson (1993), a tether does not only fail when it is severed, but fails when it becomes incapable of carrying its designed load. Depending on mission design, any degradation in performance could be considered failure. In Hayashida and Robinson (1993), the authors consider a failure to have occurred when a tether is cratered such that the impact removes half of the cross sectional area at any point on the tether. For this reason, the authors are not as concerned with the ballistic limit, which would correspond to a severed tether, as they are the minimum crater resulting in failure. Consequently, assuming the tether can be modelled as one target of uniform density and known thickness, failure is best thought of as a crater past an allowable threshold within a semi-infinite body.

The calculations in Hayashida and Robinson (1993) employ the Fish-Summers equation for a semi-infinite material, presented above, even though the failure criterion used in the work violates the definition of semi-infinite, as presented in Frost (1970). For the material constant required by the Fish-Summers semi-infinite equation, Hayashida and Robinson (1993) employs a linear interpolation using previously studied materials to find any target's material constant as a function of its density. By placing the density dependent function of material constant into the Fish-Summers equation as used in Hayashida and Robinson (1993), the penetration depth for an impactor into a semi-infinite plate is as follows:

$$p = \left(0.51296 - 0.033203\rho_t\right) m_p^{0.352} \rho_p^{\frac{1}{6}} v_n^{\frac{2}{3}} \tag{7.2}$$

Where

p = crater depth on target (cm)

m_p = projectile mass (g)

ρ_p = projectile density (g/cm^3)

ρ_t = target density (g/cm^3)

v_n = normal component of impact velocity (km/sec)

Using a linear interpolation, when indications support a theory that only two known data points were available, seems questionable. Further, considering the views of Frost (1970) with respect to applying the Fish-Summers equation to non-metal targets, one could argue that Eq 7.2 has an unacceptable level of uncertainty associated with it. However, considering the extensive work both researchers had previously performed on hypervelocity impacts, and since Cour-Palais (1969) and Frost (1970) are both referenced in Hayashida and Robinson (1993), it is only fair to assume the calculations and assumptions made in Hayashida and Robinson (1993) are appropriate. There is no indication identified in Hayashida and Robinson (1993) that the experimental results did not correspond to the anticipated results using the Fish-Summers equation for semi-infinite bodies. For these reasons, although there is reasonable doubt about the applicability of Eq 7.2, one cannot immediately rule out the work and results presented in Hayashida and Robinson (1993) without further investigation.

7.1.2 Rockwell

Hayashida and Robinson (1991) state that the Rockwell equation was developed using aluminium impactors and targets with impact velocities up to 8 km/sec. Using material hardness, target density, and projectile density, the Rockwell equation is presented in Hayashida and Robinson (1991) as in Eq. 7.3.

$$\begin{aligned} p &= 1.38 d^{1.1} B H^{-0.25} \rho_p^{0.5} \rho_t^{0.167} v_n^{0.67} \\ t_b &= 1.8 p \\ t_s &= 3.0 p \end{aligned} \tag{7.3}$$

Where

p = crater depth on target (cm)

t_b = target thickness for ballistic limit (cm)

t_s = target thickness for spallation limit (cm)

d = projectile diameter (cm)

ρ_p = projectile density (g/cm^3)

ρ_t = target density (g/cm^3)

BH = Brinnell hardness for target

v_n = normal component of impact velocity (km/sec)

7.1.3 Cour-Palais

At the same time as the Rockwell equation, NASA developed a second equation called the Cour-Palais equation. While similar to the Rockwell equation, the Cour-Palais equation has a stated restriction, identified by Hayashida and Robinson (1991), that the ratio of projectile density to target density must be less than 1.5 to ensure valid results. While the purpose for this limiting density ratio is not explained in Hayashida and Robinson (1991), and any justification for this limit would be speculative in nature without input from the experimentalists involved in the creation of the equation, it may be reasonable to assume that the non-linear regression trends discussed in Yu *et al.* (1994) began to dominate the results and became evident to experimentalists after this ratio was exceeded. As the Cour-Palais equation employs the normal velocity term raised to the power 2/3, as discussed in Yu *et al.* (1994), this explanation for the reason a limiting density ratio is presented for the Cour-Palais equation is reasonable. Hayashida and Robinson (1991) presented the Cour-Palais equation as in Eq. 7.4.

$$\begin{aligned} p &= 5.24 d^{1.056} BH^{-0.25} \rho_p^{0.5} \rho_t^{-0.167} E^{-0.33} v_n^{0.67} \\ t_b &= 2.0 p \\ t_s &= 3.0 p \end{aligned} \tag{7.4}$$

Where

p = crater depth on target (cm)

t_b = target thickness for ballistic limit (cm)

t_s = target thickness for spallation limit (cm)

d = projectile diameter (cm)

ρ_p = projectile density (g/cm^3)

ρ_t = target density (g/cm^3)

BH = Brinnell hardness for target

E = Young's modulus for target (GPa)

v_n = normal component of impact velocity (km/sec)

7.1.4 Modified Cour-Palais

The Cour-Palais equation was modified and released in 1991 as the Modified Cour-Palais equation, presented as follows:

$$p = 5.24 d^{\frac{19}{18}} BH^{-0.25} \left(\frac{\rho_p}{\rho_t}\right)^{0.5} \left(\frac{v_n}{C}\right)^{\frac{2}{3}}$$
$$t_b = 1.8p \qquad (7.5)$$
$$t_s = 2.2p$$

Where

p = crater depth on target (cm)

t_b = target thickness for ballistic limit (cm)

t_s = target thickness for spallation limit (cm)

d = projectile diameter (cm)

ρ_p = projectile density (g/cm^3)

ρ_t = target density (g/cm^3)

BH = Brinnell hardness for target

v_n = normal component of impact velocity (km/sec)

E = Young's modulus for target (GPa)

C = speed of sound in the target (km/sec)

$$C = \sqrt{\frac{E}{\rho_t}}$$

As one can see by examination, the Modified Cour-Palais equation appears to have adopted some aspects of the Rockwell equation during its modification from the original form of the Cour-Palais equation.

7.1.5 1992C

According to both Penson and Burchell (2003) and McBride and McDonnell (1999), after conducting hypervelocity impact tests with impact velocities up to 16 km/sec and further verifying such results with "impact plasma to > 100 km s^{-1}", McDonnell and Sullivan developed the '1992C' equation at Kent University. In subsequent work, this equation was used as a prediction tool for tether impacts in work such as McBride and Taylor (1997) and Penson and Burchell (2003). The '1992C' equation is presented in Eq. 7.6.

$$F_{max} = 1.64 d_p^{1.056} v_n^{0.805} \left(\frac{\rho_p \rho_{Al}}{\rho_{Fe} \rho_t} \right)^{0.476} \left(\frac{\sigma_{Al}}{\sigma_t} \right)^{0.134} \tag{7.6}$$

Where

F_{max} = ballistic limit (m)

d_p = impactor diameter (m)

v_n = normal component of impact velocity (km/sec)

ρ_p = projectile density (kg/m^3)

ρ_t = target density (kg/m^3)

ρ_{Al} = density of aluminium (kg/m^3)

ρ_{Fe} = density of iron (kg/m^3)

σ_t = yield stress of target (MPa)

σ_{Al} = yield stress of aluminium (MPa)

Although not explicitly stated in Penson and Burchell (2003) or McBride and Taylor (1997), the 1992C equation both exhibits characteristics of a standard thin-plate equation and is applied as such. With regards to its characteristics, the normal velocity component is not raised to the 2/3-power as in all other semi-infinite hypervelocity impact equations, but is instead raised to the power 0.805. This is consistent with both the Fish-Summers and Schmidt-Holsapple equations for thin-plates. With regards to its application, the 1992C equation is employed in Penson and Burchell (2003) and McBride and Taylor (1997) to model when a tether is fully severed. This is in conflict with the failure criterion of Hayashida and Robinson (1993), which argues that a tether may have functionally failed even if it is not completely severed. Because the basic strength criterion associated with a tether-based system is dependent on cross sectional area, it is logical to assume that a significant reduction in cross sectional area will render a structural tether component unusable. For this reason, the 1992C equation is not considered a relevant equation for the purposes of this study, even though it had been previously employed for hypervelocity impact work with tether materials.

7.2 Conformance to current common knowledge

The equations presented herein were produced using linear regression techniques based on various relationships apparent after an examination of the data. According to Yu *et al.* (1994), both the studies that produced the equations presented herein and a number of other various studies conducted between 1958 and 1965, which reportedly included no fewer than 1700 data points, all demonstrate similar relationships that support certain assumptions about the nature of hypervelocity impacts.

7.2.1 Energy and temperature issues

All of the equations presented above that apply to semi-infinite targets support the relationship between crater depth and impact energy. In an examination of past empirical work presented in Yu *et al.* (1994), nine equations developed between 1958 and 1965 and reported to account for over 1700 data points, as well as between18 and

45 data points collected and presented in Yu *et al.* (1994), are shown to support an energy-based explanation that relates crater depth to the normal impact velocity raised to the 2/3-power. In addition to a 2/3-power velocity relationship, the data presented in Yu *et al.* (1994) further supports a 2/3-power relationship with regards to impactor density that is supported by seven of the historic equations.

All of the aforementioned equations characterising crater depth in a semi-infinite material employ this 2/3-power to the impact velocity term. This relationship appears to be derived from the intuitive concept that impact energy has a direct relationship to crater formation. However, none indicate the direct incorporation of both the iso-deviation law and isotropic expansion concepts as presented in Yu *et al.* (1994), nor the significant emphasis placed on material strength that Yu *et al.* (1994) suggests is necessary. Combined with indications contained in Yu *et al.* (1994) that the authors feel these relationships only hold for set conditions, there is reason to believe that a valuable re-examination of commonly accepted and held assumptions and presumptions could produce meaningful results.[xi]

7.2.2 An oblique problem

Most concerning when examining traditionally assumed concepts as they are applied to the empirical hypervelocity equations presented in the literature is the fact that nowhere in Yu *et al.* (1994) is there an attempt to reconcile the energy and isotropic-based theories with oblique impacts. While it is a common assumption that only the normal component of impact velocity is relevant when assessing the effects of a hypervelocity impact, there is no indication that the aforementioned equations examined datasets that included oblique impacts.

Questions have been raised in works such as Burchell and Grey (2001) and Burchell and Whitehorn (2003) regarding the validity of such an assumption and the conditions under which such an assumption is valid. The concerns regarding this relationship raised in Burchell and Whitehorn (2003) further support the concept expressed in Yu *et al.* (1994) that these relationships may only hold for like materials, further offering an indication of why the Cour-Palais equation may contain the 1.5 density ratio limit stated in Hayashida and Robinson (1993). If there are doubts that have been raised

with regards to the normal impact velocity component assumption, it is prudent to re-examine oblique impact data that may be relevant.

7.3 Relevance of these equations to space tether research

There is no evidence that the equations presented above are acceptable for analysing a space tether system. Even though Hayashida and Robinson employed the Fish-Summers equation in their 1993 lifetime assessment of the tether material designed for the TSS-2 mission, as presented in Hayashida and Robinson (1993), more than 20 years earlier Frost stated in Frost (1970) that the equation was not appropriate for analysing non-metallic targets. Further, considering the complex manner in which other equations characterize material properties, it does not seem intuitively reasonable that such characteristics could be modelled using a linear interpolation based on two data points, as is done in Hayashida and Robinson (1993).

While the Fish-Summers equation, as utilised in the TSS-2 mission analysis, may not be ideal for that purpose, it is the only equation presented within whose constituent variables can be inputted with the least uncertainty. For example, the Rockwell, Cour-Palais, and Modified Cour-Palais all require a Brinnel hardness value. For tether materials, obtaining such a value could not be done without significant reservations regarding its fundamental validity. Further, considering the strength of tether structures and their constituent strands (*fibre bundles*) is directionally dependent, it is not clear that accounting for the material strength would improve the accuracy of a penetration prediction in a manner equivalent to cases involving a semi-infinite material whose strength is not directionally dependent. Additionally, for tether systems that employ aramid fibres, Chapter 7 proves that the strain rate directly affects the strand break strength, a fact that has a currently unknown and unstudied effect on the validity of the strength criterion in an empirical hypervelocity impact model.

Further, it is highly likely that a significant portion of the hypervelocity impacts occurring with a momentum exchange space tether system will be oblique in nature. This is a reasonable assumption, considering the fact that the system is constantly rotating relative to the velocity vector of its central facility. Quantitatively, 90% of all

momentum exchange tether system orientations will produce oblique impacts of greater than 9-degrees for a perpendicularly acting debris field. For the genre of momentum exchange tether systems, this could produce significant concerns because the reservations contained in the literature with regards to the current treatment of impact angle could have a significant influence on the lifetime analyses of momentum exchange tether systems.

Considering the functional limits of the parameters required for an empirical hypervelocity impact equation, as they apply to tether structures, it is clear that most traditionally accepted equations are not sufficient for assessing a tether system. Further, it is clear that the uncertainty associated with various impact assumptions, like the assumption that only the normal component of impact velocity must be accounted for during hypervelocity impact, may not be sufficient for systems where the probability that a non-normal impact will be encountered is much higher. For these reasons, it seems prudent to reassess the conventional wisdom associated with empirically derived hypervelocity impacts without the constraints of traditional theory.

7.4 New answers for old data

This investigation poses a re-examination of publicly available data for hypervelocity impacts in which the impact velocity, angle of incidence, and impactor and target properties are significantly varied. While it was stated in Yu *et al.* (1994) that prior investigations included no fewer than 1700 data points, the avoidance of impact angle in the document offers little indication that the data contained a suitable proportion of oblique impacts. Further, given the ease with which many authors intertwine theoretical causation and the fitting of actual results, this investigation undertakes a clean, unbiased investigation to fit an empirical hypervelocity impact equation using Markov Chain Monte Carlo (MCMC) techniques to a diverse dataset that includes a wide range of impact angles and densities. Both ranges of target density and impact obliquity include the angles and densities likely to be associated with a momentum exchange tether system, and the proposed equation uses variables that are both consistent with current empirical equations and directly relevant to space tether structures.

7.4.1 Rebuilding the Fish-Summers equation

Because it is traditional that empirical hypervelocity impact equations are derived using linear regression techniques, it may be of use to demonstrate that an MCMC technique can create an empirical hypervelocity impact equation. To do so, this section will present an equation that has been derived using MCMC techniques, incorporating data points that were created using the Fish-Summers equation, as modified for and presented in Hayashida and Robinson (1993). The new equation that is to be presented in this sub-section will be called the Fish-Summers (Rebuild) equation. If the difference between the predictions made by the Fish-Summers equation and the Fish-Summers (Rebuild) equation are insignificant for identical input data, it could be assumed that the two equations are functionally identical.

Background information on MCMC methods and techniques is more fully discussed in literature such as Gilks *et al.* (1995). As an overview, MCMC methods are a type of Bayesian analysis technique where, through use of observed data and a prior distribution for each unknown model parameter (i.e., a quantitative approximation that defines each random variable in the model that is employed to represent each parameter, a choice that is based only on expert guidance), a posterior distribution can be understood through analysis of a Markov chain. A Markov chain is a series of points that, starting from set initial conditions and selected based on the most recently selected point through use of a simulation technique known as Gibbs sampling, are selected directly from the posterior distribution defining the random variable that represents each parameter. The posterior distribution characterises the random variation within a model parameter to a high level of accuracy, dependent upon both the observed data and the prior distribution that is set by the analyst.

In theory, if the parameter being defined by a posterior distribution were to be observed an infinite number of times, the posterior would become equivalent to a histogram of the observations. This should be true if the model *converges*, as discussed in literature such as Gilks *et al.* (1995), Best *et al.* (1996), and Spiegelhalter *et al.* (2003). As clearly stated in Best *et al.* (1996) and Spiegelhalter *et al.* (2003), while there are a number of analytical routines for mathematically assessing

convergence in a MCMC model, "it is not possible to say with certainty that the sample is representative of the underlying stationary [i.e., the posterior] distribution." When selecting appropriate parameters for each model, this research relied on the general convergence assessment technique recommended in Spiegelhalter *et al.* (2004). Such criteria state that, for multiple chains with diverse initial conditions, convergence is likely to have occurred when all of the chain histories are observed to be overlapping one another. Such a condition, which can be observed through examination of Fig. 7.2 through Fig. 7.6, will occur after a burn-in period, as it is referred to in accepted literature such as Gilks *et al.* (1995), Best *et al.* (1996), and Spiegelhalter *et al.* (2004). Once the Markov chain histories are observed to overlap each other such that it is reasonable to assume the chains are likely converging, an analyst can assume that all points selected for the Markov chain are being selected directly from the posterior distribution. Once observation indicates convergence has occurred, Spiegelhalter *et al.* (2004) recommends continuing the simulation until the Monte Carlo error for each parameter is less than 5% of the sample standard deviation. If both conditions have been met, Spiegelhalter *et al.* (2004) indicates that it is reasonable to assume a histogram of the points selected for each Markov chain will represent the posterior distribution.

The MCMC analysis package used to derive the Fish-Summers (Rebuild) equation is WinBUGS, v2.01, which is a Beta version released in November 2004. The specifics of this version are discussed in Spiegelhalter *et al.* (2004), and indications of its acceptance for analytical aerospace applications is evident by its use in research presented in papers such as Garber and Paté-Cornell (2004), Guikema and Paté-Cornell (2004), and Guikema and Paté-Cornell (2005). Using WinBUGS, the goal of this investigation is to determine a normally distributed parameter for crater depth, p, which has a mean value equal to the right hand side of Eq 7.7. As with all later derivations, the standard deviation of this crater depth will be modelled as one divided by the square root of a Gamma function with parameters 0.001 and 0.001. This selected standard deviation model was chosen in accordance with the guidance offered in Spiegelhalter *et al.* (2004) regarding non-informative priors (i.e., a prior that does not inappropriately bias the results). The Fish-Summers (Rebuild) equation is derived using the model presented in Eq. 7.7.

$$p = v_n^{\beta_1} \rho_p^{\beta_2} m_p^{\beta_3} \rho_t^{\beta_4} \tag{7.7}$$

Where:

p = crater depth on target (m)

m_p = projectile mass (kg)

ρ_p = projectile density (kg/m^3)

ρ_t = target density (kg/m^3)

v_n = normal component of impact velocity (km/sec)

Within this model, it is assumed that the exponential parameters can be represented as normally distributed random variables. This assumption of normalcy is modelled by making the prior distribution for each exponent a standard normal distribution with a standard deviation of 0.5. These prior distributions were chosen in a manner consistent with Spiegelhalter *et al.* (2004) and Gilks *et al.* (1995) to ensure model convergence.

The data used to derive the Fish-Summers (Rebuild) equation was generated using the Fish-Summers equation, as modified in Hayashida and Robinson (1993). Each of the 72 penetration depth values, p, used to derive the Fish-Summers (Rebuild) was calculated using a randomly and independently selected set of values representing impact velocity, target and impactor densities, particle mass, and a normally distributed error. Each randomly selected parameter was generated using the relationships presented in Eq. 7.8 through Eq. 7.11. For velocity, each sample was taken from a uniform distribution between the values of 2 km/sec and 17 km/sec, as identified in Eq. 7.8. The values of density for both the impactor and target were uniformly distributed between 2450 kg/m3 and 2950 kg/m3, as identified in Eq. 7.9; while not specifically required for the Fish-Summers equation, this range of densities ensures the threshold ratio of 1.5 stated as a requirement of Cour-Palais is not violated by a sample point. For particle mass, to select a range of sample points that is roughly similar to that present in the orbital environment, a logarithmic relationship is

modelled using a uniform distribution as in Eq. 7.10. Finally, since it is assumed that the Fish-Summers equation was created using linear regression techniques with normally distributed error, a standard normal error term is added to each calculation of p. Because the literature does not state the error associated with predictions calculated with the Fish-Summers equation, this model assumes a standard normal error with a standard deviation of 70μm. This value is based on an assumption that no error produced by the Fish-Summers equation will be greater than 500μm, or 0.5mm. While this assumption is not supported by the literature, considering the average size associated with a tether structure, a more significant error would severely decrease the utility of any results obtained through use of the Fish-Summers equation. As the Fish-Summers equation has been used by practitioners for tether applications, as in Hayashida and Robinson (1993), this research assumes that the error associated with the equation is not likely to be more significant than that identified in Eq. 7.11.

$$v = U(2,17) \tag{7.8}$$

$$\rho = U(2450,2950) \tag{7.9}$$

$$m_p = \frac{1}{10^{12[U(0,1)]}} \tag{7.10}$$

$$\sigma = N\left(0,7_{10^{-5}}\right) \tag{7.11}$$

With the model defined, each chain is started with initial values ranging between zero and one. Three Markov chains per parameter are modelled simultaneously through 20,000 iterations. The analysis of the posterior presented in Table 7.1 and Fig. 7.1 through Fig. 7.6 disregards the first 4,999 iterations of each chain to accommodate for a sufficient burn-in period. The analytical results for the three chains are presented in Table 7.1; Fig. 7.1 presents an aggregate histogram accounting for all three Markov chains; and Fig. 7.2 through 7.6 present the histories for each parameter, identifying the overlap identified in Spiegelhalter *et al.* (2004) as an indication of model convergence. From examination of Table 7.1, it is clear that the Monte Carlo error is less than the 5% threshold recommended in Spiegelhalter *et al.* (2004) to ensure each posterior is suitably refined. From these two facts, it is assumed that the results of the MCMC analysis are reasonable.

Table 7.1 Statistics for the MCMC simulation for the Fish-Summers (Rebuild) equation, assuming a burn-in period for each chain of 5000 iterations.

	mean	sd	MC_error	val2.5pc	median	val97.5pc	start	sample
beta1	0.6645	0.0269	6.07E-04	0.6126	0.6638	0.7192	5000	45003
beta2	-0.04345	0.167	0.006754	-0.3793	-0.04674	0.2893	5000	45003
beta3	0.3529	0.007385	3.71E-05	0.3388	0.3527	0.3676	5000	45003
beta4	-0.3171	0.1715	0.00694	-0.6579	-0.3135	0.02569	5000	45003
sigma	0.005504	4.80E-04	3.50E-06	0.004665	0.005472	0.006534	5000	45003

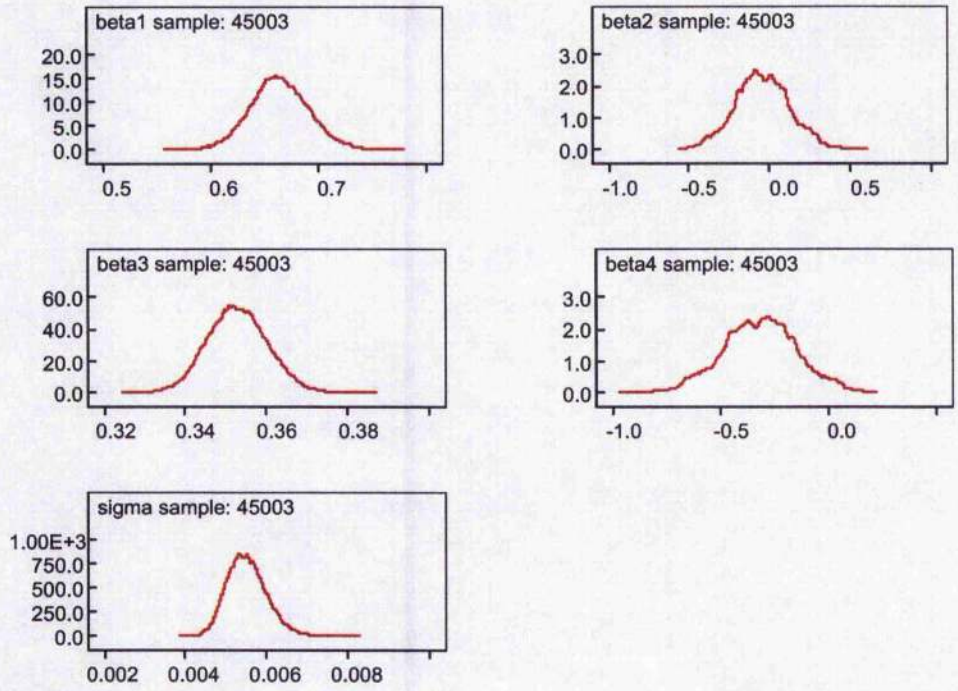

Figure 7.1 Posterior distributions for each exponent in the Fish-Summers (Rebuild) equation.

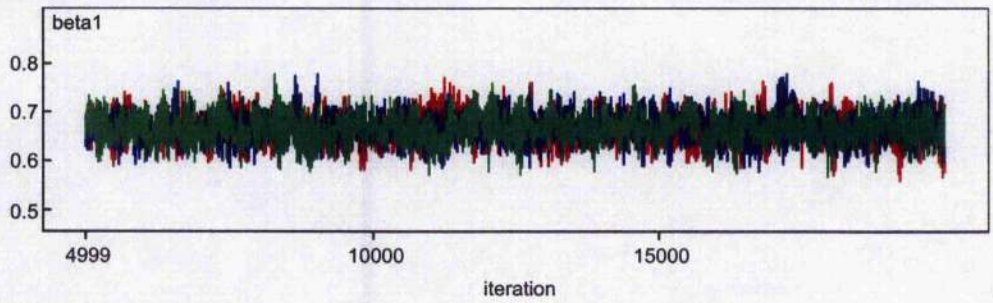

Figure 7.2 Chain histories for the Beta 1 variable.

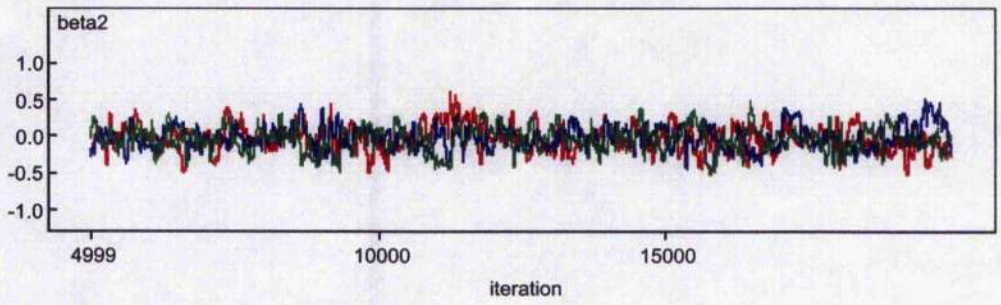

Figure 7.3 Chain histories for the Beta 2 variable.

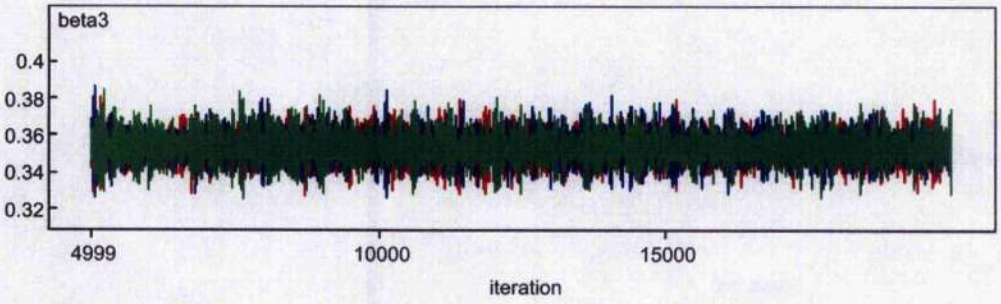

Figure 7.4 Chain histories for the Beta 3 variable.

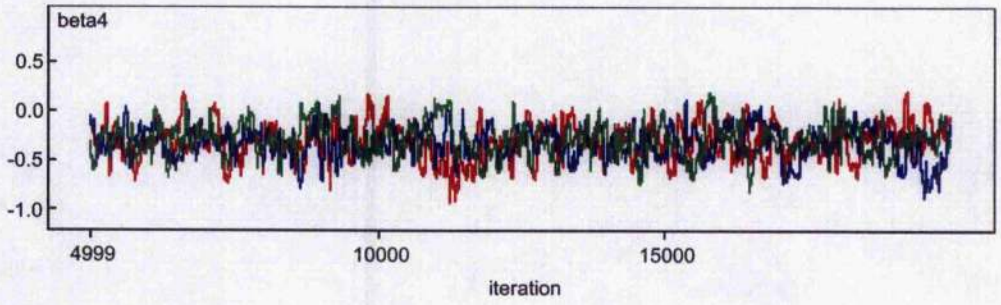

Figure 7.5 Chain histories for the Beta 4 variable.

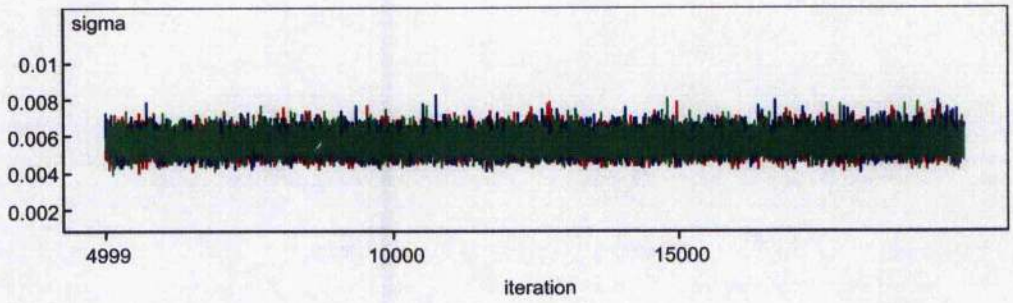

Figure 7.6 Chain histories for the standard deviation associated with the calculated penetration depth.

Table 7.1 presents a numerical characterisation of the posterior for each exponent identified in Eq. 7.7. While the mean and standard deviation presented in Table 7.1 is based on an assumption that the distribution of each parameter is normally distributed, this assumption of normalcy may not hold for the posterior, even if it is assumed for the prior, as is done for the Fish-Summers (Rebuild) derivation. While an inspection of the distribution can be made through examination of Fig. 7.1, an approximation of the skewness of each parameter can be made within Table 7.1. In the table the first column is the mean of all points selected by the Gibbs sampling method when it simulated each Markov chain; the second column is the standard deviation associated with this mean, assuming the points making up the Markov chains are normally distributed; the third column is the Monte Carlo error for each parameter, which decreases proportionally to the square-root of the number of simulated samples; and the next three columns identify the lower boundary, median, and upper boundary of the 95th percentile, which can be used to assess the normalcy of the results. Considering the symmetry between the upper and lower boundaries, combined with similarity between the mean and median estimates, it is reasonable to assume the posteriors are sufficiently normal. Assuming analytical validity, the Fish-Summers (Rebuild) equation is expressed as in Eq. 7.12.

$$p = v_n^{0.665} \rho_p^{-0.0435} m_p^{0.353} \rho_t^{-0.317} \tag{7.12}$$

When comparing against the Fish-Summers equation, as modified and presented in Hayashida and Robinson (1993), the velocity and mass terms are identical to within 0.002. While the density exponents identified in Eq. 7.12 are not in direct agreement with those employed by the Fish-Summers equation as presented by Hayashida and Robinson (1993), when comparing penetration predictions calculated with both equations using more than 10000 randomly sampled points, the average percentage difference between the predictions is –0.3% with a standard deviation of 1.4%. Such close agreement, which will be further demonstrated later in this work, indicates that the technique for creating the Fish-Summers (Rebuild) equation is suitable.

7.4.2 Data set used to derive the Draper (72) equation

This work uses 72 actual data points to reassess the applicability of the aforementioned empirical hypervelocity effects equations. The bulk of dataset comes from work completed at the University of Kent by researchers such as Burchell, Gardner, Grey, and Whitehorn, in works such as Burchell and Grey (2001), Burchell Whitehorn (2003), Burchell et al. (1999), Gardner and Burchell (1997), and Grey and Burchell (2004), with the remaining data points coming from a study presented in Christiansen *et al.* (1993), which was conducted at the NASA Johnson Space Center. The data set was selected to offer impacts of uniform projectiles onto uniform targets that present a wide range of material and target densities, impact velocities, and impact angles. Studies of uniform projectiles and targets were chosen so as to limit any unknown variability caused by the interaction of internal surfaces. To ensure the accuracy of the results are not biased towards a certain type of impact condition, the points were qualitatively and quantitatively selected to ensure wide variability. While a purely qualitative assessment of the data points implies that the points are widely varied, quantitatively assessing the product of each input variable (i.e., velocity, projectile density, projectile mass, target density, and impact angle[xii]) shows a standard deviation that is more than double the mean. This large standard deviation offers a further quantitative measure supporting an opinion that the data set is widely diverse.

The first 13 points are taken from Grey and Burchell (2003). These points were gathered from a series of tests that fired steel impactors at targets of ammonia rich ice.

While all of the tests were conducted with no impact angle, this data set offers both a wide variation in target densities and a significant difference between impactor and target density. As most tests relating to space systems are conducted to simulate aluminium on aluminium impacts, such narrow data restrictions may cause the resulting equation to be wholly unusable for tether-based systems. This concept is supported by examinations in the literature that further emphasize the importance of the impactor and target densities Yu *et al.* (1994). With an average impactor density to target density ratio of 8.31, which is much greater than standard tests with ratios closer to 1; and a standard deviation of 22.06 about the mean target density, this first set of data points offers a variation in the data set that will heighten the probability that the resulting empirical equation will be applicable to space tether systems.

Table 7.2: Data from hypervelocity impact tests using steel impactors and ammonia rich ice targets.

No.	Impact velocity (km/sec)	Impactor density (kg/m3)	Impactor mass (kg)	Target Density (kg/m3)	Impact angle (deg)	p (mm)
1	4.9	7700	4.03E-06	933	0	12.910
2	4.51	7700	4.03E-06	933	0	11.090
3	4.49	7700	4.03E-06	933	0	12.490
4	4.96	7700	4.03E-06	962	0	10.300
5	4.6	7700	4.03E-06	962	0	9.970
6	4.9	7700	4.03E-06	900	0	9.900
7	4.83	7700	4.03E-06	918	0	11.600
8	4.79	7700	4.03E-06	885	0	10.800
9	5.05	7700	4.03E-06	901	0	9.400
10	4.87	7700	4.03E-06	930	0	12.600
11	4.77	7700	4.03E-06	930	0	7.400
12	4.79	7700	4.03E-06	930	0	12.100
13	4.86	7700	4.03E-06	930	0	9.900

Data points 14 through 31 were taken from Burchell and Grey (2001). These points represent oblique hypervelocity impacts onto thick glass targets. By using aluminium impactors and glass targets, the magnitude of the density relationship is consistent with traditional space system impact analysis conditions, although inverted. Because it does not seem likely that impacting glass with aluminium would produce significantly different results than the reverse, the greatest benefit of this data set is

the range of oblique impacts. By maintaining a constant density relationship while offering a wide range of impact angles, this data set offers insight into the sole effect of impact angle.

Table 7.3: Data from oblique hypervelocity impact tests using aluminium impactors onto glass targets.

No.	Impact velocity (km/sec)	Impactor density (kg/m3)	Impactor mass (kg)	Target Density (kg/m3)	Impact angle (deg)	p (mm)
14	5	2700	1.41372E-06	2500	0	1.900
15	4.95	2700	1.41372E-06	2500	10	2.020
16	5.11	2700	1.41372E-06	2500	20	1.900
17	5.12	2700	1.41372E-06	2500	30	1.830
18	5.01	2700	1.41372E-06	2500	40	1.850
19	5	2700	1.41372E-06	2500	45	1.950
20	5.11	2700	1.41372E-06	2500	45	1.690
21	5.18	2700	1.41372E-06	2500	45	1.860
22	4.96	2700	1.41372E-06	2500	45	1.620
23	4.94	2700	1.41372E-06	2500	50	1.680
24	5.18	2700	1.41372E-06	2500	55	1.580
25	5.08	2700	1.41372E-06	2500	60	1.500
26	5.31	2700	1.41372E-06	2500	65	1.280
27	5.18	2700	1.41372E-06	2500	70	1.010
28	5.16	2700	1.41372E-06	2500	70	1.050
29	5.1	2700	1.41372E-06	2500	70	1.340
30	5.48	2700	1.41372E-06	2500	75	0.690
31	5.05	2700	1.41372E-06	2500	80	0.350

The final Burchell data set comes from Burchell and Whitehorn (2003). This data presents the results of oblique hypervelocity impacts of steel impactors onto granite. Using the data in Burchell and Whitehorn (2003) does not seem to offer a consistent means of calculating the target density, so the density of the granite used is assumed to be 2691 kg/m^3, as per Simetric (2006). With a greater magnitude of density ratio than that seen with data points 14-31, the equivalently diverse impact angles are thought to contribute to a greater understanding of the relationship between impact angle and penetration depth, a characteristic often ignored by even some of the most respected papers such as Yu *et al.* (1994).

Table 7.4: Data from oblique hypervelocity impact tests using steel impactors onto granite targets.

No.	Impact velocity (km/sec)	Impactor density (kg/m3)	Impactor mass (kg)	Target Density (kg/m3)	Impact angle (deg)	p (mm)
32	1.08	7700	3.22537E-05	2691	0	2.880
33	2.22	7700	3.22537E-05	2691	0	4.810
34	3.03	7700	3.22537E-05	2691	0	6.750
35	3.85	7700	3.22537E-05	2691	0	7.890
36	4.8	7700	3.22537E-05	2691	0	7.980
37	5.5	7700	3.22537E-05	2691	0	8.700
38	5.7	7700	3.22537E-05	2691	0	7.940
39	5.92	7700	3.22537E-05	2691	0	9.160
40	5.5	7700	3.22537E-05	2691	0	1.400
41	5.7	7700	3.22537E-05	2691	0	1.800
42	5.07	7700	3.22537E-05	2691	18	1.000
43	5.46	7700	3.22537E-05	2691	30	0.700
44	5.43	7700	3.22537E-05	2691	37	1.400
45	5.31	7700	3.22537E-05	2691	41	1.000
46	5.22	7700	3.22537E-05	2691	45	0.700
47	5.32	7700	3.22537E-05	2691	49	1.500
48	5.5	7700	3.22537E-05	2691	50	1.500
49	5.36	7700	3.22537E-05	2691	55	0.700
50	5.43	7700	3.22537E-05	2691	60	0.700
51	5.31	7700	3.22537E-05	2691	68	0.700
52	5.47	7700	3.22537E-05	2691	76	0.700
53	5.15	7700	3.22537E-05	2691	80	1.000
54	5.25	7700	3.22537E-05	2691	85	0.700

The final data set was created from the aluminium on aluminium impact tests presented in Christiansen *et al.* (1993). As Christiansen did not present the impact results in a table, the data points presented in Table 7.4 were generated using the graph of penetration as a function of impact angle presented in Christiansen *et al.* (1993). The document makes no distinction as to the impact velocity for each test except to state that all impact velocities are between 6.5 and 7.0 km/sec. As it would be arbitrary to assume these velocities are distributed according to a specific distribution, this examination of the data considers the impact velocities to be uniformly distributed, and performs its calculations using the midpoint of the range. While this uncertainty associated with the impact velocity is not desirable, this data set is valuable for its range of impact angles on targets of similar density.

Table 7.5 Data from hypervelocity impacts of aluminium impactors on aluminium targets.

No.	Impact velocity (km/sec)	Impactor density (kg/m3)	Impactor mass (kg)	Target Density (kg/m3)	Impact angle (deg)	p (mm)
55	6.75	2790	1.46084E-06	2700	0	2.160
56	6.75	2790	1.46084E-06	2700	0	2.085
57	6.75	2790	1.46084E-06	2700	30	1.850
58	6.75	2790	1.46084E-06	2700	45	1.670
59	6.75	2790	1.46084E-06	2700	45	1.650
60	6.75	2790	1.46084E-06	2700	60	1.065
61	6.75	2790	1.46084E-06	2700	65	0.945
62	6.75	2790	1.46084E-06	2700	70	0.675
63	6.75	2790	1.46084E-06	2700	72	0.580
64	6.75	2790	1.46084E-06	2700	74	0.610
65	6.75	2790	1.46084E-06	2700	76	0.515
66	6.75	2790	1.46084E-06	2700	78	0.335
67	6.75	2790	1.46084E-06	2700	80	0.170
68	6.75	2790	1.46084E-06	2700	82	0.240
69	6.75	2790	1.46084E-06	2700	84	0.180
70	6.75	2790	1.46084E-06	2700	85	0.255
71	6.75	2790	1.46084E-06	2700	86	0.165
72	6.75	2790	1.46084E-06	2700	88	0.130

7.4.3 The Draper (72) equation

The Draper (72) equation takes an identical approach to that of the Fish-Summers (Rebuild) equation, raising each input parameter to exponents that will be solved for through a MCMC simulation. Unlike the empirical impact equations presented above, the Draper (72) equation makes no assumption as to the relationship between velocity and the normal component of the impact angle. The prior distribution for each exponent, β_1 through β_5, is represented as a standard normal with standard deviation equal to one. The WinBUGS "model" from which the Draper (72) equation is derived is presented in Eq. 7.13.

$$p = v^{\beta_1} \rho_p^{\beta_2} m_p^{\beta_3} \rho_t^{\beta_4} \left[\cos(\theta)\right]^{\beta_5} \tag{7.13}$$

Where:

p = crater depth on target (m)

m_p = projectile mass (kg)

ρ_p = projectile density (kg/m^3)

ρ_t = target density (kg/m^3)

v = impact velocity (km/sec)

θ = impact angle (deg)

Each parameter for the Draper (72) equation was modelled with three Markov chains, each 40,000 samples in length, with the first 9,999 samples of each chain eliminated as a burn-in period. As with the Fish-Summers (Rebuild) equation, the quantitative results for each parameter are presented in Table 7.6, the posterior distributions for all parameters are presented in Fig. 7.7, and the chain histories for each parameter are presented in Fig. 7.8 through Fig. 7.13. Through examination of the Monte Carlo error presented in Table 7.6, which is less than 5% of the standard deviation; and the histories presented in Fig. 7.8 through Fig. 7.13, which identify significant overlap between all of the chains; both criteria identified by Spiegelhalter *et al.* (2004) are met, which indicates that the model converges.

Table 7.6 Results for the Draper (72) equation fitting

	mean	sd	MC_error	val2.5pc	median	val97.5pc	start	sample
beta1	0.04196	0.6611	0.01398	-1.149	-0.00176	1.489	10000	90003
beta2	0.6129	0.3773	0.006765	0.03809	0.5519	1.53	10000	90003
beta3	0.07554	0.22	0.004803	-0.4335	0.08951	0.4791	10000	90003
beta4	-1.348	0.3675	0.007763	-2.207	-1.302	-0.7576	10000	90003
beta5	0.8211	0.654	0.01352	-0.2015	0.731	2.277	10000	90003
sigma	0.005771	5.00E-04	2.62E-06	0.004893	0.005736	0.006851	10000	90003

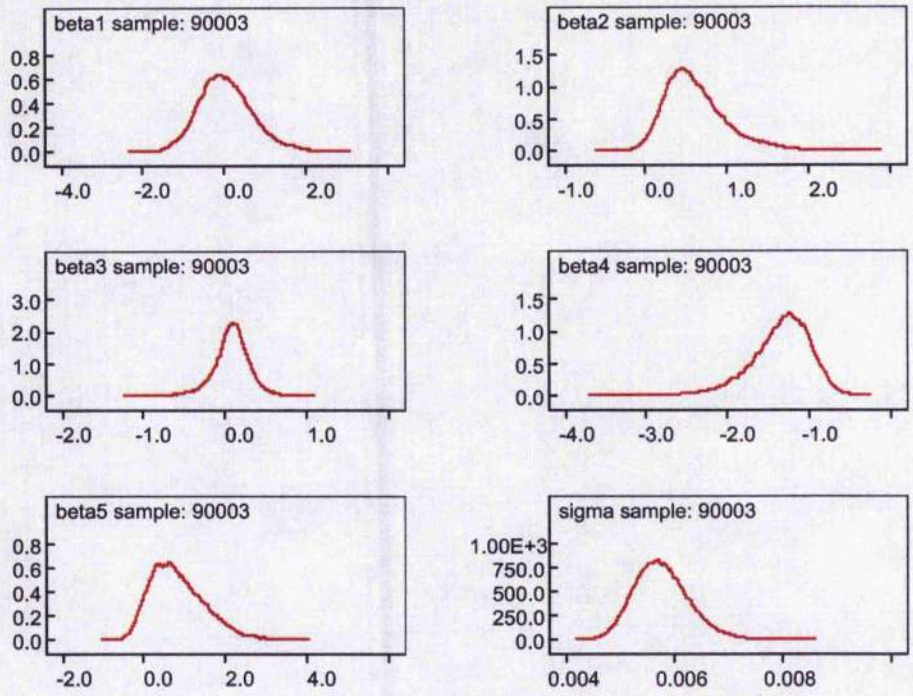

Figure 7.7 Posterior distributions for the Draper (72) equation exponents.

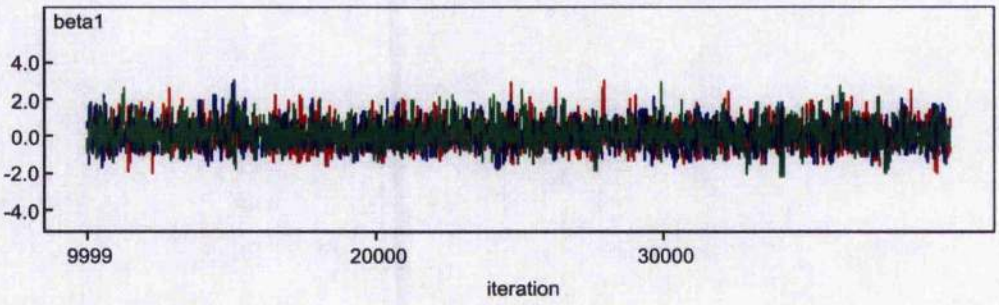

Figure 7.8: Chain histories the Beta 1 variable.

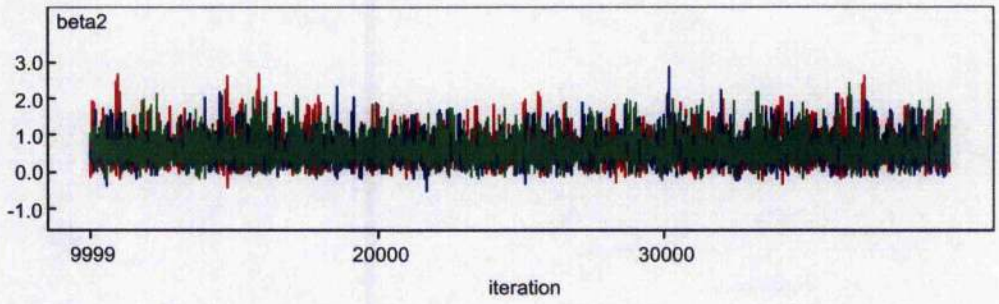

Figure 7.9 Chain histories the Beta 2 variable.

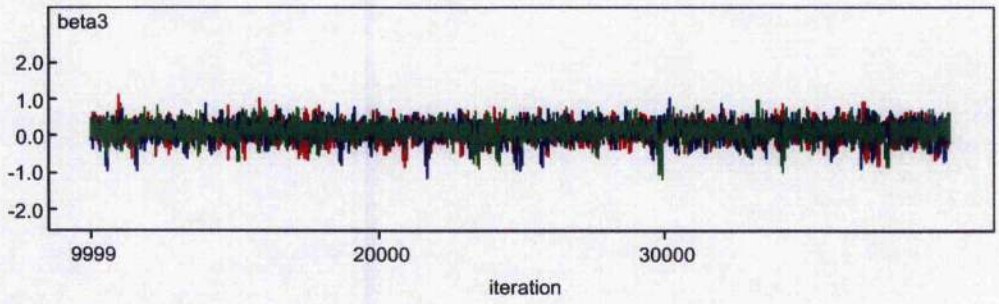

Figure 7.10: Chain histories the Beta 3 variable.

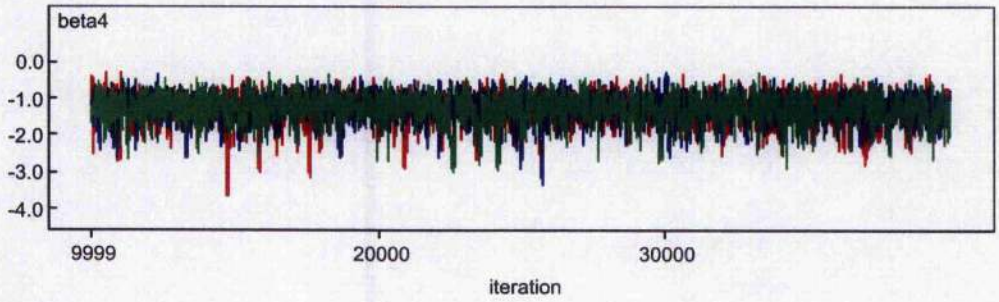

Figure 7.11: Chain histories the Beta 4 variable.

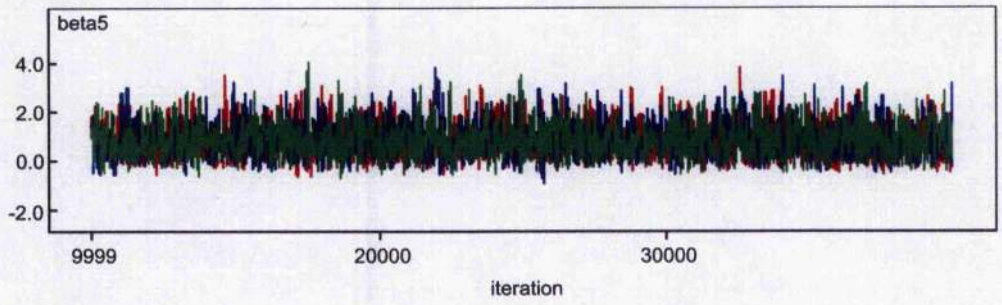

Figure 7.12: Chain histories the Beta 5 variable.

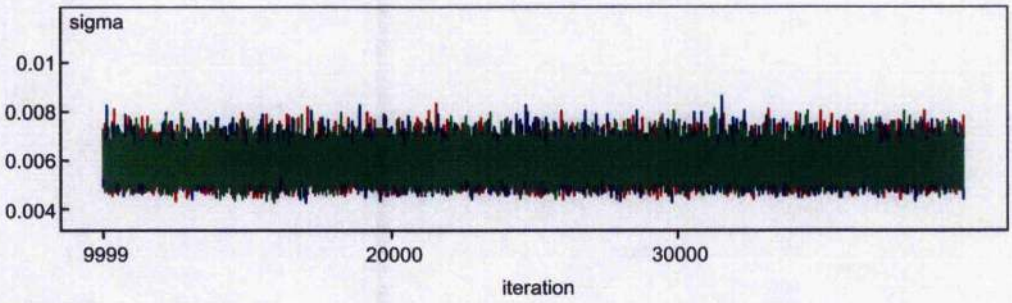

Figure 7.13: Chain history for the standard deviation associated with the calculated penetration depth.

Since all parameters are assumed to converge, the Draper (72) equation is thus assumed to be valid as presented in Eq. 7.14.

$$p = v^{0.042} \rho_p^{0.613} m_p^{0.076} \rho_t^{-1.348} \left[\cos(\theta)\right]^{0.821} \tag{7.14}$$

It is immediately evident that the mean estimates for each of the parameters presented in Table 7.6, and identified as it is applied within the Draper (72) equation in Eq. 7.14, are not identical to comparable parameters identified in any previously presented equation. In itself, this fact is neither proof that the equation is incorrect, nor is it proof that the commonly accepted theories with regards to empirically modelling hypervelocity impacts are not valid.

7.5 Examining traditional relationships

Nearly every empirical equation produced supports the energy-based theory that there exists a direct relationship between penetration depth and the normal component of the impact velocity. This theory is implemented in most empirical equations using the magnitude of the impact velocity multiplied by the cosine of the impact angle, raised to the 2/3-power. While this theory is not refuted by the Draper (72) equation at the 5% significance level, it is not strongly supported, either. At the same time, the Draper (72) equation does not strongly refute the 2/3-relationship with regards to impactor and target density supported by Yu *et al.* (1994) at the 5% significance level, while also not offering any strong evidence in its favour.

It is noted in works such as Yu *et al.* (1994) and Hayashida and Robinson (1991) that these 2/3-relationship theories are valid when the materials are similar in density. Further, the exponents that characterise the Draper (72) equation indicate that the material densities are of much higher importance than the impact velocity or impactor size. In tandem, these two observations offer an indication that the approach currently taken when performing regression fits directed by energy-based effect theories may need revision.

The Draper (72) equation is intended as an engineering model that is more capable than traditional empirical equations of producing accurate hypervelocity impact affects predictions for tether materials. In doing so, it offers an indication that traditional assumptions and theories that are commonly employed when empirically modelling the resulting craters after hypervelocity impacts may need to be re-examined. At the same time, the Draper (72) equation has not offered conclusive evidence that such assumptions are incorrect.

It is highly unlikely that the limited variable approach employed in developing the Draper (72) equation accounts for all of the mechanisms governing the effect of a hypervelocity impact. Additionally, it is likely that the Draper (72) equation may not account for enough material characteristics to make its conclusions applicable to points outside the range of the examined data set. The limited applicability of the Draper (72) equation is not unique, and is a quality that is common with empirical

models. While the following section compares the predictions of the Draper (72) equation to both the actual data; the Fish-Summers equation as modified by Hayashida and Robinson; and an equation developed identically to the Fish-Summers (Rebuild) and the Draper (72) equations, but using only the data presented in Christiansen *et al.* (1993); calibrating the Draper (72) equation using a data set that bounds the conditions expected for impacts with space tether components intuitively indicates that the Draper (72) equation should be more appropriate for space tether system analyses.

The equation produced using only the data from Christiansen *et al.* (1993) was developed to compare whether it would exhibit any similarities to the Fish-Summers (Rebuild) equation. The Christiansen equation, as it is referred to herein, is as follows:

$$p = v^{-0.103} \rho_p^{-0.471} m_p^{0.782} \rho_t^{-0.440} \left[\cos(\theta)\right]^{0.057} \tag{7.15}$$

The MCMC calculation predicts the standard deviation about the penetration depth to be 11mm. From initial inspection, this equation does not appear to hold any similarities to either Fish-Summers equation or the Draper (72) equation. However, at the 5% significance level, the differences observed in the Christiansen equation are not statistically significant.

7.6 Comparing results

It is reasonable to compare the actual test results to the predictions made by each equation in a manner that allows trends to be observed. To do this, the comparative analysis will be conducted in groupings defined by the paper from which they were borrowed.

7.6.1 Steel impactors on ammonia rich ice

The error in prediction for each of the Fish-Summers, Christiansen, and Draper (72) equations are presented in Fig 7.9 relative to the test number for which the calculation was performed. The errors are in millimetres and found by subtracting the actual crater depth from the predicted depth.

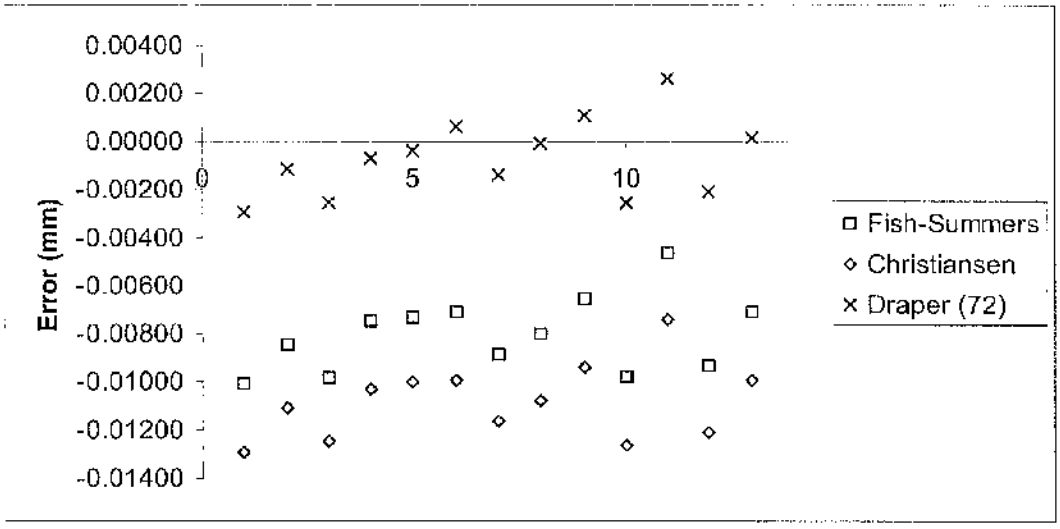

Figure 7.14 Error (mm) for points 1 through 13.

From observation, it is clear that the Draper (72) equation is the most accurate for all of the tests presented in Fig 7.14. However, the Draper (72) equation is the only equation calibrated using densities as low, and density ratios as high, as those present in the experiments that produced this data set. Also through observation, it is difficult to recognize any clear trends in the error. At the same time, there are no clear trends in the experimental inputs. While both the impact velocity and target density experienced some random variation between tests, the impact angle remaining at zero for all tests, there were no constant changes in these input characteristics that would cause a clear trend in the results or the error.

Table 7.7 Average and standard deviation of error for points 1 through 13.

	Rish-Summers error	Fish-Summers (Rebuild) error	Chr'sen error	Draper error
Average	-8.03865	-8.05721	-10.80457	-0.71165
STD	1.56902	1.57049	1.55566	1.61735

Table 7.7 offers a summary of the average error and the standard deviation about that random error using each of the four equations discussed above. While the Fish-Summers (Rebuild) equation is presented in the table, it is not presented in Fig 7.14 because of its insignificantly small variation from the traditional Fish-Summers equation.

7.6.2 Aluminium impactors onto glass targets

The errors presented in Fig 7.10 may be somewhat surprising. While the Fish-Summers equation employs the assumption that the normal component of impact velocity need be the only impact velocity consideration, the Christiansen equation was calibrated using a MCMC approach using data with a varying impact angle, and the Fish-Summers equation is seen to be the more accurate of the two. From observation, it appears true that the Fish-Summers equation is actually more accurate than the Draper (72) equation for all but one impact condition studied throughout this series of points, an observation that is supported by the improvement in overall accuracy with regards to the Draper (72) equation, as presented using the average error value in Table 7.8.

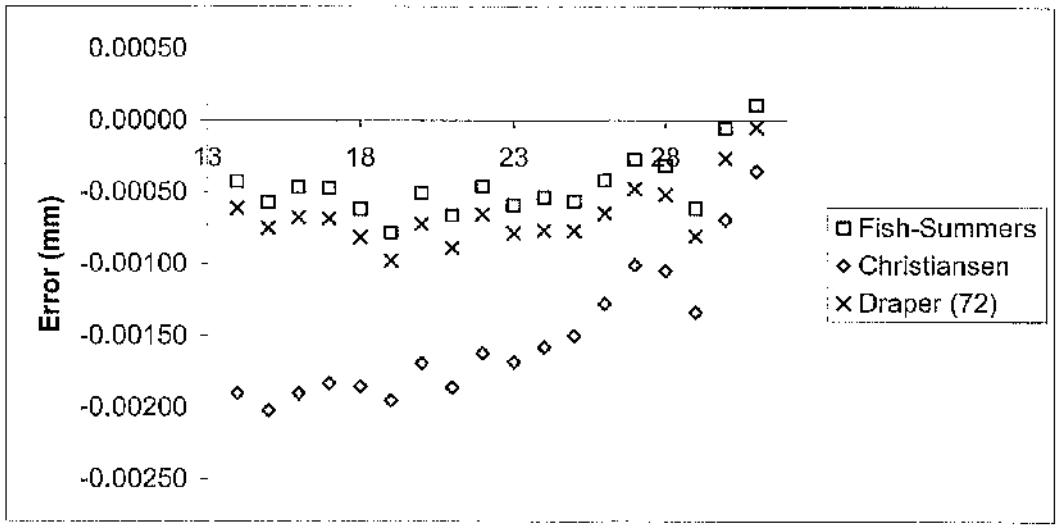

Figure 7.15 Error (mm) for points 14 through 31.

This improved accuracy with regards to the Fish-Summers equation relative to the Draper (72) equation for this data set may be a result of the fact that the test conditions contain a density ratio that is closer to unity. In these situations, it is hypothesized in Yu *et al.* (1994) that the impact energy may dictate crater depth. Such a concept does not appear to be unsupported by this data.

Table 7.8 Average and standard deviation of error for points 14 through 31

	Rish-Summers error	Fish-Summers (Rebuild) error	Chr'sen error	Draper error
Average	-0.45569	-0.44173	-1.50554	-0.65756
STD	0.21553	0.21347	0.46891	0.22294

An examination of the theories presented in Yu *et al.* (1994) may offer support for claiming that the Fish-Summers equation is more appropriate than the Draper (72) equation for these impact conditions. However, those same theories support the idea that equations are likely inappropriate for modelling tether impacts when they are derived with impact data from tests that only employ impactors and targets with density ratios close to unity. This is because the density ratio for an orbital debris impactor striking a tether segment will not be similar to those density ratios at which the Fish-Summers equation is most accurate.

7.6.3 Steel impactors onto granite targets

The results presented in Fig 7.11 may be distressing for any argument supporting the employment of any of these empirically derived models. For points on the left-hand side of the x-axis (i.e., points 32 through 39), each of the equations becomes less conservative as the impact velocity increases. This trend does not offer strong support for the idea that these equations can be applied for hypervelocity impacts where the impact velocity is nearer 10 km/sec.

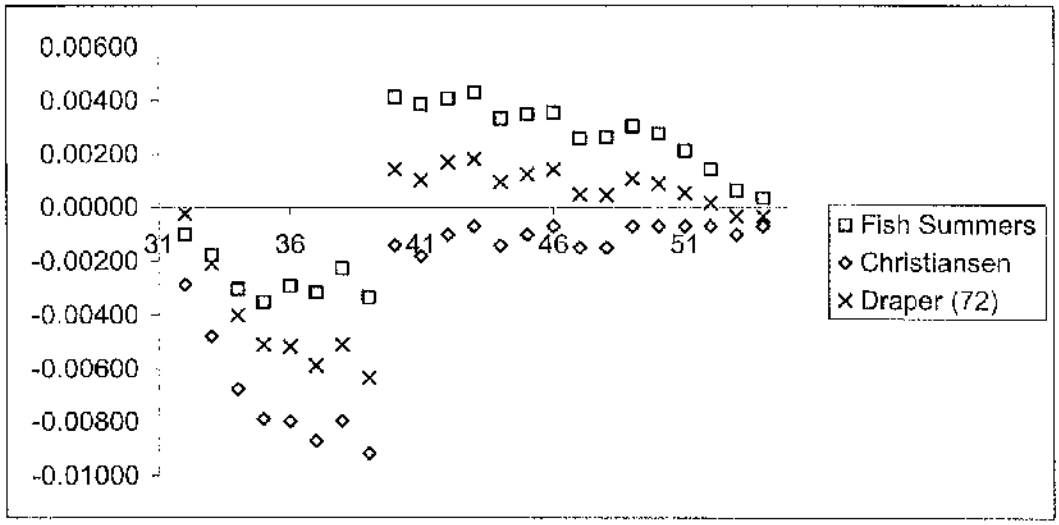

Figure 7.16: Error (mm) for points 32 through 54.

At point 40, though, all of the equations go from being un-conservative to being conservative. It is at point 40 that the test conditions drop the impact velocity, and they begin to incorporate an impact angle that increases for the remainder of the test conditions.

While the Draper (72) equation become more accurate after point 40 than the Fish-Summers equation, it is not known whether this accuracy would lessen in a rapid manner for higher velocities, as possibly indicated by the earlier tests within this group.

Table 7.9: Average and standard deviation of error for points 32 through 54.

	Rish-Summers error	Fish-Summers (Rebuild) error	Chr'sen error	Draper error
Average	0.92545	0.15055	-3.11336	-0.93009
STD	2.87321	2.88035	3.16729	2.78722

7.6.4 Aluminium impactors on aluminium targets

For the final section of the data set, again the Fish-Summers equations are more accurate than the Draper (72) equation. When accounting for the history of the Fish-Summers equation, this is not surprising as the impact conditions tested by Christiansen would likely be similar to those employed by Fish and Summers. While offering no explanation, it is interesting to note that all of the equations appear to decrease in error with an increase in impact angle.

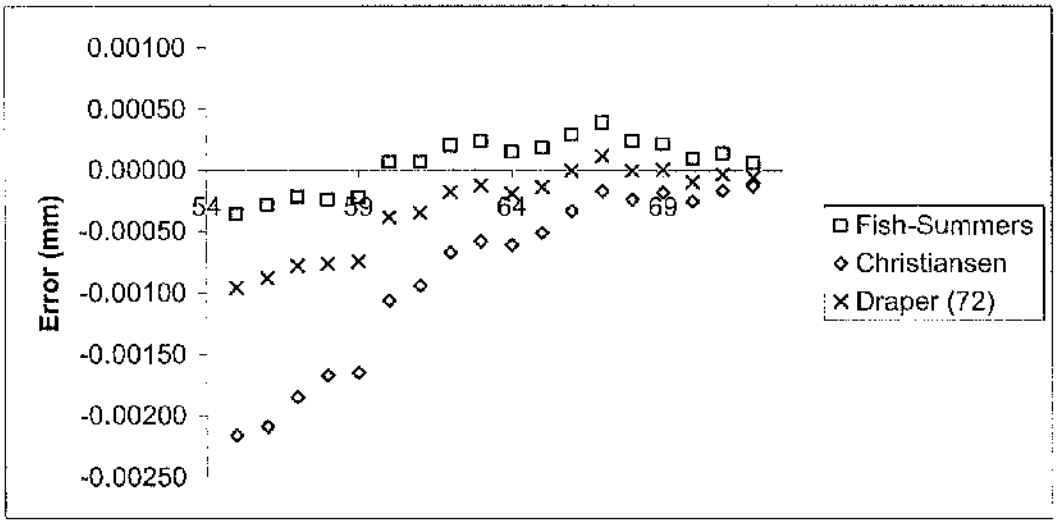

Figure 7.17: Error (mm) for points 55 through 72.

As expected, Table 7.10 identifies the Fish-Summers equations as being more accurate than both the Christiansen and the Draper (72) equations. Additionally, the Christiansen equation is most accurate for this data set, when compared to the other data sets. Such a conclusion may seem obvious, considering the general nature of empirically derived equations, discussed earlier.

Table 7.10: Average and standard deviation of error for points 55 through 72.

	Rish-Summers error	Fish-Summers (Rebuild) error	Chr'sen error	Draper error
Average	0.05935	0.05718	-0.84887	-0.30846
STD	0.22331	0.22577	0.71835	0.35393

When averaging over the whole 72-point data set, it may be intuitively obvious that the Draper (72) equation is the most accurate since it was the only equation calibrated in a manner that incorporates the entire data set. When examining Table 7.11, it is clear that the Draper (72) model has the lowest average error of the examined options, even though all equations are un-conservative.

Table 7.11: Average and standard deviation of all errors.

	Rish-Summers error	Fish-Summers (Rebuild) error	Chr'sen error	Draper error
Tot Ave	-1.25488	-1.50282	-3.53397	-0.66711
Tot STD	3.68280	3.55873	4.03743	1.71656

When examining the average error for the Christiansen equation, it is important to note that the data used for calibration contained no variation in impact velocity. For this reason, since most of the data points were at a velocity that is significantly different from that used for all the Christiansen calibration points, the Christiansen equation is not expected to be accurate over a wide range of impact conditions. In many ways, it should be held out as a note of caution against attempting to apply empirically derived equations outside their calibrated remit.

7.6.5 Applicability to tether systems

With that note of caution, it is important to realize that the Draper (72) equation was constructed with a data set that should allow the equation to find reasonable predictions for tether-based systems. Assuming the density ratio is of concern, as

argued by Yu *et al.* (1994), it must be noted that the Draper (72) equation is more accurate than the other equations for a wider range of density ratios.

Through observation of Fig 12, this higher level of accuracy at a wider range of density ratio can be seen in the plot of all prediction errors over the whole data set. Also identified in Fig 12 is the density ratio associated with an orbital debris impact on both Twaron and Spectra tethers. If density ratio is the driving concern for impact prediction, Fig 12 seems to indicate that the Fish-Summers equations and the Draper (72) equation are comparable with regards to accuracy. For density ratios closer to unity, the Fish-Summers equations appear to be the more accurate predictors of crater depth, while for higher ratios, like those seen with advances that will allow greater strength to weight ratios in tether structures, the Draper (72) equation is the most relevant.

While Fig 12 appears to offer further support for the Fish-Summers equations, indicating that the Draper (72) equation may not offer significant analytical accuracy for tether systems, this emphasis on the density ratio is not fully supported by the exponents derived within the Draper (72) equation. With the more significant exponent associated with target density, the ratio of the impactor to target density may not be as important as the target density itself. If this is valid, the Draper (72) equation is more appropriate for analysing tether target impacts because it is calibrated to more accurately analyse target densities more similar to those of the likely tether substances. The other equations are not as capable in this area.

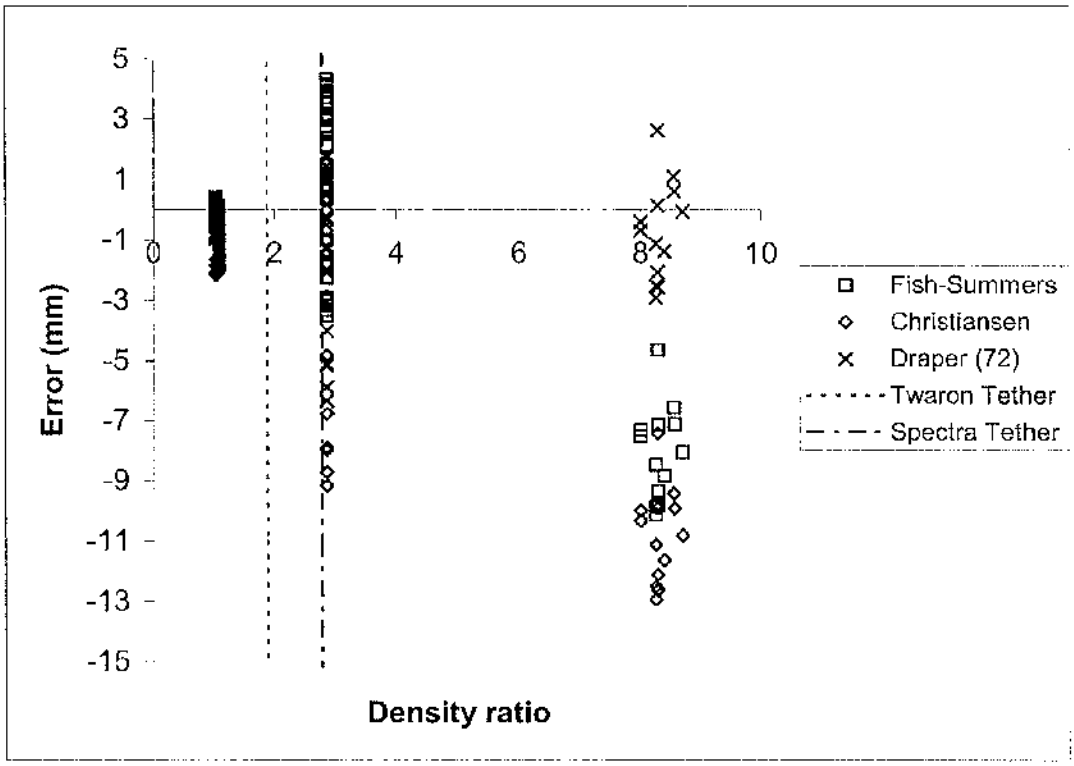

Figure 7.18 Error (mm) as a function of density ratio.

While previous results seems to indicate that crater depth is dependent on the normal component of impact velocity, Fig 7.19 offers further support that such a relationship may need to be more closely examined. Through examination of Fig 7.19, it is clear that the Draper (72), and its unconventional relationship between impact angle and crater depth, is more accurate than either the Fish-Summers equations or the Christiansen equation. This effect diminishes at greater angles where the crater depth and the cosine of the impact angle approach zero.

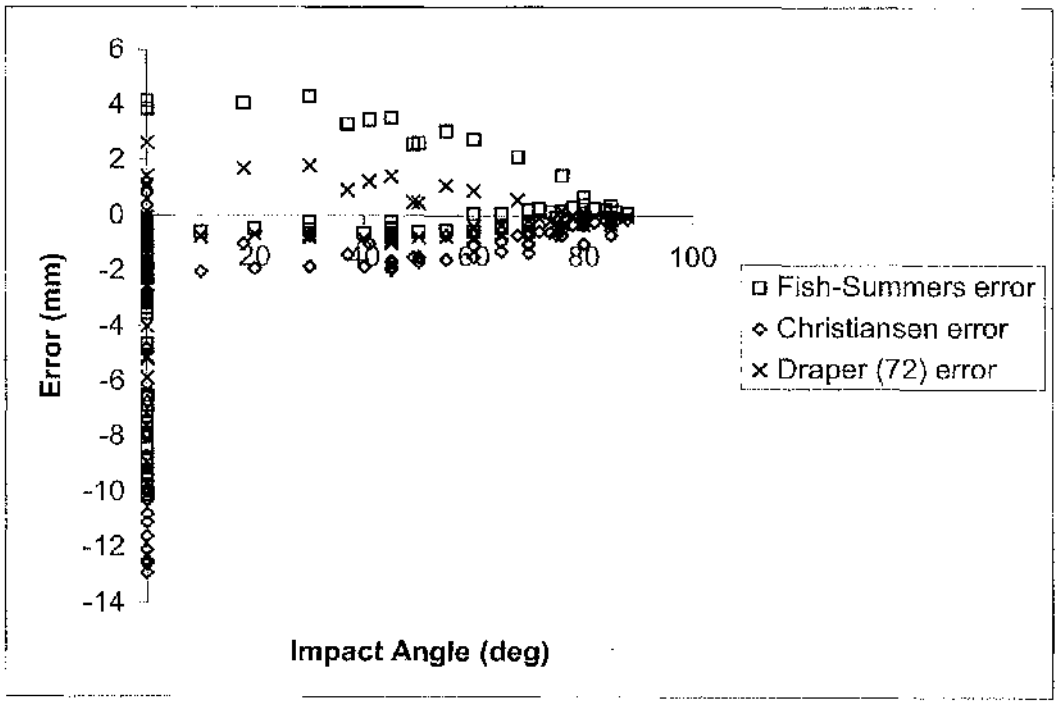

Figure 7.19 Error as a function of impact angle.

7.7 Unexamined effects

While logical given the current literature on empirically modelling hypervelocity impacts, the aforementioned work may not be suitably relevant for tether systems because it does not consider thermal properties of the material. When examining the results contained in the next chapter of this thesis in conjunction with the results presented in McBride and Taylor (1997), it is clear that (i) tether fibres in the impact location appear to have failed as a result of melting and (ii) the Spectra fibre failures examined and presented in McBride and Taylor (1997) appear to sustain greater damage from the same impactor when compared against the Twaron results presented in Chapter 8. Considering both (i) the isotropic expansion theory discussed in Yu *et al.* (1994) and (ii) the fact that the melting point of Spectra is significantly below that of Kevlar, there is anecdotal support for an empirical equation governing hypervelocity space tether impacts that considers the thermal properties of the tether material.

At the same time, given the conclusions of Allen *et al.* (1992), Benhoulo *et al.* (1997), and Wang and Xia (1999), it would be reasonable to assume that the significant

temperature variation produced by the space environment would have a significant effect on the validity of any empirical model. As environmental temperature variations that affect the tether material were not identified or recorded in the data employed by this research for constructing the Draper (72) equation, no consideration for such influences was made. This is a further potential limitation of the Draper (72) equation, but not one that is not shared by other equations that are commonly accepted by the space analyst community.

7.8 Conclusions

This examination of empirical hypervelocity impact equations that have previously been employed for spacecraft analysis has offered indications that the Draper (72) equation may be a more acceptable approximation of crater depth for hypervelocity impacts involving high strength and light weight tether structures. While too narrow in scope and data to conclusively prove any previous theory invalid, this research does offer indications that currently held concepts and assumptions used in the empirical modelling of hypervelocity impacts may need to be revisited. However, in line with the intent of this investigation, the improved accuracy over a wide range of impact conditions like those expected on space tether missions indicates that the Draper (72) equation may be a more appropriate choice for risk assessment practitioners examining space tether systems.

Chapter 8

Impactor Dispersion

The observed variation in tether strength as a function of load rate indicates that conventional hypervelocity impact modeling assumptions may be inappropriate for assessing tether-based space structures. High reliability tether system designs assume a single hypervelocity impact causes a single tether failure. Like the assumptions employed in hypervelocity impact models, it is reasonable to investigate whether this single-impact-single-failure assumption is valid.

8.1 Current assumption

Currently accepted tether-based system analysis like Hoyt and Forward (1998) assumes that an impactor that strikes a tether strand will not be capable of striking a second tether strand. For single-line thethers, this assumption is obviously true. However, for multi-strand tethers arranged in a tubular manner, like those discussed in Hoyt and Forward (2000), there is a high likelihood that multiple tether lines may be located along the same line of impact. This is illustrated using a span cross-section composed of eight independent tethers in Fig 8.1.

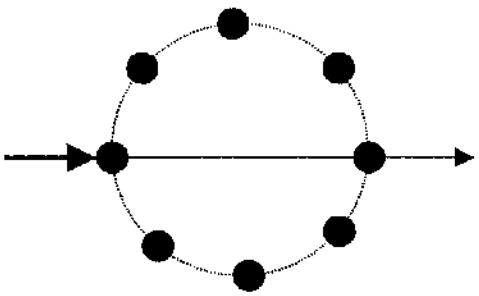

Figure 8.1 Theoretical eight-line span cross section, identifying the condition in which a single impactor, if it survives an initial impact and remains intact, could strike a second line

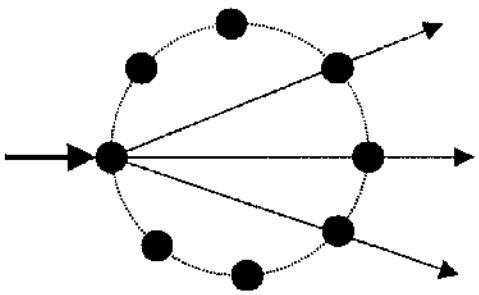

Figure 8.2 Theoretical eight-line span cross section, identifying the condition in which a single impactor, if it breaks up after the initial impact, could cause mulitple failures

Examination of Fig 8.1 demonstrates that it is possible for an impactor, which stays intact, to impact another tether line. Even if an impactor stays intact, the probability of two failures per impact could be significant enough to require a reanalysis of the

conclusions presented in Hoyt and Forward (2000). If an impactor breaks up upon impact, the products could disperse so as to cause many more than a single failure. If a single impact has a significant probability of causing multiple failures, the calculations performed in Hoyt and Forward (2000) would be invalid.

The concept that an impactor could form into a debris cloud after impact is not a unique concept. This phenomenon is widely observed and discussed relative to hypervelocity impacts with thin and semi-infinite plates in many works such as Stilp (1997), Gardner and Burchell (1997), Christiansen *et al.* (1993), Christiansen *et al.* (1992), Cour-Palais (1985), Frost (1970), Orphal (1999), Orphal and Anderson (2001), Schonberg (1989), and Schonberg and Ebrahim (1999). Considering prior analysts such as McBride and Taylor (1997), Hayashida and Robinson (1993), and Penson and Burchell (2003) assumed that the mechanics associated with a tether failure under hypervelocity impact conditions are sufficiently similar to those modelled with the thin or semi-infinite plate hypervelocity impact equations used within each respective paper, it is logical to assume that this secondary debris cloud observed after a thin plate impact is likely to form after impact with a tether structure.

This work examines hypervelocity impacts between glass impactors and Twaron targets, the remnants of those impacts being captured by both an aluminium witness plate and an aluminium witness plate with a piece of Aerogel affixed to it. By examining the witness plates and the Aerogel, this work hopes to determine whether (i) impactors that strike a Twaron tether remain intact, fracture, or vaporise; (ii) if the impactors either remain intact or break into discernable fragments, will the products remain on the initial trajectory, or they scatter; and, (iii) if the products break into fragments of significant size, would these products remain capable of causing another tether line to fail.

8.2 General set up

Three impact tests were conducted on 21 November 2005 at the hypervelocity impact testing facility within the University of Kent at Canterbury. All three tests used the two-stage light gas gun described in Burchell *et al.* (1998) to fire spherical, glass impactors at targets of braided Twaron strands. Targets made solely of braided

Twaron were chosen because (i) aramid fibres are used in other space tether concepts and designs such as Hayashida and Robinson (1993) and (ii) the uniform qualities of the target are assumed to remove uncertainties that would arise at the boundary of two unlike substances. To analyse how the impactors were affected by the impact, all tests used aluminium witness plates. For the final test, an irregularly shaped piece of Aerogel was affixed to the witness plate.

Each set of targets incorporated braided Twaron ropes identical to those that underwent the tensile tests discussed earlier. Each Twaron strand employed by the target ropes is stated by Teijin Twaron to have a linear density of 1780 dtex and a volumetric density of 1440 kg/m^3. This relationship between linear and volumetric density results in a calculated effective cross sectional diameter per strand of 396μm. When loaded into the target clamps, as shown in Fig. 8.2, the 8-strand targets had an average profile diameter of 1.60mm that expanded to 1.65mm at the clamped ends. The 4-strand targets, loaded as shown in Fig 8.3 and Fig 8.4, had an average profile area of 0.87mm that did not significantly broaden at the clamped end. For the first test, which used 8-strand targets, the average distance between tether targets was 2.30mm. For the 4-strand targets, the average distance between target tethers was 1.75mm for the second test and 1.44mm for the final test. Each target had a longitudinal diameter of 60mm exposed within the target region. When loading the tether targets into the clamps, the tethers were subjected to an unrecorded pre-load that caused all targets to be taut.

The impactors fired at the tether targets were made of a glass with density 2500kg/m^3. The glass impactors had a reported diameter of 254μm with a standard deviation of 1.5%, or 3.81μm. For the first test, a number of impactors less than 50 were used. For the second and third tests, the number of impactors used was more than 50.

The aluminium witness plates had a thickness of 1.48mm. The surface of the witness plate facing the tether targets was offset from the back of the targets by 110.2mm for each of the three tests.

8.3 Probability and number of likely impacts

Based on the size and offset of the targets associated with each test, there is a varying probability of impact associated with each impactor. For test one, there was a 47.54% chance of hitting a target tether in any manner (i.e., including impacts ranging from a slight graze to a direct hit) and a 34.51% chance of a direct hit (i.e., an impact where all parts of the impactor strike wholly within the target profile). For the second test, these probabilities change to 48.61% and 26.60% for impacts including grazes and those impacts that are only direct hits, respectively. For the third test, there is a probability of 42.82% for any impact and 23.47% for a direct hit. These probabilities are calculated using a simple geometric probability using the aggregate target profile area verses the total target containing all targets.

All tests were conducted with tens of impactors loaded into the savo, which is the expendable two-stage light gas gun component identified in Burchell *et al.* (1999) that holds the imapctors prior to them being fired at the target. The first test had somewhere between 30 and 50 impactors loaded into the savo, the second and third tests were conducted with significantly more than 50 impactors initially loaded into the gun. As per Burchell *et al.* (1999), the two-stage gas gun operates such that only around 6% of all impactors loaded into the gun reach the target. With this percentage, each test may see approximately 12 impactors reaching the target area.

For each test, there is more than a 50% chance that an impactor will result in a "clean miss," such that it strikes the witness plate without contacting any of the Twaron targets. Based on the Fish-Summers equation, a glass impactor similar to those used in these tests travelling around 5 km/sec, as were all impactors used in these tests, should cause a 0.35mm deep crater in a semi-infinite aluminium plate. As the impact tests produced craters in both the first and second witness plates similar in size to that predicted by the Fish-Summers equation, it is suspected that these two craters were caused by a glass impactor missing all of the tether targets and impacting directly with the aluminium witness plate.

8.4 Test 1

Test 1 was conducted with 10 tether targets spanning across the target area, each tether target composed of 8 tether strands braided without pre-loading or pre-twisting. All tethers were secured within the target area, using an unmeasured preload, such that all targets were taught. For this first test, the impactors travelled towards the target at a speed of 5.02km/sec.

For the first test, two indirect hits were observed in the target tethers and one suspected clean miss was observed in the witness plate. If three impactors reached the target area intact, this represents between 6% and 10% of all impactors initially loaded into the gun, in agreement with the previous calculations based on data supplied by Burchell (2001). Both impacts are identified in Fig 8.3 using various levels of magnification.

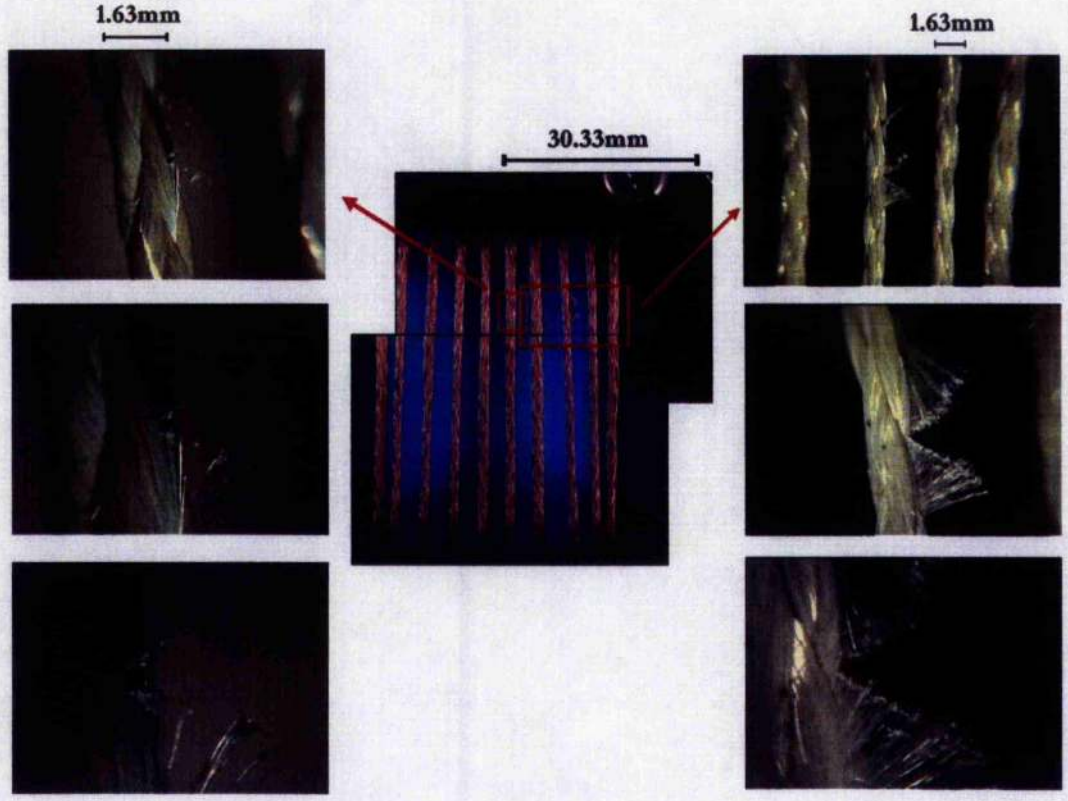

Figure 8.3: Aggregate picture of targets used in first test and close-up impages of the two identified impact locations.

The left-hand set of pictures presented in Fig 8.3 clearly shows the damage area. As each impactor diameter is approximately one-sixth the width of each target, it appears from examination of Fig 8.3 that the impactor glanced off the target. The second impact location also appears to result from a glancing impact, although it appears the impact is more significant judging by the relative number of severed fibres.

Examination of the witness plate identified two main regions containing small impact sites. These regions are identified in Fig 8.4. Between these two main regions is what appears to be a clean miss.

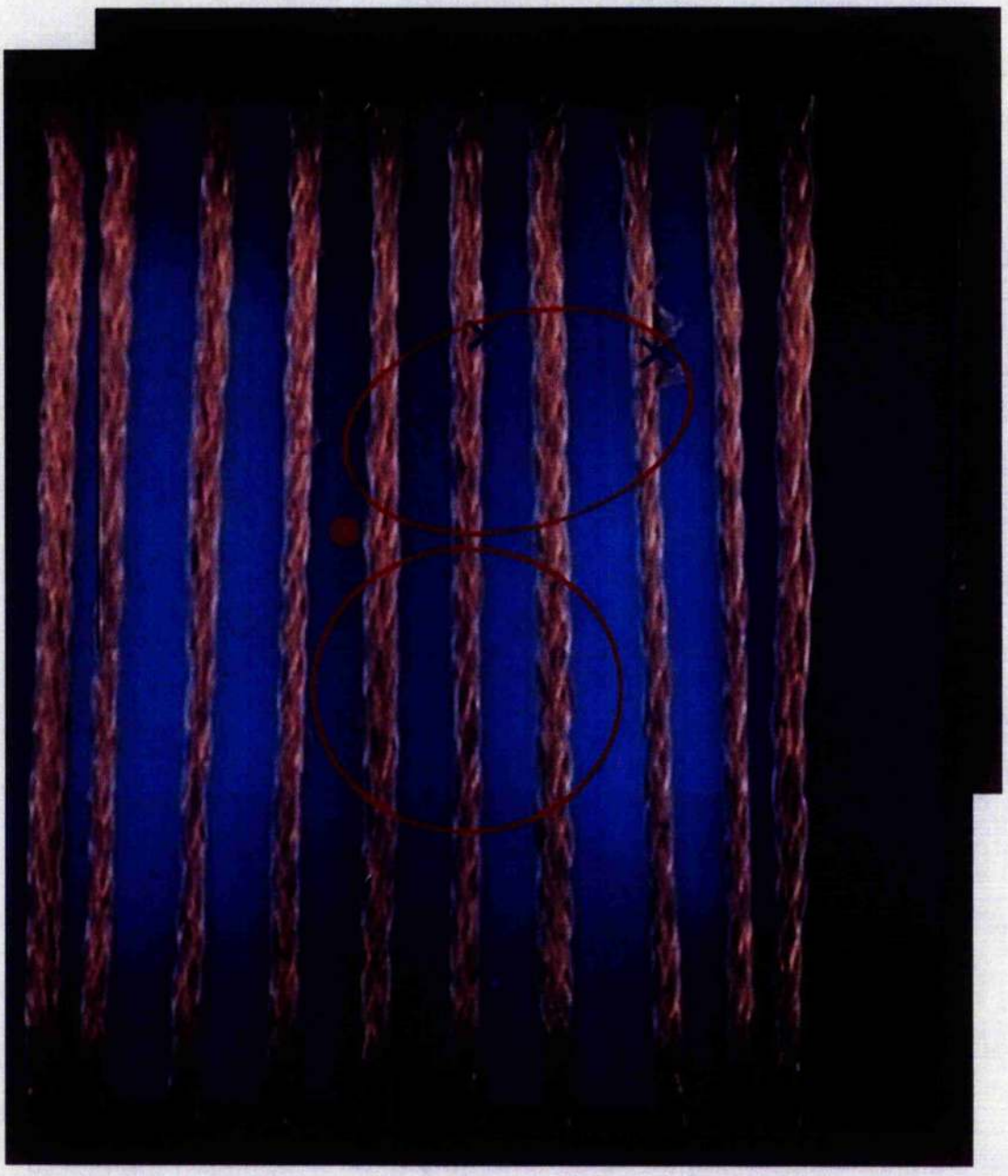

Figure 8.4: Test one with tether impacts marked with X, the location of the observed crater on the witness plate identified with a red dot, and the approximate boundary of small cratering marked with a red line.

The upper region of small craters identified on the witness plate of Test 1 seems to be located in the general proximity of the two identified impact locations. Contained within an ellipse that is approximately 15 mm by 10 mm along the major and minor

axes, respectively. If the craters within this upper region can be attributed to the impactors that struck at the identified impact locations, the debris dispersion appears to be contained within a 9-degree cone.

While it would be convenient to attribute this upper region to debris clouds formed by the two identified impacts, such a conclusion does not explain why the centre of the region is offset from the impact locations. Nor does such a conclusion explain the lower region, which appears to be independent, while the craters within are visually similar to those within the upper region. It is possible, though, that the upper region could be formed by the debris travelling away from the identified impacts, which the lower region is not, without causing an intellectual inconsistency.

As identified in Burchell (1998), not all impactors that begin the test in the savo reach the target at the end of the two-stage light gas gun. While only 6% of all loaded impactors are expected to reach the target intact, it is not unusual for glass impactors to break up in flight. If one of more impactors break up in flight, it is likely the debris formed by such an impact would remain close to the longitudinal axis of the gun. This assumption that the products would remain close to the flight axis is based on the logic that all impactors that stray significantly from the impact axis will not reach the target because of the restriction ring discussed in Burchell (1998).

8.5 Test 2

Test 2 was conducted with 16 tether targets spanning across the target area, each tether target composed of 4 tether strands braided without pre-loading or pre-twisting. For the second test, significantly more than 50 glass impactors were loaded into the savo. The impactors travelled towards the target at a speed of 4.97km/sec.

For the second test, there were three observed hits, one of which being direct, and one suspected clean miss. This number of impacts indicates that nearly 8% of all impactors initially loaded into the light gas gun reached the target area.

There are two areas identified in Fig 8.5, within which the three tether impacts were observed. In the pictures along the top of Fig 8.5, the direct impact is identified and

shown using a range of magnifications. In the pictures along the left-hand side, two impacts are identified. In the pictures along the left hand side, the two impacts are located on the two left-most targets. The most obvious impact shows a large number of fractured fibres, and is the focus of the bottom-left picture. The second picture of this left-hand set identifies the third impact to the below and left of this main impact (to assist in identifying this third impact, it may be of benefit to examine Fig 8.6, which identifies each impact with a blue 'x'). While both of these impacts appear to be indirect impacts, the smallest appears to be an extremely minor glancing blow.

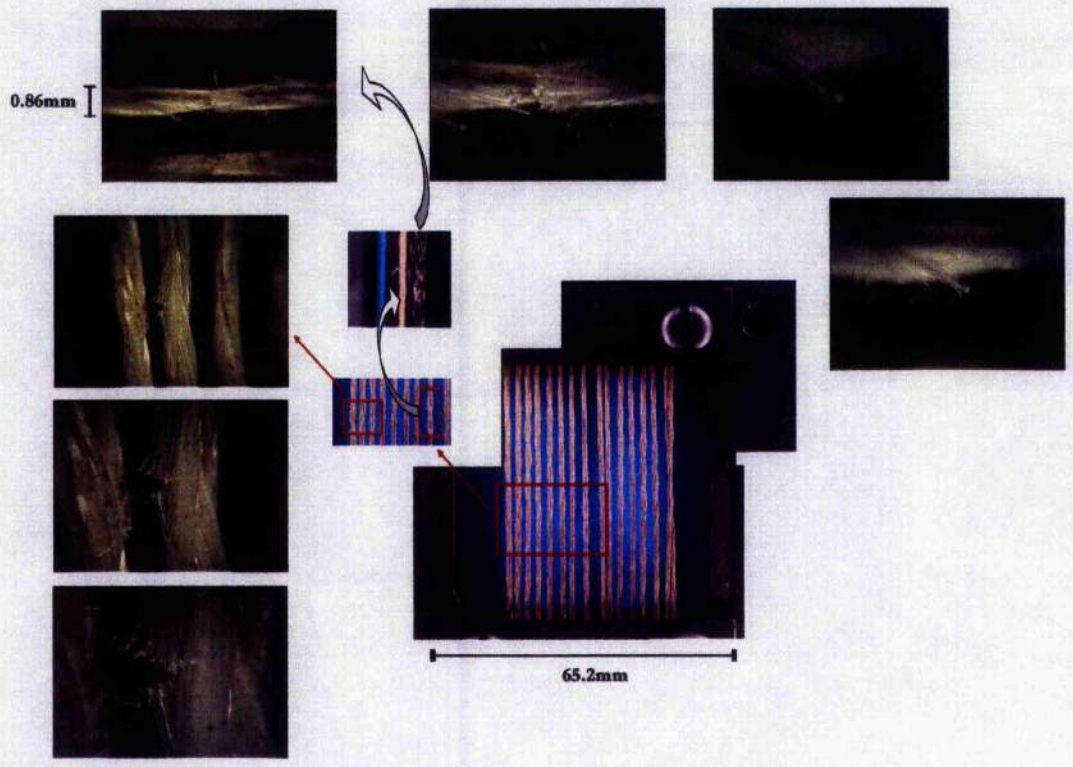

Figure 8.5: Aggregate images of second test rig after impacts, with close up images identifying the three impact locations. From left to right, impact 1 is contained on the far left tether in the leftmost close-up picture. In the same picture, impact 2 is shown in two further close-up images directly below the first. Impact 3 is identified in a side-on image, and then in a profile image with the target's longitudinal axis running horizontally, with further close-ups of the impact location and the severed tether ends.

Examination of the direct impact may be of interest from a modeling perspective. The Draper (72) equation predicts that a glass impactor that directly strikes a Twaron line as defined within should penetrate 889μm into the material. Since each strand has a calculated diameter of 396μm, it would seem logical to assume a direct impact would sever multiple tether strands. However, the damage appears contained within a single strand. This is likely due to boundary effects that are neither currently understood, nor for which enough background research has currently been performed. It is not fully understood, nor is this single data point sufficient for drawing any significant assumptions, but the fact that the damage is contained within a single strand could indicate that each strand can be treated as a single material for the purposes of hypervelocity impact modeling. Between strands, however, this single data point indicates that the failure affects may not allow for modeling the whole line as a single semi-infinite material, a conclusion that would be in conflict with the failure analysis research of Hayashida and Robinson (1993). While not conclusive, such data further supports the idea that the Draper (72) equation is suitably conservative for a tether-based system reliability analysis.

As with the first test, an aluminium witness plate was used to identify the debris travelling away from the target tethers. Identical to Test 8.1, it appears that a single impactor reached the witness plate intact without striking any tethers. While Fig 8.3 used circular boundaries to identify two distinct regions, Fig 8.6 identifies the location of each significant secondary crater. Increasing the contrast on an image of the witness plate identified these locations. This technique was possible for this witness plate because its surface was more finely finished than the other two plates. However, it is clear that not every secondary impact crater is identified using this technique. Because some of the secondary impacts are so small, many could be easily confused with surface abrasions when employing this contrast technique. To avoid erroneous results, any surface damage that could possibly be assumed as surface damage is not identified in Fig 8.6.

Examining the identified secondary craters relative to the regions identified in Fig 8.3 offers an indication that the number of points censored from Fig 8.6 may have resulted in an overly conservative estimation of the secondary debris affects. If it is

assumed that the secondary impacts identified can be attributed to the central tether impact, Fig 8.6 does not contradict the 9-degree dispersion concept proposed as a result of Test 8.1.

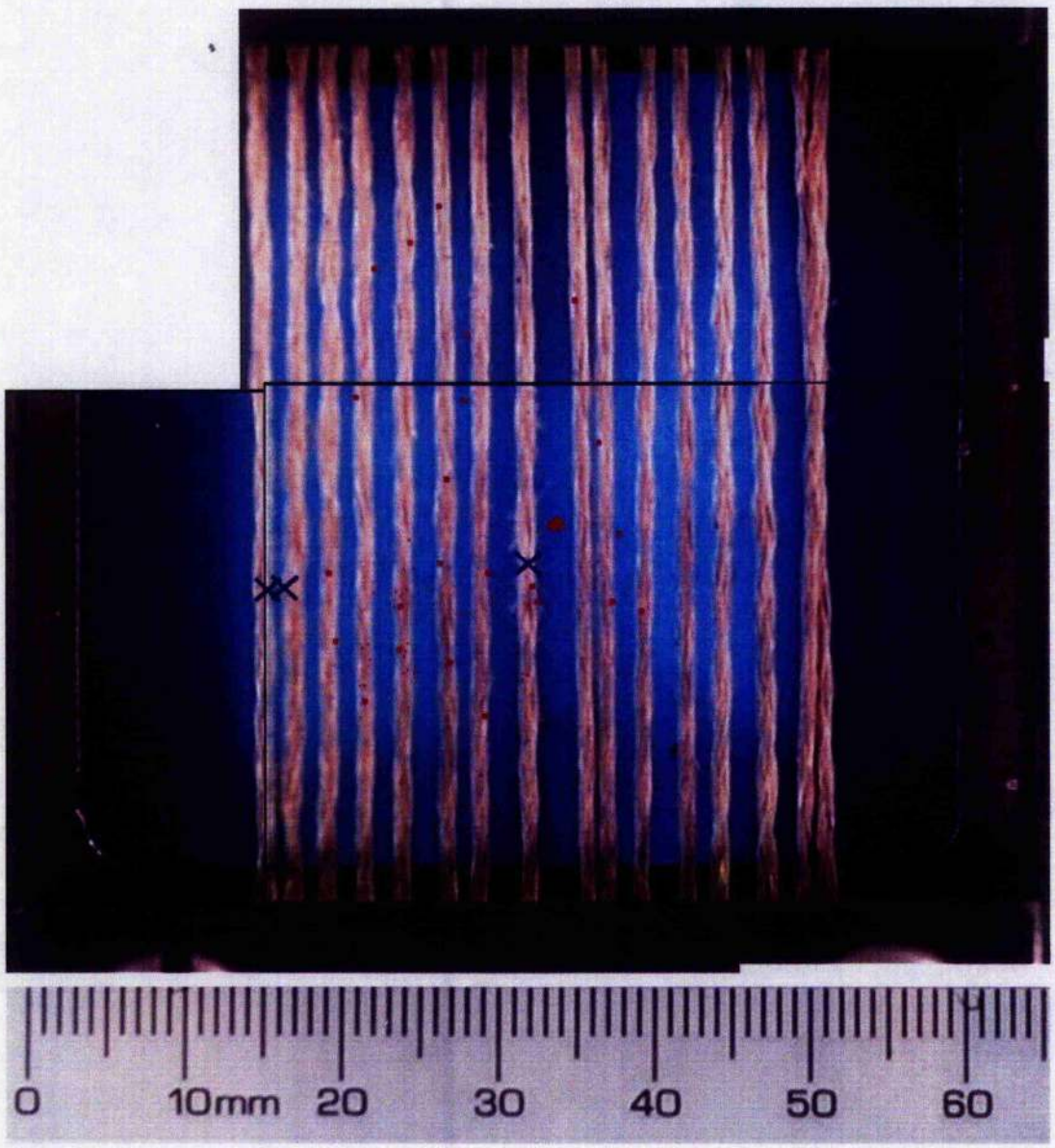

Figure 8.6: Superposition of the impacted tether strands and the locations of craters found on the witness plate associated with the second test. The blue X marks indicate the three identified impacts observed in the target tethers.

8.6 Test 3

Identical to Test 2, Test 3 was conducted with 16 tether targets spanning across the target area. The impactors travelled towards the target at a speed of 5.07km/sec. In addition to the aluminium witness plate, an irregular piece of Aerogel was attached near the target centre to capture any secondary debris. The location of this Aerogel piece is identified using the green trapezoid in Fig 8.8.

For Test 3, two impacts were identified on the tether targets, an indication that two impactors arrived at the target tethers intact. These two impacts indicate that 4% of the initial impactors reached the target. While on the low side, this percentage is still consistent with the calculations performed as a result of the information presented in Burchell (1998).

The Aerogel used for Test 3 was irregular in shape because it was a piece of scrap remaining from previous work. The profile of the Aerogel piece was wholly contained within a trapezoidal area where the left and right sides were both at right angles to the top, being of dimensions 26.88mm, 24mm, and 33.44mm, respectively. The average depth of the Aerogel was just over 25mm. The Aerogel was reported to have an approximate density of 99kg/m^3.

Figure 8.7 identifies the two tether impacts, again with varying levels of magnification. While the left-hand images appear similar to previous partial impacts, the right-hand side pictures appear unsymmetrical with regards to the number of fibres severed on the top half of the impact verses the lower half of the impact. This is a purely visual phenomenon, as the impact occurred on a section of the target where the braiding was causing the strand to rotate away from view. Examination of the specimen itself revealed that the facture was symmetric in the number of fibres severed, which is both logical and expected.

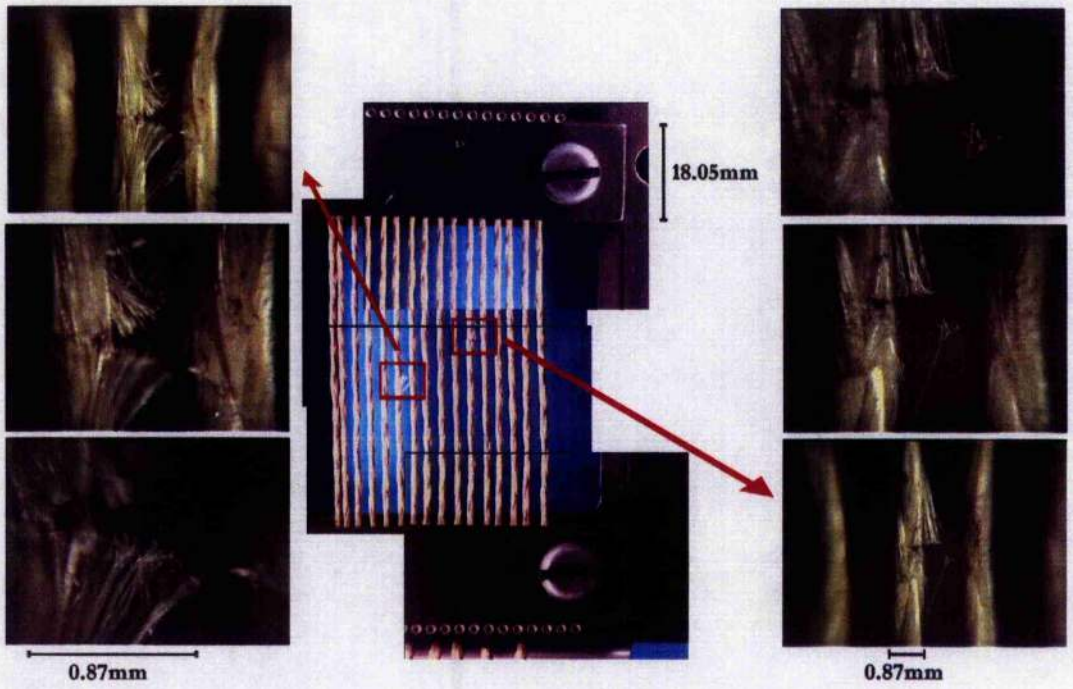

Figure 8.7: Aggregate image of the target tethers associated with test three and close-up images of the tethers at each of the two observed impact locations.

Figure 8.8 presents both where the tether impacts occurred, using a blue 'x' for each; where each of three significant debris piece was captured within the Aerogel, using a yellow 'x'; and an area that mostly encompasses the locations of the 13 smaller fragments found in the Aerogel. The fragments found in the Aerogel, identified from left to right with the yellow 'x' marks, are presented in Fig 8.9, Fig 8.10, and Fig 8.11, respectively. Figure 8.12 identifies one of the 13 small impactors that were located within the yellow circle marked on Fig 8.8.

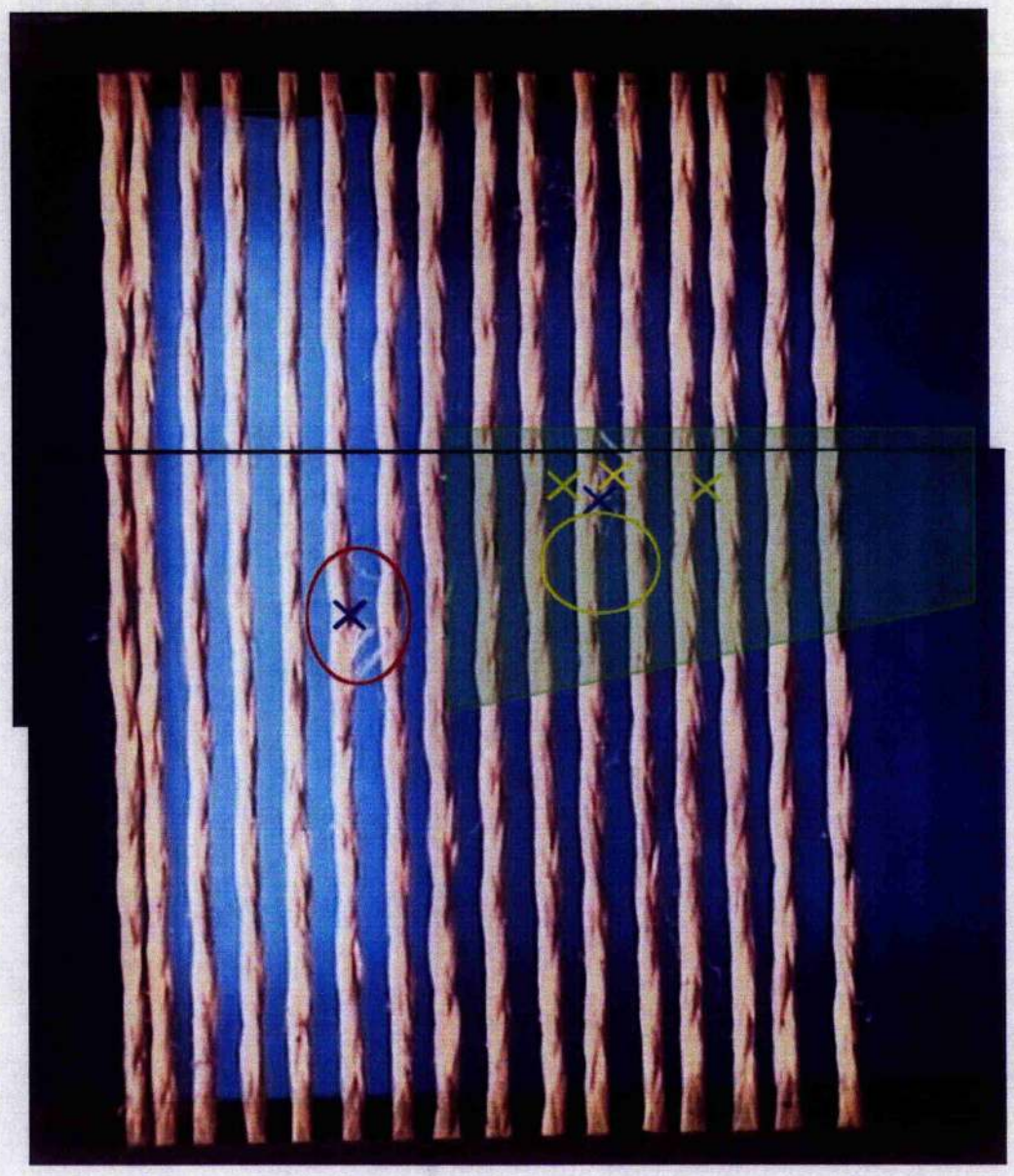

Figure 8.8: Impacts with tether observed after the third test marked with blue X, the location of surface craters on the witness plate bounded by a red line, significant impacts in the Aerogel marked with yellow X, and surface impacts into the Aerogel bounded by a yellow line.

As discussed above, impactors are decelerated and captured within Aerogel, leaving a track from the point where it entered the Aerogel to the location where it came to rest. For an Aerogel target with a density of 99kg/m^3, as is the sample attached to the

aluminium witness plate during the third test, the track an impactor makes within the Aerogel at velocities consistent with those used for these tests is empirically found by Burchell (2005) to be 100 times the diameter of the impactor. The three major tracks presented in Fig 8.9, Fig 8.10, and Fig 8.11, all had lengths of lengths 3.1mm, 5.09mm, and 4.5mm, respectively. Figure 8.12 shows one of the approximately 13 minor tracks, all of which had track lengths between 1mm and 1.67mm.

In Fig 8.9 through Fig 8.12, a scale is placed against the image that identifies the fragment diameter. For these four fragments, the diameter to track length ratio is consistent with the 1:100 ratio observed at similar velocities by Burchell (2005). This consistency appears to support a theory that very little velocity is lost between the original impactor and any fragments that are travelling away from the impact location.

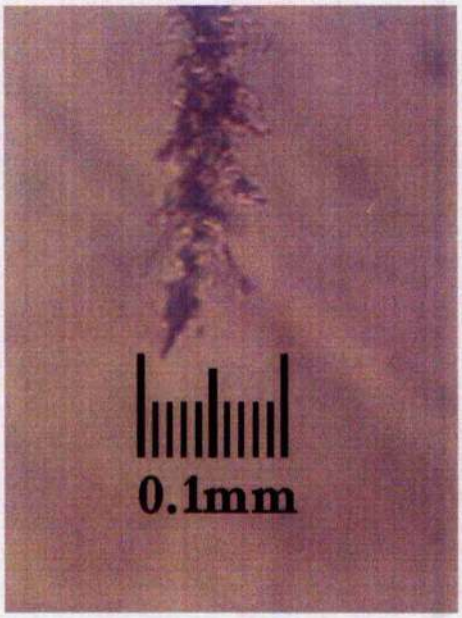

Figure 8.9: Track of length 3.1mm, and impactor located at end of the track identified as being on the order of 0.03mm.

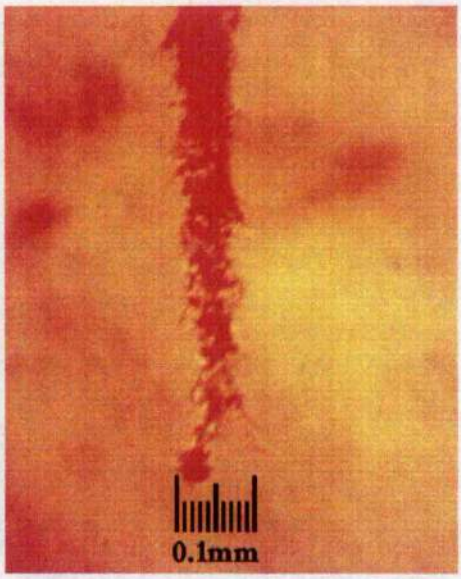

Figure 8.10: Track of length 5.09mm with impactor identified as being on the order of 0.05mm in diameter.

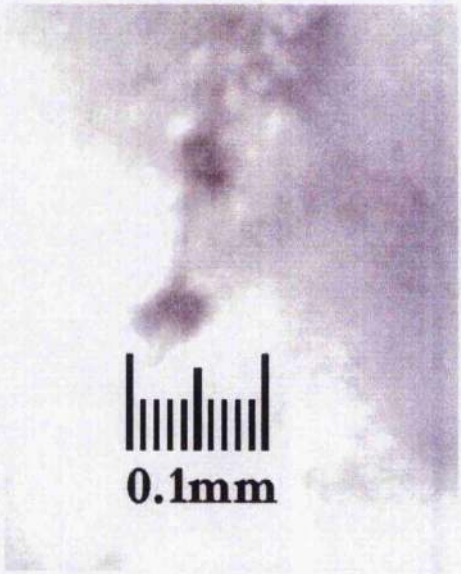

Figure 8.11: Track of length 4.5mm with impactor identified as being on the order of 0.05mm in diameter.

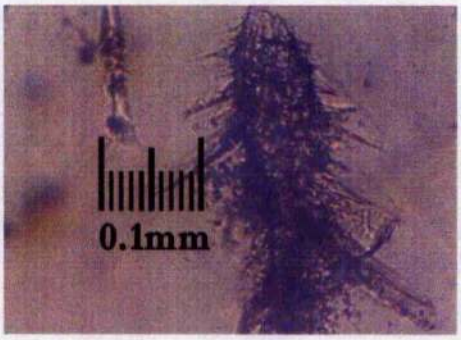

Figure 8.12: Example of one of 13 small surface impact tracks, with an impactor identified on the order of 0.02mm in diameter.

The location of these fragments in the Aerogel and on the witness plate offers a further indication that all dispersion is contained well within a 9-degree cone. With regards to the impact that did not occur over the Aerogel target, the dispersion appears to be tighter still, considering a debris patch was not observed on the far left side of the Aerogel specimen.

With regards to the size and velocity of the debris travelling away from the impact, while the 1:100 diameter to track length relationship appears to support a theory that the debris has not slowed down significantly upon formation, the size of each captured debris piece raises questions as to where the bulk of each impactor went. When looking at the three major fragments captured in the Aerogel, and adding the volume of 13 smaller fragments assuming a diameter of 15μm each, the total volume captured is calculated to be less than 2% of the original impactor mass.

8.7 Conclusions

This series of tests offers data points that contribute to the general knowledge of how semi-infinite aluminium plates and tethers react when being impacted at hypervelocities. Additionally, this series of tests offers the first known public examination of how the resulting debris associated with a hypervelocity tether impact forms and propagates. Due to the small number of tests and observed impacts, these tests cannot prove or disprove any theory when used in isolation. However, the observations one can make from these tests do offer possible trends that could be confirmed by further replicating these tests with some further modifications.

8.7.1 Tether impacts

The damage associated with each tether resulting form a hypervelocity impact does not disprove the Fish-Summers equation nor the Draper (72) equation proposed within. For the single direct impact observed throughout these tests, the Fish-Summers equation predicts that an intact impactor would fracture approximately 0.39mm of the target tether, while the Draper (72) equation predicts a depth of penetration on the order of 0.89mm. As each tether strand is calculated to have an

effective tether diameter of 0.396mm, and only one tether strand was fractured, there is no evidence contained in this impact that disproves the applicability of the Fish-Summers equation. At the same time, the Fish-Summers equation as it is employed was not calibrated for densities as low as the Twaron targets, so such agreement may be the result of random chance. It seems more logical that the boundary conditions in existence between tether strands is not fully understood, a conclusion arrived at after an examination of the predictions obtained using the Draper (72) equation.

8.7.2 Impactor fracture

There is no evidence that an impactor remains intact after an impact with a tether target. This lack of evidence comes from the fact that no crater present on any witness plate that could correspond to an intact impactor impact was located behind a target tether. Further, the only surface damage or fragments contained within the Aerogel that were within a reasonable distance from the impact location were significantly smaller than an intact impactor. While there were only 13 observed surface impacts and three other significantly sized impacts contained in the Aerogel, the aggregate mass of these impactors is still not equal to one intact impactor. Therefore, if these all came from the same impactor that fractured after striking the tether, the impactor must fracture into no fewer than 20 fragments of varying size.

8.7.3 Fragment velocity

There is no indication that any of the fragments striking the Aerogel have significantly reduced in velocity following the impact. Based on the size of the observed impactors contained within the Aerogel and the track caused by each, all seem to conform to the track length verses impactor diameter relationship observed by Burchell for an Aerogel of specified density.

8.7.4 Fragment dispersion

There is no conclusive proof to link any fragment cratering or captured fragments to any specific impact location. If it can be assumed that the fragment craterings at a given location on the witness plate or within the Aerogel can be associated with the nearest tether impact, this would result in an approximate limit on any fragment dispersion being 9°.

8.8 Recommendations and future work

The results of these experimentation lead to two major recommendations for future testing of tether materials and for analytical work on space tether systems.

8.8.1 Testing improvements

More testing must be conducted to verify that the results presented herein are repeatable. This testing should also include techniques, such as foil covers that can more clearly report on the location of arriving and departing impactors, that can offer more evidence of which resulting impacts can be attributed to which impactors. The current inability to directly verify how many impactors are reaching the targets, and which debris products can be attributed to which initial impactor, is a significant limitation to the current work.

8.8.2 Analytical assumptions

Current space tether analyses assume that a single impact will only cause a single failure. While not conclusive, this work has offered an indication that such a relationship may not be exclusively valid. For this reason, in addition to an analysis employing the one-impact-one-failure assumption, a secondary analysis should be preformed that accounts for possible debris dispersion. As this secondary analysis should be conservative enough to parameterise the true failure scenario, this work recommends employing an assumption that each impactor breaks into a lethal debris cloud that disperses at an angle of 9-degrees.

Chapter 9

TetherLife Analysis Program

With an understanding of the physical properties associated with aramid fibres such as Twaron, an empirical equation for calculating the product of impacts with such fibres, and insight into the likely secondary effects of such impact, a predictive assessment of the susceptibility of a tether-based system to orbital debris and micrometeorite impacts can be made. To do so, a program called *TetherLife* was created to support this research.

9.0 General approach

TetherLife is a Monte Carlo discrete element approach, which breaks down each large tether system into small components on the order of one meter in length, and randomly selects a large number of elements for analysis. As discussed in literature such as Liou *et al.* (2002), on-orbit lifetime analysis tools are only valid for constructing long-term average effect calculations on objects that are uniformly susceptible to a specific environment over the analysis period. By breaking down the entire span of the examined tether system into small elements, TetherLife is able to analyse each discrete element in a valid manner. After sampling a significant number of elements at a significant number of times throughout the defined mission, an average failure rate per discrete element is found. With this average failure rate, and knowing how these discrete elements interact with each other when forming each tether span, TetherLife then computes the failure rate for the entire span.

Over the lifetime of a mission, a momentum exchange tether system will go through many operational states and will be subjected to a wide range of environments. By defining specific system and mission parameters, TetherLife uses these specifications to determine how likely it is that the system being analyzed would be in a specific state. For example, because it is assumed that the system facility travels in a Keplerian manner, TetherLife can determine what percentage of the system's time on orbit is spent between two angles that are 10 degrees on either side of perigee. Using

similar calculations, TetherLife can randomly select randomly generated system states that comply with the system and mission definition.

After TetherLife has selected a suitable system state, it then randomly selects a discrete element on that system, and determines what environment that element is currently facing or has previously faced. For example, for a tether system that retracts after use, the system tips will be exposed to the space environment for more time than tethers close to the system facility. For this reason, discrete elements of the tether near the tip will be more significantly degraded by atomic oxygen as the mission progresses. Consequently, and because the tip is travelling faster than points on the sub-span nearer the system facility, the same size piece of debris at some point in the mission is more likely to cause a failure at the tip than at other locations on the sub-span, where it would not have likely caused a facture at any location some time earlier in the mission.

After selecting the suitable mission state and generating a reasonable history for each discrete element, TetherLife then generates a current environment for that element based on probabilistic models of the space environment. By calculating what environment the examined discrete element is likely facing given the system state, location, and event time, TetherLife is able to calculate whether an impact is likely to occur, and whether that impact would result in a failure. By examining a number of these randomly generated scenarios, the analysis package predicts an average probability of failure for the system as a whole over the course of the entire mission.

The overall flow of the TetherLife program is presented in Fig 9.1. Each element listed on the top-level flow chart will be discussed below.

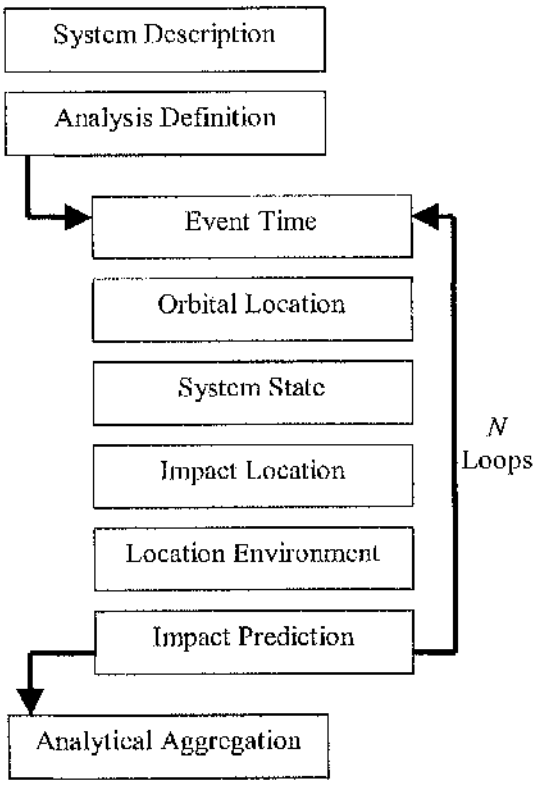

Figure 9.1 Overview of the how the probability of failure is computed for each sub-span by TetherLife.

TetherLife is a research tool designed in support of this analysis, currently in version 1.2. As with any other research tool designed to be similar in scope and fidelity to a commonly accepted engineering model, TetherLife accepts minor losses in fidelity for significant gains in efficiency. For example, when assessing the probability of failure due to a hypervelocity impact, TetherLife employs the Draper (72) equation for semi-indiscrete targets instead of employing a costly hydrocode analysis. Such an approach is well supported by the literature in works such as Frost (1969), Cour-Palais (1970), and Hayashida and Robinson (1993), and offers suitable first-order analysis results.

9.1 Setting up a TetherLife analysis

To begin a TetherLife analysis, the user must define the system he or she wishes to be analyzed, and the mission parameters within which the tether system will operate. The variables required for setting up a TetherLife analysis are discussed below.

9.1.1 System description

TetherLife is capable of performing analyses on both a passive momentum exchange tether system, which uses the force imbalances associated with long objects on elliptical orbits to produce angular rotation in the system; and an MMET system, which uses a motor in the system facility to cause its two tether spans to counter-rotate. Illustrative examples of each system are presented in Fig 9.2.

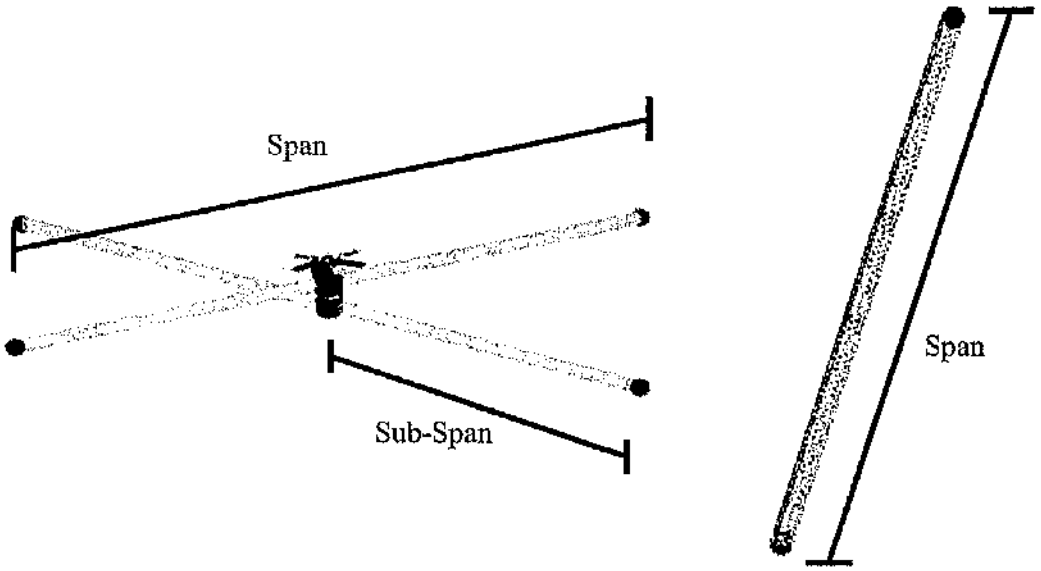

Figure 9.2: Example of a MMET system (left) and a passive momentum exchange tether system. The *span* and *sub-span* are identified, as applicable. Span graphics are based on the Hoytether graphics obtained from the Tethers Unlimited website (http://www.tethers.com/Hoytether.html).

If TetherLife is employed to assess a MMET system, it is assumed that all four sub-spans are of equal length and one span is twice the sub-span length identified by the user. For passive systems, the length identified by the user is the total span, and it is assumed that the spin axis, about which the system rotates, is at the midpoint of the system. For some situations (i.e., when a passive system employs large counterweights where the spin axis is significantly shifted to one end of the system), this assumption that the spin axis is at the midpoint of a passive system could cause a significant shift in the distribution of impact velocities, thus altering the local

environment observed by the modeled system. However, it is assumed that any conservatism in the local environment that would be observed at one end of the modeled system, resulting from a decrease in the average impact velocity, would be sufficiently countered by the corresponding loss of conservatism at the other end.

After defining what type of system is to be analyzed (i.e., a MMET or a passive system), the general parameters of the system must be set. Such parameters include the characteristic length of the system, L, which corresponds to a sub-span for a MMET and a span for a passive system; the tether material density (ρ) and break strength (S_B), which determine the maximum operational angular velocity that can be achieved by the system; the operational angular velocity, which is the rotational velocity about the system spin axis (i.e., the system facility for a MMET, and the midpoint of a passive system) at the time the payload is released; the reaction efficiency of the tether material, η_R, which determines how quickly the tether material wears away when exposed to the atomic oxygen environment, thus decreasing the diameter of each tether strand; and the diameter of primary lines (i.e., lines that are designed to bear the forces required by the mission under normal operation) and secondary lines (i.e., lines that are designed to each partly substitute for a single primary lines in the event that the primary line fails).

Within each span, there are likely to be multiple tether lines. How these lines are organized has a direct affect on how the system reacts to a failure in one line if it happens to be impacted by an object on orbit. In Fig 9.3, three different tether line orientations are presented. On the far left, a span is made of one tether line. For this system, the probability that the system would fail is equal to the probability that this single line fails. Considering the length of such tethers and the density of the debris environment, such a configuration is likely to fail very soon after it is introduced to the orbital environment.

The second orientation presented in Fig 9.3, center, represents a span composed of three tether lines, each identically capable of bearing the load required by the mission. While, similar to the first orientation presented on the far left, a failure anywhere on each line will cause the whole line to fail. However, unlike the first example, a failure

of one line will not cause a failure of the system. Assuming each line is capable of independently bearing all the loads required by the mission, all three tethers must fail before the system fails. If there is a 20% chance that the first orientation will fail over the course of a day, there is only a 0.8% chance that the second orientation will fail over the course of that same day. While a tremendous increase in reliability, such a technique for increasing reliability does require significant gains in system weight. If the mission requirements cannot afford the weight increases required to support reliability gains using such a design method, system designers must begin looking towards *cross-strapping* techniques.

Many systems work because a group of sub-systems are all working in series to perform a certain task. This is very similar to the far left illustration in Fig 9.3. So long as the single tether line is unbroken, the system is operational. The center picture then increases the reliability of the system by increasing the number of lines. However, the far right illustration in Fig 9.3 is an example of cross-strapping using a Hoytether design. This design allows for multiple breaks in a single primary strand, something that was impossible in the two other un-strapped examples.

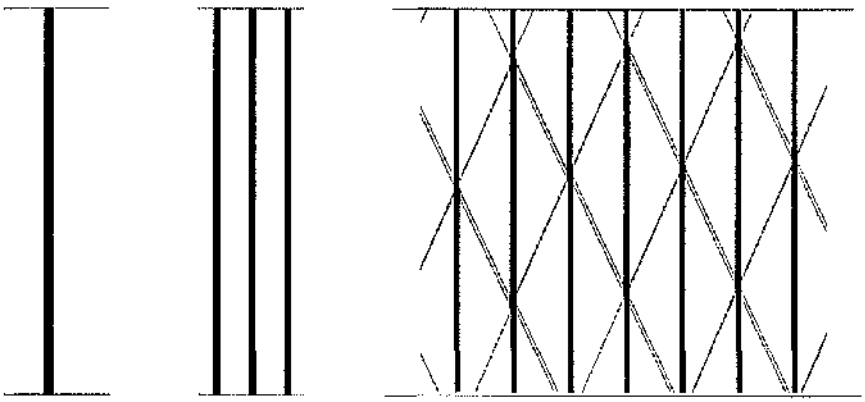

Figure 9.3: A system span composed of one primary line (left), multiple primary lines (center), and primary and secondary lines arranged in a Hoytether configuration.

The Hoytether works like any other cross-strapped mechanical system; when a component fails, its task is allocated to its surrounding components. By interlinking

primary strands with secondary lines, the Hoytether has essentially divided each primary line into a series of sub-lines, each sub-line independent of the sub-line either following or proceeding. When a sub-line fails, the load that was carried by that component is distributed to its surrounding components. This is illustrated in Fig 9.4.

Figure 9.4: The force previously supported by the now broken primary tether is distributed along the surrounding, dark black secondary lines. Span graphics are based on the Hoytether graphics obtained from the Tethers Unlimited website (http://www.tethers.com/Hoytether.html).

TetherLife allows the analyst to assess a system using any combination of the three different tether line orientations presented in Fig 9.3. If the analysis is assessing spans that use either of the un-strapped configurations, the user must define the number of primary lines required, the number of redundant primary lines, and the diameter of each primary line, d_P. If the analyst is using spans that incorporate a Hoytether method of cross-strapping, the user must define the number of primary lines, the number of redundant primary lines, the number of secondary lines associated with each primary line, and the diameters of both the primary and secondary lines, d_P and d_S, respectively.

9.1.2 Mission and analysis definition

After defining the system, the user must define the mission that will be analyzed. Such mission analysis parameters include the start and end dates of the mission, T_0 and T_1, respectively; the orbital parameters for the tether system being analyzed, such

as eccentricity, e, height at perigee, h_p, and orbital inclination, α_{inc}; the operational angular velocity, ω_{op}; the orbital angle from system perigee at release, θ_R; the ratio between the time the system is on to the time it is off, t_{on}; the ratio of the time the system is at its operational angular velocity to the total time it is operating, t_{op}; and the time step used by the analysis, Δt. After defining these model parameters, the user defines the number of randomly generated states he or she wishes to be included in the analysis, as well as a threshold term that defines the accuracy of any iterative calculations (i.e., if the user defines 0.001 as the threshold, iterative calculations will be completed when the difference between iterations is less than that value).

With the mission and analysis parameters, TetherLife generates an array of discrete steps along the orbit. Throughout the analysis, this array will be used to select the orbital location of the system. For smaller increments of time, the array will contain more points since locations on the orbit are generated based on the time it takes the system centre to travel between the orbital locations. If an orbital position is chosen from this array using a uniform distribution of array locations, the orbital location of the system will always be a valid random location based on the distribution of possible orbital positions throughout the mission.

9.2 Generating a data point

To achieve its goal of generating a number of acceptable random event scenarios, TetherLife loops through a selection and assessment process. In selecting an event, the following flow is maintained.

9.2.1 Event time and solar state

The first step TetherLife takes when generating a random event scenario is to select when the event happened. Every sample is modeled to occur within the start and end date of the mission. As inputted by the user, TetherLife selects a moment in time that represents the time each randomly generated event would occur at from a uniform distribution identified as follow:

$$f(t) = U(T_0, T_1) \tag{9.1}$$

To achieve this, TetherLife uses the following to generate the time T_i using the Microsoft Visual Basic C++ 8 (Beta2) compiler, where all variables are long unsigned doubles:

$$T_i = \frac{\text{rand()}}{\text{RAND\_MAX}} \tag{9.2}$$

As is with any computer number generator, the random numbers generated are only pseudorandom numbers. To ensure, as much as reasonably possible, that the numbers are random relative to each other within the program and relative to each other on various runs, the rand() function is re-seeded to the user's computer clock time at the beginning of every TetherLife analysis.

All numbers generated using a uniform distribution in TetherLife will be generated using the method described above. While the numbers are theoretically pseudorandom, considering the technique's wide use in solutions using commonly accepted engineering analysis software such as MatLab, this techniques is assumed to offer sufficiently random values for the purposes of an analysis performed by TetherLife.

As described in more detail when discussing the environmental models, TetherLife cannot sample an instantaneous moment in time, but must sample a discrete time increment. While terms such as "moment" or "instant" are often used in this study to refer to the time at which a selected impact condition is assessed, the model of the impact condition is really happening over a time span defined as follows:

$$t \geq T_i \cap t < T_i + \Delta t \tag{9.3}$$

For the purposes of selecting appropriate values from the distributions, etc., TetherLife calculations are made under the assumption that Δt is appropriately small such that the values obtained at the time T_i can be assumed valid over the entire time step Δt.

With the event time, the level of solar activity can then be found. Solar activity is a driving element of the environment, and occurs in 11-year cycles. It is accounted for in the literature as an *F10.7 value*, which corresponds to a 13-month smoothed solar flux. Based on a quantitative analysis of the available data for solar cycles 20 and 23, TetherLife models the solar cycle using the following formula:

$$S(\text{F10.7}) = 27.061\left|T_i - T_C\right|^{\frac{3}{2}} \exp\left[-\left(\frac{\left|T_i - T_C\right|}{5.3}\right)^{\frac{5}{2}}\right] + 70 \tag{9.4}$$

Where T_C is used to place the current time into its appropriate location relative to solar cycle 23, and is found as follows:

$$T_C = 1996 + 11\left(\text{int}\left[\frac{T_i - 1996}{11}\right]\right) \tag{9.5}$$

This use of a fitted curve for solar cycle 23, and even the use of solar cycle 23, is a significant approximation. However, relative to its later use in the orbital debris model, a variation of 20% in this model near the beginning and tail end of the solar cycle has only a 0.2% to 0.3% affect on the orbital debris flux value. At the peak of the cycle, this effect can increase to between an 11% to 20% change in the orbital debris flux approximation. However, considering the uncertainties associated with the orbital debris environment, the uncertainty associated with using this model based on solar cycle 20 and 23 is assumed insignificant.

9.2.2 System state

After finding the time of the randomly generated analysis point, TetherLife constructs a likely system state for that time. The foundation of this generated system state, as alluded to earlier, is the random selection of the system location on its orbit. This is done because all momentum exchange tether systems are designed to operate in a manner that is coupled with the orbital dynamics of their orbit. For a passive momentum exchange tether system, the system could begin to tumble, thus producing the angular velocity that allows the system to impart significant tangential velocities

to a payload located at the system tip, when there is an imbalance in the local velocities and forces of the system relative to the gravity gradient, with which the system was originally oriented while hanging on orbit. Such an imbalance arises when the system, while travelling on a highly elliptical orbit, approaches perigee. For this reason, if TetherLife randomly selects an orbital position that is close to perigee for a passive momentum exchange tether system, TetherLife will assume that is highly likely the angular velocity of the system is close to its operational angular velocity. However, TetherLife does not use the orbital dynamics of the system to calculate what that operational angular velocity is at any moment in time. TetherLife assumes that the angular velocity inputted by the user is appropriate for the system, and makes very general, normally distributed assumptions as to the angular velocity relative to the proximity of the central facility to the perigee of its orbit.

These assumptions are made because, while work is ongoing in this area, there is no publicly available data that would allow TetherLife to make assumptions that better apply for all systems. For this reason, especially for passive momentum exchange tether systems, mission planners intent on using the package for a specific mission would require specific changes to be made to the model. Such changes would include either modifying the distributions used within TetherLife, or allowing for non-standard distributions be created within the model using suitable orbital dynamic models.

Unlike a passive momentum exchange tether system, a MMET does not rely on imbalances in the orbital dynamics of the system to produce the operational angular velocity in the system spans. Because a MMET relies on a motor in its system facility to produce angular velocities in its counter-rotating spans, it can make use of the orbital benefits afforded a system launching at apogee. While both a MMET and passive momentum exchange tether system have the same limiting operational capabilities as a result of their material, the MMET is potentially capable of delivering its maximum velocity increment to a payload at a much higher altitude than a passive system, thus making the system more effective from the standpoint of direct payload transfer. Consequently, TetherLife assumes a MMET will be at its operational angular velocity at apogee, and makes a similar approximation for generating an

angular velocity for the system relative to apogee as it does for a passive system at perigee.

Regardless of the system, after selecting the location of that system using the orbital position array as discussed above, the angular velocity is generated as a normally distributed random variable with a standard deviation based on the orbital location, θ_i, relative to the system release point, θ_R. The standard deviation of the normal random variable is as follows:

$$\sigma_\omega = \exp\left(\left|\theta_R - \theta_i\right|\right) - 1 \tag{9.6}$$

With this standard deviation, a standard normal random variable is generated using two uniformly distributed variables x_1 and x_2, both generated identically to the uniformly random selection of time within the mission, as follows:

$$y_1 = \cos(2\pi x_1)\sqrt{-2\log(x_2)} \tag{9.7}$$

From this generation of y_1, the angular velocity at T_i is the operational angular velocity multiplied by one less the product of y_1 and σ_ω. While it is true that this use of the exponential function is relatively arbitrary with regards to generating the standard deviation, it is a logical choice in a situation where no better data is currently available in the public domain. For an MMET system, verifying such an approximation would require a further study of the angular acceleration and deceleration associated with various motor sizes and types, work that is currently ongoing at the University of Glasgow. For a passive system, there are a number of orbital dynamic and operational considerations that must be further explored for each mission, including how one stabilizes a passive system after use, relative to the gravity gradient. Without such studies, the use of the exponential as it is in this approximation of standard deviation is consistent with available data.

Once TetherLife has selected a location and an angular velocity, it then selects an appropriate span length. For MMET systems, the operational model incorporated into

TetherLife and being explored at the University of Glasgow for its dynamical and operational advantages assumes that the system receives its payloads when the tether sub-spans are retracted into the system facility. As full retraction of the sub-spans means the moment of inertia is at a minimum, it is assumed that the facility will spin-up to its full operational angular velocity at this time. Based on the power required to angularly accelerate the system in a retracted verses an extended orientation, spinning up to the operational angular velocity before retracting the tether sub-spans is the most efficient use of energy. It is at this point of maximum angular velocity that the sub-spans would be released. As the sub-spans will increase the moment of inertia for the system, more power will be required by the system facility as the moment of inertia increases just to maintain the same angular velocity. By finding the most efficient power usage profile, the release rate of the sub-spans can be calculated. In addition to power considerations, especially for aramid fibers, there may be a loading rate that is optimal for the tether material. All of these factors must be taken into consideration with each system to determine the distribution of lengths a MMET system will see throughout the course of its mission.

As such knowledge of system power consumption and how to harness the benefits of the strain-rate dependency exhibited by the tether material is unknown at this time, TetherLife uses four main assumptions when randomly generating the state of the sub-spans:

1. When the system is at its operational angular velocity, the sub-spans will either be at full length, or will be approaching their full length,
2. When the system facility is stopped, the sub-spans will either be fully retracted or will be retracting,
3. When the angular velocity of the system facility is changing, the sub-spans will either be fully retracted or at full length, and
4. The sub-spans will release and retract in an identical, smooth, and continuous manner.

With the first three assumptions, a selection criterion of state can be created. As shown in Fig 9.5, once the angular velocity is known, the four assumptions above

require the span length to be restricted to a specific state. For example, if the angular velocity is not at either its maximum or minimum, there is assumed to be a 50% chance that the span is either fully extended or fully retracted as per the identical nature of extension and retraction made in the fourth assumption. For situations where the angular velocity is either at its maximum or at its minimum, TetherLife needs a probability distribution for determining the likely state of the tether spans.

System Operating	Operational State	$\omega_i = \omega_{op}$	$L_i = L$
	Changing State	$\omega_i = \omega_{op}$	L_i = increasing
		$\omega_i = 0$	L_i = decreasing
		ω_i = increasing	$L_i = 0$
		ω_i = decreasing	$L_i = L$
System Idle	Rest State	$\omega_i = 0$	$L_i = 0$

Figure 9.5: Various states of angular velocity and span length as defined by TetherLife.

However, since there is currently no publicly available work with the orbital dynamics of a MMET system that can be studied to find an appropriate distribution function, TetherLife employs the arctangent function to achieve a malleable distribution that provides random values in accordance with the requirements of the fourth assumption. To generate these distributions, TetherLife employs the $t_{\omega r}$ and t_{op} ratios cited earlier in this work, as well as the t_{oL} and $t_{\omega L}$ terms that must also be inputted by the user.

If it can be assumed that the total time that the system exists is represented by unity, the portion of its lifetime that the system spends carrying out a mission, verses the time it is just sitting on orbit waiting for the next mission to begin, is equal to $\frac{t_{on}}{t_{on}+1}$. For example, if t_{on} equals 0.5, that means that 33% of the system lifetime is spent

performing for and shutting down from a mission, while 67% of its lifetime is spent idly on orbit.

As illustrated by Fig 9.5, within that time that the system is operating, a certain percentage of that time will be spent such that that the system is operating at its operational angular velocity. This percentage of that operational time spent when the system is operating at its maximum operational angular velocity is t_{op}. Relative to the total lifetime of the system, the portion of the entire system life that the system is operating at is maximum operational angular velocity is then $\frac{t_{\omega n} t_{op}}{(t_{\omega n}+1)}$. For example, if that same system that operates 33% of its time also operates at its operational angular velocity such that t_{op} a equals 0.5, these ratios would be combined to find that, out of the entire life of the system, 16.5% of that time is spent at its maximum operational angular velocity. Understanding these ratios allows the analyst to adjust the rate at which the system accelerates up to its operational angular velocity and the rate at which the system is used on orbit.

To understand the state of the tether spans at the i^{th} instant, L_i, one must also consider the t_{oL} and $t_{\omega L}$ terms. The t_{oL} term states what percentage of the time that the system is operating at its maximum operational angular velocity is done with the sub-spans at full extension. For efficient systems where the payload is released very soon after the system is ready to launch, this t_{oL} term will be very small. The larger this number gets, the more inefficient the system is likely to be relative to an optimal launch. Here, an optimal launch is one where the system spins up, reaches its full operational angular acceleration and the sub-spans are fully out exactly at the release point, releases its payload, and near instantly begins to shut down after the mission. As achieving this state seems intuitively rare, it is reasonable to assume that an actual MMET system will have a relatively significant t_{oL} value. The $t_{\omega L}$ term is the ratio between how long the system takes to accelerate and decelerate to and from its operational angular velocity and how long the system takes to extend or retract the sub-spans to and from their full length. As it is assumed that the system takes an equivalent time to both accelerate or decelerate and extend and retract, these two

terms are the final requirements for solving all of the time relationships identified in Fig 9.5.

When the sub-spans are either expanding or retracting, the sub-span length at the i^{th} instant is found using the arctangent function. As previously discussed, there is currently no information available with regards to how an operational MMET system would accelerate or decelerate, accounting both for efficient motor operation in the facility and the orbital dynamic equations governing the system. By using the arctangent function, a random variable that is uniformly distributed between zero and unity, y_i, can be used to select random lengths that transition smoothly from zero to L as follows:

$$L_i = \frac{L}{\pi}\left[\arctan\left(\left[20y_i\right]-10\right)+\frac{\pi}{2}\right] \tag{9.8}$$

The use of arctangent and the use of the constants 20 and 10 was an arbitrary selection made on qualitative grounds. The use of arctangent offered results that appear intuitively logical, meaning the system will take more time during the beginning and the end of each process than it will once the process is underway. This is why arctangent was chosen over a linear relationship between time and extension. However, arctangent produces results that are not so unique to a specific assumption of how the orbital dynamics and motor performance will interact that it would produce egregiously erroneous results. Further, the use of the constants 20 and 10 were chosen to minimize the discontinuity in the function at the extremities. By using these constants, the arctangent function generates random length variables between 3% and 97% of the total length. While it would be ideal to have these values contain the whole range of span lengths, a qualitative assessment of the results indicates that such a minor discrepancy is not outside the scope of an engineering model.

For passive systems, it is assumed that the system is at its full span length for all points throughout the analysis. For this reason, users wishing to assess a passive system only need define the t_{on} and t_{op} ratios. It must be noted that these ratios are dependent on the system and mission description defined above. TetherLife does not

detect errors in user inputs that would cause the system and mission definitions for a passive system to be invalid. The results produced by TetherLife for a passive momentum exchange tether system are highly dependent on the inputs being consistent with an assessment of the orbital dynamics driving the system.

The final system state parameter that must be generated by TetherLife is the span orientation, φ. The span orientation is the angle between the longitudinal axis of the sub-span on which the discrete element will be chosen and the gravity gradient. By knowing this angle, TetherLife can locate a discrete element, discussed in the following section, relative to the center of the Earth. By doing this, it can then assess the orbital environment at that location. As it is assumed the angular velocity of a MMET span is not significantly affected by the force of gravity, the span orientation is modeled as a uniformly distributed random variable between zero and 2π, with the value for each instant chosen accordingly.

9.2.3 Discrete element location

TetherLife models each tether line as a series of segments. Each of these segments defines one of the discrete elements analyzed by this model. For a span that incorporates a Hoytether formation, every joint is the start and end point of a segment. The user must define the length of each primary and secondary segment, L_P and L_S, respectively. For analyses of independent lines, each line is modeled as a series of segments that are one meter in length each.

TetherLife assumes every strand is equally accessible to the debris environment. This assumption is based on the significantly large spacing between tether strands, when considered in conjunction with the uncertainty of debris trajectories approaching the system. As such, this assumption allows the analysis to investigate a segment solely from the perspective of its distance from the system facility. TetherLife selects an element by selecting a random value between zero and unity, and multiplying that value by L_i, which is the length of the sub-span, for a MMET system, or full span, for a passive system, and locates that point relative to the overall length L.

It is very important that the point be randomly selected using L_i yet analyzes it relative to its location on L. This is because only the tether segments currently exposed to the environment at that instant are susceptible to the environment at that instant, but the segments closer to the span tips are susceptible to the environment for a longer period of time each mission than those located near the system facility. As discussed later, it is this time of exposure that dictates the amount of degradation seen on the tether surface, effectively reducing the tether diameter more quickly for segments that are closer to the span tips.

With the segment location selected, and the distance from the system spin axis to that location known, the local velocity of that segment relative to the system facility can be calculated as the cross product of the system angular velocity at that instant and the radius from the system spin axis to that location. This local velocity, in conjunction with the diameter of the segment after accounting for atomic oxygen degradation, is vital in the later probability of failure due to debris and micrometeorite impact.

When calculating the likely orbital debris and micrometeorite environment, the most important aspect of the discrete element location is its altitude, or height above the surface of the Earth, h_i. This is found by adding $L_i \cos(\phi)$ to the height of the system facility. Because the spans of the proposed tether systems are so large, this change in height can be significant from an analysis perspective. The ability of TetherLife to account for both the variation of environment and local velocity across the system is what makes the results less uncertain than conventional analysis approaches.

9.2.4 Orbital debris environment

TetherLife characterizes the orbital debris environment, as it does the micrometeorite environment, using equations presented by Tribble, originally in Tribble (1995) and again in Tribble (2004). The Tribble equations calculate the average planar flux per year (F_{OD}) for orbital debris of a particular diameter. This equation for this flux is as follows:

$$F_{OD} = H(d_{OD})\Phi(h_i, S)\Psi(\alpha_{inc})[F_1(d_{OD})g_1(T_i) + F_2(d_{OD})g_2(T_i)] \qquad (9.9)$$

Where:

$$H(d_{OD}) = \left\{ 10^{\exp\left[-\left(\frac{\log(d_{OD}) - 0.78}{0.637} \right)^2 \right]} \right\}^{\frac{1}{2}} \tag{9.10}$$

$$\Phi(h_i, S) = \frac{\Phi_1(h_i, S)}{\Phi_1(h_i, S) + 1} \tag{9.11}$$

$$\Phi_1(h_i, S) = 10^{\left[\frac{h_i}{200} - \frac{S}{140} - 1.5 \right]} \tag{9.12}$$

$$F_1(d_{OD}) = \left(1.22 10^{-5}\right) d_{OD}^{-2.5} \tag{9.13}$$

$$F_2(d_{OD}) = \left(8.1 10^{-5}\right) (d_{OD} + 700)^{-6} \tag{9.14}$$

$$g_1(T_i) = (1 + q)^{(T_i - 1988)} \tag{9.15}$$

$$g_2(T_i) = 1 + p(T_i - 1988) \tag{9.16}$$

These equations are calibrated to be accurate through 2011, the g_1 and g_2 terms being growth terms with the variables q and p within those functions being 0.05 and 0.02, respectively. There is a further inclination dependence, characterized in the equation as $\Psi(\alpha_{inc})$. The values for this inclination term as it is used in TetherLife are presented in (Tribble 1995).

While these equations do produce specific flux values, it must be understood that the orbital debris environment is "not well defined or understood, and the number of small (<1 cm) [orbital debris] above 700 km is virtually unknown" (Tribble 1995). This uncertainty is a product of both the limitations inherent in the equipment used to observe the orbital debris environment and the relative lack of exhaustive studies

aimed at characterizing the environment. However, the use of predictive models that calculate the debris flux at a certain location on orbit is common.

The latest NASA model characterizing the near earth orbit debris environment is ORDEM2000. ORDEM2000 uses a discrete element model of the debris environment to generate either average flux values for a spacecraft traveling along a specific orbit or the number of particles an observatory would see passing in front of it if located at a specific location. The ORDEM2000 model also incorporates NASA breakup and drag models, which predict how the environment will grow over a significant amount of time. Very similar to ORDEM2000, the ESA Master99 model incorporates the same level of functionality as ORDEM2000 and takes the same analytical approach. When directly compared, the results from both programs do not substantially differ in most cases.

The ORDEM version prior to 2000 was ORDEM96. While ORDEM2000 took a discrete element approach, ORDEM96 used a series of equations for calculating the probability that both a spacecraft on its designated trajectory and a series of debris bands on specific inclinations would be located within the same volume of space. When compared in Liou *et al.* (2001), the approach taken and results presented by ORDEM96 do not seem inconsistent with research done after 1996 and prior to 2000 since the model outputs differ quite minimally compared against ORDEM2000 results for identical missions.

Both the ORDEM96 and ORDEM2000 cite the same uncertainties with the orbital debris environment that are cited by Tribble (1995). As a result of the inherent uncertainty associated with the system being modeled, and the relative complexity of incorporating either the ORDEM96 or ORDEM2000 packages into the TetherLife model, it was assumed that the uncertainty associated with the Tribble model was no more significant than the uncertainty inherent in either ORDEM model. Support for the Tribble model as a valid engineering model was further bolstered when the same equations were re-released, after both ORDEM models were available, in Tribble (2004) with no substantial changes.

9.2.5 Micrometeorite environment

Micrometeorite flux as a function of mass is observed to be constant at a significant distance from the Earth. Equation 9.17 represents this background flux, as it is characterized within Tribble (1995).

$$F_{MM} = 3.156 10^{7} \left[A^{-4.38} + B + C \right] \tag{9.17}$$

Where:

$$A = 15 + 2.2 10^{3} m_{MM}^{0.306} \tag{9.18}$$

$$B = 1.3 10^{-9} \left(m_{MM} + 10^{11} m_{MM}^{2} + 10^{27} m_{MM}^{4} \right)^{-0.306} \tag{9.19}$$

$$C = 1.3 10^{-16} \left(m_{MM} + 10^{6} m_{MM}^{2} \right)^{-0.85} \tag{9.20}$$

This background flux does not stay constant for locations closer to the surface of the Earth. Of the three main factors that affect the micrometeorite flux at a particular point close to the Earth, the first is the gravitational focusing effect. The gravitational forces of Earth attract micrometeorites so as to cause them to change course towards the Earth. This effect diminishes as the distance from the Earth increases. Therefore, the closer a point is towards the surface of the Earth, the higher the micrometeorite flux. This effect is defined by using the following equation. This gravitational focusing term is multiplied to the background flux to estimate the flux associated with a point at the height, in kilometers, incorporated into the gravitational focusing term.

$$F_{grav} = 1 + \frac{R_E + 100}{R_E + h_i} \tag{9.21}$$

The next factor affecting micrometeorite flux at a point close to the surface of the Earth is the planetary shielding factor. Because it is assumed that the background

micrometeorite environment is effectively directionless, the closer a point to the surface of the Earth, the less likely background micrometeorites will be approaching the system from the direction of the Earth. This decrease in micrometeorite density is called the Earth shielding factor, and is presented mathematically as follows. To apply the shielding factor, it is multiplied to the product of the background flux and the gravitational focusing factor.

$$F_{shield} = \frac{1+\cos(\eta)}{2} \tag{9.22}$$

$$\eta = \arcsin\left(\frac{R_E + 100}{R_E + h_i}\right) \tag{9.23}$$

The final factor affecting the local micrometeorite flux for points near the surface of the earth is the spacecraft direction factor. Depending on which direction the discrete element is facing, the micrometeorite flux is significantly affected. Because of their orientation, locations on a spacecraft that either face the Earth or are opposite the direction the spacecraft is traveling will see the debris flux, which is found as the product of the background flux and all previously discussed factors, reduced by a factor of 10. For locations facing all other directions, the local micrometeorite flux must be multiplied by the following directional factor:

$$F_{dir} = \frac{1.8 + 3\sqrt{1-\left(\frac{R_E + 100}{R_E + h_i}\right)^2}}{4} \tag{9.24}$$

9.2.6 Atomic oxygen environment

Atomic oxygen is, functionally, an abrasive that removes exposed surfaces of an object in space. This change in thickness of an exposed surface as a function of time is directly related to the atomic oxygen flux during exposure and the reaction efficiency of the material. This is discussed and expressed mathematically within Tribble (1995) using an equation that is presented in this section as Eq. 9.25.

$$\frac{dx}{dt} = \eta_R \Phi_{AO} \tag{9.25}$$

The atomic oxygen flux is found in the same manner as the debris flux for the orbital debris models by multiplying the atomic oxygen *number density* by the velocity of the system as it travels through that density of particles. TetherLife finds the number density for a particular altitude using an approximation of the US Standard Atmosphere 1976 presented in Tribble (1995). This approximation is as follows:

$$\rho_{AO} = \begin{cases} -9.99_{10}{}^{17} h_i + 2.0_{10}{}^{20} & h_i \le 200\,\text{km} \\ -1.25_{10}{}^{13} h_i + 1.25_{10}{}^{16} & h_i > 200\,\text{km} \end{cases} \tag{9.26}$$

As TetherLife is not a deterministic model, it is not possible to deterministically track the atomic oxygen flux for every line segment. Consequently, the atomic oxygen flux for every exposed location on the system over the course of the mission is assured to be similar to the atomic oxygen flux observed at the system facility. For high-altitude systems with long spans, this approximation would be a conservative estimate of the atomic oxygen affect, while for systems at significantly lower altitudes this assumption would underestimate the affect. For example, if the altitude of the system facility were 800 km above the surface of the earth, the tip of a 200 km long tether would experience an increase or decrease of 100%. However, this decrease would result in an atomic oxygen number density of zero, while the increase would only have a change in surface thickness of $7.6 10^{-9}$ cm/sec if the tether span were coated with a material similar in reaction efficiency to Kapton. Considering the change in degradation is so small, and considering a span tip will only be subjected to such a large variation in altitude for less than 0.5% of all the time the system is at full extension (which, the time the system is at full extension itself, should be a relatively short amount of time is the mission is optimised to be operating in an efficient manner), this assumption that the atomic oxygen flux for all locations on the system is sufficiently equivalent to the flux at the system facility is assumed to be a suitable approximation for an engineering model.

To find the average atomic oxygen flux experienced by the system, this calculation must take into account the orbital parameters for non-circular orbits. As the atomic oxygen flux is the product of the atomic oxygen number density and the velocity of the system at that the time the system encountered that density, TetherLife examines the orbital velocity of the system facility at all of the locations contained within the orbital array discussed earlier and calculates the product of that velocity and the numeric density at that location. Taking the average of these calculations allows TetherLife to arrive at an average atomic oxygen flux for all points on the orbit, given the previous assumption that all locations experience a significantly similar flux to that of the system facility.

While these equations and assumptions allow TetherLife to assess the atomic oxygen flux associated with a specific location at any point throughout the mission, they do not account for the fact that not every location will be exposed to the atomic oxygen environment for the entirety of the system lifetime nor the entirety of the mission. To account for this, TetherLife uses the state equations for sub-span length discussed above to determine, based on the location of the line segment being analyzed relative to the sub-span tips, what percentage of the mission that location has been exposed to the environment. This calculation calls the various operational ratios discussed above and the arctangent assumption previously used. With this exposure factor, the time of exposure for each randomly generated point at some time T_i within the planned mission can be assessed based on the mission parameters inputted by the analyst.

These calculations for incorporating the degrading affect of atomic oxygen require a number of assumptions. It is believed that these assumptions are suitable for an engineering model for a number of reasons. First, it must be noted that the effect of atomic oxygen degradation on these tether elements is very small. Considering the number density of atomic oxygen at 800 km altitude, it would take 10 years of constant exposure before a tether line is compromised. As discussed, no tether strand will be constantly exposed to the environment over the mission lifetime. Since the system is extending and releasing, and it is not anticipated that the system will transition from one mission immediately to the next, the majority of segments will

only be exposed to the atomic oxygen environment for a small percentage of the system lifetime.

Further, TetherLife has minimized computational complexity by taking a Monte Carlo analytical approach that relies on the selection of independent, random variables. Because atomic oxygen degradation is the only significantly time dependent factor being considered, increasing the fidelity of the atomic oxygen analysis would be computationally costly. Considering the fact that the atomic oxygen affect is so small, increasing the analytical fidelity of TetherLife would have significant cost implications for little added benefit. For this reason, it is assumed that the treatment of atomic oxygen employed by TetherLife is suitable for the purposes of an engineering model.

9.2.7 Impact prediction

TetherLife assumes that a momentum exchange tether system will fail as a result of hypervelocity impact. As previously mentioned, TetherLife calculates this probability of failure by randomly selecting a sizable number of moments in time and determining whether it is likely a fatal impact would occur given the states and conditions associated with that random moment. By making these random moments so short in duration, and the impact locations so small relative to the analytical tools employed, TetherLife assumes that one instant is capable of modeling one, independent debris piece and its likelihood of impacting one, independent line segment. By keeping each time step so small and each line segment so short, every impact prediction generated by TetherLife should have a probability of occurrence that is much less than unity. By having a probability of occurrence that is much less than unity, it is assumed that TetherLife need only account for the case of one impact per segment per instant. Therefore, after selecting the state of the system and the location of the segment that is to be analysed, TetherLife randomly generates a single orbital debris piece and one micrometeorite to examine the likelihood that each will impact the randomly generated line segment in its randomly generated location and state.

After a qualitative and quantitative assessment of the literature, it became clear that the probability that an orbital debris piece or a micrometeorite would be less than or equal to a certain value at all altitudes could be represented by a single function for each. This single function for each would effectively be a cumulative histogram, and considered a pseudo-CDF for the purposes of this investigation. The data presented in the literature of debris flux verses debris diameter, for a range of altitudes, is recreated in Fig 9.6. As one can qualitatively deduct through observation, the distribution of flux as a function of diameter is consistent across the altitudes.

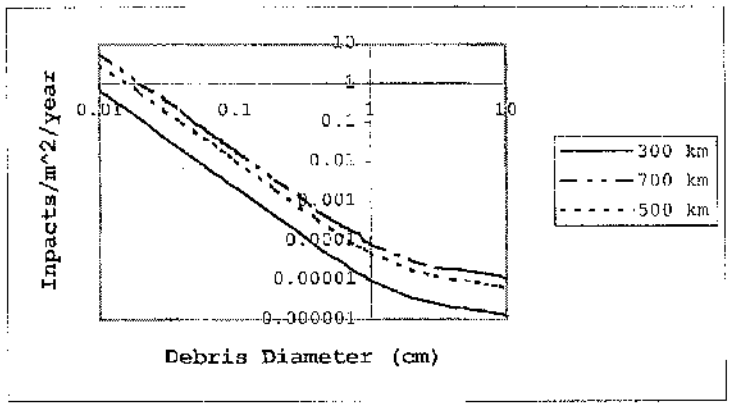

Figure 9.6: Re-creation of the flux as a function of orbital debris diameter data for various altitudes, as presented in Liou *et al.* (2001).

When creating a pseudo-CDF of particle diameter using the data for each of the three altitudes identified in Fig 9.6, the standard deviation about the average value was less than or equal to 0.1% of the average value. Such a minimal variation is assumed a suitable trade-off in fidelity for the purposes of the increased efficiency that a single pseudo-CDF would provide the TetherLife program in its current version. For future versions of TetherLife, it is assumed that these will take a discrete element approach to the debris environment identical to the ORDEM2000 approach, thus rendering this issue of variability about the average irrelevant in future versions.

The reason a debris diameter pseudo-CDF had to be approximated for this work and has not come up before is of interesting note. For a conventional orbital risk assessment, the system being examined often has a known and constant susceptibility

to particles of a specific size. For this reason, the analyst will often take this threshold size and compute the flux observed by the vehicle when accounting for all debris elements of an equivalent or larger size. For a momentum exchange tether system, the system is not constantly or uniformly susceptible to a debris element of a particular size. At one time for one location, the characteristics of an impact that would result in failure may vary significantly from that at another time and location. For example, if identical impactors approaching the system in an identical manner were to strike both (i) near the tip of a span or sub-span and (ii) near the system facility, the impactor striking nearer the span tip would be more likely to cause failure because the local impact velocity is significantly greater. As a result, the Monte Carlo approach taken by TetherLife requires the failure analysis to account for not just the threshold debris size and the assumed approach rate of the system facility, but must randomly generate all aspects of the impact to include local velocity and tether diameter as a function of time. For this reason, a pseudo-CDF of each the orbital debris and micrometeorite environments must be constructed for use in TetherLife, where they were not previously required.

Based on the altitude dependent flux verses impactor diameter graphs available in the literature, the pseudo-CDF for the orbital debris and micrometeorite environments used in TetherLife are presented in Fig 9.7 and Fig. 9.8, respectively. As a point of caution, when observing the pseudo-CDF for orbital debris diameter and making visual comparisons between that and the data presented in Fig 9.6, it is important to note that the y-axis in Fig 9.6 is logarithmic, while the y-axis for both the orbital debris and micrometeorite pseudo-CDF in Fig. 9.7 and Fig. 9.8 is uniform.

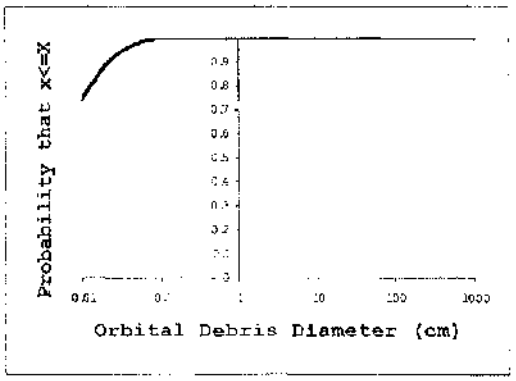

Figure 9.7 Pseudo-CDF for orbital debris diameter at all altitudes.

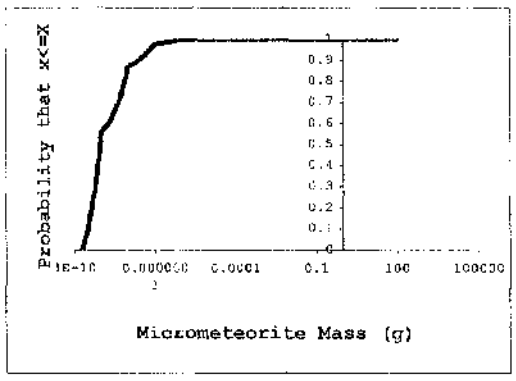

Figure 9.8 Pseudo-CDF for micrometeorite mass at all altitudes.

While the orbital debris pseudo-CDF was generated using data presented in Fig 9.6, which had already been generally smoothed with assumptions of a logarithmic relationship between debris size and flux, the micrometeorite pseudo-CDF was generated using the composite function originally presented in Kessler (1996) and again in Tribble (1995). Because it is a composite function, the resulting pseudo-CDF also contains a number of discontinuities. As the pseudo-CDF is used solely for the purpose of extracting random values of micrometeorite mass that an aggregated histogram of the selected values is representative of the environment, it is assumed that these discontinuities do not produce an error in the generated random variables that is more significant than that inherent in the process by which the originating functions were generated or that inherent in the procurement of the data set.

To select the randomly generated orbital debris and micrometeorite impactors, TetherLife uses two uniformly distributed random variables and the respective pseudo-CDF, as done previously for other system state parameters. After TetherLife generates a random time, system state, analysis location, and impactor sizes, it is able to calculate the probability that each of those impactors would strike and cause a failure of that tether component. With all of the variables for the impact set, TetherLife calculates the probability that a failure would occur using historically accepted failure criteria.

To offer the user a greater understanding of the risk posed to the system by the orbital environment, the probability that the system will be impacted at any instant is calculated and presented separate of the probability that the impact would cause a failure. By doing so, the probability of failure at any instant is mathematically presented as follows:

$$\Pr(\text{fail}) = \Pr(\text{impact})\Pr(\text{fail}|\text{impact}) \tag{9.27}$$

9.2.7.1 Probability of impact

The TetherLife probability of impact calculation employs the well-supported concept of geometric probability, based on projections into an impact plane. At any instant, it is assumed that there is an impact plane perpendicular to system velocity vector. At that instant, the projection into the impact plane of the analysed segment constitutes the *casualty area.*

The probability of impact is equal to the casualty area multiplied by the debris density associated with the debris size that has been previously selected. This is presented in terms of debris flux and casualty area, and equated in to standard geometric probability, as follows:

$$\Pr(\text{impact}) - \Phi A_c = N_{deb}\frac{A_c}{A_{deb}} \tag{9.28}$$

Where:

$\Pr(\text{impact})$ = probability of impact

Φ = impactor flux ($1/m^2$)

A_c = projection of the suseptible item into the impact plane (m^2)

N_{deb} = number of impactors in the impact plane

A_{deb} = area of the impact plane (m^2)

As mentioned earlier, if either the impactor flux or casualty area is too large, the product would violate the laws of probability theory. This is the reason TetherLife assesses Hoytether configurations on a segment level, and artificially divides tether strands that run the length of the span into one metre long segments.

To calculate the impactor flux at an impact plane, this is found as either the orbital debris or micrometeorite flux, after all required modifications are accounted for, calculated using Eq. 9.9 and Eq. 9.17, respectively, multiplied by the analysis time step, Δt. While the user defined Δt is of a discrete length and not instantaneous, as implied with the use of a the term 'impact plane,' there is no significant loss in accuracy if it can be assumed that the expected change in conditions associated with the element and the local environment is insignificant over that time step.

The main conceptual alternative that is held out to the impact plane approach is that of *swept volume*. The concept of assuming the probability of impact is directly related to the number of debris particles contained within a volume swept over a time step by the object profile relative to its velocity vector is presented in Gittins *et al.* (2003). As proposed, Gittins *et al.* (2003) states that the probability of tether failure could be computed as follows:

$$P = \rho A v t \tag{9.29}$$

Where

P = collision and sever probabilities

ρ = debris density

A = tether cross sectional area

v = relative velocity

t_G = time interval

The equation and discussion presented in Gittins *et al.* (2003) does not specify the units associated with each parameter, although the equation is dimensionally correct if

SI units are assumed. However, it is clear that the debris density is defined as the volumetric density of debris that is capable of severing the tether being analysed. It is unclear from where this data set detailing volumetric impactor density as a function of position originates. For small time intervals where the volumetric debris density is uniform throughout the swept volume and the system velocity is defined by the dynamics of a Keplerian orbit, the following relationship is valid:

$$\rho v t = \Phi \tag{9.30}$$

The swept volume approach presented in Gittins *et al.* (2003) is widely employed for space launch aircraft impact safety analyses when the debris cloud is known and the aircraft size and velocity are known, and both are case specific. For orbital applications, it has been previously demonstrated that equations defining the planar impactor flux, Φ, for locations in space are widely accepted. For this reason, the swept volume approach of Gittins *et al.* (2003) presents no real benefit over the planar method.

Using the impact plane approach, TetherLife computes the probability of impact at each location. After aggregating these results, an average probability of impact at any instance can be computed with a normally distributed approximation of the standard deviation about the calculated mean.

9.2.7.2 Impact outcome

With the probability of impact computed in the manner identified above, the conditional probability of failure for the randomly generated analysis point must be computed. This conditional probability is found by examining each randomly generated set of impact conditions, assessing whether a failure would occur given those impact conditions, and aggregate the result of every analysis point to find a mean probability of failure conditional on an impact and the standard deviation associated with that mean, assuming normalcy in the data set.

It is assumed by this research that all impacts occurring on obit and relevant to a space tether lifetime analysis are hypervelocity impacts. As accepted from the conclusions

of Hayashida and Robinson (1993) presented earlier in this work, a tether can fail without severing. If the tether segment is not capable of holding its designed load, it is assumed that the tether will be considered in a state of failure. It is further assumed that this state of failure occurs when the penetration depth equals the maximum allowable wile retaining the definitional validity of a semi-indiscrete plate, which is 25% of the target thickness.

From an earlier discussion of the empirically derived hypervelocity impact equations currently accepted as valid for the purposes of space system analysis, it was concluded that an equation which is calibrated over densities more relevant to a space tether member may be more appropriate for the kind of analyses performed by TetherLife. For this reason, TetherLife adopts the Draper (72) equation for the assessing the depth of a crater crated by a hypervelocity impact. For convenience, the Draper (72) equation is re-stated as Eq. 9.31.

$$p = v^{0.042} \rho_p^{0.613} m_p^{0.076} \rho_t^{-1.348} \left[\cos(\theta)\right]^{0.821} \tag{9.31}$$

The Draper (72) equation is adopted into TetherLife using the following inequality derived using the stated assumption of failure:

$$\frac{d_t}{4} \leq v^{0.042} \rho_p^{0.613} m_p^{0.076} \rho_t^{-1.348} \left[\cos(\theta)\right]^{0.821} \tag{9.32}$$

With d_t being equal to the tether diameter at the time of impact, when this inequality is valid, it is assumed the tether is in a state of failure. After assessing this relationship for a significant number of randomly generated samples, the average is assumed to be the average probability of failure for a tether segment, assuming an impact has occurred.

9.3 Analysing the results

The probability of failure for any time segment is assumed constant over the entire mission.[xiii] Because of this, the probability of failure at any instant is considered constant over the entire mission. From reliability engineering, we know that the

probability that a component fails some time after t but before $t + \Delta t$ is equal to the component's failure rate multiplied by the time step, Δt. This is expressed mathematically as follows:

$$\lambda(t)\Delta t = P\{\mathrm{t} < t + \Delta t \mid \mathrm{t} > t\} \tag{9.33}$$

As previously noted, the failure rate for each component is a constant failure rate, by design. Therefore, it does not vary as a function of time, and is found and presented as follows:

$$\lambda = \frac{P\{\mathrm{t} < t + \Delta t \mid \mathrm{t} > t\}}{\Delta t} \tag{9.34}$$

From the exponential distribution, which is used for continuously operating systems with a constant failure rate, the component's PDF is as follows:

$$f(t) = \lambda e^{-\lambda t} \tag{9.35}$$

This leads, though integration, to the following CDF for the component:

$$F(t) = 1 - e^{-\lambda t} \tag{9.36}$$

From the previous CDF, the reliability of the system may be written as follows:

$$R(t) = e^{-\lambda t} \tag{9.37}$$

As the mean time to failure (MTTF), a common metric in reliability analysis, is defined as follows:

$$MTTF = -\int_0^{\infty} t\frac{dR}{dt}dt = -tR(t)\Big|_0^{\infty} + \int_0^{\infty} R(t)dt \tag{9.38}$$

$$MTTF = \int_0^\infty R(t)dt \tag{9.39}$$

$$MTTF = \frac{1}{\lambda} \tag{9.40}$$

For assessing the probability of failure of the system, and therefore the MTTF for the system using this inverse relationship for systems with a constant failure rate, TetherLife must account for the tether segment configuration employed by each span. TetherLife has the ability to account for both un-strapped systems and Hoytether configured systems.

9.3.1 Un-strapped systems

By design, each primary line segment on an un-strapped line is mutually exclusive to all others on that line. Therefore, the probability that a primary line will fail is equal to the probability that each segment will fail, multiplied by the number of segments. The failure rate for each line is expressed as follows:

$$\lambda_T = N_p \lambda_p \tag{9.41}$$

Where:

λ_p = Failure rate for a primary segment

N_p = Number of primary segments

λ_T = Failure rate for a primary line

With the failure rate per primary line established, the failure rate of an un-strapped span is then found by modelling it as a simple, k out of n system using the binomial distribution, as follows:

$$\lambda_{\text{Span}} = \frac{1}{\Delta t}\binom{N_{\text{P}}}{N_{\text{R,P}}+1}(\lambda_{\text{T}}\Delta t)^{N_{\text{R,P}}+1}(1-\lambda_{\text{T}}\Delta t)^{[N_{\text{P}}-(N_{\text{R,P}}+1)]} \tag{9.42}$$

9.3.2 Hoytether systems

Unlike an un-strapped span with redundant primary lines, a Hoytether is designed to allow for multiple breaks in multiple primary lines without system failure. As claimed in Hoyt and Forward (1998), a Hoytether is constructed of layers, each layer arranged in series to construct a span. While this failure criteria is identical to that used for assessing the system failure rate of an un-strapped system using line segments, the design of each Hoytether layer is what makes it superior to an un-strapped system.

Each Hoytether layer is composed of sections. The relationship between a section and a layer are identified in Fig 9.9 and Fig 9.10. As can be seen in Fig 9.9, this section example contains one primary tether segment, and two secondary segments. Depending on the relative size of these primary and secondary lines, there are a number of ways in which a segment could fail.

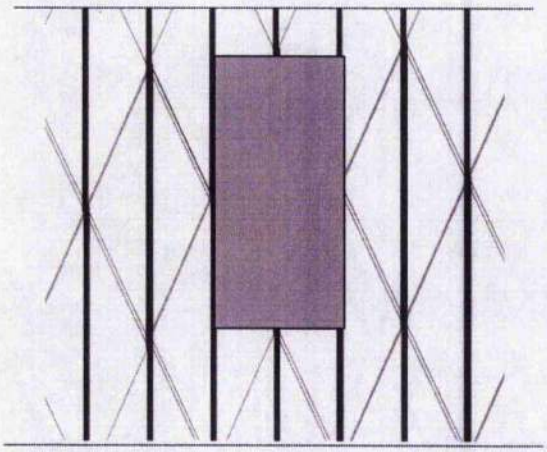

Figure 9.9 Hoytether section, identified by the highlighting box, with four redundant segments per primary segment.

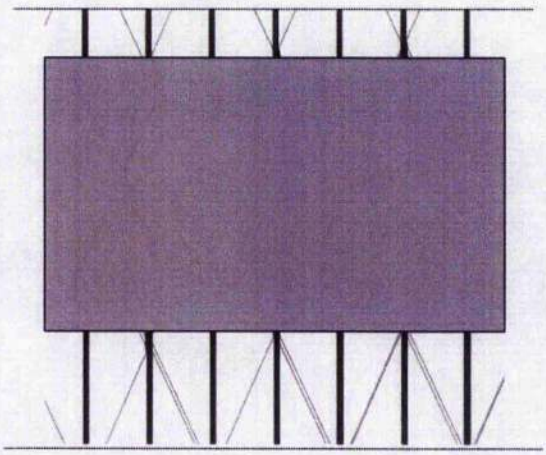

Figure 9.10 Hoytether layer, identified by the highlighting box, with seven primary lines.

For a Hoytether configuration where each secondary line has half of the cross sectional area associated with a primary line, a failure in the primary line would require both secondary lines to be operational such that the load carried by the primary line is both absorbed by the secondary lines and each layer maintains its independence. If the cross sectional area of each secondary line is less than that where, in conjunction with the other operational secondary lines, it is capable of supporting the load previously held by a primary line, the layer would not be independent of its successive layers.

If the Hoytether system is designed such that each layer is independent, if there is a failure in the primary line within one layer, the same primary line in the adjoining layer will be unaffected. As identified in Hoyt and Forward (1998), there are configurations where this independence is not valid. TetherLife assumes this layer independence is maintained when performing its calculations. Further the concept of this independence, or even the validity of the independent configuration proposed in Hoyt and Forward (1998) assumes there is no significant loss of strength at the nodes where primary and secondary lines connect. While this assumption is suspect as a result of the transverse weakness observed in the type of fibres that would likely be considered for space tether applications, such an assumption is accepted for the purposes of this work.

Assuming layer independence is valid as a result of system design, the probability failure for a span is equal to the mutually exclusive probability of failure associated with each layer. This is presented mathematically as follows:

$$\Pr(\text{fail}, \text{Span}) = N_L \Pr(\text{fail}, \text{L}) \tag{9.43}$$

Where:

$\Pr(\text{fail}, \text{Span})$ – probability that a span or sub-span will fail

N_L = number of layers

$\Pr(\text{fail}, \text{L}) = \text{probability that a layer will fail}$

When assessing the probability of failure associated with a layer, the number of redundant primary tether lines becomes important. As with the un-strapped span, failure in the span occurs when the number of primary lines that fail is greater than those that are redundant. When carried forward to the Hoytether design, failure in a layer occurs when the number of failed sections contained within that layer is greater than the number of redundant primary lines. This is expressed as follows:

$$\Pr(\text{fail}, \text{L}) = \prod_{x=1}^{N_{R,P}+1} \Pr(\text{fail}, \text{S}_x | \text{S}_x \subset \text{L}) \left[\prod_{x=1}^{N_{R,P}+1} \Pr(\text{S}_x \subset \text{L}) \right] \tag{9.44}$$

Where:

$\Pr(\text{fail}, \text{L}) = \text{probability that a layer will fail}$

$\Pr(\text{fail}, \text{S}_x | \text{S}_x \subset \text{L}) = \text{probability that the } x^{\text{th}} \text{ section will fail, conditional on the } x^{\text{th}} \text{ section being contained within the layer}$

$\Pr(\text{S}_x \subset \text{L}) = \text{probability that the } x^{\text{th}} \text{ section is contained within the layer}$

$N_{R,P} = \text{number of redundant primary lines contained within each layer}$

Similar to failures in a layer, where the threshold number of section failures must be associated with the same layer, the failure of a section requires the primary segment and all redundant lines plus one to fail within the same segment. Therefore, the probability that a segment will fail is equal to the probability that a primary will fail multiplied by the probability that each of the required secondary tethers will fail. This is expressed mathematically as follows:

$$\Pr(\text{fail},\text{S}) = \Pr(\text{fail},\text{P}) \prod_{x=1}^{N_{\text{R,H}}+1} \Pr(\text{fail},\text{H}_x | \text{H}_x \subset \text{S}) \left[\prod_{x=1}^{N_{\text{R,H}}+1} \Pr(\text{H}_x \subset \text{S}) \right] \qquad (9.45)$$

Where:

$\Pr(\text{fail},\text{S})$ = probability that a section will fail

$\Pr(\text{fail},\text{P})$ = probability that a primary line segment will fail

$\Pr(\text{fail},\text{H}_x|\text{H}_x \subset \text{S})$ = probability that x^{th} Hoytether secondary line will fail, conditional on the x^{th} Hoytether secondary line being within the section

$\Pr(\text{H}_x \subset \text{S})$ = probability that the x^{th} Hoytether secondary line will be within the section

$N_{\text{R,H}}$ = number of redundant Hoytether secondary lines associated with each primary line

As a note, while the Hoytether is passively viewed as having only two secondary lines per tether, this work does not assume that is an exclusive design. For example, if the Hoytether is thought of as not just being a tube where primary lines are contained along the surface, but as a cluster of primary lines, it is feasible that some primary lines could have many more than just two secondary lines associated with each primary segment. Because TetherLife computes the probability of failure associated with each segment, it is capable of offering data from which such a configuration could be solved. However, it does not directly address this unconventional Hoytether design.

As discussed, TetherLife is only concerned with a passive Hoytether design where each primary has two secondary lines, for which the secondary line design criteria ensures independence between the layers. Using the failure rate for a primary and Hoytether secondary segment, λ_P and λ_H, respectively, the following equations can be represented using the analytical inputs required by TetherLife:

$$\lambda_S = \lambda_P \lambda_H \Delta t \left[\frac{1}{N_P N_L} \right] \tag{9.46}$$

$$\lambda_L = \frac{1}{\Delta t} \binom{N_P N_L}{N_{R,P}+1} (\lambda_S \Delta t)^{N_{R,P}+1} (1-\lambda_S \Delta t)^{[N_P N_L - (N_{R,P}+1)]} \tag{9.47}$$

$$\lambda_{Span} = N_L \lambda_L \tag{9.48}$$

One problem with the calculations presented above is the fact that the tether segments at the span tip will be exposed more frequently than those near the system centre. This was the same problem experienced when looking at an atomic oxygen degradation methodology, and it has been treated in an identical manner here. While it is true that this calculation will be conservative at the system centre and un-conservative at the span tips, it is assumed that this imbalance in fidelity is not great enough to counter the increase in efficiency of the model. As previously discussed, considering the uncertainty associated with the debris environment, which drives the failure rates being used in these calculations, combined with the uncertainty associated with the MMET deployment and retraction profile, this imbalance in conservatism relative to the span length is considered acceptable for this initial version of TetherLife.

Chapter 10

LSM Mission Analysis

In the previous chapter, the methodology behind the TetherLife analysis program was explained. This section discussed the results obtained after employing TetherLife, v1.2, for an analysis of the MMET systems proposed by the LSM mission.

10.0 Defining the operational characteristics

While the orbital dynamics of the LSM mission are clearly defined in Cartmell *et al.* (2004), there is some variability within the requirements of the mission and the planned operation of an MMET. It is clear that both systems are at full extension at handover. Because there is significant uncertainty in the orbital insertion capability of a Delta II, this analysis assumes the rendezvous between the conventional first stage and the initial MMET occurs when the MMET spans are retracted. Because the LSM mission assumes the upper tether is fully extended for the duration of the mission, the parameters for the elliptical Earth orbit (EEO) MMET system are selected to reflect this operational constraint.

To implement these requirements, the analysis made the time ratio assumptions presented in Table 10.1.

Table 10.1 Time ratios employed for the LSM mission analysis

	LEO MMET	EEO MMET
t_{on}	2	10
t_{op}	0.5	0.001
t_{oL}	0.05	0.9
$t_{\omega L}$	1	1

These ratios identified in Table 10.1 can be identified as inputs into the analysis by examining the screen-shots presented in Fig 10.1 and Fig 10.2.

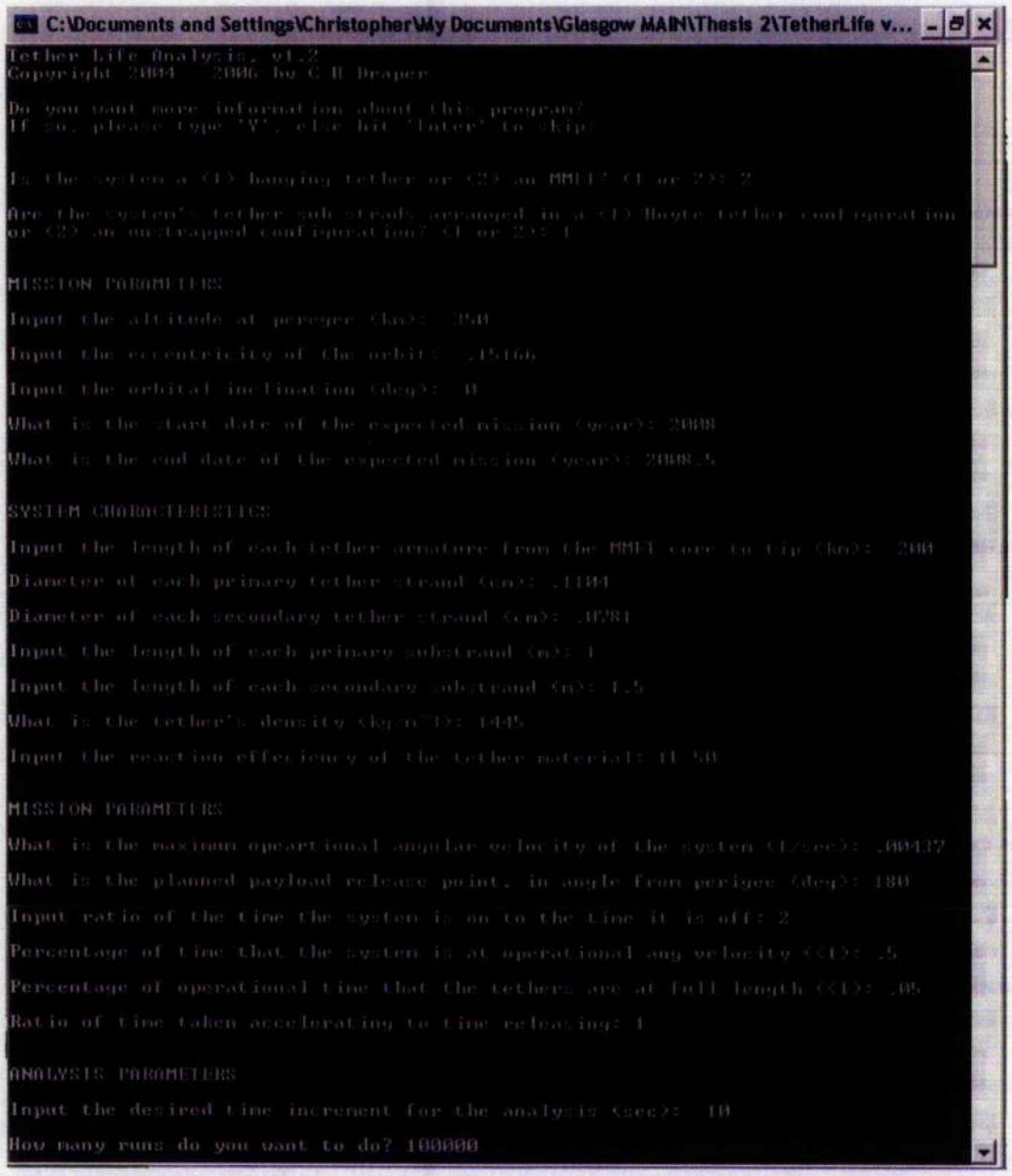

Figure 10.1: Edited screenshot of TetherLife, v1.2, identifying the inputs used in assessing the LEO system of the LSM mission.

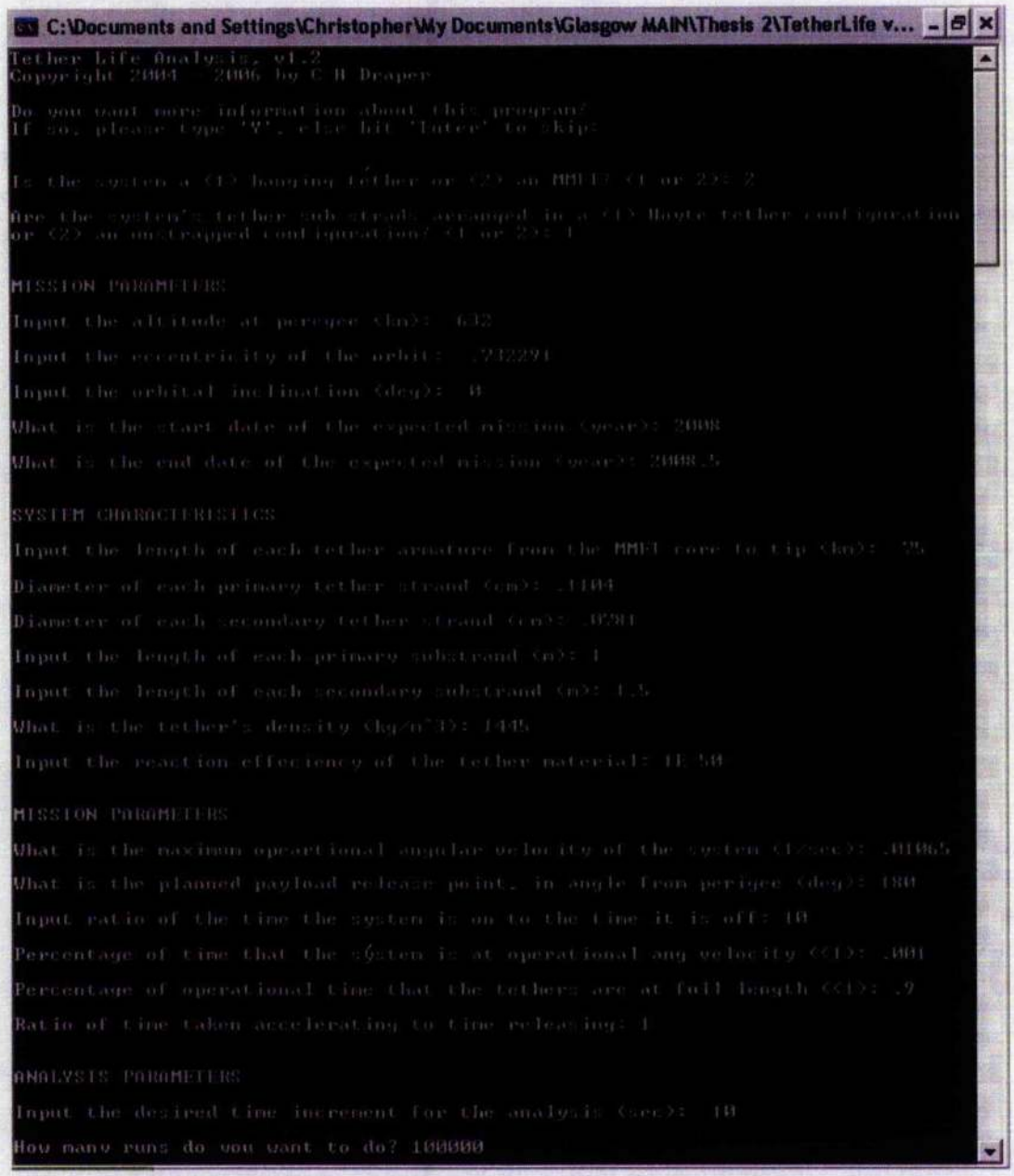

Figure 10.2: Edited screenshot of TetherLife, v1.2, identifying the inputs used in assessing the EEO system of the LSM mission.

In terms of the state chart presented in Fig 9.5, the percentage of time the system spends in each of the identified states can be computed using these parameters. The results of such a computation are presented in Table 10.2.

Table 10.2 Total percentage of mission time spent in a particular state, as defined by Fig 9.5

		Percentage of total LEO Mission	Percentage of Total EEO Mission
System Operating	Operational State	1.67%	0.08%
	Changing State	31.67%	90.92%
System Idle	Rest State	33%	9%

It is important to note three main things when examining the percentages present in Table 10.2: (i) the rest state accounts for the time between missions; (ii) if the system is changing state, it is either not operating at its operational angular velocity, not fully extended, or a combination of the two so long as the system is not fully retracted nor stopped; and (iii) the different percentage in rest time does not require the LEO mission to take longer than the EEO mission.

As stated in Chapter 9, the ratios are developed as a guide for how quickly the system changes state. They do not directly dictate the amount of time a process takes. For example, for the LEO mission, it is known that 1.67% of the time associated with each mission is spent in an operational state. Using the graphs of B.W. Augenstein, which are reproduced in Thomson (1986), the 20-degrees bounding apogee takes approximately 11 minutes to traverse. If this 20-degrees is an acceptable distance through which the LEO system is in an operational state, such that it is ready to release the payload, 1.67% of each mission takes 11 minutes. Therefore, the parameters here would assume a mission occurs approximately every 11 hours, or roughly twice a day. At this rate, the MMET system would be conducting 60 missions a month. Depending on the start-up costs and the system reliability, this rate may pose a financially feasible option when compared against an equivalent conventional launch system.

However, it is important for the analyst to understand that the mission length, orbital parameters, the timing ratios, and the release tolerances are all interlinked because of the inter-coupling within the orbital dynamics. By setting 20-degrees as an acceptable tolerance for LEO release, the selected parameters for the EEO mission determine the release parameters that are acceptable for that orbit. If the LEO system is only operating at its maximum angular velocity for 10-degrees on either side of apogee, the EEO system would only have 30 seconds to receive and release its payload. Considering the angular velocity of the system, 294 seconds is required to execute this activity. Understanding this, for the time relationships identified, there would need to be around 100 hours between missions, which only allows seven per month. For many scenarios, this may not be acceptable.

The significantly greater percentage of mission time attributed to a changing state, with regards to the EEO mission, is due to the very small t_{op} parameter. By having the system on for such a significant percentage of the time, and so much of that time at the operational angular velocity ready for release, these parameters make the required timing associated with the EEO system more precise. However, it also allows the EEO system to accelerate and decelerate at a much slower pace, likely resulting in an energy savings, which could prolong mission life.

As all of these elements are interconnected, the flatter acceleration and deceleration profiles associated with the EEO mission mean it will sit idle on orbit for less time. However, as before, the start and end of each mission will coincide. Considering these current parameters, the LEO system would sit idle on orbit for over a day between missions, while the EEO would sit idle for less than one-third of that time.

When thinking of the system being idle, this is not necessarily a bad thing. When idle, the system is fully retracted and is not able to fail as a result of debris impacts. This is not true with the EEO system as it is modelled here. For areas of greater debris density, such as LEO, it would be better to spin-up more quickly if the probability that a strike results in a failure is very high. For areas of lesser debris density, taking a more energy efficient spin-up and spin-down approach may be reasonable as the risk of failure would be less.

10.1 Analysis results

With a 10 second time increment, Δt, and 100 000 samples, the system failure rates are presented in Fig 10.3 through 10.8 for a range of system configurations and failure assumptions. Each system assumes a primary strand is made of the eight-strand braided Twaron examined in Chapter 6, and the secondary strands are made of the four-strand Twaron to ensure layer independence.

10.1.1 One-impact-one-failure

When examining the system from a one-impact-one-failure perspective, Table 10.3 presents the lifetime and maximum payload available to various span configurations. Table 10.4 presents equivalent information for the EEO MMET system.

Considering the payload sizing and safety factor considerations discussed in Chapter 3 regarding research currently being conducted at the University of Glasgow, the configurations presented in Table 10.3 are capable of accommodating a payload masse plus safety factor totalling either 2.5 tonnes or 3 tonnes. The maximum payload mass is computed by evenly dividing the mass among the primary lines.

Table 10.3: Results of a TetherLife, v1.2, analysis for the LEO system proposed in the LSM Earth to moon mission.

N Primary	8	8	9	10	10	10	11	12
N Redundant Primary	0	0	1	2	0	0	1	2
N Secondary per Primary	0	2	2	2	0	2	2	2
MTTF (hours)	2.7E-05	1.9E+00	1.2E+06	1.2E+12	3.8E-05	1.9E+00	1.2E+06	1.2E+12
MTTF (years)	3.0E-09	2.2E-04	1.4E+02	1.4E+08	4.4E-09	2.2E-04	1.3E+02	1.3E+08
Max Payload (kg)	2,643	2,643	2,643	2,643	3,303	3,303	3,303	3,303
Sub span mass (kg)	2,213	5,533	6,916	8,299	2,766	6,916	8,299	9,683
Dual-span mass (kg)	8,853	22,132	27,665	33,198	11,066	27,665	33,198	38,731

When examining the MTTF for the LEO system, it is clear that the minimum configuration for ensuring a reasonable lifetime for each payload mass is a Hoytether

with one redundant primary line. For the 2.5 tonne payload, the Hoytether with no redundant line increases the MTTF by over 7,000,000% of that predicted for the un-strapped system, while the Hoytether with one redundant primary line increases the MTTF by a further 63,000,000%. For the LEO system, these gains in reliability come at mass increases of 149% and 25%, respectively. By adding a redundant primary line for the Hoytether span, the MTTF increases from two hours to 140 years.

Table 10.4: Results of a TetherLife, v1.2, analysis for the EEO system proposed in the LSM Earth to moon mission.

N Primary	16	16	17	18	19	19	20	21
N Redundant Primary	0	0	1	2	0	0	1	2
N Secondary per Primary	0	2	2	2	0	2	2	2
MTTF (hours)	5.0E-04	1.7E+00	3.2E+05	9.8E+10	1.1E-03	1.7E+00	3.2E+05	9.5E+10
MTTF (years)	5.7E-08	1.9E-04	3.7E+01	1.1E+07	1.3E-07	1.9E-04	3.6E+01	1.1E+07
Max Payload (kg)	2,537	2,537	2,537	2,537	3,012	3,012	3,012	3,012
Sub span mass (kg)	1,660	4,150	4,668	5,187	1,971	4,928	5,446	5,965
Dual-span mass (kg)	6,640	16,599	18,674	20,749	7,884	19,711	21,786	23,861

Similar results are observed with the EEO system. While a Hoytether with no redundant lines is only able to deliver an untenable MTTF of just less than two hours, adding a single redundant primary line increases the MTTF so it is just above 35 years. These significant increases in reliability are achieved for the EEO system with increases in mass that are less than 15%.

If it is assumed that one impact causes only one failure, the Hoytether demonstrates a significant superiority over an un-strapped system.

10.1.2 Lethal dispersion

As concluded based on the results of Chapter 8, it may not be sufficient to assume a single impact causes only a single failure. If the conclusions of Chapter 8 are implemented, such that a 9-degree lethal dispersion occurs upon impact, this work implements this by assuming a single impact is capable of causing a section behind

the impact to fail. When this is done, while the Hoytether is still superior, its superiority decreases immediately and significantly.

Table 10.5 presents the same configurations from 10.3 for the LEO system. By examination, while the MTTF increases by 900% when two redundant primary lines are added to a mission designed for 2.5 tonne payloads, the mass increase is 271% and the MTTF is still only on the order of seconds.[xiv]

Table 10.5 Results of a TetherLife, v1.2, analysis for the LEO system proposed in the LSM Earth to moon mission, assuming an impact of either a primary or secondary tether causes secondary impacts with sufficient size and dispersion to cause a section failure.

N Primary	8	8	9	10	10	10	11	12
N Redundant Primary	0	0	1	2	0	0	1	2
N Secondary per Primary	0	2	2	2	0	2	2	2
MTTF (hours)	1.9E-05	1.9E-05	5.2E-05	1.9E-04	1.8E-05	1.8E-05	4.0E-05	1.2E-04
MTTF (years)	2.2E-09	2.2E-09	5.9E-09	2.2E-08	2.1E-09	2.1E-09	4.6E-09	1.4E-08
Max Payload (kg)	2,643	2,643	2,643	2,643	3,303	3,303	3,303	3,303
Sub span mass (kg)	2,213	5,533	6,916	8,299	2,766	6,916	8,299	9,683
Dual-span mass (kg)	8,853	22,132	27,665	33,198	11,066	27,665	33,198	38,731

With significant levels of redundancy, the MTTF is again increased to acceptable levels, as identified in Table 10.6.

Table 10.6: Results of a TetherLife, v1.2, analysis for the LEO system proposed in the LSM Earth to moon mission, assuming an impact of either a primary or secondary tether causes secondary impacts with sufficient size and dispersion to cause a section failure.

N Primary	8	8	21	22	10	10	24	25
N Redundant Primary	0	0	13	14	0	0	14	15
N Secondary per Primary	0	2	2	2	0	2	2	2
MTTF (hours)	1.9E-05	1.9E-05	1.7E+05	1.4E+06	1.8E-05	1.8E-05	2.1E+05	1.7E+06
MTTF (years)	2.2E-09	2.2E-09	1.9E+01	1.6E+02	2.1E-09	2.1E-09	2.4E+01	1.9E+02
Max Payload (kg)	2,643	2,643	2,643	2,643	3,303	3,303	3,303	3,303
Sub span mass (kg)	2,213	5,533	23,515	24,898	2,766	6,916	26,281	27,665
Dual-span mass (kg)	8,853	22,132	94,060	99,593	11,066	27,665	105,126	110,659

For the EEO system, the MTTF is identified, again, for the initially examined orientations in Table 10.7, and for those with more significant redundancy in Table 10.8.

Table 10.7: Results of a TetherLife, v1.2, analysis for the EEO system proposed in the LSM Earth to moon mission, assuming an impact of either a primary or secondary tether causes secondary impacts with sufficient size and disperstion to cause a section failure.

N Primary	16	16	17	18	19	19	20	21
N Redundant Primary	0	0	1	2	0	0	1	2
N Secondary per Primary	0	2	2	2	0	2	2	2
MTTF (hours)	5.2E-05	5.2E-05	7.0E-05	1.3E-04	5.8E-05	5.8E-05	6.6E-05	1.1E-04
MTTF (years)	6.0E-09	6.0E-09	8.0E-09	1.5E-08	6.6E-09	6.6E-09	7.5E-09	1.2E-08
Max Payload (kg)	2,537	2,537	2,537	2,537	3,012	3,012	3,012	3,012
Sub span mass (kg)	1,660	4,150	4,668	5,187	1,971	4,928	5,446	5,965
Dual-span mass (kg)	6,640	16,599	18,674	20,749	7,884	19,711	21,786	23,861

Table 10.8: Results of a TetherLife, v1.2, analysis for the EEO system proposed in the LSM Earth to moon mission, assuming an impact of either a primary or secondary tether causes secondary impacts with sufficient size and dispersion to cause a section failure.

N Primary	16	16	32	33	19	19	36	37
N Redundant Primary	0	0	16	17	0	0	17	18
N Secondary per Primary	0	2	2	2	0	2	2	2
MTTF (hours)	5.2E-05	5.2E-05	1.1E+05	6.9E+05	5.8E-05	5.8E-05	1.0E+05	6.0E+05
MTTF (years)	6.0E-09	6.0E-09	1.3E+01	7.8E+01	6.6E-09	6.6E-09	1.2E+01	6.9E+01
Max Payload (kg)	2,537	2,537	2,537	2,537	3,012	3,012	3,012	3,012
Sub span mass (kg)	1,660	4,150	12,449	12,968	1,971	4,928	13,746	14,265
Dual-span mass (kg)	6,640	16,599	49,796	51,871	7,884	19,711	54,984	57,058

10.1.3 Reliability over time

The reliability as a function of time is presented in Fig 10.3 and Fig 10.4 for the span configurations identified when employed for the LEO and EEO missions, respectively, in which the payload mass is a maximum of 2.5 tonnes.

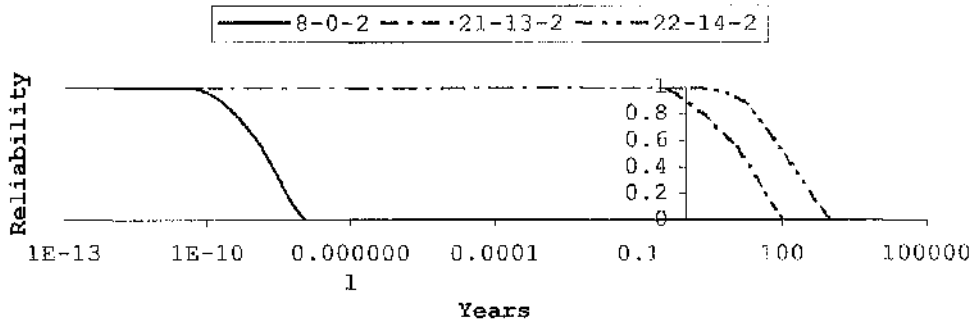

Figure 10.3 Reliability over time for three LEO systems, assuming lethal debris dispersion occurs

The curves progress to the right with increasing MMET, as expected. What may not be expected, though, is how soon the reliability of each system drops below the 99.7% reliability level. For the LEO systems, the reliability drops below this value at a mere fraction of a minute, 18 days, and 6 months, respectively. For the EEO mission, the identified configurations drop below this reliability level at a fraction of a minute, 10 days, and 3 months, respectively.

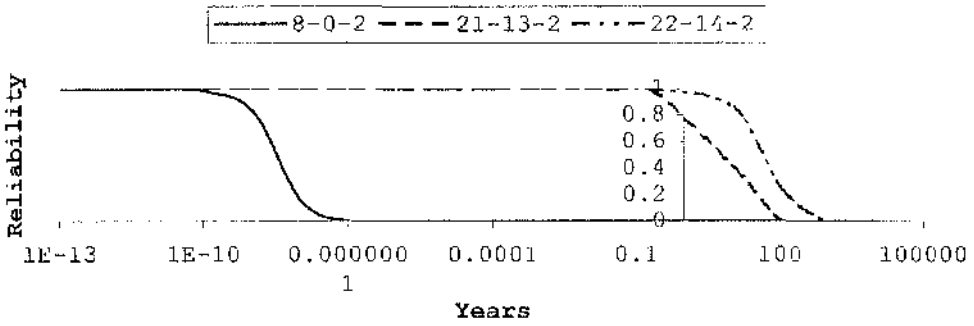

Figure 10.4 Reliability over time for three EEO systems, assuming lethal debris dispersion occurs

While the MTTF for these missions is significant, it must also be appreciated that the variance of the MTTF for the uniform failure rate case is equal to the MTTF squared. As a result, even with a mean time to failure on the order of a few hundred years, the probability of success for each mission may force the system to pose a higher risk than its conventional alternative.

When examining the values obtained using TetherLife, v1.2, to assess a Hoytether similar to that presented in Hoyt and Forward (1998), the results do agree. While agreement does not verify the techniques presented in Hoyt and Forward (1998), it does offer an indication that the calculations performed by TetherLife, v1.2, are in agreement with the current literature.

10.2 LSM mission: lifetime risk

Assuming each system will be designed to last on the order of 30 years, and considering the parameters of the LSM mission and the time relationships identified result in a mission-to-mission time of 102 hours, the following probability of failure for the first mission is generated for each system. This calculation assumes the payload mass is no more than 2.5 tonnes, and considers the probability of failure on the mission to be equal to the failure rate multiplied by the duration of the mission. Further analyses in the next Chapter will take a higher fidelity approach to a similar analysis.

Table 10.9 Values currently calculated for the LSM mission risk assessment.

	Conventional	MMET-based
C_{LV}	\$254M	\$70M
$C_{MMET,1}$	--	
$C_{MMET,2}$	--	
$p_{f,LV}$	0.003000	0.003000
$p_{f,H1}$	--	0.003000
$p_{f,T1}$	--	0.000072
$p_{f,H2}$	--	0.003000
$p_{f,T2}$	--	0.000147

Without accounting for the recurring cost of the MMET systems, the risk of a conventional system is calculated to be 0.762, while the risk of an MMET-based system is 0.643. While the MMET-based system appears to have the lower risk, thereby making it the more reasonable choice within the framework presented in this thesis, the lifetime costs are yet to be calculated.

Chapter 11

Feasibility assessment

With the system reliabilities known for both of the MMET systems employed in the LSM mission, and for the conventional systems, a choice between two reasonable options can be made based on the total system risk. Depending on the capital cost associated with initially deploying each MMET, an acceptable failure rate for a known number of missions can be determined.

11.0 The full choice

As previously stated, this thesis presents two reasonable launch system options, and selects the option with the least risk. We recall from Chapter 2 that there are two components to risk: (i) the probability of system failure and (ii) the magnitude of the effect resulting from that failure. This thesis focuses on the financial risk of a launch system. The financial risk posed by a launch system on any launch, as discussed in Chapter 2, is equal to the cost of the launch system for each launch, C_L, multiplied by the probability that the system will fail on that launch, $p_{f,L}$. After examining the financial risk posed by various launch system options, the option with the least risk is the reasonable choice, so long as all options are reasonable options.

As previously discussed, a reasonable option is one where probability of failure is not so large that it is inconsistent with other options available within the market. By examination of the true probability of success midpoint estimates presented in Draper *et al.* (2004), in conjunction with the concept of acceptable risk within the commercial market as discussed in documents such as DOT (2001), it is assumed in this research that a reasonable option a reliability of no less than 90%.

As previously identified in Chapter 10, the reliability associated with an MMET operation decreases as a function of time. Because this decrease in reliability results from broken tether segments, this decrease does not produce a time-dependent effect on the other sources of failure. For example, the probability of failure associated with each handover is not dependent on how many MMET sub-strands are broken.

Therefore, the probability of failure associated with the entire MMET-based unconventional launch system must be assessed when examining it as a reasonable option, and not just the failure rate of the MMET components.

11.1 Recouping mission cost

The first component examined for risk calculation purposes is the cost per mission. For each mission that employs an MMET-based unconventional launch system, there is a cost associate with the conventional launch vehicle and all MMET systems that are required to complete the mission. While a conventional launch system is a recurring cost for each launch, a large investment in each MMET system must be made to deploy the system before any missions can begin, after which all monies received as a result of operations are paid against this initial investment. The cost of deploying an MMET system would include costs such as the materials and labour required to build the system, the cost of boosting the system into orbit, and the cost of making the system usable after it has been placed on orbit. This significant capital investment in each MMET would be paid back in the form of a mission fee, charged to the customer, at the onset of each mission. If the cost of deploying an MMET is known, as well as the number of missions that the system can complete before its probability of failure per mission falls below acceptable levels, one could determine the minimum cost per mission that must be charged to both recoup the deployment costs and make a suitable return on investment.

If a launch service provider is interested in deploying an MMET-based unconventional launch system, this research assumes the MMET systems required will be a capital asset in which the provider must invest. As stated, the capital cost of deploying an MMET would be recouped through a mission price charged for each use of the system, C_m. When determining what this cost would be, it is assumed that price stickiness exists, based on the observations presented in Chapters 2 and 3. Therefore, the price charged should be assumed equivalent for each MMET mission.

Since the price the supplier will charge the customer for each mission is assumed constant over the lifetime of the system, this price will be modelled herein as annuity payments against the present value of the capital invested plus a suitable return, C_0,

in the presence of a suitable discount rate per mission, r_{disc}. Employing the standard equation for calculating the payments associated with an annuity as presented in works such as Brealey and Myers (2003), Eq. 11.4 rearranges the basic equation such that the price that the provider must charge per mission, C_m, for an MMET whose capital plus return is identified as C_0, is the subject of the equation.

$$C_m = \frac{C_0 r_{disc}}{\left[1 - \frac{1}{(1+r_{disc})^N}\right]} \tag{11.1}$$

Given an opportunity cost of capital based on the returns cited in quarterly reports such as Boeing (1999), it is assumed in this research that a mission discount rate for application in Eq. 11.4 should be based on an annualised discount rate of 7%.

If both the cost of deployment and the discount rate are known, an analyst must still work to determine the number of missions each MMET can complete. Approximations of this number can be calculated using reliability estimates developed in accordance with Chapter 10.

11.2 Probability of failure and its effect on the reasonable system

While Chapter 10 provides a methodology for determining both the failure rate and the MTTF for an MMET system, a launch service customer will not be interested in how the MMET system operates in isolation. As discussed previously, an MMET-based unconventional launch system must be capable of attaining a suitable reliability in its entirety relative to its conventional competition. This section discusses how such an assessment is conducted.

11.2.1 Uniform failure model

Systems that are susceptible to random failures are often modelled with a uniform failure rate. While the probability that such a system will fail over any set time period of time, Δt, is equal at any point in time, the probability that the system will fail

before a time, t, is calculated through use of the CDF of the exponential distribution, identified in Eq. 11.2.

$$F(t)=1-e^{-\lambda_{un}t} \tag{11.2}$$

Within Eq. 11.2, the uniform failure rate is represented by λ_{un}. If the failure rate for a system is known, and that system is known to be operating over a constant time, the probability that the system will fail during that time can be calculated with Eq. 11.2. If taken from system deployment, one can calculate when system reliability falls below an acceptable level. For the MMET-based unconventional launch system concept required for the LSM mission, however, this uniform failure rate may not be appropriate.

11.2.2 Failure allocation across the LSM mission

As with most engineering systems, an MMET-based unconventional launch system is not operating at a uniform failure rate across the whole mission. Identical to the highly contentious issue of failure allocation as it applied to conventional launch vehicles, as discussed in DOT (2002), the various events associated with an MMET-based unconventional launch system produce spikes in the failure rate over time. For example, while Chapter 10 assumes both the conventional launch and the handoff have the same probability of failure on each mission, the handoff operation is likely to take more than an hour, while the conventional launch will take no less than a few hours. If the failure rate within each operation is assumed uniform, the failure rate for the handoff operation can be many times greater than that of the conventional launch vehicle. Figure 11.1 identifies the probability of failure associated with each operation over the time the operation is occurring.

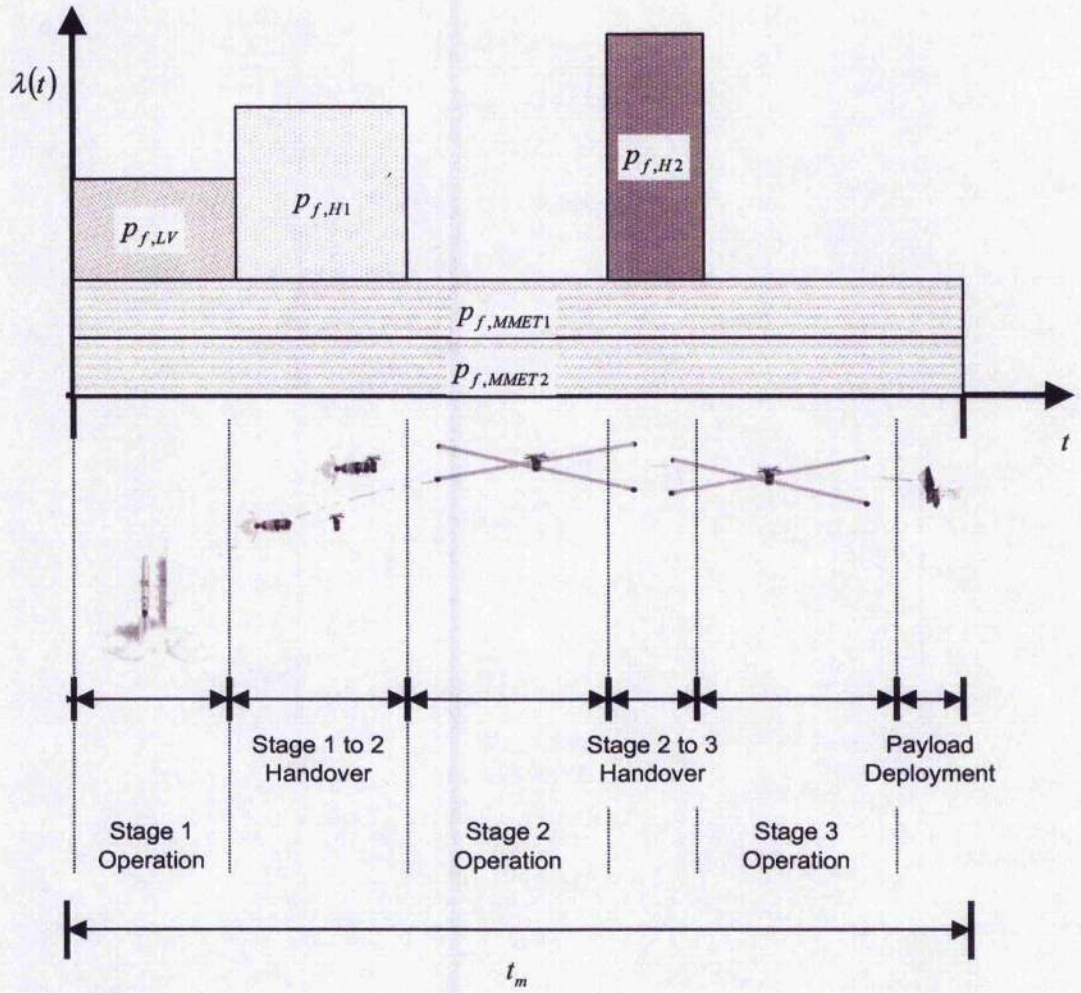

Figure 11.1 The probability of failure (upper) for each component of the MMET-based unconventional launch system required for the LSM mission, as identified (lower).

Given the probability of failure for each operation, the time over which each operation is acting, and Eq. 11.2, the failure rate for each element can be calculated, a not to scale representation of which is identified in the upper portion of Fig. 11.2. Equation 11.2 must be employed in this situation because it is not appropriate to assume that the time increment is infinitesimally small, unlike in Chapter 10. Considering all failure modes are assumed to be independent, the lower portion of Fig. 11.3 identifies the probability of failure associated with the system as a function of time.

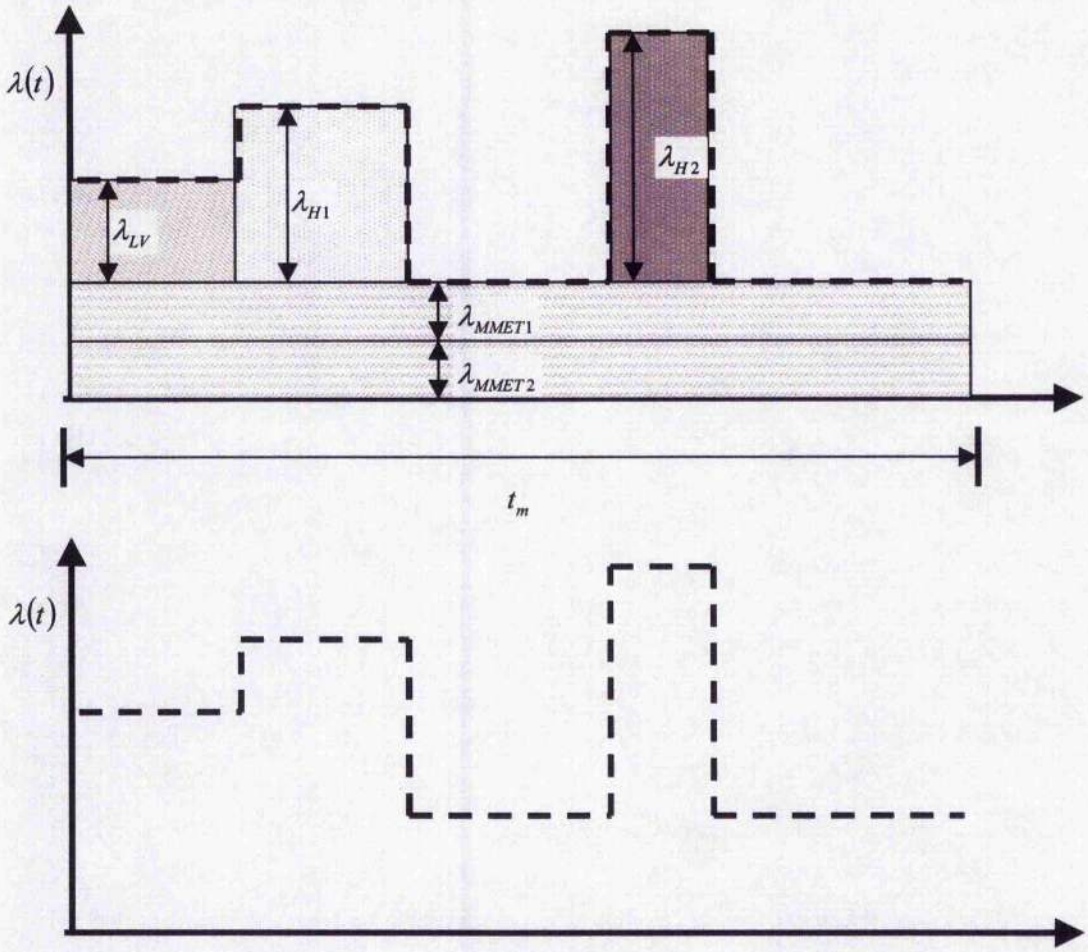

Figure 11.2 The magnitude of failure rate for each component in the MMET-based unconventional launch system proposed for the LSM mission (upper), and the system failure rate as a function of time (lower).

While it is clear that the failure rate for the MMET system is not uniform as a function of time, and is cyclical in nature, it is also important to note that understanding where within the mission that failure occurs is not as vital to the final risk calculation as it is to understanding whether the mission succeeds or fails. For this reason, this research will model operation of the MMET-based unconventional launch system required for the LSM mission not as a continuously operating system, but as a series of identical and finite events separated by a non-trivial time that is equal to the length of each mission.

11.2.3 System reliability

In accordance with standard texts such as Lewis (1996), reliability is the "the probability that a system survives for some specified period of time." With this understanding of reliability, and removing the assumption that the MMET-based unconventional launch system required for the LSM mission can be modelled as a system with a uniform failure rate, the probability that the LSM mission will survive to complete the n^{th} mission is calculated using Eq. 11.3.

$$R(n) = \left(1 - \left[\left(1 - p_{f,LV}\right)\left(1 - p_{f,H1}\right)\left(1 - p_{f,MMET1}\right)\left(1 - p_{f,H2}\right)\left(1 - p_{f,MMET2}\right)\right]\right)^n \qquad (11.3)$$

From Eq. 11.3, if the probability of failure for each MMET system is known, the number of missions, N, which can be completed before violating the acceptable system reliability level, can be readily found. For MMET systems with a known MTTF, the probability of success for any mission of length, t_m, can be found using Eq. 11.4.

$$p_{f,MMET} = 1 - e^{-\frac{t_m}{MTTF_{MMET}}} \qquad (11.4)$$

11.2.4 Calculating the number of missions per MMET

As per the assumptions presented in Chapter 9, the failure rate estimates for each MMET system examined within this research are uniform across an entire mission, and all missions run consecutively.[xv] For an MMET-based unconventional launch system that employs only one MMET, the number of missions that can be completed before the system ceases to be a reasonable launch option is defines by the single MMET system and represented by a solitary value, N. Since the price per mission developed for this research is based on the cost of capital plus the required return, there is no penalty to using each system until the end of its useful life, and then replacing it. For systems that employ a single MMET system, this useful lifetime of the MMET system is equal to the useful lifetime of the entire unconventional system. For MMET-based unconventional launch systems like those required for the LSM mission, which employ multiple MMET systems that may have varying MTTF

estimate, replacing both systems at the same time may not be making best use of the asset.

As identified in Chapter 10, the cost of deploying a system is related to its MTTF as a result of the system mass. In an effort to increase a systems MTTF, the system mass must increase. This increase in mass results in a need for the deploying systems to be larger. Consequently, a trade-off must be made and understood where the cost of increasing the MTTF for a system is weighed against the number of missions the system is capable of completing. If the number of missions that can be completed is not large enough, relative to the cost of deployment, such that the cost required per mission to recoup the capital investment associated with deploying the MMET makes the system risk too high, the system concept will no longer be financially feasible.

The minimum MTTF required for each MMET system can be related to the minimum system reliability, expressed previously in terms of the maximum allowable probability that the system will not fail prior to the time t, and the number of missions, N, that can be completed in that time. For each MMET system, knowing what level of reliability at the end of its useful life would be sufficient for ensuring the restrictions developed in accordance with Eq. 11.3 are not violated, the minimum MTTF required to achieve the required number of missions, N, sufficient for producing a suitable return on investment relative to the required risk level can be calculated using Eq. 11.5.

$$\text{MTTF} \geq -\frac{Nt_m}{\ln[R(N)]} \tag{11.5}$$

Deriving Eq. 11.5 requires the reorganisation of Eq. 11.2 so as to make the minimum MTTF the subject, in terms of the reliability after the completion of N mission, $R(N)$. Using this equation, an acceptable minimum boundary can be found iteratively for the MMET system if it is to be a reasonable choice. For example, if the system operates every 11 hours, and requires 100 missions to recoup the deployment costs, the MTTF would need to be greater than 1.2 years.

11.3 Mission risk

To be a financially feasible option, assuming it is a reasonable choice as determined through the above relationships and work, the risk posed by an MMET-based unconventional system must be less than that of its conventional alternative. For an MMET-based unconventional launch system like that required for completing the LSM mission proposed within this research, calculating this risk is more complex than examining just the employed MMET system in isolation. For the LSM mission, two MMET systems are required, identified as systems *MMET*1 and *MMET*2 for the LEO and EEO orbits, respectively.

As all failure probabilities and prices are uniform, the risk is identical for every mission, and is calculated using Eq. 11.6. In Eq. 11.6, all of the parameters employed are as previously discussed, the subscript *MMET*1 and *MMET*2 identifying parameters that are specific to the LEO and EEO MMET systems, respectively, for purposes of assessing the LSM mission.

$$Risk = \left(1 - \left[\begin{array}{l} \left(1 - p_{f,LV}\right)\left(1 - p_{f,H1}\right)\times \\ \left(1 - p_{f,MMET1}\right)\left(1 - p_{f,H2}\right)\times \\ \left(1 - p_{f,MMET2}\right) \end{array} \right] \right) \times$$

$$\left[C_{LV} + \left(\frac{C_{0,MMET1} r_{disc}}{\left[1 - \frac{1}{\left(1 + r_{disc}\right)^{N_{MMET1}}} \right]} \right) + \left(\frac{C_{0,MMET2} r_{disc}}{\left[1 - \frac{1}{\left(1 + r_{disc}\right)^{N_{MMET2}}} \right]} \right) \right] \quad (11.4)$$

11.4 Optimising system design for the LSM mission

With a target risk for a reasonable conventional alternative, Eq. 11.2 and Eq. 11.4 must be considered simultaneously in an iterative optimisation process. The process must be iterative because, as previously discussed, there is a direct relationship between the MTTF of each MMET system as its mass. Considering how this relationship effects the initial capital required and the cost per mission, the following subsection provides an initial assessment of the risk associated with the LSM mission.

11.4.1 Initial assessment

From the results presented in Chapter 10, in conjunction with the approximation above of a minimum MTTF of 1.2 years, the LEO system required for the LSM mission would require a Hoytether span with a 24-14-2 configuration, assuming lethal dispersion. Such a system has a sub-span mass greater than 26 tonnes. With a sub-span mass of 26 tonnes, the system mass would be no less 105 tonnes, without the central facility. Wade (2006) states that the Delta IV Heavy, currently the largest heavy-lift vehicle operated by a US manufacturer, has a capability of 25,800 kg to a 185 km orbit. Based on the energy of this orbit, the Delta IV Heavy should be able to deliver 21.2 tonnes to the LEO orbit proposed in the LSM mission, and 6.5 tonnes to the EEO orbit. These values to not indicate that a MMET with this level of reliability given an assumption that a hypervelocity impact is likely to produce lethal debris would be able to be placed onto an orbit suitable for completing the LSM mission. By excluding this assumption that a lethal debris cloud is generated after an initial impact, the decrease in system size could allow for smaller vehicles to be employed during initial installation.

Examining the next smallest launch vehicles, in terms of payload capacity, the Ariane 5G is capable of lifting 13.6 tonnes to the LEO orbit or 4.1 tonnes to the EEO orbit, according to an energy calculation based on data provided by Wade (2006). The Ariane 5G list price is stated as $180 million in 2005 US Dollars.[xvi] The next size after the Ariane 5G is that of the Delta IV Medium, Atlas V, and Zenit 3SL. Each of these could lift approximately 9.6 tonnes and 2.9 tonnes to the LEO and EEO orbits, respectively. While the price of Delta IV and Atlas V is stated at $138 million each, the Zenit 3SL is stated at $90 million. With the 11-1-2 configuration for the LEO MMET sub-span mass equal to 8.3 tonnes, and the 20-1-2 configuration of the EEO MMET sub-span mass equal to 5.4 tonnes, each system would require multiple launches to place it onto orbit.

Out of those options presented, only the Delta IV Heavy is capable of launching the EEO MMET system onto its orbit. If this research assumes that the central facility is approximately 20% of the system mass, deployment of the EEO system required by the LSM mission would cost $1.3 billion. Using equivalent logic, combined with the

Zenit 3SL being chosen as the lowest cost option with suitable capability, deployment of the LEO MMET system would cost $450 million. As neither price includes the manufacture of the system, deploying the hardware necessary to carry out the LSM mission, alone, would cost over $1.7 billion.

Given the probabilities of failure assumed for the conventional vehicle, each handover, and the failure rate for the 11-1-2 and 20-1-2 configured MMET systems, the probability of failure for the system would be 0.937%. With this estimate, the system would be a feasible launch option. Further, with the calculated MTTF values for each MMET system and a mission time of 102 hours, the LEO and EEO systems would be able to complete 11,764 missions and 3,137 missions while retaining a probability of failure less than 9% during the time span required to complete those missions.

Taking the number of missions for each system, plus a discount rate per mission of 0.082% based on the annualised 7% discount rate stated earlier, the cost per mission for the LEO and EEO MMET systems for the LSM mission would be $0.37 million and $1.15 million, respectively. Added to the $70 million per mission required for the conventional launch system used to boost each payload up to the LEO MMET system, the total cost per mission would be around $71.4.

With this cost per mission and the previously calculated probability of failure, the risk per mission for the LSM mission, employing the 11-1-2 and 20-1-2 configuration spans for the LEO and EEO MMET systems, respectively, would be 0.669. As previously discussed in section 10.2, the risk associated with completing the LSM mission using conventional means is 0.762. Considering these risk values, the LSM mission could be feasibly completed, as proposed by Cartmell *et al.* (2004).

Chapter 12

Conclusions and Future Work

The analyses provided by this work support the use of the MMET for commercial applications. However, the scope of such a determination must be assessed and understood in the context of future work.

12.0 Analytical limitations

The analysis performed and described in this thesis is limited. Many of the limitations involve uncertainty with regards to the data available, whether that data be financial, physical, or operational in nature.

12.0.1 Financial data

As discussed, financial data on the price a supplier charges a customer is a closely guarded secret. This is guarded because the small number of participants in the market makes such knowledge competitively damaging. Consequently, the data that is publicly available is likely to be somewhat unreliable. Considering the recent commercial space lift market crash, with no current prediction for a turnaround in the near future, it is likely that the costs associated with commercial launches both are, and will continue to be, even lower than publicly presented or projected. This decrease in costs would affect the risk calculations, with the expected change in predictions being uncertain.

12.0.2 Operational data

This analysis does not take into account operational factors that may affect the risk assessed for each system. While such risks could be accounted for in the values produced, thus retaining the small number of final inputs into the analysis, they are not considered in this thesis. This is because doing so would be unrealistic from a data assurance point of view, and the impact relative to model fidelity is assumed to be minimal, if not insignificant. Further, as discussed with regards to the handover between tethers, the kind of equipment to be used is currently unknown and would certainly depend on the orbital dynamics of the system. When the system motion has

been determined to a high level of certainty, including accounting for the motor characteristics and power supply reliability and performance, the operational impact on system performance may be found to be minimal. However, considering such issues are currently unknown without the completion of accompanying work at the University of Glasgow, this research is unable to make a more accurate approximation of operational uncertainty than that proposed here.

12.0.3 Environmental data

The orbital debris and micrometeorite data that is currently available is known to have a high level of intrinsic uncertainty. This is understood and widely accepted by experts in the field, as noted by Liou *et al.* (2001). Like similar analyses performed prior to this one, the environmental data available in the public domain is assumed to be suitable. It is outside the scope or capability of the current research efforts at the University of Glasgow to improve on such models, which is why such an undertaking was neither considered, nor initiated, for this thesis.

12.0.4 Material data

As identified in this thesis, the public knowledge on how aramid fibres would react under hypervelocity impact conditions is anecdotal, at best. While it was not possible to perform enough tests to reach concrete conclusions, the material and impact testing performed in support of this research offered an indication that the current assumptions may not be fully supported through experimentation. Further, while the dataset used for calibrating the Draper (72) equation may not fully account for the characteristics important to an aramid rope, it is clear that previous work was neither calibrated for the type of densities that would be expected for a tether impact, nor did it address non-planar target surfaces. While an increase in data could lead to improvements in the equations and assumptions used by TetherLife for characterising hypervelocity impacts with tether structures, it is likely that the techniques employed within this work offer an incremental improvement in the field, when considering the small amount of publicly available data on the topic.

12.0.5 Time dependence

While texts such as Lewis (1994) support the use of a uniform failure rate as it was used in the TetherLife program, the conservatism of the Monte Carlo approach cannot be assessed without further work into deterministic models of the system. As this work was being conducted in tandem with the orbital dynamic modelling necessary for building such models, a comparison may be made in the near future. However, without such a model, the time dependence on failure rate could only be assumed.

12.0.6 Environmental focus

TetherLife only focuses on impact failures resulting from the orbital debris and micrometeorite environment. No work was performed with regards to the plasma environment and its effect on the tethers, nor was any work undertaken regarding the general space environment and its effect on any general components required for system operation. The scope of such an examination is extraordinary, especially in such early stages of the work when orbital dynamic assessments are not fully completed. While the data present and employed for this analysis has a high degree of inherent uncertainty, the approach and uncertainty associated with the results of the TetherLife program are consistent with commonly accepted models.

12.1 Other concerns

In addition to the limitations of the analysis, there are a number of other concerns regarding the conclusions that could be drawn based on the results of the analysis conducted and presented in support of this research. The two most significant concerns about the MMET system and the analysis performed here are the following:

12.1.1 Number of missions

The number of missions proposed by this analysis is unreasonable for the foreseeable future. With only five commercial launches performed under DOT license in 2005, it seems unlikely that the necessity for 85 missions per year to the moon will emerge in the near future. However, this concern is one of speculation based on current uses for space. If the use of space and the moon changes significantly, it is likely that the launch requirements for supporting such activities could also change.

12.1.2 Tether separation

Examination of Boeing (2002) indicates that the maximum payload size that could be contained within a Delta IV fairing is 9m in length with a diameter of 5m. While such a volume indicates that each span could fit within the fairing, it also indicated that the maximum distance between counter-rotating spans would be less than 18 metres. For 200 km span, this distance is 0.009% of the span length. This separation would mean that, if a perturbation of 1:10,000 of a degree exists in each span, there is a significant likelihood that the tethers would collide and cause a failure. While this study does not rely on an analysis of the system orbital dynamics, such a perturbation seems intuitively likely. Unfortunately, this failure mode is inherent in the system design, and cannot be designed out without significantly decreasing the span lengths, which would require resulting increases in the operational angular velocity.

12.2 Recommended future work

As discussed, future risk assessment work on the MMET must make use of the orbital dynamics specific to each vehicle. While the assumptions made in this work are reasonable, based on the quality and quantity of available data, this model must be proved against a deterministic equivalent. Once the orbital dynamics are more fully finalised for analysing an operational system, future risk work would be capable of examining the components required to operate the system. Within such research, an examination of the required ground systems and likely safety concerns associated with frequent system operation could be undertaken.

With so little currently defined about the MMET system in its operational form, much of the work that must be completed before a further risk assessment can be carried out is in system definition. Only upon completion of such work can a more complete risk assessment be conducted.

12.3 Concluding remarks

This work offers an indication that the MMET could be a suitable unconventional launch system component for commercial applications. While this analysis of the current system concept indicates there are many issues that must be investigated before the system can be deployed, issues that are both minor and intrinsic, this top-

level analysis proves that further work is necessary and important. While this thesis is only a starting point from which future risk analyses may continue, its conclusions are appropriate in the context of the information available.

Endnotes

Chapter 1

i. A COLA is generally performed for only the initial full orbit of a satellite, after which the orbital perturbations during its useful life are not assumed significant enough such that the satellite becomes a hazard to objects known at that time, or those that will be placed in accordance with a valid COLA analysis. However, for on-orbit launch systems like momentum exchange tethers that rely on orbital dynamic mechanisms to operate, these systems will experience significant travel from any initial orbit. While it is public knowledge that the uncertainty associated with large, tether-based objects has caused the delay or cancellation of ESA missions out of concern for other systems already on orbit, neither this research nor that of Patera (2002) addresses the kinds of operationally focused calculations that would be required to prove an operating MMET would avoid all other objects. It is assumed herein that a COLA-type analysis would be completed for each operation performed on orbit, an analysis that would ensure the launch operation would avoid all other assets of value on orbit, and, after each orbit, the system would return to a rest state and orbit that is known to pose limited risk to other assets of value that are on orbit at the time. As consistent with current government oversight for commercial operations, implemented because United Nations treaties hold a nation responsible for the actions of its citizen with regards to space operations, it is assumed that the operator will take responsibility for this task of ensuring a collision will not occur. As previously stated, though, how the operator does this is not discussed in this thesis.

ii. Primary failures, in this context, refer to failures such as debris impacts or handover failures that are the direct result of the environmental or operational factors investigated by this thesis. This use of the word primary should not be confused with later discussions of primary and secondary lines within a Hoytether configuration. In this context, issues such as electronic component reliability or unanticipated COTS failures are secondary failures from the perspective of the unconventional launch

system concept discussed within this research, and are not discussed. These are left out of the analysis due to the current lack of system definition, which would make valid component selection unrealistic.

iii. This work is only concerned with the transport of a single payload form the surface of the earth to the moon. The analysis was scoped in this way as a result of the significant uncertainty surrounding the orbital dynamics of the non-symmetric handover scenario. If the effect of a non-symmetric payload release is relatively insignificant, it may be possible to transfer two payloads per mission. However, as this is unproven, the second "payload" that is required to balance the MMET system is ignored, with the assumption that it could be a dummy payload that is discarded when the payload of interest is transferred to the second MMET system.

Chapter 2

iv. The use of the product rule for calculating the probability of failure is only valid when no one component is so significant that is dominates the others. The product rule is assumed acceptable within this research because, by design, the MMET is only considered a reasonable system so long as its reliability does not fall below a stated threshold. This ensures that the system success rate will not fall to such a significantly low level that it will then dominate the failure calculation for the entire unconventional system.

v. This research is only concerned with the financial risk associated with the operation of an MMET-based unconventional launch system in which all components are already installed on their proper obit. This research does not account for the probability of failure associated with installing the required MMET systems, a factor that would affect the total capital investment required to get the system up and running. While a slight oversight, so long as the reliability of the systems employed for such a task is suitably high, this will not have a significant affect on the end calculations or results relative to the inherent uncertainty associated with the research as a whole.

Chapter 4

vi. As will be clarified through information presented later within section 4.2, and the worked example presented in section 4.2.2, the shape and size constants are found using an iterative solution technique that uses the observed vehicle flight history as the input data. Prior to performing an analysis, nothing is known about the shape and size parameters, and cannot be determined without the solving of equations 4.5 and 4.5.

vii. The issues associated with selecting an appropriate reference date are neither fully explored nor understood through the limited examination performed in support of this research. In many cases, an analyst's opinion of an appropriate result may dominate his or her definition of "appropriate reference date," a scenario that would have an equivalent affect even if a quantitative metric were to have been presented in support of this research. As noted within section 4.2.2, the reference date does have a significant impact on the results of the calculation and, while it is clear that results obtained using two different reference dates cannot be compared, it is highly likely that the logic behind choosing one reference date over another cannot be suitably determined using solely numerical means.

viii. The Julian date system employed within this research is equivalent to that employed for Microsoft-based software packages, where the date having a serial value of 1 is equal to 1 January 1900.

ix. Flight histories were developed using the "Orbital Launch Vehicle Alphabetical Index," Encyclopedia Astronautica [online database], URL: http://www.astronautix.com/lvs/orbindex.htm [cited 7 December 2003], which were verified against Isakowitz (1999), Chang (1996), and Chang (2000) for all applicable flights.

Chapter 6

x. The author would like to thank Nicolas LeClanche of Culzean Fabrics in Kilmarnock, Scotland, for his company's support and supply of the Twaron samples tested for this work.

Chapter 7

xi. It must be noted that the work of Shanbing, Y, Gengchen, S., and Quingming, T., "Experimental laws of cratering for hypervelocity impacts of spherical projectiles into thick targets," *International Journal of Impact Engineering*, Vol. 15, No. 1, pp 67-77, was consulted through the course of this reserach, and it is unclear why a reference to this work and its results was omitted from the original text of this thesis.

xii. Any impact angle equal to zero for the purposes of this single calculation was represented as 1E-5, so as to avoid the product of dissimilar datasets being equivalent.

Chapter 9

xiii. This assumption that the failure rate is constant over the entire mission is sufficient so long as the rest time between missions is not significant. When the number of missions is on the order of that examined for the purposes of this research, it is assumed that the difference between the number of failures observed while the system is operating verses the number of failures observed while the system is at rest is not so significant that the operational phase dominates the rate of observed failures. Assuming this condition is met, which would likely be best verified using a deterministic model, the requirements outlined in Lewis (1996) for when the uniform failure rate is applicable would then be met. If the rest time is significant relative to the probability of time that the system is operating, which would occur if the number of missions per unit time is significantly reduced, this use of the uniform failure rate assumption would not be valid.

Chapter 10

xiv. Examining the results presented in Table 10.5 when compared to those present in Table 10.3, the MTTF values presented may not seem intuitively logical. As seen in Table 10.5, the MTTF for the 8-0-0 is less than it is when lethal dispersion is ignored, the results of such calculations presented in Table 10.3. This reduction in the MTTF may not seem

logical since a secondary impact requires an initial impact. If the MTTF is interpreted in a deterministic manner as the time of first impact, it is not logical for the values calculated for the 8-0-0 tether configuration presented in Table 10.5 to differ with those presented in Table 10.3. However, as the MTTF is an average value, the higher number of early failures associated with the calculations performed under the assumption that a lethal cloud would form shifts the mean approximation of the failure distribution, thereby reducing the MTTF estimate. While the histograms of the failure times are not examined for this research, this decreasing MTTF value could indicate that the distribution associated with the MTTF approximation is significantly skew, causing the normalcy approximation employed by the MTTF calculation to be insufficient for a high fidelity analysis in an equivalent manner to how it is employed by TetherLife, v1.2.

Chapter 11

xv. This analysis does not independently examine the probability that the system will be capable of carrying out the next mission. Ensuring an asset that is on orbit has not become unusable between missions, or between the specific times when the system is required, is of vital importance to the space industry, most notably with regards to the Shuttle tiles. Whether employing fibre optics or other methods for assessing the system state while on orbit, either actively or passively, knowing the system state before an operation occurs will likely be required by any end customer. This research assumes such an analysis is not necessary as a result of the reliability threshold limit imposed on the system, but this may not be sufficient in an operational environment.

xvi. All prices in this Chapter or used in this thesis for comparative purposes are listed in 2005 US Dollars, and, when necessary, converted with the US Department of Commerce Price Producer Index, as previously discussed.

References

Air Force Space Command, (1997), Eastern Western Range 127-1 Range Safety Requirements Handbook, Range Safety Office, Patrick Air Force Base, Florida, 31 December 1997

Air Force Space Command, (2004), "Range Safety User Requirements," AFSPCM 91-710, 1 July

Allen, S., Roche, E., Bennett, B., and Molaison, R., (1992), "Tensile deformation and failure of poly(p-phenylene terephthalamide) fibres," Polymer, Vol. 33, No. 9, pp. 1849-1854

Anderson, C.E., Jr., (1987), "An Overview of the Theory of Hydrocodes," Int. Journal of Impact Engineering, Vol. 5, pp. 33-59

Ansell, J., Quigley, J., and Walls, L., (1997), "Growth and innovation through reliability testing," Stochastic Modelling in Innovative Manufacturing/ Christer, A., Osaki, S, and Thomas, L., (eds), Springer-Verlag, Berlin

Ansell, J., Walls, L., and Quigley, J., (1999), "Achieving growth in reliability," Annals of Operations Research, Vol. 91, pp. 11-24

Anselmo, L., and Pardini, C., (1999) "Assessing the impact risk of orbital debris on space tethers," Space Debris, Vol. 1, No. 2, pp. 87-98

Anselmo, L., and Pardini, C., (2005), "The survivability of space tether systems in orbit around the earth," ACTA Astronautica, No. 56, pp. 391-396

Armstrong, J.S., (1985) Long-Range Forecasting, John Wiley, New York

Arnold, W., and Schafer, F.K., (1999) "Behind Armor Blast (BAB) Caused by Shaped Charges," Int. Journal of Impact Engineering, Vol. 23, No. 1, pp. 13-25

Ashford, D., (2002), Spaceflight Revolution, Imperial College Press, London

Baker, J.R., (1995), "Hypervelocity Crater Penetration Depth and Diameter - A Linear Function of Impact Velocity?" Int. Journal of Impact Engineering, Vol. 17, pp. 25-35

Baker, J.R., and Persechino, M.A., (1993), "An Analytical Model of hole Size in Finite Plates for Both Normal and Oblique Hypervelocity Impact for all Target Thicknesses up to the Ballistic Limit, Proc. 1992 Hypervelocity Impact Symp." Int. Journal of Impact Engineering, Vol. 14, pp. 73-84

Baumung, K., Kanel, G.I., Razorenov, S.V., Rusch, D., Singer, J., and Utkin, A.V., (1997), "Shock-Melting Pressure from Non-Planar Impacts," Int. Journal of Impact Engineering, Vol. 20, pp. 101-110

Bedingfield, K.L., Leach, R.D, and Alexander, M.B., (1996), "Spacecraft Systems Failures and Anomalies Attributed to the Natural Space Environment," NASA RP-1390, August

Bekey, I., (1983), "Tethers open new space options," Astronautica and Aeronautics, Vol. 21, pp. 32-40

Bendisch, J., Bunte, K.D., Krag, H., Sdunnus, H., Wegener, P., Walker, R., Wiedemann, C., and Rex, D., (2000), "MAS-GEN-FR [Upgrade of ESA's MASTER Model]," ESA Contract 12318/97/D/IM, 23 June

Benloulo, I., Rodriquez, J., Martinez, M., and Galvez, V., (1997), "Dynamic tensile testing of aramid and polyethylene fiber composites," International Journal of Impact Engineering, Vol. 19, pp. 135-146

Berger, B., (2006), "Fender Bender: NASA's DART Spacecraft Bumped into Target Satellite," Space.com [http://www.space/com/missionlaunches/050422_dart_update.html], cited 29 March

Bernhard, R.P., Christiansen, E.L., Hyde, J. and Crews, J.L., (1995), "Hypervelocity Impact Damage into Space Shuttle Surfaces," Int. Journal of Impact Engineering, Vol. 17, pp. 57-68

Bierbaum, R.L., Brown, T.D., and Kerschen, T.J., (2002), "Model Based Reliability Analysis", IEEE Transactions on Reliability, Vol. 51, No. 2, pp 133-140

BNA, (2005a), "Lockheed Martin, Boeing to resubmit joint venture proposal to US authorities," *Federal Contracts Report*, Vol. 84, No. 11, pp 298

BNA, (2005b), "SpaceX protests plan to award EELV contracts on to Boeing, Lockheed Martin," *Federal Contracts Report*, Vol. 84, No. 11, pp 306

Boeing Company, (1998a), 1998 First Quarter Earnings Report, www.boeingmedia.com

Boeing Company, (1998b), 1998 Second Quarter Earnings Report, www.boeingmedia.com

Boeing Company, (1998c), 1998 Third Quarter Earnings Report, www.boeingmedia.com

Boeing Company, (1999a), 1998 Annual Earnings Report, www.boeingmedia.com

Boeing Company, (1999b), 1999 First Quarter Earnings Report, www.boeingmedia.com

Boeing Company, (1999c), 1999 Second Quarter Earnings Report, www.boeingmedia.com

Boeing Company, (1999d), 1999 Third Quarter Earnings Report, www.boeingmedia.com

Boeing Company, (2000a), "Delta II Payload Planners Guide," MDC 00H0016, October 2000, page 58.

Boeing Company, (2000a), 1999 Annual Earnings Report, www.boeingmedia.com

Boeing Company, (2000b), 2000 First Quarter Earnings Report, www.boeingmedia.com

Boeing Company, (2000c), 2000 Second Quarter Earnings Report, www.boeingmedia.com

Boeing Company, (2000d), 2000 Third Quarter Earnings Report, www.boeingmedia.com

Boeing Company, (2001a), 2000 Annual Earnings Report, www.boeingmedia.com

Boeing Company, (2001b), 2001 First Quarter Earnings Report, www.boeingmedia.com

Boeing Company, (2001c), 2001 Second Quarter Earnings Report, www.boeingmedia.com

Boeing Company, (2001d), 2001 Third Quarter Earnings Report, www.boeingmedia.com

Boeing Company, (2002a), 2001 Annual Earnings Report, www.boeingmedia.com

Boeing Company, (2002b), 2002 First Quarter Earnings Report, www.boeingmedia.com

Boeing Company, (2002c), 2002 Second Quarter Earnings Report, www.boeingmedia.com

Boeing Company, (2002d), 2002 Third Quarter Earnings Report, www.boeingmedia.com

Boeing Company, (2002e), Comments and Proprietary Cost Impact Analysis (Confidential), Department of Transportation Docket Management System, Docket Number FAA-2000-7953-28, 23 October

Boeing Company, (2003a), 2002 Annual Earnings Report, www.boeingmedia.com

Boeing Company, (2003b), 2002 Annual Report, http://www.boeing.com/companyoffices/financial/finreports/annual/02annualreport/f_mda16.html#del

Boeing Company, (2003c), 2003 First Quarter Earnings Report, www.boeingmedia.com

Boeing Company, (2003d), 2003 Second Quarter Earnings Report, www.boeingmedia.com

Boeing Company, (2003e), 2003 Third Quarter Earnings Report, www.boeingmedia.com

Boeing Company, (2004a), 2003 Annual Earnings Report, www.boeingmedia.com

Boeing Company, (2004b), 2004 First Quarter Earnings Report, www.boeingmedia.com

Boeing Company, (2004c), 2004 Second Quarter Earnings Report, www.boeingmedia.com

Boeing Company, (2004d), 2004 Third Quarter Earnings Report, www.boeingmedia.com

Boeing Company, (2005a), 2004 Annual Earnings Report, www.boeingmedia.com

Boeing Company, Lockheed Martin Corporation, International Launch Services, Orbital Sciences Corporation, and Sea Launch Corporation, (2000), Consolidated Industry Response to FAA NPRM, Licensing and Safety Requirements for Launch, Department of Transportation Docket Management System, Docket Number FAA-2000-7953-17, 25 October

Boeing Company, Lockheed Martin Corporation, International Launch Services, Orbital Sciences Corporation, and Sea Launch Corporation, (2002), Consolidated Industry Response: FAA SNPRM, Licensing and Safety Requirements for Launch, Department of Transportation Docket Management System, Docket Number FAA-2000-7953-31, 28 October

Brealey, R A, and Myers, S C, (2003), Principles of Corporate Finance, International Edition, McGraw-Hill, Boston

Burchell, M., and Grey, J., (2001), "Oblique hypervelocity impacts on thick glass targets," Materials Science and Engineering, Vol A303, pp 134-141

Burchell, M., and Whitehorn, L., (2003), "Oblique incidence hypervelocity impacts on rock," Mon. Not. R. Astron. Soc., Vol 341, pp 192-198

Burchell, M., Cole, M., McDonnell, J., and Zarnecki, J., (1999), "Hypervelocity impact studies using the 2 MV Van de Graaff accelerator and two-stage light gas gun of the University of Kent at Canterbury," Meas. Sci. Technol., Vol 10, pp 41-50

Burington, R., and May, D., (1970), Handbook or Probability and Statistics with Tables, Second Edition, McGraw-Hill Book Company, New York

Burt, R, and Christiansen, E., (2001), Hypervelocity Impact Tests on Hubble Space Telescope (HST) Solar Array Cells, NASA JSC-28307

Campbell, J., and Vignjevic, R., (1997), "Development of Lagrangian Hydrocode Modelling for Debris Impact Damage Prediction," Int. Journal of Impact Engineering, Vol. 20, pp. 143-152

Carroll, J., (1986), "Tether applications in space transportation," ACTA Astronautica, Vol. 13, pp. 165-174

Cartmell, M., (1996), "Report on rotating, inertial, space vehicle propulsion concept for the European Space Agency," European Space Technology and Research Centre, Noordwijk, Holland

Cartmell, M., (1997a), "Feasibility assessent of a space-based spinning tether propulsion system for the European Space Agency," ESTEC, Noordwijk, Holland

Cartmell, M., (1997b), "Supplementary Report -- Feasibility assessment of a space-based spinning tether propulsion system for the Eurpean Space Agency," ESTEC, Noordwijk, Holland

Cartmell, M., (1998), "Generating velocity increments bymeans of a spinning motorised tether," 34th AIAA/ASME/SAE/ASEE Joint Propulsion Conference and Exhibition, Cleveland Conference Center, Cleveland, OH, USA, 3-5 July

Cartmell, M., and D'Arrigo, M., (2005), "Simultaneous forced and parametric excitation of a space tether," XXXIII Summer School on 'Advanced Problems in Mechanics,' Russian Academy of Sciences, St. Petersburg, Russia, 28 June - 5 July

Cartmell, M., and Ziegler, S., (1999), "The use of symmetrically laden motorised tethers for continuous two-way interplanetary payload exchange," 35th

AIAA/ASME/SAE/ASEE Joint Propulsion Conference and Exhibit, Bonaventure Hotel and Conference Center, Los Angeles, CA, USA, 20-24 June

Cartmell, M., and Ziegler, S., (2000), "Terrestrial scale model testing of a motorised propulsion tether," 36th AIAA/ASME/SAE/ASEE Joint Propulsion Conference and Exhibit, Huntsville, AL, USA, July

Cartmell, M., and Ziegler, S., (2001), "Experimental scale model testing of a motorised momentum exchange propulsion tether," 37th AIAA/ASME/SEA/ASEE Joint Propulsion Conference and Exhibition, Salt Lake City, UT, USA, 8-11 July

Cartmell, M., McInnes, C., and McKenzie, D., (2004), "Proposals for an Earth-Moon mission design based on motorised momentum exchange tethers," XXXII Summer School on 'Advanced Problems in Mechanics,' Russian Academyof Sciences, St. Petersburg, Russia, June

Cartmell, M., Ziegler, S., and Neill, D., (2002), "On the scale modelling of motorised momentum exchange tethers," XXX Summer School on 'Advanced Problems in Mechanics,' Powerpoint presentation, Russian Academy of Sciences, Repino, St. Petersburg, Russia, 27 June - 6 July

Cartmell, M., Ziegler, S., and Neill, D., (2003), "On performance prediction and scale modelling of a motorised momentum exchange propulsion tether," STAIF 2003, University of New Mexico, Albuquerque, NM, USA, 2-6 February

Castillo, E., Conejo, A.J., Minguez, R., Castillo, C., (2003), "An alternative approach for addressing the failure probability-safety factor method with sensitivity analysis," Reliability and System Safety, Vol. 82, pp. 207-216

Chang, I., (1996), "Investigation of space launch vehicle catastrophic failures," Journal of Spacecraft and Rockets, Vol. 33, No 2

Chang, I., (2000), "Overview of world space launches," Journal of Propulsion and Power, Vol. 16, pp. 853-866

Chobotov, V., and Mains, D., (1999), "Tether satellite system collision study," Acta Astronautica, Vol. 44, pp. 543-551

Christiansen, E., (1998), Orbiter Meteoroid/Orbital Debris Impacts: STS-50 (6/92) through STS-86 (10/97), NASA JSC-28033, 1998

Christiansen, E., Cykowski, E., and Ortega, J., (1993), "Highly Oblique Impacts into Thick and Thin Targets," Int. Journal of Impact Engineering, Vol. 14, pp. 157-168

Christiansen, E., Hyde, J., and Snell, G., (1992), "Spacecraft Survivability in the Meteoroid and Debris Environment, AIAA Paper No. 92-1409" AIAA Space Programs and Technologies Conference, 24-27 March

Christiansen, E., Hyde, J., Lear, D., (1997), "Meteoroid/Orbital Debris Impact Damage Predictions for the Russian Space Station Mir," Proceedings of the Second European Conference on Space Debris, 17-19 March

Collani, E. and Dräger, K., (2001), Binomial Distribution Handbook for Scientists and Engineers, Birkhäuser, Boston

Collins, G., (2002), "An introduction to Hydrocode Modelling," Unpublished lecture notes, August 2

Commercial Space Transportation Advisory Committee (COMSTAC), (1997), Report of the COMSTAC Technology & Innovation Working Group: Commercial Spacecraft Mission Model Update, http://ast.faa.gov/files/pdf/geo.pdf, May

Commercial Space Transportation Advisory Committee (COMSTAC), (1998), Report of the COMSTAC Technology & Innovation Working Group: Commercial Spacecraft Mission Model Update, http://ast.faa.gov/files/pdf/comstac.pdf, May

Cosmo, M., and Lorenzini, E., (1997), "Tethers in space handbook, Third Edition," NASA Marshall Space Flight Center, December

Cour-Palais, B., (1969), "Meteoroid Environment Model - 1969 [Near Earth to Lunar Surface]," NASA SP-8013, March

Cour-Palais, B., (1985), Hypervelocity impact investigations and meteoroid shielding experience related to Apollo and Skylab. Orbital Debris (D.J. Kessler and S-Y Su, Eds.), NASA CP-2360

Cour-Palais, B., (2001), "The Shape Effect of Non-Spherical Projectiles in Hypervelocity Impacts," Int. Journal of Impact Engineering, Vo. 26, pp. 129-143

Dahl, J., and Schultz, P., (2001), "Measurement of Stress Wave Asymmetries in Hypervelocity Projectile Impact Experiments," Int. Journal of Impact Engineering, Vol. 26, pp. 145-155

Davison, L., Grady, D., and Shahinpoor, M., (1996) High Pressure Shock Compression of Solids II: Dynamic Fracture and Fragmentation, Springer, New York

Decker, R., (2004), "Defense space activities: continuation of evolved expendable launch vehicle program's progess to date sujcct to somc uncertainty," GAO report GAO-04-778R Evolved Expendable Launch Vehicle, Washington, DC, 24 June

DeGoot, M., and Schervish, M., (2002), Probability and Statistics, Third Edition, Addison Wesley, New York

Demichela, M., Piccinini, N., Ciarambino, I., and Contini, S., (2003), "On the numerical solution of fault trees," Reliability and System Safety, Vol. 82, pp. 141-147

Department of Transportation, (1996), Federal Aviation Administration, Office of the Associate Administrator for Commercial Space Transportation, LEO Commercial Market Projections, http://ast.faa.gov/files/pdf/leo-b.pdf, 5 April 1996

Department of Transportation, (1998a), Associate Administrator for Commercial Space Transportation (AST), 1998 LEO Commercial Market Projections, http://ast.faa.gov/files/pdf/leo-d.pdf, May 1998

Department of Transportation, (1998b), Associate Administrator for Commercial Space Transportation, Commercial Space Transportation: 1997 Year in Review, http://ast.faa.gov/files/pdf/1997yir.pdf, January 1998

Department of Transportation, (1999a), Associate Administrator for Commercial Space Transportation, Commercial Space Transportation: 1998 Year in Review, http://ast.faa.gov/files/pdf/1998yir.pdf, January 1999

Department of Transportation, (1999b), Federal Aviation Administration's Associate Administrator for Commercial Space Transportation (AST) and the Commercial Space Transportation Advisory Committee (COMSTAC), 1999 Commercial Space Transportation Forecasts, http://ast.faa.gov/files/pdf/leo-99.pdf, May 1999

Department of Transportation, (2000a), Associate Administrator for Commercial Space Transportation, Commercial Space Transportation: 1999 Year in Review, http://ast.faa.gov/files/pdf/1999yir.pdf, January 2000

Department of Transportation, (2000b), Federal Aviation Administration's Associate Administrator for Commercial Space Transportation (AST) and the Commercial Space Transportation Advisory Committee (COMSTAC), 2000 Commercial Space Transportation Forecasts, http://ast.faa.gov/files/pdf/AST2000.PDF, May 2000

Department of Transportation, (2001a), Associate Administrator for Commercial Space Transportation, Commercial Space Transportation: 2000 Year in Review, http://ast.faa.gov/files/pdf/YIR_00.pdf, January 2001

Department of Transportation, (2001b), Federal Aviation Administration, Licensing and Safety Requirements for Launch, section A417.25 (b)(5)(ii), FR No. 67, Vol. 146, page 49518

Department of Transportation, (2001c), Federal Aviation Administration's Associate Administrator for Commercial Space Transportation (AST) and the Commercial Space Transportation Advisory Committee (COMSTAC), 2001 Commercial Space Transportation Forecasts, http://ast.faa.gov/files/pdf/0501forcast.pdf, May 2001

Department of Transportation, (2002a), 14 Code of Federal Regulations: Aeronautics and Space, Chapter III, 1 January 2002

Department of Transportation, (2002b), Supplimental Notice of Proposed Rulemaking: Licensing and Safety Requirements for Launch, July 2002

Department of Transportation, (2002c), Associate Administrator for Commercial Space Transportation, Commercial Space Transportation: 2001 Year in Review, http://ast.faa.gov/files/pdf/2k1ASTYIR.pdf, January 2002

Department of Transportation, (2002d), Federal Aviation Administration's Associate Administrator for Commercial Space Transportation (AST) and the Commercial Space Transportation Advisory Committee (COMSTAC), 2002 Commercial Space Transportation Forecasts, http://ast.faa.gov/files/pdf/ForecastMay2k2GSO_NGSO.pdf, May 2002

Department of Transportation, (2002e), "Liability risk-sharing regime for US commercial space transportation: study and Analysis," Federal Aviation Administration, April

Department of Transportation, (2003a), Associate Administrator for Commercial Space Transportation, Commercial Space Transportation: 2002 Year in Review, http://ast.faa.gov/files/pdf/2002yir.pdf, January 2003

Department of Transportation, (2003b), Federal Aviation Administration's Associate Administrator for Commercial Space Transportation (AST) and the Commercial Space Transportation Advisory Committee (COMSTAC), 2003 Commercial

Space Transportation Forecasts, http://ast.faa.gov/files/pdf/Forecast_05-19-03.pdf, May 2003

Department of Transportation, (2004) Associate Administrator for Commercial Space Transportation, Commercial Space Transportation: 2003 Year in Review, http://ast.faa.gov/files/pdf/YIR03.pdf, January 2004

Department of Transportation, (2006), US commerical space developments and concepts, Department of Transportation, Washington, DC, 2006

Dooling, D., and Finckenor, M., (1999), "Material Selection Guidelines to Limit Atomic Oxygen Effects on Spacecraft Surfaces," NASA/TP-1999-209260, June

Draper, C., McKenzie, D., and Cartmell, M., (2004), "Increasing luanch site capability using a motorized momentum exchange tether," 40th AIAA/ASME/SEA/ASEE Joint Propulsion Conference and Exhibition, Ft. Lauderdale, FL, USA, 11-14 July

Drolshagen, G., (1997), "HST solar array impact survey: Revised damage laws and residue analysis," Adv. Space Res., Vol 19

Drolshagen, G., (2002), "Models and Tools for Meteoroids/Debris Impact Analyses", SPENVIS Workshop, ESTEC, 27-28 May

Eftis, J., Carrasco, C., and Osegueda, R., (2001), "Simulations of Hypervelocity Impact Damage and Fracture of Aluminum Targets Using a Constitutive-Microdamage Material Model," Int. Journal of Impact Engineering, Vol. 26, pp. 157-168

Eichner, A., (1976), The megacorp and oligopoly: Micro foundations of macro dynamics, Cambridge University Press, Cambridge

Eiden, M., and Cartmell, M., (2003), "Overcoming the Challenges: Tether Systems Roadmap for Space Transportation Applications," AIAA/ICAS International Air & Space Symposium and Exposition, Dayton Convention Center, Dayton, Ohio, USA, 14-17 July

Elfer, N., (1996), Structural Damage Prediction and Analysis for Hypervelocity Impacts - Handbook, NASA CR 4706, Feb

Fahrenthold, E., and Horban, B., (1999), "A Hybrid Particle-Finite Element Method for Hypervelocity Impact Simulation," Int. Journal of Impact Engineering, Vol. 23, pp. 237-248

Fahrenthold, E., and Horban, B., (2001), "An Improved Hybrid Particle-Finite Element Method for Hypervelocity Impact Simulation," Int. Journal of Impact Engineering, Vol. 26, pp. 169-178

Fahrenthold, E., and Koo, J., (1997), "Energy Based Particle Hydrodynamics for Hypervelocity Impact Simulation," Int. Journal of Impact Engineering, Vol. 20, pp. 253-264

Fellner, W., (1949), Competition among the few: oligopoly and similar market structures, Alfred A Knopf, Inc, New York

Figler, A., (2001), "Talk about sky-high taxes," Cable World, (http://www.findarticles.com/p/articles/mi_m0DIZ), 23 July

Finkelstein, M., (2003), "The expected time lost due to an extra risk," Reliability and System Safety, Vol. 82, pp. 225-228

Fisher, F., (1970), "Tests of Equality between Sets of Coefficients in Two Linear Regressions: An Expository Note," Econometrica, Vol. 38, pp. 361-366

Forward, R., and Hoyt, R., (1995), "Space tethers with multidecade lifetimes," 46th International Astronautical Congress, Oslo, Norway, 2-6 October

Forward, R., and Hoyt, R., (1999), "Space tethers," Scientific American, February

Forward, R., and Nordley, G., (1999), "Mars-Earth rapid interplanetary tether transport (MERITT) system: initial feasibility analysis," AIAA-99-2151

Fragola, J., and Collins, E.,(2004), "Risk forecasting using heritage-based surrogate data," 2004 Proceedings: Annual Reliability and Maintainability Symposium, pp. 628-633

Franzen, R., Orphal, D., and Anderson, C. Jr., (1997), "The Influence of Experimental Design on Depth of Penetration (DOP) Test Results and Derived Ballistic Efficiencies," Int. Journal of Impact Engineering, Vol. 19, No. 8, pp. 727-737

Friedman, J., (1983), Oligopoly Theory, Cambridge University Press, Cambridge

Fries, A., and Easterling, R., (1999), "Annual testing of strategic missile systems," Proceedings of the American Statistical Association Section on Physical and Engineering Sciences, pp. 132-134

Frost, V., (1970), "Meteoroid Damage Assessment," Aerospace Corporation, NASA SP-8042, May

Gabler, E., (1992), "Product and Service Pricing: Launch vehicles," Space Economics, Progress in Astronautics and Aeronautics, Vol 144

Garber, R., and Pate-Cornell, M., (2004), "Modeling the effects of dispersion of design teams on system failure risk," Journal of Spacecraft and Rockets, Vol. 41, pp. 60-68

Gardner, D., and Burchell, M., (1997), "Thick target hypervelocity impact crater morphology: the influence of impact angle, speed and density ratio," Proceedings of the Second European Conference on Space Debris, ESOC, Darmstadt, Germany, 17-19 March, pp. 481-486

Gates, S., Koss, S., and Zedd, M., (2001), "Advanced tether experiment deloyment failure," Journal of Spacecaft and Rockets, Vol. 38, pp. 60-68

Gerassimenko, M., (2001), "Modeling of Measured Target Pressure Profiles in Three Hypervelocity Impact Experiments," Int. Journal of Impact Engineering, Vol. 26, pp. 221-230

Geroski, P., Philips, L., and Ulph, A., (1985), "Oligopoly, Competition and Welfare: Some Recent Developments," Oligopoly, Competition, and Welfare, Basil Blackwell, Oxford

Gilks, W., Richardson, S., and Spiegelhalter, D.,(1995), Markov chain Monte Carlo in practice, Chapman and Hall, New York

Gittins, G., Swinerd, G., Lewis, H., and Williams, D., (2004), "A studey of debris impact collision probabilities to space tethers," Advances in Space Research, Vol. 34, No. 5, pp. 1080-1084

Goldstein, R., (1998), Radar observations of space debris, Planetary Space Science, Vol. 46, No. 8, pp. 1007-1013

Graham, G., McBride, N., Kearsley, A., Drolshagen, G., Green, S., McDonnell, J., Grady, M., and Wright, I., (2001), "The Chemistry of Micrometeoroid and Space Debris Remnants Captured on Hubble Space Telescope Solar Cells," Int. Journal of Impact Engineering, Vol. 26, pp. 263-274

Grant, J., Willenberg, H., Tillotson, B., Stemler, J., Bangham, M., and Forward, R., (2000), "Hypersonic airplane space tether orbital launch - HASTOL: A two-stage comerical launch system," AIAA-2000-3841

Grey, I., and Burchell, M., (2004), "Hypervelocity impact craters in ammonia rich ice," Icarus, Vol 168, pp 467-474

Guerin, F., Dumon, B., and Usureau, E., (2003), "Reliability estimation by Bayesian method: definition of prior distribution using dependability study," Reliability and System Safety, Vol. 82, pp. 299-306

Guikema, S., and Pate-Cornell, M, (2004), "Bayesian analysis of launch vehicle success rates," Journal of Spacecraft and Rockets, Vol. 41, pp. 93-102

Guikema, S., and Pate-Cornell, M, (2005), "Probability of infancy problems for space launch vehicles," Reliability Engineering and System Safety, Vol. 87, pp. 303-314

Guikema, S., and Pate-Cornell, M., (2002), "Component choice for managing risk in engineered systems with generalized risk/cost functions," Reliability Engineering and System Safety, Vol. 78, pp. 227-238

H/Srz, F., Bernhard, R., See, T., and Brownlee, D. (1993), "Natural and Orbital Debris Particles on LDEF's Trailing and Forward-Facing Surfaces," Proceedings of the 3rd LDEF post-retrieval symposium, NASA CP 3275, pp.415-430

Hanselman, D., and Littlefield, B., The Student Edition of MATLAB, Version 5, User's Guide, Prentice Hall, Upper Saddle River, NJ, 1997, ISBN 0-13-272550-9

Hayashida, K. and Robinson, J., (1991), "Single Wall Penetration Equations", NASA TM-103565, December

Hayashida, K., and Robinson, J., (1993), "TSS Tether Cable Meteoroid/Orbital Debris Damage Analysis," NASA TM-108404, April

Hayhurst, C., Ranson, H., Gardner, D., and Birnbaum, N., (1995), "Modelling of Microparticle Hypervelocity Oblique Impacts on Thick Targets," Int. J. Impact Engng, Vol. 17, pp. 375-386

Hays, W., and Winkler, R., (1970), Statistics, Volume II, Probability, Inference, and Decision, Holt, Rinehart and Winston, Inc., New York

Hiermaier, S., Konke, D., Stilp, A., and Thoma, K., (1997), "Computational Simulation of the Hypervelocity Impact of Al-Spheres on Thin Plates of Different Materials," Int. Journal of Impact Engineering, Vol. 20, pp. 363-374

Holtz-Eakin, D., (2003), "NASA's space flight operations contract and other technologically complex government activities conducted by contractors," Gongressional Budget Office, 29 July

Hörz, F., (1999), Optical Analysis of Impact Features in Aerogel From the Orbital Debris Collection Experiment on the Mir Station, NASA TM-1999-209372

Hoyt, R., and Forward, R., (1998), "The Hoytether: A Failsafe Multiline Space Tether Structure," Tether Technology Interchange Meeting, NASA/CP-1998-206900, Jan

Humes, D., (1993), "Small Craters on the Meteoroid and Space Debris Impact Experiment," Proceedings of the 3rd LDEF post-retrieval symposium, NASA CP 3275, pp.287-322

Hyde, J., Christiansen, E., and Kerr, J., (2001), "Meteoroid and Orbital Debris Risk Mitigation in a Low Earth Orbit Satellite Constellation," Int. J. Impact Engng, Vol. 26, pp. 345-356

Isakowitz, S., Hopkins, J., and Hopkins, J., (1991), International reference guide to space launch systems, American Institute of Aeronautics and Astronautics, Reston

James, B., Norton, O., and Alexander, M., (1994), "The Natural Space Environment: Effects on Spacecraft", NASA Reference Publication 1350, November

Jewell, W., (1984), "A general framework for learning curve reliability growth models," Operations Research, Vol. 32, pp. 547-558

Johnson, L, Gilchrist, B., and Lorenzini, E., (1999), "Overview of future NASA tether applications," Advances in Space Research, Vol. 24, pp. 1055-1063

Johnson, N., (2001), "NASA's new breakup model of EVOLVE 4.0," Adv. Space Res., Vol. 28, No. 9, pp. 1377-1384

Johnson, R., and Smith, P., (1998), "Future spacelift projections," Space Policy, Vol. 14, pp 145-151

Kaplan, S., (1990), "On the inclusion of precursor and near miss events in quantitative risk assessment: a bayesian point of view and a Space Shuttle example," Reliability Engineering and System Safety, Vol. 27, pp. 103-115

Kessler, D, (1970), Meteoroid Environment Model -- 1970 [Interplanetary and planetary],NASA SP-8038, October

Kessler, D, (1972), "A guide to using meteoroid-environment models for experiment and spacecraft design models," NASA TN D-6596, March

Kessler, D, (1991), "Meteoroids and orbital debris. In Space Station Program Natural Environment Definition for Design," NASA SSP-30425/Rev.A

Kessler, D, (1996), "A Computer-Based Orbital Debris Environment Model for Spacecraft Design and Observation in Low Earth Orbit," NASA TM-104825

Kessler, D., (1981), "Derivation of the collision probability between orbiting objects: The lifetimes of Jupiter's outer moons," ICARUS, Vol. 48, pp. 39-48

Kessler, D., (1981), Derivation of the collision probability between orbiting objects: The lifetimes of Jupiter's outer moons, ICARUS, Vol. 48, pp. 39-48

Kessler, D., (1993), "Origin of Orbital Debris Impacts on LDEF's Trailing Surfaces," Proc. of the 2nd LDEF Post-Retrieval Symposium, NASA CP-3194, pp.585-593

Kessler, D., Reynolds, R., and Anz-Meador, P., (1988), "Orbital debris environment for spacecraft designed to operate in low Earth orbit," NASA TM 100471, September

Kiureghian, A., (2001), "Risk assessment of satellite launch with reusable launch vehicle," Reliability Engineering and System Safety, Vol. 74, pp. 353-360

Koop, G., (2003), Bayesian Econometrics, Wiley, West Sussex

Kotz, S., and Johnson, N., (1986), Encyclopedia of Statistical Sciences, John Wiley and Sons, New York

Koucky, M., (2003), "Exact reliability formula and bounds for general k-out-of-n systems," Reliability and System Safety, Vol. 82, pp. 229-231

Krige, J., (1999), "The commerical challenge to Arianespace: the TCI affair," Space Policy, Vol. 15, pp 87-94

Krisko, P., (2000), EVOLVE 4.0 User's Guide and Handbook, LMSMSS-33020

Kumar, K., Yasaka, T., and Sasaki, T., (2004), "Orbit transfer of service vehicle/payload through tether retrieval," Acta Astronautica, Vol. 54, pp. 687-698

Kyroudis, G., and Conway, B., (1988), "Advantages of tether release of satellites from elliptic orbits," Acta Astronautica, Vol. 11, pp. 441-448

Laird, D., and Palazotto, A., (2003), "Gouge Development During Hypervelocity Sliding Impact," Int. Journal of Impact Engineering, Vol. 28, No. 2, pp 205-223

Lamontage, C., Maneulpillai, G., Taylor, E., and Tennyson, R., (1999), "Normal and Oblique Hypervelocity Impacts on Carbon Fibre/Peck Composites," Int. J. Impact Engng.; Vol. 23, pp. 519-532

Lennert, S., and Cartmell, M., (2003), "Analysis and design of a friction brake for momentum exchange propulsion tethers," Fifth IAA International Conference on Low-Cost Planetary Missions, ESA/ESTEC, September

Levine, A.S. (1991), LDEF.69 months in space: The first post-retrieval symposium, NASA CP-3134

Levine, A.S. (1992), LDEF.69 months in space: The second post-retrieval symposium, NASA CP-3194

Levine, A.S. (1993), LDEF.69 months in space: The third post-retrieval symposium, NASA CP-3275

Lewis, E., (1996), Introduction to Reliability Engineering, Second Edition, John Wiley & Sons, Inc., New York

Liou, J., Matney, M., Anz-Meador, P., Kessler, D., Jansen, M., and Theall, J., (2002), "The New NASA Orbital Debris Engineering Model ORDEM2000," NASA/TP-2002-210780, May

Littlefield, D., (2001), "The Use of r-Adaptivity with Local, Intermittent Remesh for Modeling Hypervelocity Impact and Penetration," Int. Journal of Impact Engineering, Vol. 26, pp. 433-442

Livesey, F, (1987), Economics for Business Decisions, Pitman Publishing, London

Lockheed Martin Corporation, (2003), 2002 Annual Report, http://www.lockheedmartin.com/data/assets/314.pdf

Lorenzini, E., Cosmo, M., Kaiser, M., Bingham, M., Vonderwell, D., and Johnson, L., (2000), "Mission analysis of spinning systems for transfers from low orbits to geostationary," Journal of Spacecraft and Rockets, Vol. 37, pp. 165-172

Lugtigheid, D., Banjevic, D., and Jardine, A., (2004), "Modelling repairable system reliability with explanatory variables and repair and maintenance actions," IMA Journal of Management Mathematics, Vol. 15, pp. 89-110

Lyle, K., Padula, S., and Stockwell, A., (2003), "Application of probabilistic analysis to aircraft impact dynamics," AIAA-2003-1482, 2003

Lynch, N., (1999), "Constant Kinetic Energy Impacts of Scale Size KE Projectiles at Ordnance and Hypervelocity," Int. Journal of Impact Engineering, Vol. 23, pp. 573-584

Matney, M., Kessler, D., and Johnson, N., (2004), "Calculations of collision probabilities for space tethers," 51st International Astronautical Congress, IAA Paper 00-IAA-6.5.02, 2-6 October, Rio de Janeiro, Brazil

Mazzuchi, T.A., and Soyer, R., (1993), "A Bayes Method for Assessing Product-Reliability During Development Testing," IEEE Transactions on Reliability, Vol 42, pp. 503-510

McBride, N., and McDonnell, J., (1999), "Meteoroid impacts on spacecraft: sporadics, streams, and the 1999 Leonids," Planetary and Space Science, Vol. 47, pp. 1005-1013

McBride, N., and Taylor, E., (1997), "The risk to satellite tethers from meteoroid and debris impacts," Proceedings of the Second European Conference on Space Debris, ESOC, Darmstadt, Germany, 17-19 March, pp. 643-648

McCartney, et al., (1993), Atlas/Centaur AC-71 Failure Investigation: Final Report, General Dynamics Space Systems Division, 27 January

McKenzie, D., and Cartmell, M., (2004), "On the performance of a motorized tether using a ballistic launch method," 55th International Astronautical Congress 2004, Vancouver Convention and Exhibition Center, Vancouver, 5-8 October

McKenzie, D., and Cartmell, M., (2005), "On the performance of a motorised tether with payload deployment," XXXIII Summer School on 'Advanced Problems in Mechanics,' Russian Academy of Sciences, St. Petersburg, Russia, 28 June - 5 July

McManus, H., Hastings, D., and Warmkessel, J., (2004), "New methods for rapid architecture selection and conceptual design," Journal of Spacecraft and Rockets, Vol. 41, pp. 10-19

Mell, R., and Wertz, G., (2001), "Testing and Optimization of Electrically Conductive Spacecraft Coatings," NASA/CR-2001-211411, December

Meriam, J., and Kraige, L., (1997), Engineering Mechanics: Dynamics, Fourth Edition, John Wiley & Sons

Moosman, A., (2002), "Risk models for new and established launch vehicles," CoreTech Meeting, Colorado Springs, Colorado, USA, November

Morris, W., White, N., and Debeling, C., (1996), "Analysis of Shuttle orbiter reliability and maintainability data for conceptual studies," AIAA Space Programs and Technologies Conference, Huntsville, AL, 24-26 September

Mouterde, F., Cartmell, M., and Wang, Y., (2004), "Computational simulation of feedback linearised control of a motorised momentum exchange tether on a circular Earth orbit," Sixth World Congress on Computational Mechanics, Beijing Hotel, Beijing, China, 5-11 September

NASA, (1995), "NASA Safety Standard: Guidelines and Assessment Procedures for Limiting Orbital Debris," NSS-1740.14, August

National Oceanic and Atmospheric Administration, (1995), "Preliminary report and forecast of solar geophysical data," published weekly by the joint NOAA-USAF Space Environment Services Center, SESC PRF 1053, 7 November

Neish, M., and Kibe, S., (1997), "Hypervelocity impact damage equations for Kapton multi-layered insulation and teflon second surface Mirrors," Proceedings of the 3rd European Space Debris Conference, ESA SP-473

Nilsen, T. and Aven. T., (2003), "Models and uncertainty in the context of risk analysis," Reliability and System Safety, Vol. 79, pp. 309-317

Office of Commercial Space Transportation, (1995), LEO Commercial Market Projections, http://ast.faa.gov/files/pdf/leo.pdf, 17 May

Office of Commercial Space Transportation, (1997), LEO Commercial Market Projections, http://ast.faa.gov/files/pdf/leo-c.pdf, 25 July

Orbital Sciences Corporation, (2003), 2002 Annual Report, http://www.orbital.com/Investor/FinancialDocuments/documents/AR_02.pdf, 2003

Orphal, D., (1999), "Highly oblique impact and penetration of thin targets by steel spheres," Int. Journal of Impact Engineering, Vol. 23, pp. 687-698

Orphal, D., and Anderson, C., Jr., (1999), "Streamline Reversal In Hypervelocity Penetration," Int. Journal of Impact Engineering, Vol. 23, pp. 699-710

Orphal, D., and Anderson, C., Jr., (2001), "Target Damage from Highly Oblique Hypervelocity Impacts of Steel Spheres Against Thin Laminated Targets," Int. Journal of Impact Engineering, Vol. 26, pp. 567-578

Parkinson, R., (1999), "The hidden costs of reliability and failure in launch systems," Acta Astronautica, Vol. 44, pp. 419-424

Pass, C., and Lowes, B., (1993), Collins Dictionary of Economics: Second Edition, Harper Collius Publishers, Glasgow

Patera, R., (2002), "Method for calculating collision probability between a satellite and a space tether," Journal of Guidance, Control, and Dynamics, Vol. 25, pp. 940-945

Patsuris, P., (2001), "Communications satellite tax out of this world," Forbes.com, 18 July

Paul, K.G., Igenbergs, E., and Berthoud, L., (1997), "Hypervelocity impacts on solar cells — observations, experiments, and empirical scaling laws," International Journal of Impact Engineering, Vol. 20, pp. 627-638

Penson, J., and Burchell, M., (2003), "Hypervelocity Impact Studies on Space Tethers," 54th International Astronautical Congress, Paper IAC-03-1.5.04, Bremen, Germany

Pfefferman, J., and Cernuschi-Frias, B., (2002), "A Non-Parametric Non-Stationary Procedure for Failure Prediction", IEEE Transactions on Reliability, Vol. 51, No. 4, December

Philipson, L., (1989), "A simple method for obtaining approximate systems failure rate uncertainty distributions," Reliability Engineering and System Safety, Vol. 25, pp. 371-382

Philipson, L., (1995a), "Risk profile derivations for space and missile launch hazards," Reliability Engineering and System Safety, Vol. 49, pp. 217-236

Philipson, L., (1995b), "Anomalies in Bayesian launch range safety analysis," Reliability Engineering and System Safety, Vol. 49, pp. 355-357

Port, O., (2004), "Commentary: Space travel: Bringing costs down to Earth, NASA should give startups room to maneuver," Business Week Online, http://www.businessweek.com/magazine/content/04_05/b3868097.htm, February 2

Porter, R., (1985), "On the incidence and druation of price wars," Oligopoly, Competition, and Welfare, Basil Blackwell, Oxford

Quigley, J., and Walls, L., (1999), "Measuring the effectiveness of reliability growth testing," Quality and Reliability Engineering International, Vol. 15, pp. 87-93

Quigley, J., and Walls, L., (2003), "Confidence intervals for reliability growth models with small sample sizes," IEEE Transactions in Reliability, Vol. 52, pp. 257-262

Rex, D., (1997), "Space debris mitigation and space systems design," Acta Astronautica, Vol. 41, pp. 311-316

Robinson, J., (1999), "Orbital Debris Impact Damage to Reusable Launch Vehicles," Int. Journal of Impact Engineering, Vol. 23, pp. 783-794

Ross, S., Westerfield, R., and Jordan, B., (2000), "Fundamentals of Corporate Finance, Fifth Edition" Irwin McGraw-Hill, Boston

Sabath, D., and Paul, K., (1997), "Hypervelocity impact experiments on tether materials," Advances in Space Research, Vol. 20, pp. 1433-1436

Sachs, L., (1984), "Applied Statistics: A Handbook of Techniques." 2nd edition, Springer-Verlag, New York

Sarhan, A., (2003), "Non-parametric empirical Bayes procedure," Reliability and System Safety, Vol. 80, pp. 115-122

Schonberg, W., (1989), "Penetration and Ricochet Phenomena in Oblique Hypervelocity Impact," AIAA Journal, Vol. 27, No. 5, pp. 639-646

Schonberg, W., and Ebrahim, A., (1999), "Modelling Oblique Hypervelocity Impact Phenomena Using Elementary Shock Physics," Int. Journal of Impact Engineering, Vol. 23, pp. 823-834

Schonberg, W., and Yang, F., (1993), "Response of Space Structures to Orbital Debris Particle Impacts," Int. Journal of Impact Engineering, Vol. 14, pp. 647-658

Sea Launch Company, LLC, (2002), Comments and Cost Impact Analysis (Confidential), Department of Transportation Docket Management System, Docket Number FAA-2000-7953-29, 28 October

Settecerri, T., and Stansbery, E., (1997), Measurements of the orbital debris environment: Comparison of the Haystack and HAX radars, JSC-27971

Shackelford, J., (1996), Introduction to Materials Science for Engineers, Fourth Edition, Prentice Hall, Upper Saddle River, NJ

Shim, V., Lim, C., and Foo, K., (2001), "Dynamic mechanical properties of fabric armour," International Journal of Impact Engineering, Vol. 25, pp. 1-15

Silverman, E., (1995a), "Space Environmental Effects on Spacecraft: LEO Materials Selection Guide," NASA CR-4661, Part 1, August

Silverman, E., (1995b), "Space Environmental Effects on Spacecraft: LEO Materials Selection Guide," NASA CR-4661, Part 2, August

Simetric, (2006), "Mass, weight, density or specific gravity of bulk materials," [http://www.simetric.co.uk/si_materials.htm], last cited 13 April 2006

Smith, J., Appleby, P., Hilton, J., Richardson, N., and Hermida, J., (1997), "Risk management in commerical launches," Space Policy, Vol. 13, pp 145-152, May

Smith, M., (2005a), "Space launch vehicles: Government activities, commerical competition, and satellite exports," CSR Issue Brief for Congress, 27 May

Smith, M., (2005b), "U.S. Space Programs: Civilian, Military, and Commercial," CSR Issue Brief for Congress, 17 November

Snedecor, G., and Cochran, W., (1989), Statistical Methods, Eighth Edition, Iowa State University Press, Ames, IA

Sorensen, K., (2003), "Momentum eXchange Electordynamic Reboost (MXER) Tether Technology Assessment Group Final Report," In-Space Propulsion Technologies Program, NASA Marshall Space Flight Center, 24 July

Souder, W., Sherman, J., and Davies-Cooper, R., (2005), "New product development performance and the interaction of cross-functional integration and knowledge management," Journal of Product Innovation Management, Vol. 22, pp. 399-411

Spiegelhalter, D., Thomas, A., Best, N., and Lunn, D., (2003), WinBUGS User Manual, http://www.mrc-bsu.cam.ac.uk/bugs/winbugs/manual14.pdf, January

Spiegelhalter, D., Thomas, A., Best, N., and Lunn, D., (2004), WinBUGS User Manual, Version 2.0, [http://www.mrc-bsu.cam.ac.uk/bugs] June

Stamatelatos, M., Apostloakis, G., Dezfuli, H., Everline, C., Guarro, S., Moieni, P., Mosleh, A., Paulos, T., and Youngblood, R., (2002), Probabilistic Risk Assessment Procedures Guide for NASA Manages and Practicioners, Version 1.1, NASA Office of Safety and Mission Assurance, August

Stansbery, E., (1996), "Haystack radar measurements of the orbital debris environment; 1990-1994," JSC-27436

Stansbery, E., Kessler, D., and Matney, M., (1995), "Recent Results of Orbital Debris Measurements from Haystack Radar," AIAA 95-0664, 33rd Aerospace Sciences Meeting and Exhibit, Reno, NV, January 9-12

Stansbery, E., Kessler, D., Tracy, T., Matney, M., and Stanley, J., (1994), "Haystack Radar Measurements of the Orbital Debris Environment," NASA Johnson Space Center,JSC-26655, 20 May

Stewart, J., (1995), Calculus: Early Transcendentals, Third Edition, Brooks/Cole Publishing Company ITP

Stilp, A., (1997), "Hypervelocity impact research," Proceedings of the Second European Conference on Space Debris, ESOC, Darmstadt, Germany, 17-19 March, pp. 399-404

Stockman, A., (1999), Introduction to Microeconomics, 2nd Edition, Dryden Press, Fort Worth

Stradling, G., Idzorek, G., Shafer, B., Curling, H., Collopy, M., Blossom, A., and Fuerstenau, S., (1993), "Ultra-high Velocity Impacts: Cratering Studies of Microscopic Impacts from 3 km/s to 20 km/s, Proc. 1992 Hypervelocity Impact Symp.," Int. Journal of Impact Engineering, Vol. 14, pp. 719-727

Stronge, W., (2000), Impact Mechanics, Cambridge University Press, Cambridge, UK

Strumfels, R., (2001), "Design of space tethers for meteoroid and orbital debris impact survivability," 39th Aerospace Sciences Meeting and Exhibit, Reno, NV, USA, 8-11 January

Sutton, G., and Biblarz, O., (2001), Rocket Propulsion Elements, Seventh Edition, John Wiley & Sons

Taylor, E., Tsembelis, K., Hayhurst, C., Kay, L., and Burchell, M., (1999), "Hydrocode Modelling of Hypervelocity Impact on Brittle Materials: Depth of Penetration and Conchoidal Diameter," Int. Journal of Impact Engineering, Vol. 23, pp. 895-904

Teijin Twaron, (2005), "Twaron datasheet," Doc 04-007, September

Teijin Twaron, (2005a), "Strain rate dependence for Twaron," Doc Y4644+6649+6650+6962-Rate.xls / FigRate, September

Thomson, W., (1986), Introduction to Space Dynamics, Dover Publications, Inc., New York, NY

Title 14 Code of Federal Regulations, (2000), Chapter III, Part 401, Organization and Definitions, as amended, 3 November

Title 14 Code of Federal Regulations, (2003), Chapter III, Government Printing Office, Washington, DC

Title 49, United States Code, (2001), Subtitle IX, Chapter 701, Commercial Space Launch Activities [the Commercial Space Launch Act (CSLA)], as amended, 2 January

Todd, D., (2000), "Doubts continue as Boeing's Delta 3 rocket falls short again," Spacetrack, Airclaims Ltd, 12 September

Tribble, A., (1995), The Space Environment, Princeton University Press, Princeton, NJ

Tribble, A., (2003), The Space Environment, Princeton University Press, Princeton, NJ

Tully, S., (1985), "Europe blasts into the space business," Fortune Magazine, (http://money.cnn.com/magazines/fortune/fortune_archive/1985/05/27/65849/index.htm), 27 May

Van Der Heide, E., and Kruijff, M., (2001), "Tethers and debris mitigation," Acta Astronautica, Vol. 48, pp. 503-516

Van Noord, J., and Sturmfels, R., (2001), "Electordynamic tether optimization for the STEP-AIRSEDS mission," 37th AIAA/ASME/SAE/ASEE Joint Propulsion Conference and Exhibit, Salt Lake City, UT, USA, 8-11 July

Van Noord, J., Robinson, J., and Piekutowski, A., (2002), "Results of hypervelocity impact tests on tape tethers," 40th AIAA Aerospace Sciences Meeting and Exhibit, Reno, NV, USA 14-17 January

Vaughan, W.W., (1999), "The NASA Marshall solar activity model for use in predicting satellite lifetime," Adv. Space Res. Vol. 23, No. 4

Wade, M, (2006) "Orbital Launch Vehicle Alphabetical Index," Encyclopedia Astronautica, http://www.astronautix.com/lvs/orbindex.htm [cited 1 March 2006]

Walker, J., (2001), "Hypervelocity Penetration Modeling: Momentum vs. Energy and Energy Transfer Mechanisms," Int. Journal of Impact Engineering, Vol 26, pp 809-822

Walls, L., and Quigley, J., (2001), "Building prior distributions to support Bayesian reliability growth modelling using expert judgement," Reliability Engineering and Systems Safety, Vol. 74, pp. 117-128

Walls, L., Quigley, J., and Krashich, M., (2005), "Comparison of two models for managing reliability growth during product design," IMA Journal of Management Mathematics, Vol. 16, pp. 12-22

Walsh, J., Stradling, G., Idzorek, G., Shafer, B., and Curling, H., (1993), "Microparticle Impacts as Ultra-high Velocities: Their Relationship to Macroparticle Impacts, Proc. 1992 Hypervelocity Impact Symp.," Int. Journal of Impact Engineering, Vol. 14, pp. 775-784

Wang, Y., and Xia, Y., (1999), "Experimental and theoretical study on the strain rate and temperature dependence of mechanical behavior of Kevlar fibre," Composites Part A: Applied Science and Manufacturing, Vol. 30, pp. 1251-1257

Ward, J., (1998), "Methodologies for Assessing Launch-Vehicle Failure Probabilties," Research Triangle Institute Memo, 30 December

Weerahandi, S., (1987), "Testing Regression Equality with Unequal Variances," Econometrica, Vol. 55, pp. 1211-1215

Weigel, A., and Hastings, D., (2004), "Evaluating the cost and risk impacts of launch choices," Journal of Spacecraft and Rockets, Vol. 41, pp. 103-110

Wilhelm, S., (2000), "Boeing's Delta III rocket may be a loss leader," Puget Sound Business Journal (Seattle), 24 July

Williams, P., Blanksby, C., Trivailo, P., and Fujii, H., (2005), "In-plane payload capture using tethers," Acta Astronautica, Vol. 57, pp. 772-787

Yano, H., (1999), "Japanese contribution to in-situ meteoroid and debris measurement in the near Earth space," Earth, Planets, and Space, Vol. 51

Young, E., (2001), "Los Angeles plans to tax property in space," New Scientist, 11 July

Yu, S., Sun, G., and Tan, Q., (1994), "Experimental laws of cratering for hypervelocity impacts of spherical projectiles into thin targets," Int. J. Impact Eng., Vol 15, No. 1, pp 67-77

Zhang, J. and Kessler, D., (1993), "Orbital debris and meteoroid population as estimated from LDEF impact data," Proceedings of the 3rd LDEF post-retrieval symposium, NASA CP 3275, pp.373-384, 1993

Ziegler, S., (2003), The Rigid-body Dynamics of Tethers in Space, PhD Thesis for the University of Glasgow, September

Ziegler, S., and Cartmell, M., (2000a), "On the validity of recent predications for tethers on elliptical orbits," 11th AAS/AIAA Space Flight Mechanics Meeting, Santa Barbara, CA, USA, Vol. 108, pp. 1831-1838

Ziegler, S., and Cartmell, M., (2000b), "Investigating the use of motorised tethers for payload orbital transfer," AIAA/AAS Astrodynamics Specialist Conference and Exhibit, Denver, CO, USA, 14017 August

Ziegler, S., and Cartmell, M., (2001), "Using motorised tethers for payload orbital transfer," Journal of Spacecraft and Rockets, Vol. 38, pp. 904-913

Zukas, J., (1990), High Velocity Impact Dynamics, New York, Wiley

Zukas, J., and Gaskill, B., (1996), "Ricochet of Deforming Projectiles from Deforming Plates," Int. Journal of Impact Engineering, Vol 18, No. 6, pp 601-610